REPORT DOCUMENTATION PAGE

Form Approved
OMB No. 0704-0188

Public reporting burden for this collection of information is estimated to average 1 hour per response, including the time for reviewing instructions, searching existing data sources, gathering and maintaining the data needed, and completing and reviewing the collection of information. Send comments regarding this burden estimate or any other aspect of this collection of information, including suggestions for reducing this burden, to Washington Headquarters Services, Directorate for Information Operations and Reports, 1215 Jefferson Davis Highway, Suite 1204, Arlington, VA 22202-4302, and to the Office of Management and Budget, Paperwork Reduction Project (0704-0188), Washington, DC 20503.

1. AGENCY USE ONLY (Leave blank)	2. REPORT DATE Dec 95	3. REPORT TYPE AND DATES COVERED Final 1 Apr 93 – 30 Sep 95

4. TITLE AND SUBTITLE
High Performance Computing and Modelling of Composite Manufacturing Processes Such as Resin Transfer Molding

6. AUTHOR(S)

Suresh G. Advani

5. FUNDING NUMBERS

DAAH04-93-G-0087

7. PERFORMING ORGANIZATION NAME(S) AND ADDRESS(ES)

University of Delaware
Newark, DE   19716

8. PERFORMING ORGANIZATION REPORT NUMBER

9. SPONSORING / MONITORING AGENCY NAME(S) AND ADDRESS(ES)

U.S. Army Research Office
P.O. Box 12211
Research Triangle Park, NC   27709-2211

10. SPONSORING / MONITORING AGENCY REPORT NUMBER

ARO 31559.1-MA

11. SUPPLEMENTARY NOTES
The view, opinions and/or findings contained in this report are those of the author(s) and should not be construed as an official Department of the Army position, policy, or decision, unless so designated by other documentation.

12a. DISTRIBUTION / AVAILABILITY STATEMENT

Approved for public release; distribution unlimited

12b. DISTRIBUTION CODE

ABSTRACT *(Maximum 200 words)*

The focus was to understand and model the composite manufacturing process called Resin Transfer Molding (RTM) and develop numerical simulations to move towards virtual manufacturing in an attempt to reduce the prototype costs. Experiments were carried out to understand and isolate the important features of this process and mathematical models were developed to create a process model. These models were incorporated in numerical simulations to make them useful for manufacturing of complex structures. Numerical procedures were also developed in the process to make the simulations stable and faster. The results of numerical simulations were compared with two elaborate experimental programs, a five sided box and a cone, to verify the authenticity of the numerical simulation and the mathematical models. Different versions of the numerical simulation developed are being used at ARL, Aberdeen and by TACOM. This report gives a brief summary of the work and the details of the work are reported as appendices.

14. SUBJECT TERMS

Resin Transfer Molding, Manufacturing Simulations, Composites Manufacturing, Process Models

15. NUMBER OF PAGES

16. PRICE CODE

17. SECURITY CLASSIFICATION OF REPORT UNCLASSIFIED	18. SECURITY CLASSIFICATION OF THIS PAGE UNCLASSIFIED	19. SECURITY CLASSIFICATION OF ABSTRACT UNCLASSIFIED	20. LIMITATION OF ABSTRACT UL

Final Technical Report

Research Agreement No. DAAH04-93-G-0087

HIGH PERFORMANCE COMPUTING AND MODELING OF COMPOSITE MANUFACTURING PROCESSES SUCH AS RESIN TRANSFER MOLDING

by

Suresh G. Advani

Associate Professor of Mechanical Engineering

Affiliated Faculty with Center for Composite Materials

University of Delaware

Newark, DE 19716

phone: 302 -831-8975

fax: 302-831-3619

e.mail: advani@me.udel.edu

Other Personnel Supported by this grant

Dr. Baichen Liu

Dr. Lihwa Fong

Dr. Ram Varma

Dr. Pavel Simacek

Mr. Simon Bickerton

Ms. Wei Zhang

Mr. Patrick Murphy

DISCLAIMER NOTICE
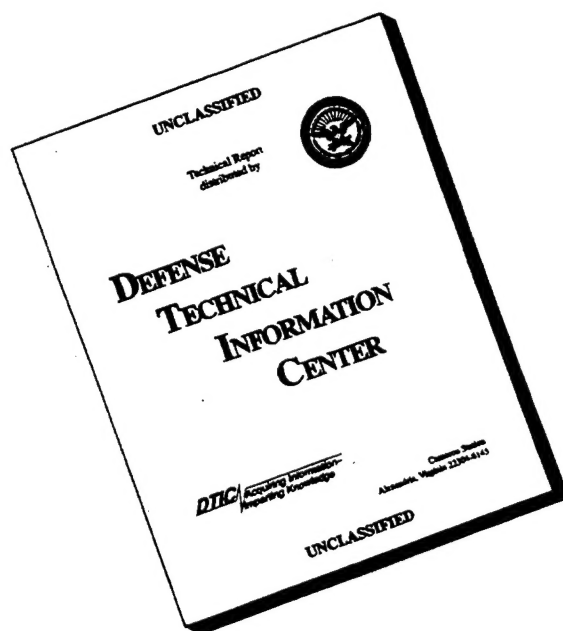
THIS DOCUMENT IS BEST QUALITY AVAILABLE. THE COPY FURNISHED TO DTIC CONTAINED A SIGNIFICANT NUMBER OF PAGES WHICH DO NOT REPRODUCE LEGIBLY.

Preamble

This report summarizes the research conducted under this grant number. The focus was to understand and model the composite manufacturing process called Resin Transfer Molding (RTM) and develop numerical simulations to move towards virtual manufacturing in an attempt to reduce the prototype costs. Experiments were carried out to understand and isolate the important features of this process and mathematical models were developed to create a process model. These models were incorporated in numerical simulations to make them useful for manufacturing of complex structures. Numerical procedures were also developed in the process to make the simulations stable and faster.

The results of numerical simulations were compared with two elaborate experimental programs, a five sided box and a cone, to verify the authenticity of the numerical simulation and the mathematical models. The report is organized in the following fashion. A brief summary of the work is given and the details of the work are reported as appendices or reports at the end that were produced during the course of this grant.

Introduction

Resin Transfer Molding (RTM) is a closed mold process in which matched male and female molds, preplaced with fiber preform, are clamped to form composite components. Resin mix is transferred into the cavity through injection ports at a relatively low pressure. Injection pressure is normally less than 690 KPa (or 100 psig). The displaced air is allowed to escape through vents to avoid dry spots. Cure cycle is dependent on part thickness, type of resin system and the temperature of the mold and resin system. The part cures in the mold, normally heated by controller, and is ready for its removal from the mold when sufficient green strength is attained.

Resin Transfer Molding is a manufacturing process for composites that has the potential to fabricate complex net shape load bearing structures. However, to make this manufacturing cost-effective, one must abandon trial and error type of approach and resort to science base approach. In the past three years we have shown the usefulness of the modeling and simulation of this process in prediction of the flow and processing parameters for a given mold geometry and injection locations.

The critical issues that we have addressed are discussed below. The eventual goal to incorporate them in a model and help develop simulations such as LIMS and DRAPER has been achieved. These simulations are being utilized by ARL at Aberdeen, MD and TACOM and does allow one to practice virtual manufacturing in real time and hence serve as a learning tool for process engineers and in addition can be used to design the tooling for mold fabrication.

Temperature Solution for Mold Filling Simulation

In many cases, the isothermal simulation of mold filling has proven sufficient for practical applications. However, in some cases we need to incorporate temperature into the solution since it influences some of the flow parameters, namely the resin viscosity. The other factor which might influence the flow is the degree of cure within the part.

The temperature solver and cure model were incorporated into LIMS program. This required certain modifications to solution procedures. The flow is modeled as two dimensional flow. This is possible because of the typical geometry of the part. Due to importance of the heat conduction in the normal direction, the energy equation has to be solved in 3-D. The operator splitting scheme was used to obtain the 3-D temperature solution. This approach takes advantage of the fact that the advection is only important in the plane of flow and conduction is important only in the thickness direction. The method offers better stability than previously used schemes, which allows for larger time steps to accelerate the calculation. The approach is described in [1].

The stability of the temperature solver remains, however, conditional. Occasional problems motivated us to perform the stability analysis of the algorithm used for the simulation. Sufficient

condition for stable behavior was established and improvements of stability due to operator splitting were confirmed. Details of the analysis are given in Appendix A

Manufacturing Considerations

The realistic simulation requires modeling of the tools and processes available in industrial practice. To provide these tools, several features were explored and added to the simulation procedures.[2]

First of these is the ability to simulate in-mold sensors and filling gates. It allows opening/closing of injection ports dependent on the flowfront position within the mold. This approach is used to optimize mold filling time or to reduce injection pressure required.

Second feature is accounting for the presence of vents. With vent locations specified, the simulation can be used to predict the changes in pressure distribution and mold filling pattern if the resin front is not directly connected to vents. Third feature is closely connected to the second one. It allows prediction of dry spot formation. The simulation code checks if air is trapped in the mold and keeps track of these trapped air pockets.

The combination of these improvements enhances the ability of the code as a designing tool that allows to detect possible flaws and correct them prior to the prototype manufacturing.

Inflatable Molds

The use of inflatable mold in resin transfer molding is aimed at overcoming issues associated with non-uniform compaction in rigid molds. These are poor permeability in densely packed areas and racetracking effects in the areas of low fiber density — corners etc.

Resin transfer mold with flexible walls is made up of one rigid tool and one flexible matched half. The flexible part is capable of inflating or deflating depending on the process

requirements. The pressure can be changed with time, allowing for example to increase the compaction during the consolidation stage.

The model of the resin transfer molding with inflatable mold was presented [3]. This model allows one to change the permeability, porosity and preform thickness depending on the pressure within mold and predicts pressures and flow fronts within the mold. Simulations were conducted that suggest that the using of inflatable mold can speed mold filling and reduce the required injection pressure.

Fabric Deformation During Draping of Mold

Preform permeability plays an important part in the physics of the mold filling process. This permeability is a function of fiber tow and mat geometry. Considerable effort was given to measure the permeability of fiber preforms in simple conditions. However, in the process of placing the flat workpiece into a contact with three-dimensional tooling the structure of the fabric deforms, often to a considerable degree. The implications of this fact are discussed in [4].

To handle this deformation, a draping simulation program DRAPER has been developed. The program allows to drape a tool surface and predict the changes in fabric geometry. These changes were accounted for and filling simulation was run for both altered and unaltered cases. They showed a considerable difference in the flow field within the mold and the inlet pressure was an order of magnitude different for the altered case [4].

The geometry provided by the program compares successfully with experimental data. The results of this comparison are provided in Appendix B.

The actual situation during draping is a bit more complex. The fabric deformation is limited. The penalty for exceeding the limits is wrinkled preform. Also, some deformed geometry might be preferable to others. If a draping simulation is to be used as a useful design tool, it has to allow for the above mentioned limits and provide ways to optimize the draping process. This problem has been analyzed in [5].

In relation with this analysis a new code is being written. This code contains hooks necessary to support the features mentioned above. The output can interface with LIMS and generate a proper permeability data, once the model for permeability is known.

Integration and Verification

An indepth study was undertaken to verify the simulations developed to account for preform draping in RTM. Three stages are required in the full process, including; prediction of preform deformation using DRAPER, calculation of local permeability tensors using DRAPER results, and filling simulations using LIMS. A mold was constructed to provide a complex tool surface, requiring the preform to undergo significant deformation during draping. The mold cavity is a thin shelled cone, with hemispherical nose. Pieces were manufactured with this mold, the aim being to analyze the resulting deformation, investigate local fiber volume fraction variation, and to compare these results with predictions given by DRAPER. This phase of the work is underway.

Utilizing a transparent female mold piece, a number of flow visualization experiments were performed with flow front progression being recorded to video tape, and injection pressures being logged with time. Flow simulations were preformed incorporating the draping and permeability prediction results. Comparison with the experimental results strongly suggests that further effort is required in the area of local permeability calculation. The flow visualization program, and simulation results are presented in [6].

An Extensive Flow Visualization Study; The Box Mold

An experimental study was completed in a mold providing a moderately complex thin-shelled cavity. Many experiments were completed, with the main goal of the study being to develop a library of flow visualization experimental data for comparison with the various RTM

mold filling simulations that have been developed. This work has also served as an introductory study into the effect known as 'racetracking' (further discussed in the following section), and provided insight into large scale void entrapment (discussed in [2]).

The mold cavity shape studied was a 'five sided box', with a base and four side walls. The mold was constructed with a transparent acrylic female tool, allowing the progression of the fluid injected into the box to be recorded to video tape, and later transferred to digital movies. Injection pressures were also logged as the mold was filled. The mold was constructed with a variety of possible injection points, pressure measurement sites, and air venting locations. This provided a wide range of possible injection schemes to be investigated, and a final total of 46 experiments were completed. This study is detailed fully in [7], some results also appear in [2].

'Racetracking' Study

Racetracking describes a common phenomenon that is encountered during the mold filling stage of RTM. The effect is due to air channels, or areas of abnormally high porosity in the preform. These high porosity regions provide paths of lower resistance to flow, and cause significant amounts of preferential flow in these portions of a mold cavity. This can lead to large unpredictable deformations of the fluid flow front, possibly creating large scale dry spots, rendering the finished part a failure. The common practice is to eliminate racetracking wherever possible, ensuring predictable mold filling. This is not always easy, and will require very careful design of the mold tool.

Air channels, and other high porosity materials, have also been used to produce better mold filling processes. Predetermined channels, or layers of high porosity material, are being used to distribute resin within a mold cavity more efficiently. With intelligent use, either injection pressures or mold filling times can be significantly reduced.

A simple method is required that will allow existing filling simulations (such as LIMS) to model racetracking. By comparing experimental flow visualization results from the box study with filling simulations of the same experiments, a simple method that has been used in the past

was verified. In this approach, elements representing air channels in a finite element mesh are assigned higher permeability values. The permeabilities that are assigned to such elements, are a function of the geometry of the actual channel, and properties of the adjacent preform material. A method was developed to measure such 'channel permeabilities' experimentally for a simple flow. Channel permeabilities were measured for a random mat fiberglass preform at three different volume fractions, and a variety of channel sizes. Such data is proving to be valuable in attempts to predict channel permeabilities analytically. The details of the experimental program, and results, are presented in [8]

Future Work

The most important issues to be solved now are associated with preforming, which means draping of the mold surface and closing the tool. This phase of the RTM process is insufficiently known and should be researched both experimentally and by analytic modeling. We cannot really model the filling process unless we have a sufficiently accurate input data. These can be only provided with knowledge of the preforming stages of RTM.

The most important issue in this group is the conversion of preform geometry data — regardless whether obtained by observation or draping models — into a reliable estimate of permeability. The values provided by currently used models fail to compare reasonably with the experimental data. Creating a manageable permeability model based on the reinforcement geometry is thus a very important task.

The handling of racetracking is an integral part of the permeability description. Initial work into analytical prediction of channel permeabilities is promising. When the geometry of an air channel is well known, e.g. when channels are used as a distribution network, analytical expressions can be derived from steady state solutions of fully developed Stoke's flow. A second type of racetracking needs to be studied, in which the geometry of an air channel may be unknown, e.g. when racetracking is unintentional. Racetracking can occur in this form when an

actual air channel is not physically present, and may be due to changes in the microstructure of a preform at the boundaries of the mold cavity.

The second problem we need to address is the compaction of preform during the closure of mold, briefly touched in [3]. This not only affects the permeability and thus the manufacturing but also influences the final product's mechanical properties. We feel strongly that compaction has to be modeled together with draping and permeability models if the predictive capabilities of the filling models are to improve.

The draping issue is far from being treated sufficiently. The development of the code should continue and really examine the optimization possibilities described in [5]. This requires some fundamental answers concerning what are viable criteria for optimization and what steps are actually possible to satisfy these criteria. Another question to be examined for the draping is the repeatability of this, usually manual, process.

There are some steps to be taken in the simulation of the filling process as well. Additional work should be spent on solving the temperature field and the cure field within the part. Also, the interfacing between the filling simulation and the models of the preforming stage has to be expanded together with the preforming models.

References Included in the Report

[1]   Liu, B. and Advani, S.G., "Operator Splitting Scheme for 3-D Temperature Solution Based on 2-D Flow Approximation," in *Computational Mechanics*, 16, 1995, pp. 1 - 9

[2]   Liu, B., Bickerton, S. and Advani, S.G., "Modeling and Simulation of Resin Transfer Molding (RTM) — Gate Control, Venting and Dry Spot Prediction," to appear in *Composites Manufacturing*

[3]   Lee Fong, L. and Advani, S.G., *"Modeling and Simulation of Composite Fabrication with Inflatable Molds,"* included report

[4]   Lee Fong, L., Advani, S.G. and Fickie, K., *"The Role of Drapability of Fiber Preforms in Resin Transfer Molding,"* included report

[5]   Simacek, P. and Advani, S.G., *"The Simulation of Draping Process,"* included report

[6]   Bickerton, S., Advani, S.G., Fickie, K. and Fong, L., *"Effects of Draping of Fiber Preforms on Process Parameters During Manufacturing with Resin Transfer Molding,"* included report

[7]   Bickerton, S. and Advani, S.G., *"Experimental Investigation of RTM, within a Box Mold,"* included report

[8]   Bickerton, S. and Advani, S.G., *"Characterization of Corner and Edge Permeabilities During Mold Filling in Resin Transfer Molding,"* included report

APPENDIX A : STABILITY ESTIMATE FOR LIMS TEMPERATURE SOLVER

Analysis

The temperature solver as implemented in LIMS version 3.3. suffers from occasional breakdown and abnormal termination due to the floating point overflow. The problem can be traced down to the temperature solver. More importantly, the problem can prevented by respecting a few simple rules derived herein. Note the cause of the problem is the method of solving equation system and not a faulty (unstable) discretization. Nonetheless, similarly to the conditionally stable discretization, the solver poses a limit on time step used within the simulation.

The governing energy equation, following Tucker and Dessenberger [1] and utilizing the dimensional analysis provided by Advani, Bruschke and Parnas [2] , is

$$\left(\rho.C_p\right)_{ef} \cdot \frac{\partial T}{\partial t} + \left(\rho.C_p\right)_r \cdot \langle v_f \rangle \cdot \nabla T = k_{ef} \cdot \frac{\partial^2 T}{\partial^2 z} + Source \quad terms \tag{1}$$

The effective heat capacity can be evaluated from constituent properties using the porosity as

$$\left(\rho.c_p\right)_{ef} = \varepsilon \cdot \left(\rho.c_p\right)_r + \left(1 - \varepsilon\right) \cdot \left(\rho.c_p\right)_f \tag{2}$$

and the temperature gradient is just a two dimensional vector within the plane of the preform, i.e.,

$$\nabla T = \begin{pmatrix} \dfrac{\partial T}{\partial x} \\ \dfrac{\partial T}{\partial y} \end{pmatrix} \tag{3}$$

The 'Source terms' include the effects of reaction, viscous dissipation and heat dissipation due to two phase system. From the practical point of view the second term is negligible [2] and the third term is neglected as well, because of insufficient data. This leaves the reaction heat as

the only source and — in most practical cases — this term is small. In the following we will assume the source term being 0 unless stated otherwise.

Note that the equation (1) is valid only in the case that the flow is fully saturated. Otherwise, the first term in (1) has to be replaced by

$$\frac{\partial}{\partial t} \cdot \left((\rho \cdot c_p)_{ef} \cdot T \right) \tag{4}$$

and (2) has to account for degree of filling Φ

$$(\rho \cdot c_p)_{ef} = \Phi \cdot \varepsilon \cdot (\rho \cdot c_p)_r + (1 - \varepsilon) \cdot (\rho \cdot c_p)_f \tag{5}$$

To simplify the problem we will assume that we are solving for the saturated flow only. This means we are not interested in the situation close to the flowfront.

The solution of the problem within LIMS program utilizes finite difference scheme in time and transverse direction z and the control volume/ finite element method in the plane of preform (x-y). The geometry of the problem is shown in Figure 1.

To apply the control volume method in x-y we need to integrate (1) over the planar area of the control volume A_i. Using integration per partes we can obtain

$$\int_{A_i} (\rho \cdot c_p)_{ef} \cdot \frac{\partial T}{\partial t} \cdot dA_i + \int_{S_i} (\rho \cdot c_p)_r \cdot T \cdot \left(\langle v_f \rangle \cdot \boldsymbol{n} \right) \cdot dS_i = \int_{A_i} k_{ef} \cdot \frac{\partial^2 T}{\partial z^2} \cdot dA_i + \int_{A_i} Source \tag{6}$$

The time and transverse (z) discretization by FDM is

$$\left(\frac{\partial T}{\partial t} \right)_{i,n}^{k-1+\theta} = \frac{T_{i,n}^k - T_{i,n}^{k-1}}{\Delta t} \tag{7}$$

and

$$\left(\frac{\partial^2 T}{\partial z^2}\right)_{i,n}^{k-1+\theta} = \theta \cdot \frac{T_{i,n+1}^k - 2 \cdot T_{i,n}^k + T_{i,n-1}^k}{\Delta z^2} + (1-\theta) \cdot \frac{T_{i,n+1}^{k+1} - 2 \cdot T_{i,n}^{k+1} + T_{i,n-1}^{k+1}}{\Delta z^2} \qquad (8)$$

where index i changes with control volume (node of FEM mesh), n with the temperature node and k with the time step. Additionally, we assume that thermal nodes are spaced equally, i.e., h_i terms in Figure 1 are all equal to Δz. Θ can take values between 0 and 1 and decides whether we are dealing with explicit ($\Theta=0$), fully implicit ($\Theta=1$) or other scheme. The acceptable value for Θ is given by the stability requirements of discretization scheme. This necessity arises in order to prevent error magnification from one time substep to another.

The second term in equation (6) stands for convection and can be discretized, assuming that the flow field (flows from element i to element j q_{ij})is known, as

$$\int_{S_i} (\rho \cdot c_p)_r \cdot T \cdot \left(\langle v_f \rangle \cdot v \right) \cdot dS_i = -\sum_{j=Neightbours} (\rho \cdot c_p)_r \cdot T_{j,n}^k \cdot q_{ij} \cdot \frac{1}{h} \qquad (9)$$

where the temperature in volume i drops out, as the flows for saturated flow sum to 0. To accommodate implicit or Crank-Nicholson scheme we can express (9) using Θ as

$$\frac{1}{h} \cdot \left(-\theta \cdot \sum_j (\rho \cdot c_p)_r \cdot T_{j,n}^k \cdot q_{ij}^k + (\theta - 1) \sum_j (\rho \cdot c_p)_r \cdot T_{j,n_{k-1}} \cdot q_{ij}^{k-1} \right) \qquad (10)$$

Note that in LIMS the flows will not depend on time, i.e., the index k. If we were interested in non-saturated flows, there would be additional terms in (10) which disappear only on condition of

$$\sum_j (\rho \cdot c_p)_r \cdot q_{ij} = 0 \tag{11}$$

The previous discretization leads to the equation

$$\frac{A_i (\rho \cdot c_p)_{ef}}{\Delta t} \cdot T_{i,n}^k + \theta \cdot \frac{1}{h} \cdot \sum_j (\rho \cdot c_p)_r \cdot q_{ij}^k \cdot \left(T_{i,n}^k - T_{j,n}^k \right) - \frac{\theta \cdot A_i \cdot k_{ef}}{\Delta z^2} \cdot \left(T_{i,n+1}^k - 2 \cdot T_{i,n}^k + T_{i,n-1}^k \right) =$$

$$= A_i \cdot Source\left(T_{i,n}^{k-1} \right) + \frac{A_i (\rho \cdot c_p)_{ef}}{\Delta t} \cdot T_{i,n}^{k-1} - (1-\theta) \cdot \frac{1}{h} \cdot \sum_j (\rho c_p)_r \cdot q_{ij}^{k-1} \cdot \left(T_{i,n}^{k-1} - T_{j,n}^{k-1} \right) + \tag{12}$$

$$+ \frac{(1-\theta) A_i \cdot k_{ef}}{\Delta z^2} \left(T_{i,n+1_{k-1}} - 2 \cdot T_{i,n}^{k-1} + T_{i,n-1}^{k-1} \right)$$

which allows solving the temperature field at time k from the known flow state and temperature field at time k-1.

The evaluation of the Source term should be also carried at time

$$t^{\theta} = t^{k-1} + \theta \cdot \Delta t \tag{13}$$

, respective it should be approximated by

$$Source\left(t^{\theta} \right) \cong \theta \cdot Source\left(t^k \right) + (1-\theta) \cdot Source\left(t^{k-1} \right) \tag{14}$$

but this is neither used within LIMS nor important given the negligible size of this term

Iterative solution of the system

The size of the system and the two-dimensional flow solution necessitates the use of iterative solver for the temperature sub-stepping. In this section we first look at sufficient condition for stable iterative solution of (12) and then examine the operator splitting and its influence on the solution process.

The iterative solution scheme solves system

by converting it into

$$K.x = F \tag{15}$$

$$x^{(i+1)} = A.x^{(i)} + b \tag{16}$$

, selecting the value $x^{(0)}$ and iterating until the value of x stops changing. For example, for Jacobi iteration

$$K = L + U + L$$

$$A = -D^{-1}(U + L) \tag{17}$$

$$b = D^{-1}.F$$

Obviously, this scheme will work only if the spectral radius of A is smaller than 1. Otherwise the error will increase with each step unless the initial guess is orthogonal to eigenvectors of A with eigenvalues bigger than 1. It can be easily demonstrated by assuming

$$x^{(i)} = x + e^{(i)} \tag{18}$$

which trivially leads to

$$e^{(i+1)} = A.e^{(i)} \tag{19}$$

and with repeated iterations the ratio of $e^{(i+1)}$ over $e^{(i)}$ will go to the largest (in magnitude) eigenvalue of A.

For the stability of simple iterative solver (such as Jacobi iteration) it is sufficient if the system matrix is diagonally dominant. In such a case the spectral radius of the matrix A is smaller than 1 and the solution will converge. Opposite is not necessarily true for some iterative schemes.

This condition of diagonal dominance can be easily applied to the system (12). It will require that

or

$$\frac{A_i \cdot (\rho \cdot c_p)_{ef}}{\Delta t} > \frac{\theta}{h} \cdot \sum_j (\rho \cdot c_p)_r \cdot \left| q_{ij}^k \right| \tag{20}$$

$$\frac{(\rho \cdot c_p)_{ef}}{(\rho \cdot c_p)_r} \cdot \frac{V_i}{\sum_j \Delta t \cdot \left| q_{ij}^k \right|} > \theta \tag{21}$$

We will postpone the discussion of this result for later. Lets just note that we have shown that, if an iterative solution is to be used, there is a condition that binds time step and Θ, different from the one obtained from the usual analysis of time stepping. The difference is that (21) is a condition to prevent growth of the error *within* a solution for a given time step, while the other [3] prevents accumulation of the error while marching through time.

Next question is an operator splitting scheme. This generally works by replacing (16) by a series of steps

$$x^{(i,1)} = A_1 \cdot x^{(i-1)} + b_1$$

$$x^{(i,2)} = A_2 \cdot x^{(i,1)} + b_2$$

$$\tag{22}$$

$$x^{(i)} = A_n \cdot x^{(i,n-1)} + b_n$$

where individual A_i matrices can actually represent a closed form solution of system of equations. This will lead to the scheme

$$x^{(i)} = \prod_{j=1}^n A_j \cdot x^{(i-1)} + \prod_{j=2}^n A_j \cdot b_1 + \quad \dots \quad + b_n \tag{23}$$

which is an ordinary iterative scheme. Consequently, to confine the error, we need

$$\rho \left(\prod_{j=1}^n A_j \right) \leq 1 \tag{24}$$

This can be easily replaced by weaker sufficient condition since the spectral radius of product has to be bounded by the product of spectral radiuses.

$$\rho(A_j) < 1 \tag{25}$$

Application to LIMS

Armed with (21), (24) and (25) we can analyze the LIMS 3.3 code temperature solver. It really uses three steps. In the first step, the convection is accounted for:

$$\dot{T}^{k,(n)}{}_i = T^{k-1}{}_i + \frac{\Delta t.(\rho.c_p)_r}{V_i.(\rho.c_p)_{ef}} \cdot \sum_j q_{ij}\left(\dot{T}^{k,(n-1)}{}_j - \dot{T}^{k,(n-1)}{}_i\right) \tag{26}$$

This is similar to the equation (12) solved by fully implicit ($\Theta=1$) scheme by Jacobi iteration. The difference are missing conduction and source terms, but these do not affect the condition (21). The spectral radius of the first step is thus limited by

$$\rho(A_1) < \max_i\left(\frac{(\rho.c_p)_r}{(\rho.c_p)_{ef}} \cdot \frac{\Delta t.\sum_j |q_{ij}|}{V_i}\right) \tag{27}$$

The second step takes care of the source term, being

$$\ddot{T}^{k,(n)}{}_i = \dot{T}^{k,(n)}{}_i + Source\left(\dot{T}^{k,(n)}{}_i\right) \tag{28}$$

if the source term is zero, this step is linear and the spectral radius of its matrix is

$$\rho(A_2) = 1 \tag{29}$$

If there is a heat generation, the analysis becomes more complex. For the cases of interest the generation is, however, small. Thus, we will assume that this step does not influence the stability of the solution.

Last step takes care about the conduction term in z direction and actually uses closed form solution from the form

$$\left(1 + 2 \cdot \frac{\alpha_{ef} \Delta t}{\Delta z^2}\right) T^{k,(n)}{}_i - \frac{\alpha_{ef} \Delta t}{\Delta z^2} \cdot \left(T^{k-1,(n)}{}_i + T^{k+1,(n)}{}_i\right) = \ddot{T}^{k,(n)}{}_i \tag{30}$$

Nonetheless, this can be easily transformed into a form corresponding to (22) by a simple matrix inversion. Moreover, we can solve for the eigenvalues of the matrix A_3 directly, since we know [3] eigenvalues of A_i^{-1}. These are described by

$$\lambda_n(A_3) = \frac{1}{\lambda_n(A_3^{-1})} = \frac{1}{1 + 2 \cdot \frac{\alpha_{ef} \Delta t}{\Delta z^2} \cdot \left(1 + \cos\left(\frac{2.n.\pi}{M+1}\right)\right)} \tag{31}$$

where M is the order of the matrix (number of temperature nodes) and n goes from 1 to M. The largest eigenvalue will thus be

$$\rho(A_3) = \frac{1}{1 + 2 \cdot \frac{\alpha_{ef} \Delta t}{\Delta z^2} \cdot \left(1 + \cos\left(\frac{2.M.\pi}{M+1}\right)\right)} \tag{32}$$

Since we assumed equidistant temperature nodes this can be expressed as

$$\rho(A_3) = \frac{1}{1 + \frac{2.\alpha_{ef} \Delta t}{h^2} \cdot (M-1)^2 \cdot \left(1 + \cos\left(\frac{M.\pi}{M+1}\right)\right)} \tag{33}$$

Note that (33) is always less than 1. Actually, if M grows the spectral radius will converge to some value smaller than 1.

Conclusions

The LIMS temperature solver was shown to be conditionally stable and little can be done to defy this fact, as the structure of the program requires an iterative solver. There are two

reasons for this. First, some of the terms in the governing equation are generally non-linear. Second, the CPU requirements are considerably lower for the current 2.5-dimensional structure.

The stability of the solution process can be — assuming negligible heat generation — guaranteed if the following holds:

$$1 > \left(\frac{1}{1 + \frac{2.\alpha_{ef}\Delta t}{h^2} \cdot (M-1)^2 \cdot \left(1 + \cos\left(\frac{M.\pi}{M+1}\right)\right)} \right) \cdot \max_i \left(\frac{(\rho.c_p)_r}{(\rho.c_p)_{ef}} \cdot \frac{\Delta t.\sum_j |q_{ij}|}{V_i} \right) > \rho(A_3).\rho(A_1) \quad (34)$$

i.e., the spectral radius of the iteration matrix is less than 1. The only parameter we can vary to satisfy (34) is the size of time substep Δt which can be always made small enough to prevent any problems. This may unfortunately increase the CPU requirements.

The second possibility is to adjust the meshing process. The number of temperature nodes through the thickness does not influence the stability too much (33). The in-plane discretization, however, influences the stability of the first substep (27). This condition basically says that the fluid volume flowing through any control volume within a time substep must not exceed the size of control volume. The ratio of heat capacities just converts this demand to requirement that the heat flow due to convection not exceeding the 'heat inertia' of the control volume. This means that (27) will require larger time substep if elongated elements are oriented along the flow than if they are oriented transverse to it.

Within the LIMS the number of time substeps within the single flow step is specified. Thus we do not have direct control over the substep magnitude, as the flow step size is automatically adjusted to fill consequent control volume. If we label the number of substeps by N we have

$$\Delta t = \frac{1}{N} \cdot \frac{V_l}{\sum_j q_{lj}} \quad (35)$$

Substituting this to (27) we can realize that, since the flow field is given, factor we can influence is of type

$$\max_i\left(\frac{1}{N}\cdot\frac{V_l}{V_i}\right) \tag{36}$$

where i goes over all volumes and V_l is the volume currently being filled. Since there is a single value of N for all steps, the lowest possible N will correspond to all elements being of similar size.

Recommendations

The steps user can undertake to avoid overflow problems during solution:

*   Set the time step so that the (34) is satisfied. Since the user sets number of sub-steps, this means increasing this value till the problem disappears.

*   Avoid unnecessary mesh refinement. Well refined mesh around inlets produces most trouble, since these volumes have the highest flow through.

The steps maintenance programmers of LIMS should take

*   Change the substepping scheme to reflect the size of a real time step. The number of substeps should be based on the actual size of the flow step and the allowable size of substep.

*   Since the flow field is needed to evaluate the conditions in (34), adaptive selection of time substep should be attempted.

References

[1]   Tucker, C.L. and Dessenberger, R.B., "Governing Equations for Flow and Heat Transfer in Stationary Fiber Beds," in *Flow and Rheology in Polymer Composites Manufacturing*, edited by S.G. Advani, Elsevier, 1994

[2]   Advani, S.G., Bruschke, M.V. and Parnas R.S., "Resin Transfer Molding Flow Phenomena in Polymeric Composites," in *Flow and Rheology in Polymer Composites Manufacturing*, edited by S.G. Advani, Elsevier, 1994

[3]   Greenberg, M.D., "*Advanced Engineering Mathematics*," Prentice-Hall, 1988
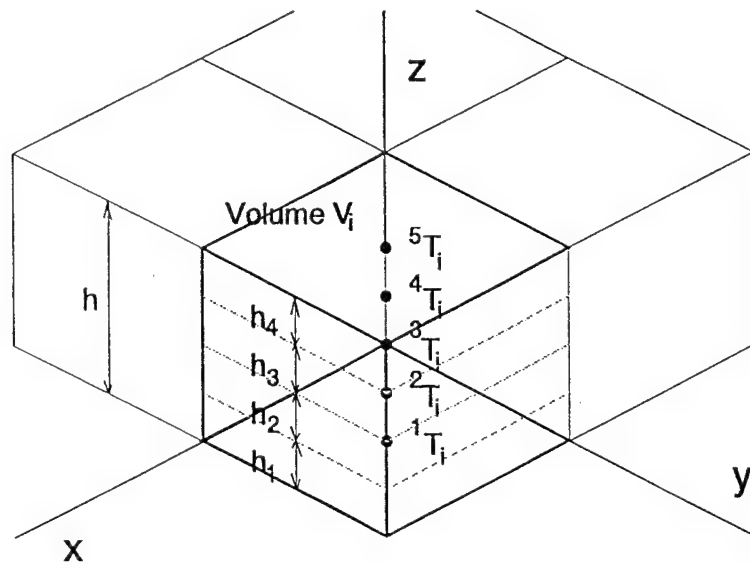
Figure 1

APPENDIX B : VERIFICATION OF DRAPING SIMULATION

ABSTRACT

The issue of draping fiber mats over complex surfaces is very important to the process of resin transfer molding. When a mat is draped over a surface, the fiber volume fraction changes in local areas and may become so great as to prevent proper resin flow into those areas. The mat may wrinkle or bridge causing adverse effects to the piece. The DRAPER computer simulation attempts to predict the behavior of the mat when it is draped on any surface. In an attempt to qualitatively determine the accuracy of DRAPER, a dome is draped, then digitized and the coordinates plotted. The resulting plot is then compared with DRAPER's output.

INTRODUCTION

The issue of draping fiber mats over complex surfaces is very important to the process of resin transfer molding. When a mat is draped over a surface, the fiber volume fraction changes in local areas and may become so great as to prevent proper resin flow into those areas. The mat may wrinkle or bridge causing adverse effects to the piece. The DRAPER computer simulation attempts to predict the behavior of the mat when it is draped on any surface.

In order to qualitatively determine the ability of draper to predict the warp and weft yarn paths, one hemisphere of a sphere was draped with a bi-directional fiberglass mat. A grid was drawn on the mat corresponding to every other warp and weft yarn. The grid point locations were determined on one quarter of the hemisphere in 3-D space with x, y, z coordinates.

Using I-DEAS the coordinates were then plotted forming a mesh. Next, the outer warp and weft path coordinates were used as constraint paths and input into DRAPER. DRAPER generated the mesh using these coordinates and the two meshes were compared.

PROCEDURE

I. Placing Grid on Mats

The grid was placed on the mats in two ways. When using bi-directional fabric it is easy to draw grid lines by hand directly on the warp and weft yarns with a magic marker. However, this is very tedious, requiring about forty-five minutes to an hour to draw the grid on a two foot by two foot mat. The advantage of drawing the grid directly onto the yarns is that the grid will deform exactly as the mat does giving better results.

The other method of placing a grid on the mats employed the use off a silk screen. A silk screen of the grid was made and using fabric paints the grid was 'printed' on the mat. While this method is much quicker it has some problems associated with it. The fabric paint tends to bleed into the mat causing blurred grid lines. This can be controlled by thickening the paint. However, if the paint is made too thick it will not flow through the silk screen. When using a woven mat, this may be the only way to print a grid as it is impossible to follow an individual yarn by hand.

II. Draping the Mat

Once the grid is printed the mat is draped. The mat is placed on the draping table and saturated with polyeurathane. The top half of the table is then clamped down over the mat using C clamps. Next, the sphere is pushed through the hole in the table using a firm but steady force until the equator is even with the top of the table. The sphere must not be allowed to rotate as it is being inserted or the warp and weft yarns will be skewed.

The polyeurathane is then allowed to cure for two to three days. The piece is then removed from the table. It is still quite rubbery at this point and must cure for a couple of more days to be completely dry. Once completely dry, the piece is ready to be digitized.

III. Digitizing the Dome

The dome was digitized using a Bridgeport CNC milling machine. The coordinates were determined in 3-D space with x, y and z axes. A pointer was fabricated and attached to the machine. The pointer was manually moved to each grid point location taking top center of the dome as point 0, 0, 0. This is excruciatingly tedious requiring eighteen hours to digitize one quarter of the globe. However, this was the most accurate method readily available at the time.

IV. Plotting Grid Points

The hand written data were entered into a spreadsheet and then converted to the universal format. The grid point were plotted using I-DEAS.

V. Plotting with DRAPER

Using the outer warp and weft yarn paths from the dome as constraint paths, DRAPER generated the mat on the surface of the sphere. The results were then observed to determine, qualitatively, the ability of DRAPER to predict the mat deformation.

APPARATUS

Draping Table

In order to try to allow uniform draping from one mat to another a "draping table" was constructed (Figure 1). The Table consists of two flat halves with a hole equal to the diameter of the sphere cut out of them. The fabric is sandwiched between the halves which are secured with C clamps. This gives uniform tension on the mat as the sphere is being inserted. The table

was fabricated from one 4'x8' sheet of 1/2' plywood with formica laminated to one side with contact cement.
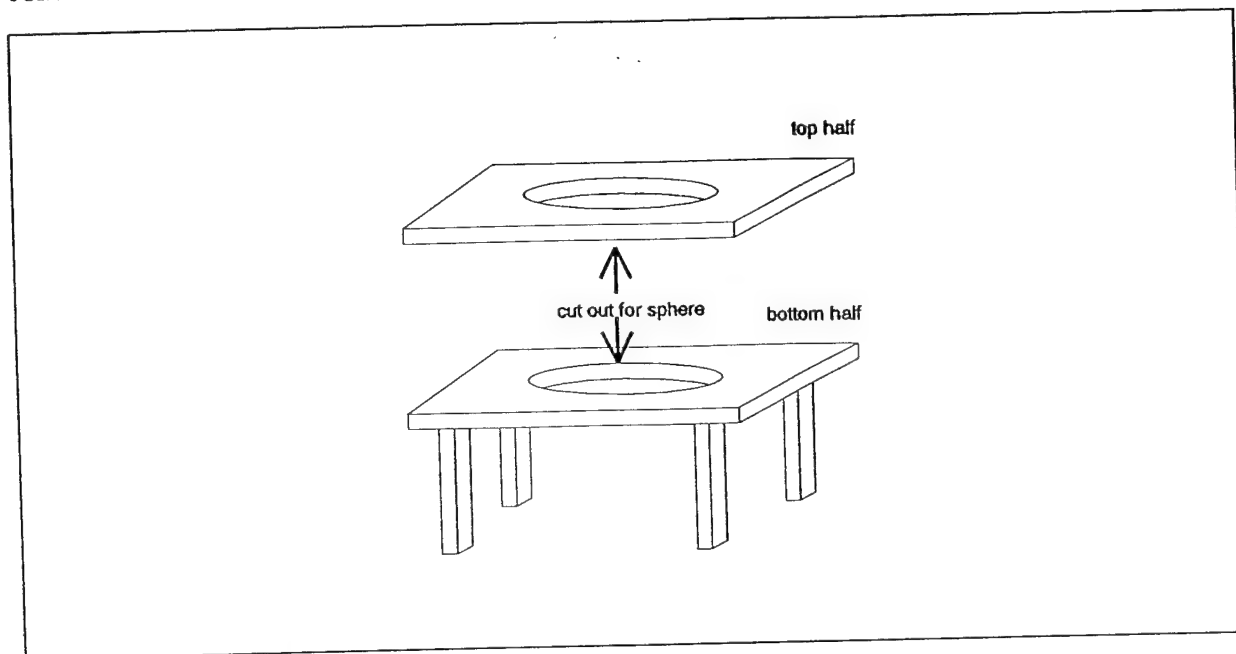
Figure 1.: Draping Table

The sheet of plywood was then cut in half. A hole of 12" diameter was cut out of the center of each half to allow the sphere to be inserted. A 12" diameter globe was used as the sphere.

RESULTS

Appendix 1 contains the experimental results and the results of DRAPER. By observation, it is seen that the two are in close agreement over the sphere. On the flange there is some difference. The simulation appears to be wrinkled or uneven. This is due to the fact that there is 90 degree edge where the flange meets the dome. Geometries used in DRAPER mast have radiused edges. Furthermore, the arc length of the radius must be longer than the distance between yarns. It was not feasible to create a grid so small that the distance between grid lines was shorter than that of the edge radius.

Other differences arise from the fact that DRAPER assumes no slippage along warp and weft yarns. This assumes a constant distance between yarns. However, slippage does occur in reality and the distance between yarn varies. The amount of slippage that occurs depends on the type of mat used, the amount of deformation required to drape the surface, the manner in which the mat is draped, and many other factors.

If further experiments of this type are to be performed, a more efficient method of digitizing the grid points must be found. Perhaps a Coordinate Measuring Machine could be employed or stereo image analysis used. The accuracy of experiment would be greatly improved. A lot of human error occurs when spending eighteen hours measuring grid coordinates and then transcribing those into a computer.

The accuracy could also be improved by building a better draping apparatus. If the sphere rotates as it is being inserted into the table the warp and weft yarns are distorted causing "wavy" gridlines. This could be eliminated by building a device which inserts the sphere instead of doing it by hand.

Although DRAPER assumes ideal conditions, it can be seen that it closely approximates the actual draping of a fiberglass mat over a sphere. By carefully controlling the draping process, improving methods of data acquisition, and creating a finer grid, the comparison between the two could be improved.
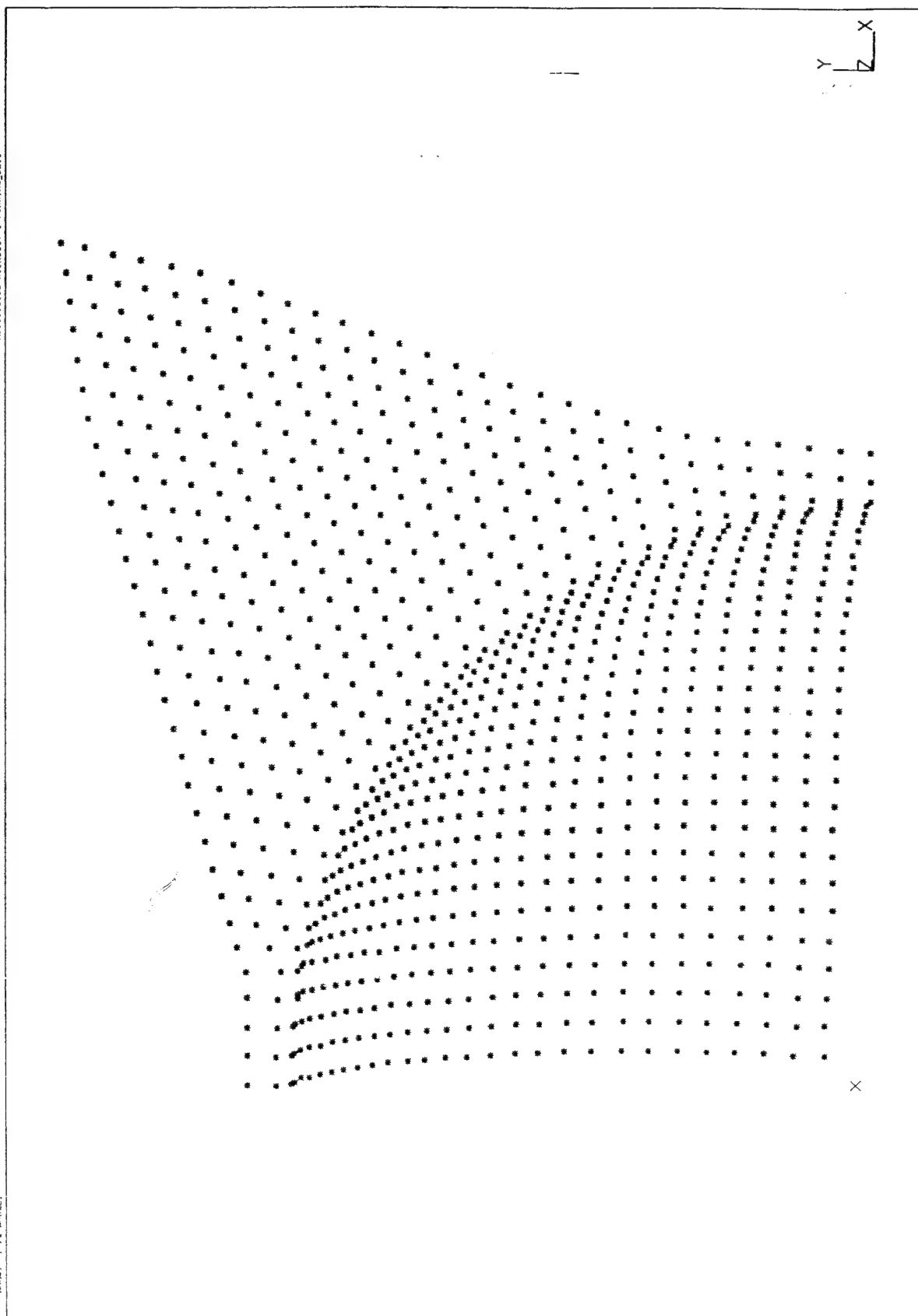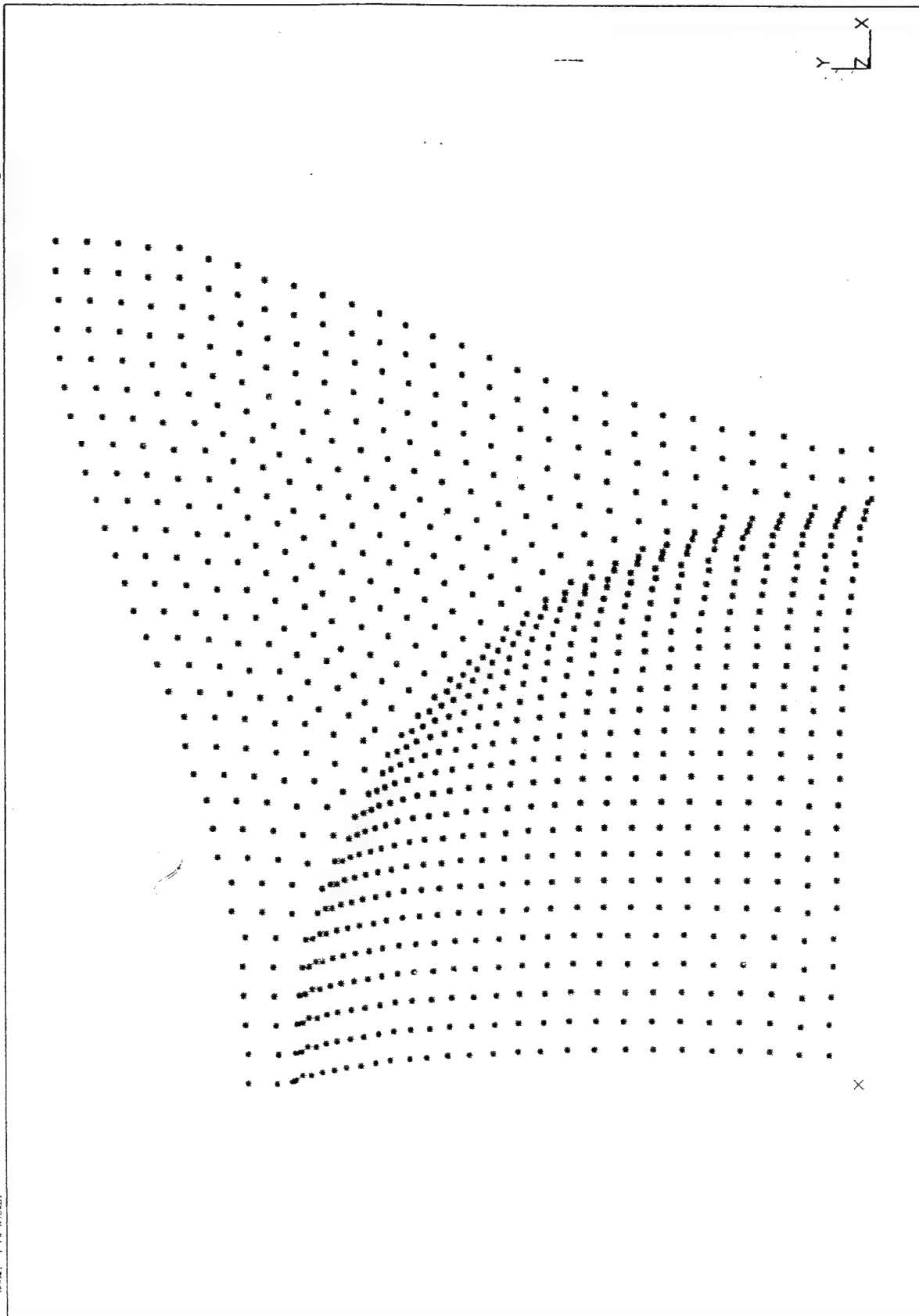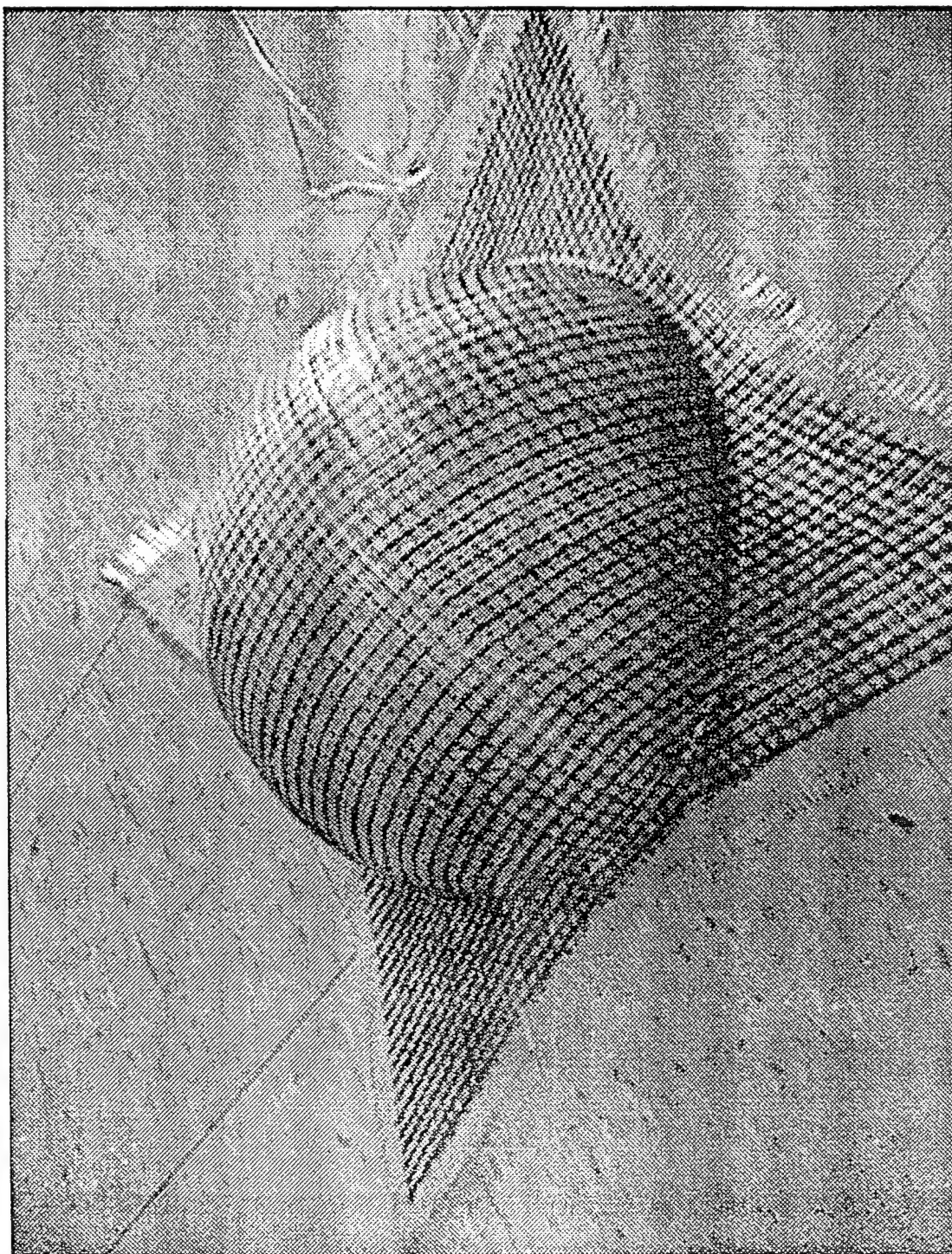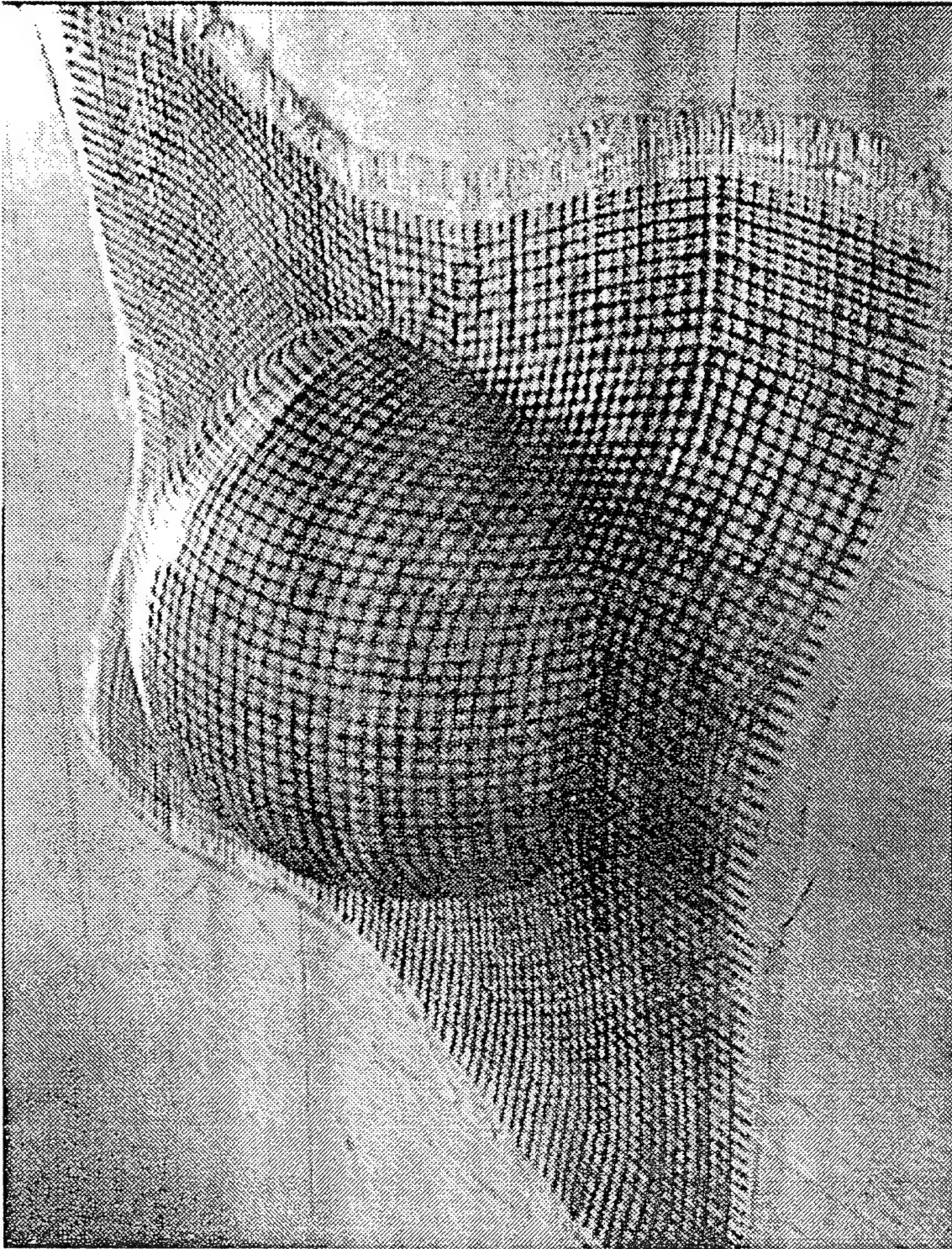
APPENDIX C : LIST OF PRESENTATIONS AND PUBLICATIONS

Presentations

(1)   S.G. Advani, Lihwa Fong and Ram Varma, "*Use of Process Simulation as Design Tools in Molding of Composites,*" Keynote Speaker, Computer Aided Design and Manufacturing Polymer Processing and Rheology Society ,Sept. 29, 1994, Kyoto, Japan

(2)   Wei Zhang and Suresh G. Advani , "*Heat Dispersion in Anisotropic Porous Media,*" ASME Winter Annual Meeting, Chicago, Nov. (1994).

(3)   Ram Varma and Suresh G. Advani, "*Three Dimensional Fillings of Resin Transfer Molding,*" ASME Winter Annual Meeting, Chicago, Nov. (1994).

(4)   Lihwa Fong and S.G. Advani, "*The Role of Drapability of Fiber Preforms in Resin Transfer Molding,*" American Society for Composites, Newark, Sept. (1994).

(5)   Lihwa Fong and Suresh G. Advani, "*The role of Dual Permeability in Mold Filling Simulation of Resin Transfer Molding,*" International Conference on Composites Engineering, New Orleans, August, 1994

(6)   Baichen Liu, Simon Bickerton and Suresh G. Advani, "*Modeling and Simulation of Resin Transfer Molding (RTM)- Venting and Void Formation,*" International Conference on Composites Engineering, New Orleans, August, 1994

(7)   Lihwa Fong, Baichen Liu and Suresh G. Advani, "*Modeling and Simulation of Resin Transfer Molding with Flexible Mold Walls,*" Pociety of Plastic Industry, Cincinnati, Jan. 1995

(8)   Simon Bickerton, Yves Parseval, Kurt Fickie and Suresh G. Advani, "*Role of Local Permeability Variations in Resin Transfer Molding,*" Nineth International Conference on Numerical Methods in Thermal Problems, Atlanta July, 1995

(9)   S. Bickerton and S. G. Advani, "*Characterisation of Corner and Edge Permeabilities During Mold Filling in Resin Transfer Molding,*" ASME Summer Meeting, Los Angeles, 1995

Publications

1. W. Zhang and S. G. Advani, "Heat Dispersion Effects in Stationary Fiber Beds," in *ASME AMD* Vol. 194, pp. 335-352, New York (1994)

2. R. Varma and S. G. Advani, "Three-Dimensional Simulations of Filling in Resin Transfer Molding," in *ASME FED* Vol. 200, pp.21-27, New York (1994).

3. Lihwa Fong and S.G. Advani, "The Role of Drapability of Fiber Preforms in Resin Transfer Molding", in *Proceedings of the 9th American Society for Composites*, p. 1246. (1994)

4. L. Fong and S. G. Advani,"The role of Dual Permeability in Mold Filling Simulation of Resin Transfer Molding," in *Proceedings of the International Conference on Composites Engineering*, p. 301 (1994).

5. B. Liu, S. Bickerton and S. G. Advani, "Modeling and Simulation of RTM - Venting and Void Formation," in *Proceedings of the International Conference on Composites Engineering*, p. 17 (1994)

6. Lihwa Fong, Baichen Liu and Suresh G. Advani, " Modeling and Simulation of Resin Transfer Molding with Flexible Mold Walls," in *Proceedings of the Society of Plastic Industry*, Session 3A pp. 1-5 (1995).

7. S. Bickerton and S. G. Advani,"Characterisation of Corner and Edge Permeabilities During Mold Filling in Resin Transfer Molding," in *Recent Advances in Composite Materials*, MD-Vol 56, pp. 143-151, (1995).

8. Simon Bickerton, Yves Parseval, Kurt Fickie and Suresh G. Advani, "Role of Local Permeability Variations in Resin Transfer Molding," in *Proceedings of the Nineth International Conference on Numerical Methods in Thermal Problems*, Part 2, pp. 1335-1347(1995).

9. D. Liu , S. Bickerton and S. G. Advani, " Modeling and Simulation of RTM:Gate Control, Venting and Dry Spot Prediction" to appear in *Composites Manufacturing* (1995).

10. B. Liu and S. G. Advani, "Operator Splitting Scheme for 3-D Temperature Solution Based on 2-D Flow Approximation, " in *Computational Mechanics*, 38, pp. 74-82(1995).

Modeling and Simulation of Resin Transfer Molding (RTM) -Gate Control, Venting and Dry Spot Prediction

Baichen Liu, Simon Bickerton, and Suresh G. Advani*
Center for Composites Material and
Department of Mechanical Engineering
University of Delaware, Newark, DE 19716

This work presents three simulation features developed in an existing mold filling simulation code for resin transfer molding (RTM) to address the processing issues encountered during manufacturing. They are gate control, venting, and dry spot formation. The first feature is achieved using numerical sensors, which simulate the sensors used in practice to control the process. This feature makes it possible to use the developed simulation code to design a control strategy to optimize mold filling time, or to reduce injection pressure required. The second feature is developed to account for the presence of vents. With vent locations specified, simulation can be used to predict changes in the pressure distribution and mold filling pattern if the resin front is not directly connected to the vent. The third feature provides for the prediction of dry spot formation. The simulation code checks if air is trapped in the mold and keeps track of these trapped air pockets. It computes the location, size, and the pressure of all dry spots formed in the filling process. The combination of these features enhances the ability of the code as a design tool. The gate control and dry spot prediction features can be used in conjunction to guide the design of optimal processing conditions. Controlled resin injection with a strategy is an indispensable way to prevent dry spot formation, and reduce operation costs. Similarly, venting and dry spot prediction can be used to detect possible flaws and to correct them before a prototype mold is constructed

Keywords: mold filling; resin transfer molding; dry spot; process control; simulation

INTRODUCTION

Resin transfer molding (RTM) is a manufacturing process developed in recent years for high performance composite materials, such as structural parts for aircraft and automobiles. A typical RTM process cycle consists of four phases. The first phase is preform manufacturing which produces the fiber reinforcement in the shape of the finished part. The second phase is mold filling during which resin is injected into the cavity of a mold containing the preplaced preform. The third phase is resin curing which may start during or

---

* To whom correspondence should be addressed

after the second phase. The fourth phase is demolding, which occurs after the curing reaction comes to completion and the part solidifies [1]. Figure 1 is a schematic of the second phase of the process, mold filling, which is the focus of this study. It addresses the basic fluid mechanics in a changing domain with a free surface.

The second phase is the core of the process. The injected resin is driven by the injection pressure to saturate the preform. The formulation to describe mold filling is modeled as flow through porous media, and shares the same physics with other problems like those widely studied in the fields of oil recovery.

Because it allows the designer the best possible control over the fiber reinforcement in the final part, RTM has become a preferred method to manufacture structural composite parts. It has also attracted researchers to explore the possibility of simulating the process numerically. Many computer programs have been developed to solve for the pressure, velocity, flow front development and temperature distribution [2-10]. However, most of these codes do not have the ability to predict dry spot formation. Han et al. recently reported a dry spot prediction scheme [10]. However, their study did not show how closely the venting conditions are related to the formation of dry spots.

Gating and venting are very practical design issues in RTM. It is not possible to mold a composite part without at least one gate to inject resin and one vent to let the displaced air out of the mold. Poorly designed gate and vent location can render a part with dry spots (also refereed to as voids, portions of the part that do not contain matrix material). For three dimensional parts, the design of gate and vent location is far from trivial due to the complexity of geometry and anisotropy of flow. In this work, models have been developed to address these issues. These models have been encorporated in LIMS (Liquid Injection Molding Simulation), a simulation developed at the University of Delaware [5,11].

Dry spots, which are regions of the composite part devoid of the resin, degrade the properties of the part significantly. Due to the presence of inserts, ribs, cores and heterogeneity in the preform lay-up in the mold, the resin flow in the mold may branch and merge around the inserts or low permeability areas. If the flow fronts merge in the absence of a vent, air gets entrapped and forms dry spots in these areas. The capability to predict dry spot formation is crucial in RTM process simulations, as it will allow one to design the preform to minimize dry spot formation, and also re-arrange vent and gate locations to let the flow fronts merge in areas where the stress concentration due to applied load is minimum. A numerical algorithm to predict dry spot formation is the main goal of this paper. The other two models are developed to enhance the understanding of the relation between the gate and vent location and dry spot formation.

2

Control of resin injection during the process is discussed. By placing sensors within the mold which are able to detect the resin flow front, the mold filling strategy can be adjusted as the mold fills. Numerical sensors have been encorporated within LIMS, and will allow for the modelling of these features in flow studies. Examples are provided to demonstrate the advantages of such an approach.

In following sections, the numerical implementation of the simulation is presented and followed by the details of the mathematical models. Simulation results are presented and discussed, and the conclusions about this contribution are stated.

NUMERICAL IMPLEMENTATION FOR RTM SIMULATION

The RTM simulation code LIMS has been developed at University of Delaware in the past [5].

The program solves a governing equation

$$\nabla \cdot \left(\frac{1}{\eta} S \cdot \nabla p \right) = 0, \tag{1}$$

subject to boundary conditions of a prescribed pressure at the flow front, no flow through the walls and known pressure or flow rate at the gate locations. In eq. (1), η is the viscosity of the resin, S is the permeability tensor of the resin, and p is the pressure. Details about the boundary conditions will be given in the next section. Equation (1) is obtained from substituting Darcy's law

$$v = -\frac{1}{\eta} S \cdot \nabla p, \tag{2}$$

into the continuity equation

$$\nabla \cdot v = 0, \tag{3}$$

where v is the velocity vector. The velocity is obtained from solving eq. (2) once the pressure is available, and the flow front pattern is approximated from the solved velocity using pseudo steady-state assumption.

Finite element method is used to solve for the pressure distribution. RTM is a moving boundary problem. In LIMS this moving boundary problem is treated as a series of pseudo-steady states as for low Reynolds number flows, because inertia terms are insignificant.

Once the pressure distribution becomes available, a control volume approach is used to compute the moving boundary at the next time step. Pressure solution and flow front advance are repeated until the mold is filled. More details about the method have been reported in [5,8].

MATHEMATICAL MODELS FOR PROCESSING ISSUES

All models for gating, venting, dry spot prediction, and gate control are implemented as modified boundary conditions for the governing equation being solved.

Gating

There are two types of processing conditions at the gate: specified pressure or specified flow rate. The specified gate pressure can be written as:

$$p = p_0(t) \quad \text{at} \quad \mathbf{x} = \mathbf{x}_{gate}, \tag{4}$$

where $\mathbf{x}$ is a location in the mold. The specified injection flow rate can be written as:

$$\nabla \cdot \left(\frac{1}{\eta} S \cdot \nabla p \right) = \frac{1}{A} q_0(t) \quad \text{at} \quad \mathbf{x} = \mathbf{x}_{gate}, \tag{5}$$

where A is the normal area of the control volume where the injection gate is located, and q is the volumetric flow rate of the injection gate. Both conditions can be functions of time. Only one of the above conditions can be applied to one gate location. However, one may switch the condition from pressure to flow rate or vise-versa at any time.

Venting

There are many ways used in practice to vent displaced air out of the mold. The simplest is drilling a few openings in the mold to let the air out. More sophisticated venting involves applying vacuum to these venting ports, i.e., vacuum assisted injection molding. To account for both conditions, it is chosen to set the pressure at all vents to be the same pressure, which is the atmosphere pressure for the former venting condition and a vacuum pressure for the latter. The pressure at the vent locations, p_{vent}, is required as a boundary condition. Before the flow front reaches the vent, the boundary condition is

$$p = p_{vent}, \text{ at the outer flow front.} \tag{7}$$

Here outer flow front refers to the front of resin flowing into an area in the mold with at least one vent in that area, while inner flow front refers to the front flowing into an area without a vent. Figure 2 gives examples to clarify the distinction.

Once the flow front has reached a vent, an additional boundary condition becomes effective:

$$p = p_{vent}, \quad \text{at} \quad \mathbf{x} = \mathbf{x}_{vent}. \tag{8}$$

The flow may pass the vent location, but the pressure at that location remains the same. This condition represents the situation that the vent is kept open after the resin starts leaking out from it. This is the case for vacuum assisted injection molding processes where the

vents are connected with the vacuum source, usually a tank or reservoir under reduced pressure. The venting ports remain open and are connected to the vacuum source until the whole mold filling process comes to a completion.

Dry spot prediction

As mentioned in the previous section, the control volume approach is used for flow front advancement. The algorithm to predict dry spot formation is carried out at each step of flow front advancement. Two arrays, of the length of the total number of control volumes, are used to register the filling status and the computation status of each control volume. There are three filling statuses, *filled*, *unfilled* and *dry*, and two computation statuses, *determined* and *undetermined*, for each control volume. Dry spot detection is done in three steps:

1. After each flow front advancement, one loop through all control volumes is carried out to find the unfilled control volumes. The computation status is registered as *undetermined* for an unfilled control volume and as *determined* for a filled one. At the same time, the filling status is registered as *filled* for filled control volumes.

2. Starting from each control volume where a vent is located, a search scheme is used to find all unfilled control volumes connected to the vent through unfilled control volumes. For these control volumes, the filling status is registered as *unfilled* and the computation status is changed to *determined*.

3. At this stage, if all control volumes are *determined*, no dry spot is formed in the mold. If there are still some control volumes *undetermined*, a search needs to be carried out to find the dry spots. This search starts from any one of the *undetermined* control volumes. The searched control volumes will be registered as *dry* and *determined*. During the search, the total volume of each dry spot is computed and the vent pressure, p_{vent}, is considered as the initial pressure of the dry spots--the collection of connected *dry* control volumes. A dry spot number is used to denote the uncovered dry spot.

Step 3 is repeated until all control volumes become *determined*. The location, size and pressure of each dry spot are stored. When the filling process continues, the size of the dry spots decreases and the pressure in the dry spots increases according to the ideal gas law, $p_{void} v_{void} / T = p_{vent} v_{initial} / T = $ constant. The pressure of each dry spot at the current time, p_{void}, is used as the boundary condition on the flow front surrounding that dry spot:

$$p = p_{void}, \text{ at inner flow front.} \tag{9}$$

Gate control is achieved by opening or closing specified gates upon certain conditions of the mold filling. The strategy used in this work is that the gates are controlled according to the filling status at the locations in the mold where sensors are placed. Once the flow front reaches a sensor, the sensor sends out a signal to control injection gates by opening or closing the valves or adjusting the pressure or flow rates. The logic unit to start injection from a gate located at x_{gate} is the following:

if (flow front has reached location x_{sensor}) then

$$p = p_0(t) \text{ at } x = x_{gate}. \tag{6}$$

The programming for other controlled operations, e.g., closing the valve of a gate or adjusting the flow rate, is done similarly.

The essence of the algorithm is applying certain boundary conditions according to the current filling status. Although the strategy of the controlled injection is extremely simple, it is very helpful in an RTM process design. Examples will be shown in the next section where various kinds of practical goals in the RTM process can be achieved by using appropriate gate control strategies.

SIMULATION RESULTS AND DISCUSSION

Dry spot formation

Dry spot formation is the least desirable situation encountered during resin transfer molding. Dry spots render the manufactured part unusable. The-state-of-the-art of preventing dry spots in industry remains a trial-and-error method. Many test runs are done before a correct molding strategy is found for making dry-spot free pieces. This can cause a significant waste of resources, and increase the cost and time of prototype development. All models developed in this work are aimed at providing a design tool to predict dry spot formation before test runs are carried out.

There are many reasons for dry spot formation. They include poorly designed gate and vent location, geometric complexity of the part, and permeability variation in the preform, just to name a few.

Figure 3 presents an example where the reason for dry spot formation is the variation in the permeability of the preform. The part represented in this example is a square two dimensional panel. Close to the center of the part there is an area (shown with light shade in Fig 3) where the permeability has been assigned a value much lower then that of the surrounding material. The permeability in the shaded area is 10^{-11} m^2, which is 100 times lower than the permeability of the remainder of the preform. This situation is

analogous to the inclusion of a high density section of preform, designed to provide the finished piece with high strength in a certain area. The flow front wraps around this area as it is more difficult to impregnate , and merges behind it to form a trapped air pocket, which is shown as dry preform in Figure 3. If the vent pressure is specified as non-zero, a dry spot will form.

Experimental Verification

A mold was constructed to provide a '5-sided box' cavity. If the process were to be carried to completion, the final piece produced would be a box with a base and four side walls. The overall dimensions of the cavity were 8"x5 1/2"x4", with the cavity thickness being 1/8" throughout the mold. The mold was constructed to provide a wide variety of possible injection schemes, with five injection and eight venting sites.[12] Two of the experiments completed during this study are presented here to demonstrate the ability of LIMS to predict the formation of dry spots.

The first experiment considered is detailed in Figures 4 through 6. Dyed corn syrup was injected at constant flowrate at the center of one of the ends of the box, the preform consisting of random fiberglass mat with a volume fraction of 14%. An image recorded during the experiment is presented in Figure 4. This image presents the base of the box at the center of the picture, while the the four sides of the box are captured in a single video frame by placing mirrors at 45 degrees to each face. Due to the presence of these mirrors, the side faces appear inverted. This particular instance was chosen as it captures the initial formation of a dry spot on the central face of the mold. In this example, a dry spot has formed due to the presence of racetracking, an effect caused by areas of relatively high porosity in the preform, or air channels. In this experiment, air gaps formed at the four edges of the base of the box, situated at the center of Figure 4.

Figure 5 presents the results of a LIMS flow front simulation of this experiment. The contours shown represent the position of the flow front at different times during filling. Racetracking was modelled by assigning higher permeability to rows of elements representing the air gaps in the mold. Figure 6 provides a close up of the central face of the mold. Superimposed on this image is the position and shape of the dry spot predicted by LIMS. Comparison between predicted and experimental dry spot formation is good. It is noted that after the dry spot was formed, the fluid was drawn into the dry spot by capillary forces, and it appeared to close up.

The second experiment considered is detailed in Figures 7 through 9. Fluid was injected at constant flowrate at the end of the box and simultaneously at the center of the central face, the preform consisting of bidirectional fiberglass mat with a volume fraction of

35%. An image recorded during the experiment is presented in Figure 7. At this particular instance a large dry spot is formed between the merging flow fronts existing within the mold In this example, a dry spot has formed due to the complications introduced through multiple injection sites, and also the presence of racetracking. As in the experiment described earlier, air gaps formed at the four edges of the base of the box.

Figure 8 presents the results of a LIMS flow front simulation of this experiment. As for the experiment described earlier, contours shown represent the position of the flow front at different times during filling. Figure 9 provides a close up of the central face of the mold, with the flow front predicted by LIMS superimposed. Comparison between predicted and experimental dry spot formation is reasonable. As noted for the earlier experiment, after the dry spot was formed, capillary forces draw the fluid into the dry spot effectively closing it up. However, the region in which the dry spot occurs is not fully saturated with fluid, and hence represents a defective portion of the finished product. After completion of filling the area initially occupied by the dry spot was lighter in color than the rest of the mold, again signifying the unsaturated nature of this region.

Dry spot prevention through Controlled Injection

The prevention of dry spot formation is an open ended problem and has multiple solutions. Here we will examine one method to prevent voids to demonstrate how the new features included in LIMS can be used to prevent dry spot formation.

Figure 10 shows an example of dry spot formation due to mild geometric complexity of the molded part. The part being molded is a flat panel with two open windows as shown in the figure. The injection gate is located at the center of bottom edge and the vent is located at the center of the top edge. When flow merges into the center portion of the part, the path for displaced air to escape is blocked by resin. A dry spot forms in the center of the part. This numerical experiment has been completed by Han et al. [10], LIMS agreeing with the position and nature of dry spot formed.

To prevent this type of dry spot forming, many possible approaches can be adopted. The location of the gate can be redesigned as suggested in [10]. If the injection gate is moved to one of the bottom corners, and the vent is moved to the opposite upper corner, the flow pattern will change and the flow fronts meet right around the vent. Thus the dry spot will not form. Alternatively, an additional vent can be placed at the center of the part shown in Figure 10 to let trapped air out and avoid the dry spot formation.

Here we propose use of controlled injection to prevent formation of the dry spot. This approach is not necessarily superior, but is presented to demonstrate the advantages of controlled injection. Figure 11 demonstrates the injection control strategy. One additional

gate is placed at the center portion of the part. On one side of the panel, a sensor is installed to detect the flow front. The sensor sends a signal for gate control when resin reaches this location. Initially, the resin is injected from the bottom center gate. Before the resin can block the air path, it reaches the sensor. The sensor sends out two control signals, one to close the valve of the bottom gate, the other to open the valve of the center gate. Thus, the resin injection is switched to the center gate, as shown in Figure 11(a), until the mold is completely filled as shown in Figure 11(b). No dry spot is formed in the part.

Operation cost reduction through Controlled Injection

It is true that guaranteeing the quality of the manufactured product is considered to be the most important issue concerning RTM. However, by employing good control strategies one can improve product quality and reduce product development time. Controlled injection during the mold filling stage of RTM has the potential to reduce operation costs of the process.

Take the very simple one dimensional part shown in Fig. 12 as an example. For a long rod as shown in the figure, the controlled injection relay can significantly reduce the operation cost, or shorten the operation time.

Assume the preform is uniform everywhere and injection is from one end initially. Solving eqs. (1-2) leads to the following conclusions:

1. if constant injection pressure is used, the time to fill the part is proportional to the square of the length, $t_{fill} \propto L^2$;

2. if constant injection flow rate is used, the injection pressure required is proportional to length, $p_0 \propto L$.

If a sensor and an additional gate are placed at the mid point of the part, as shown in Fig. 12, and the resin injection gate is switched when flow front reaches this point, then

1. the time needed to fill the whole mold will be reduced to one half in the case of constant injection pressure;

2. the highest pressure required at the inlet will be reduced to one half in the case of constant injection rate.

It is obvious that for large parts, this practice can produce substantial reductions in operation costs.

SUMMARY

The features of gate control, venting and dry spot prediction have broadened the ability of LIMS as a design tool. Eliminating dry spots, a key issue in the production of high quality

RTM pieces, can be investigated via numerical experiments with the help of the models developed in this work. Several experiments have been presented to verify LIMS with the discussed models included. LIMS has been shown to perform well with the effects of permeability variation, racetracking and multiple injection sites present within a mold. The advantages of controlling the injection strategy through the use of sensors within a mold have been presented. Controlled injection has been shown to be an effective method of preventing dry spot formation, and reducing operation costs by lowering mold pressures encountered or filling time. Utilization of numerical packages such as LIMS will save time and resources spent on tool design before actual production, and make RTM a cost effective manufacturing method.

ACKNOWLEDGMENT

REFERENCES

1. **Advani, S.G., Bruschke, M.V. and Parnas, R.** `Resin Transfer Molding' in *Flow and Rheology in Polymeric Composites Manufacturing*, Ed. Suresh G. Advani, (Elsevier, Amsterdam 1994).

2. **Fracchia, C.A., Castro, J. and Tucker, C.L. III** `A finite element / control volume simulation of resin transfer mold filling' *Proceedings of the American Society for Composites Fourth Annual Technical Conference* (1989) pp 157-166.

3. **Coulter, J.P. and Guceri, S.I.** `Resin impregnation during the manufacturing of composite material subject to prescribed injection rate' *Journal of Reinforced Plastic Composites* 7 (1988) pp 200-220.

4. **Molnar, J.A. Trevino, L. and Lee, L.J.** `Liquid flow in molds with prelocated fiber mats' *Polymer Composites* 10 (1989) pp 414-423.

5. **Bruschke, M.V. and Advani, S.G.** `A finite element / control volume approach to mold filling in anisotropic porous media' *Polymer Composites* 11 (1990) pp 398-405.

6. **Lin, R., Lee, L.J. and Liou, M.J.** `Non-isothermal mold filling and curing simulation in thin cavities with preplaced fiber mats' *International Polymer Processing* 6 (1991) pp 356-369.

7. **Subbiah, S., Trafford, D.L. and Guceri, S.I.** `Non-isothermal flow of polymers into two-dimensional, thin cavity molds: a numerical grid generation approach' *Int. J. Heat Mass Transfer* **32** (1989) pp 415-434.

8. **Bruschke, M.V. and Advani, S.G.** `A numerical approach to model non-isothermal, viscous flow with free surfaces through fibrous media' submitted to *Int. J. Numer. Method in Fluids*.

9. **Liu, B. and Advani, S.G.** `Operator splitting scheme for 3-D temperature solution based on 2-D flow approximation' submitted to *Journal of Computational Physics*.

10. **Han, K., Wu, C.-H. and Lee, L.J.** `Characterization and Simulation of Resin Transfer Molding - Race Tracking and Dry Spot Formation' *Proceedings of Ninth Annual ASM-ESD Advanced Composite Conference*, Michigan, Nov. 1993.

11. **Advani, S.G., Liu, B., and Bruschke, M.V.** `*Liquid Injection Molding Simulation - LIMS User's Manual - version 3.0.'* University of Delaware, Newark.

12. **Bickerton, S., Advani, S.G., and Fickie, K.** `Experimental Investigation of RTM, within a Box Mold', ARO report to appear.

AUTHORS

Baichen Liu was a post-doctoral Research Fellow at the Center for Composite Materials, University of Delaware. He is presently a Senior Research Engineer at The Dow Chemical Company, Midland, MI 48667. Suresh G. Advani, to whom correspondence should be addressed, is Associate Professor within the Department of Mechanical Engineering, also at the University of Delaware, Newark, DE 19716, USA. Simon Bickerton is a graduate student in the Department of Mechanical Engineering, at the University of Delaware.

Figure Captions

Figure 1.   Schematic of mold filling stage of resin transfer molding.

Figure 2.   Schematics of mold filling showing inner and outer flow fronts of resin.

Figure 3.   Mold filling simulation of a flat panel. The preform has a low permeability area around the center as shown with light shading. The permeability in the shaded area is 100 times lower than the

permeability of the surrounding preform. The simulation results show a dry spot formed in the center of the panel.

Figure 4.   Single video frame captured during box mold experiment with random mat preform.

Figure 5.   Mold filling simulation results for experiment represented in Figure 4. Contours represent equal steps in time.

Figure 6.   Close up of central face of box mold, taken from Figure 4. Corresponding void predicted by simulation is presented.

Figure 7.   Single video frame captured during box mold experiment with bidirectional mat preform.

Figure 8.   Mold filling simulation results for experiment represented in Figure 7. Contours represent equal steps in time.

Figure 9.   Close up of central face of box mold, taken from Figure 7. The corresponding void, and outer flow front predicted by LIMS are presented.

Figure 10.   Mold filling simulation of a flat panel with two open windows. Contours represent equal steps in time. The simulation result shows a dry spot formed within the center portion of the part.

Figure 11.   Mold filling simulation for the part shown in Fig. 10 using controlled injection. (a) The contour lines are filling time obtained at the moment of the switching of the injection location from bottom gate to center gate. (b) The contour lines are filling time obtained at the end of mold filling.

Figure 12.   Schematic of controlled injection strategy for a one dimensional part.

Vent

Resin

Fig. 1

Outer flow front
Inner flow front
Vent

Gate

Inner flow front
Outer flow front
Vent

Gate

Figure 2

Vent

Gate
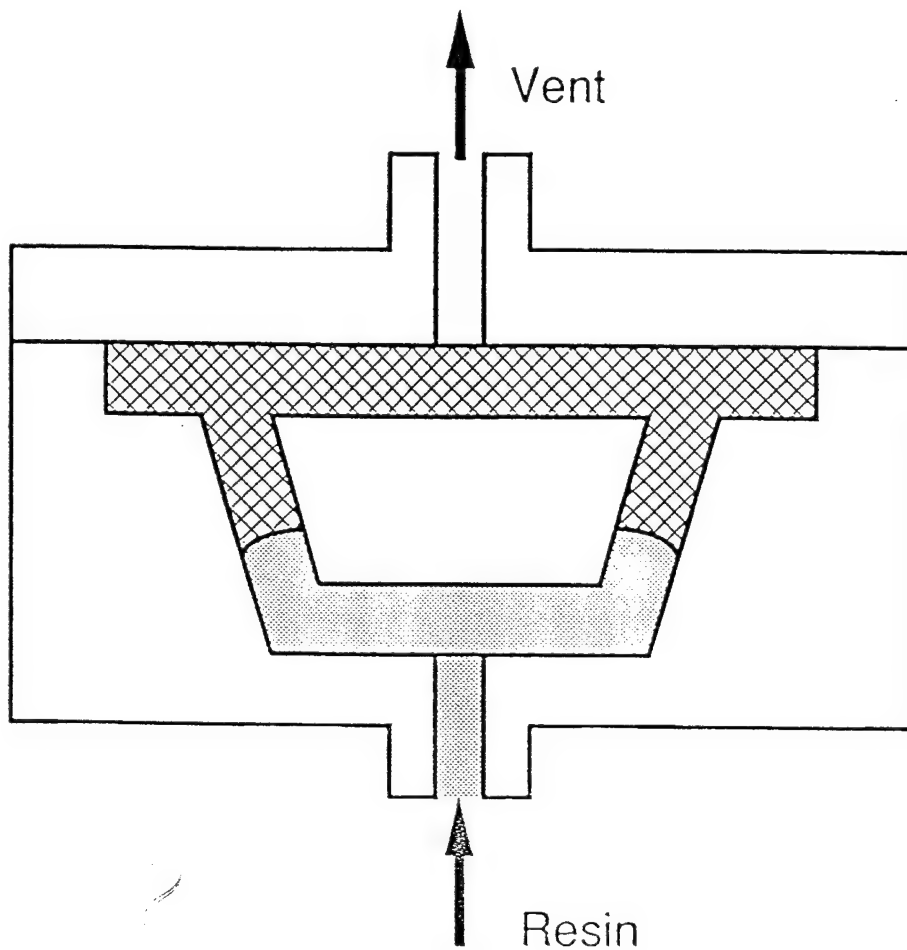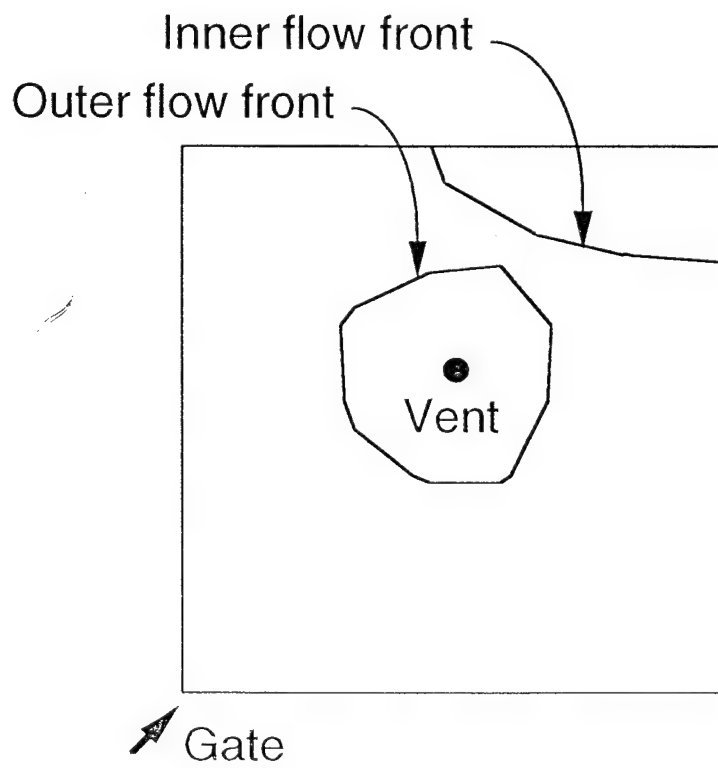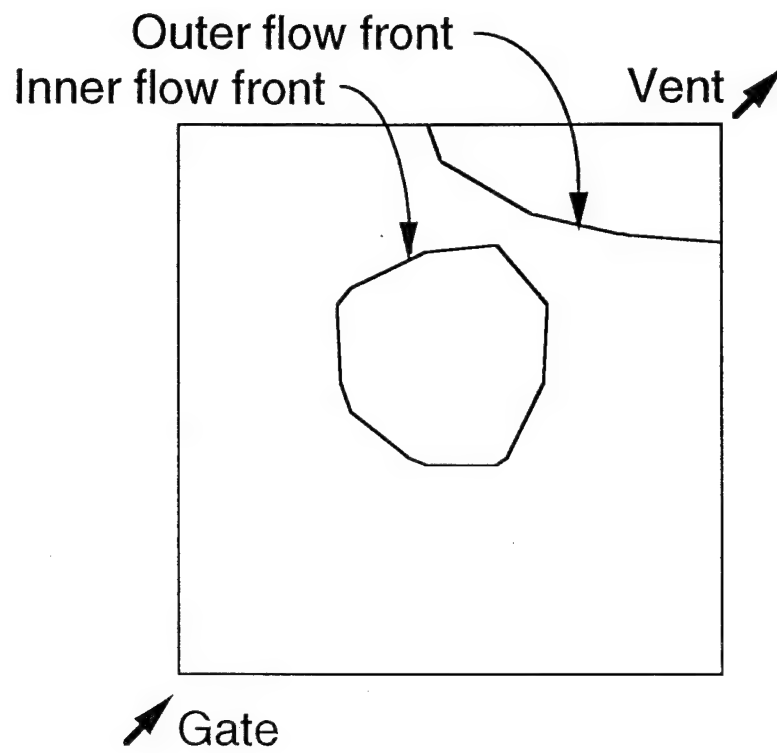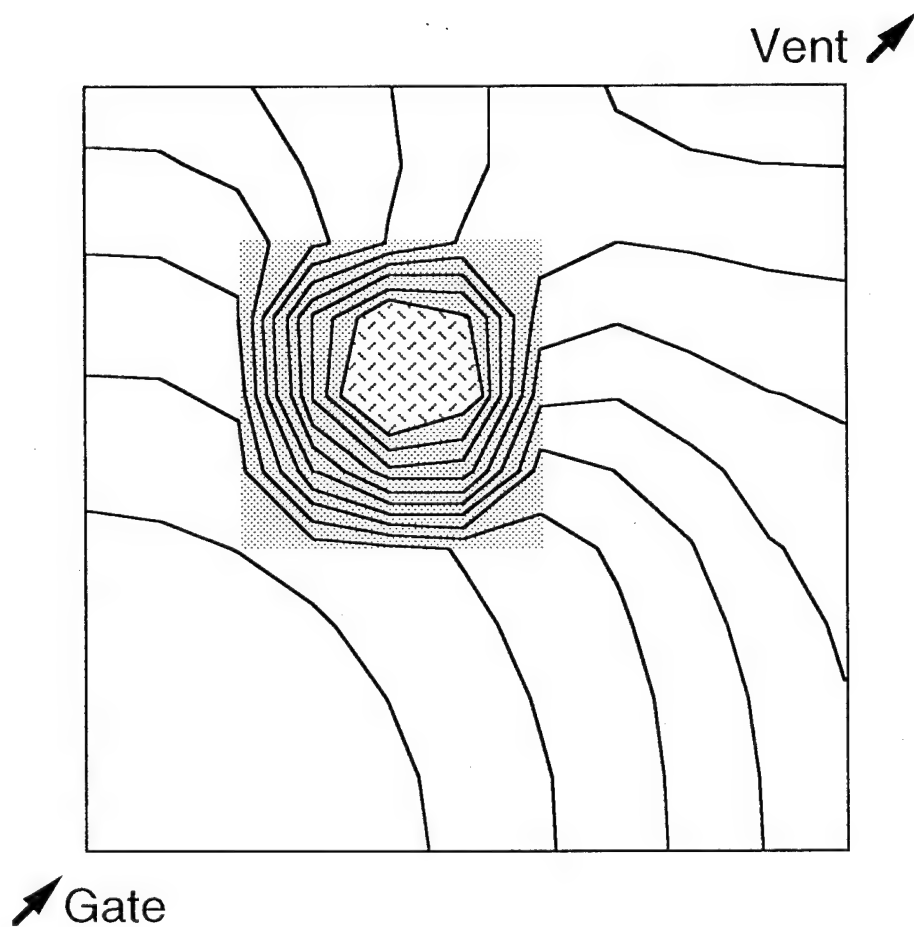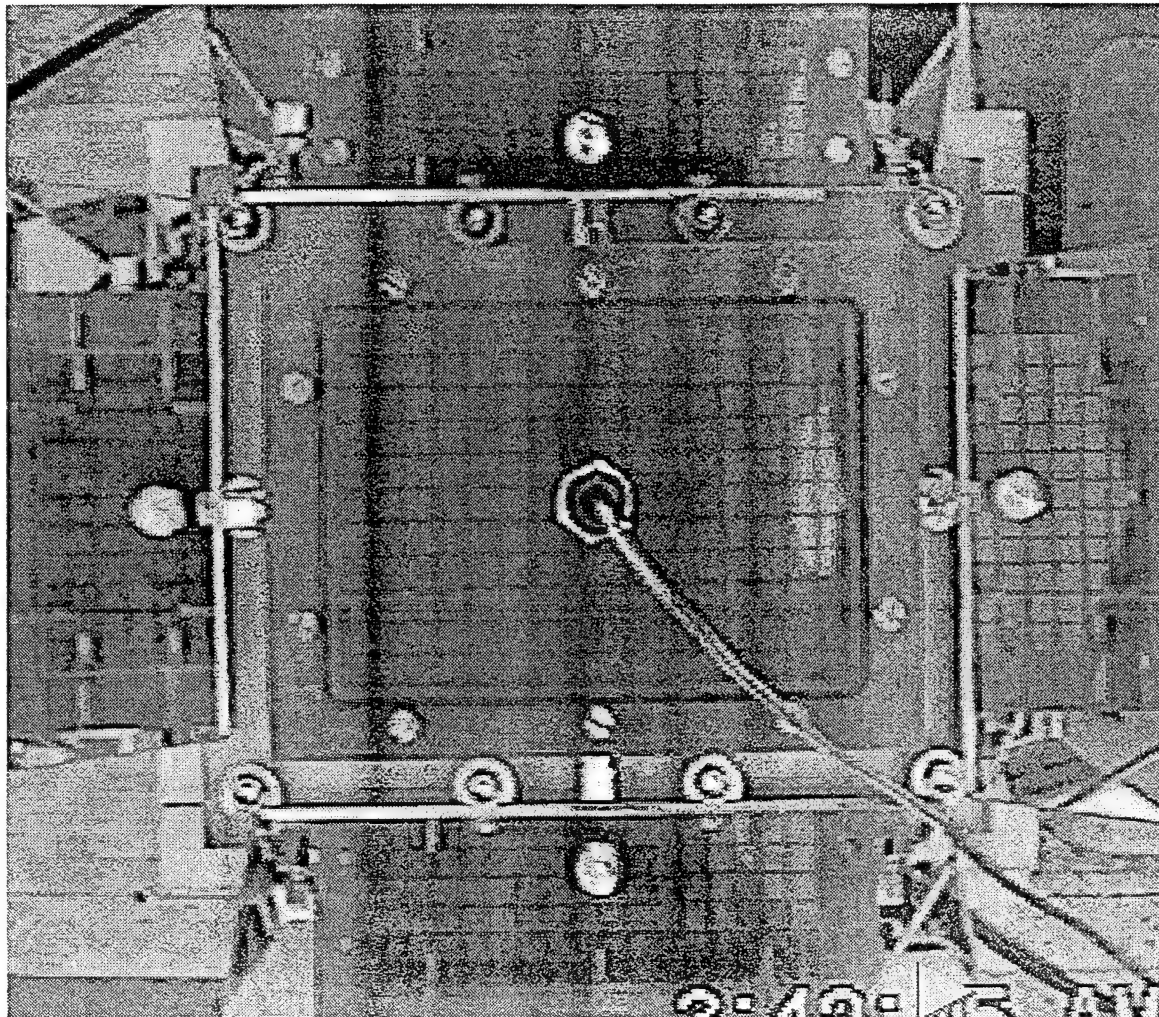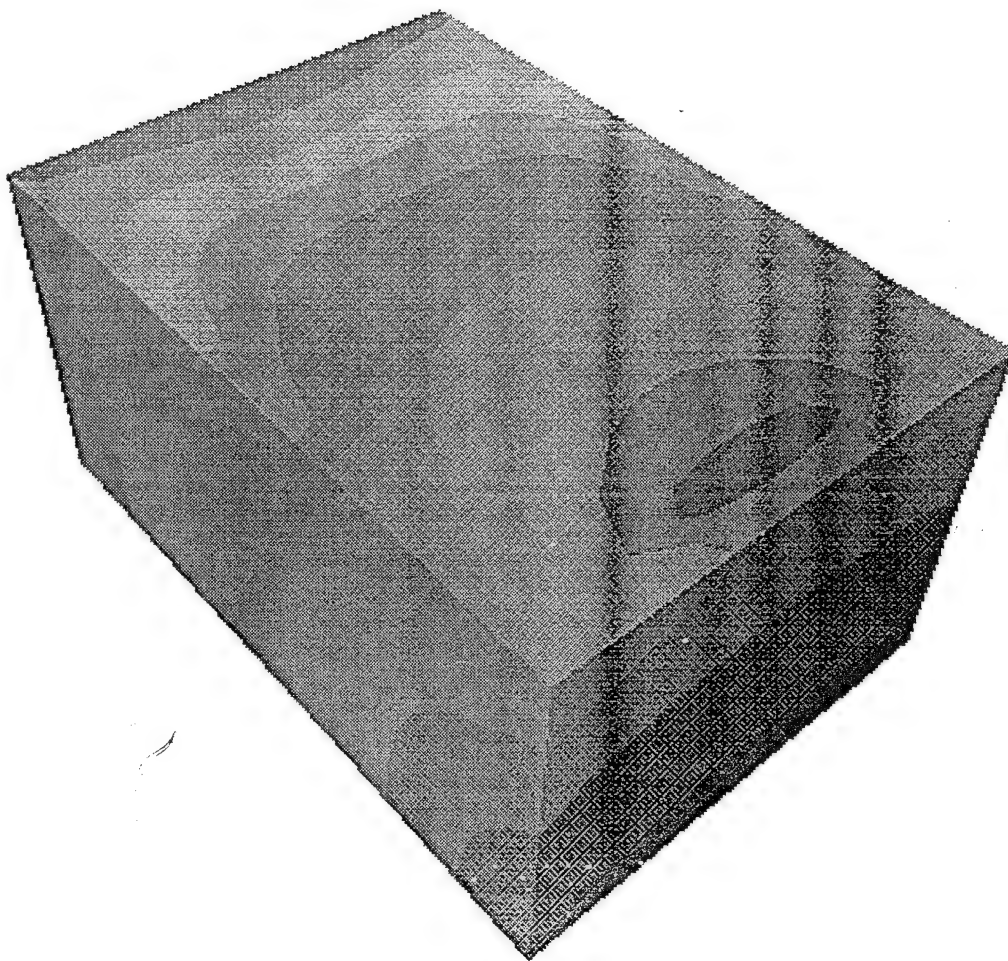
Figure 3

Figure 4

Figure 5
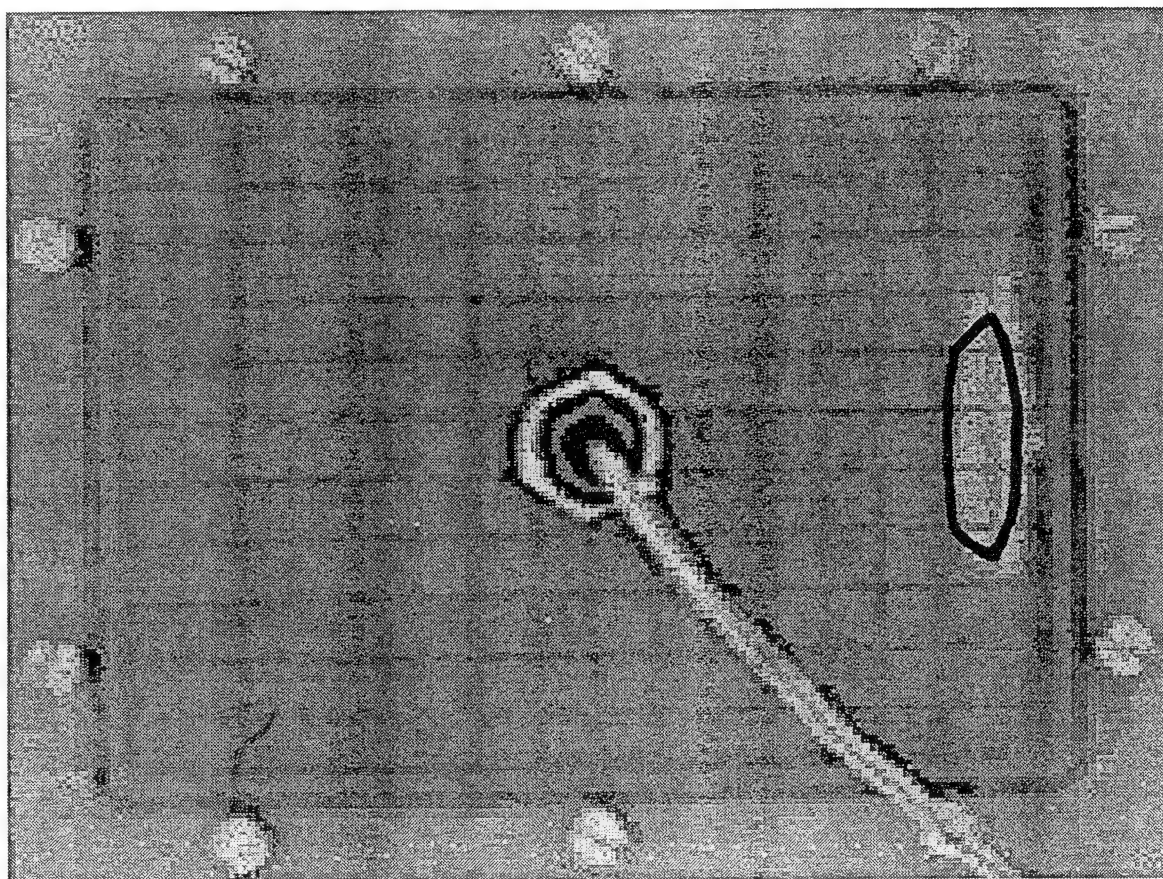
Figure 6
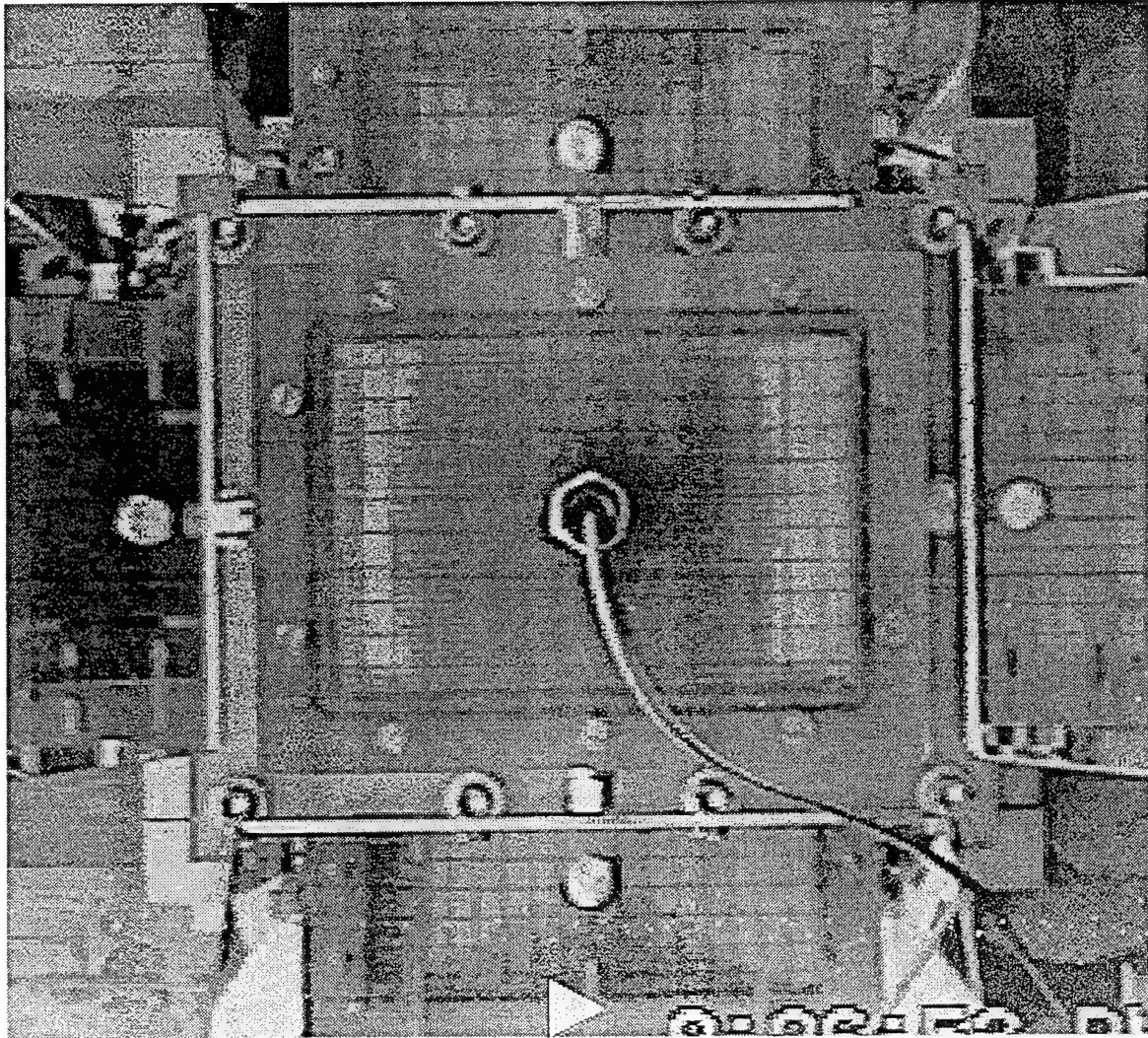
Figure 7

Figure 8

Figure 9

Vent

Void

Gate

Fig 10

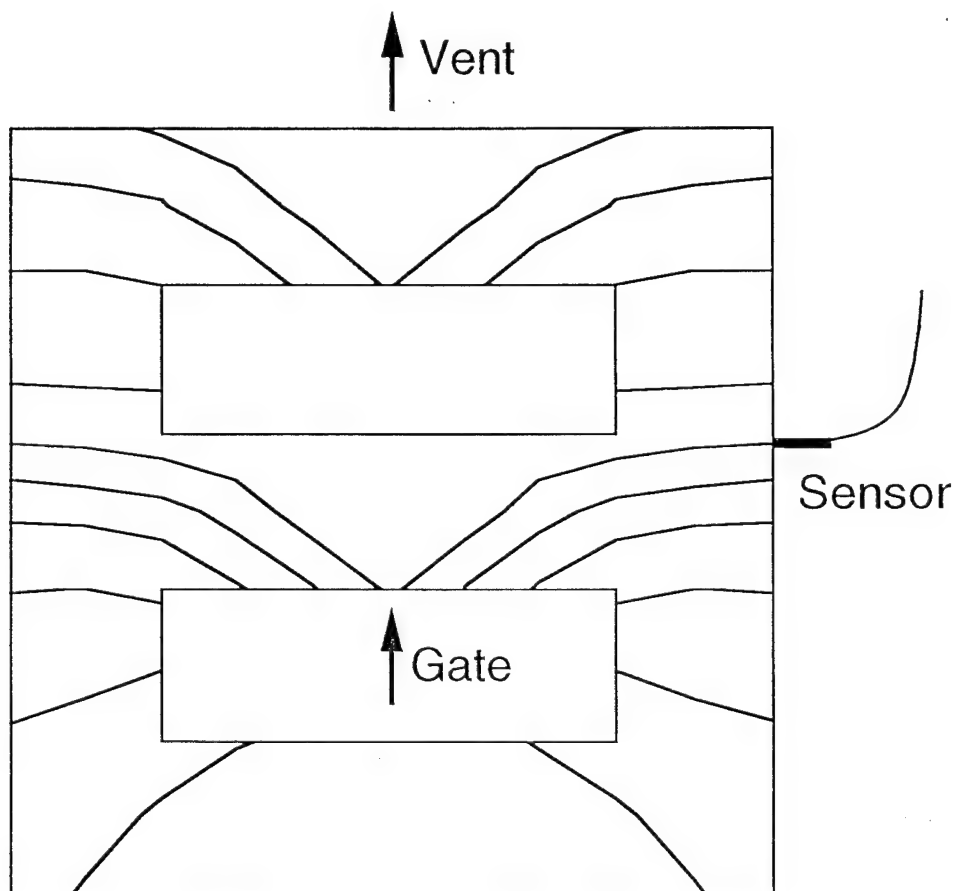Figure 11a

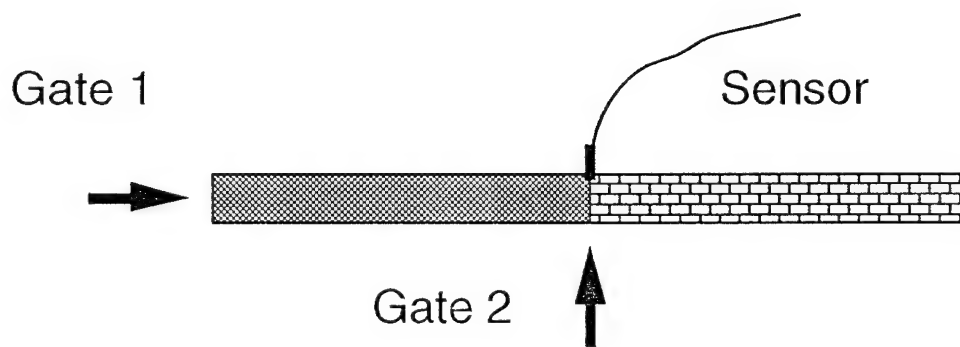Vent

Sensor

Gate

Figure 11 b

Gate 1

Gate 2

Sensor
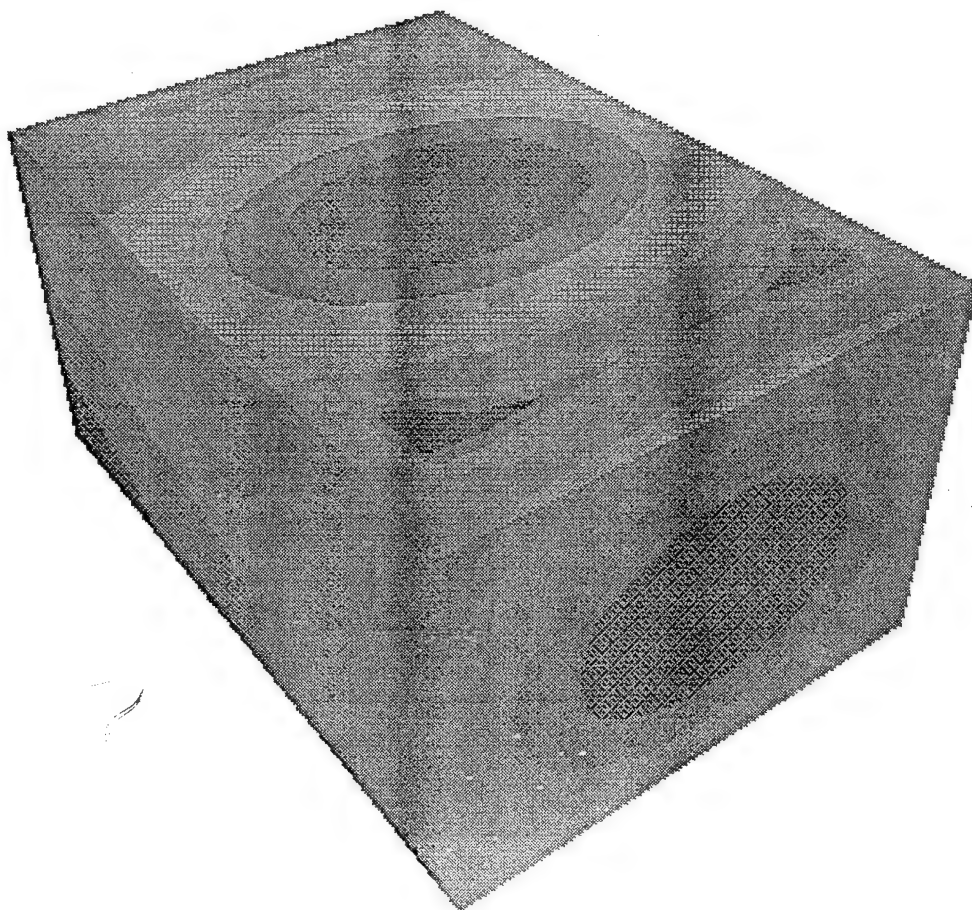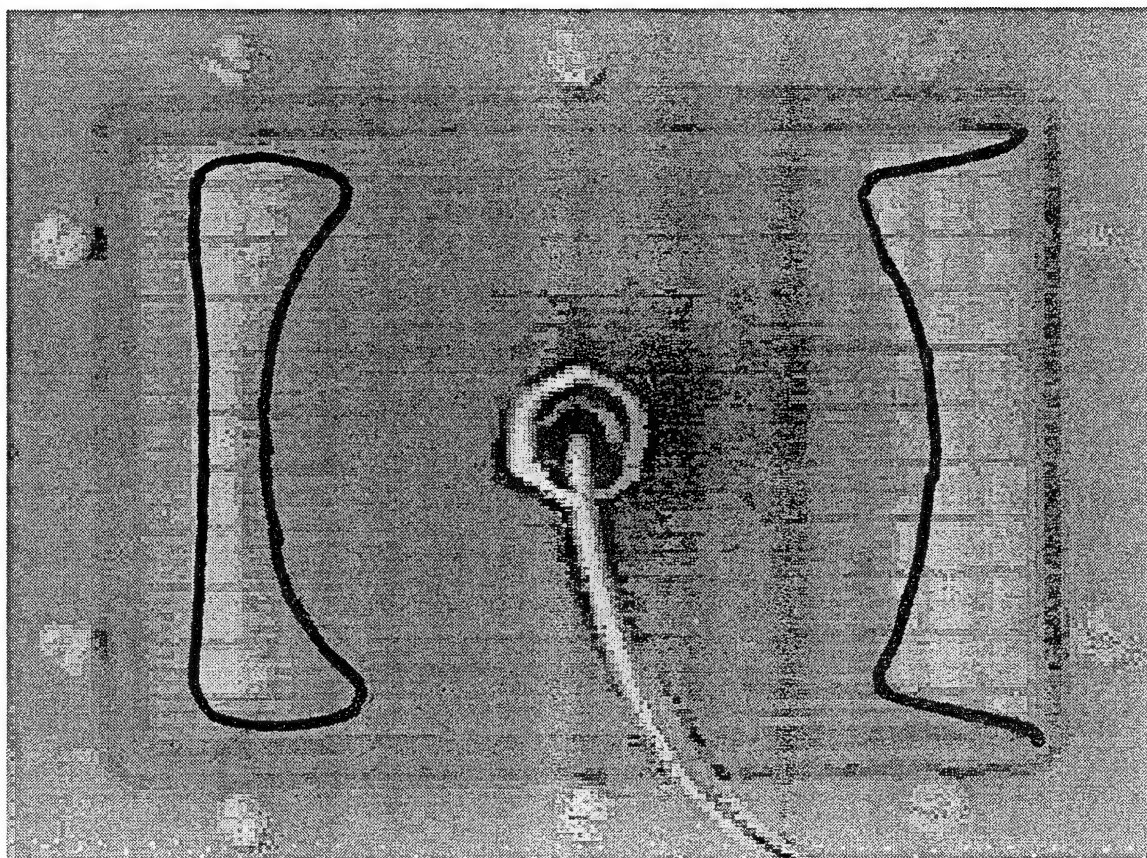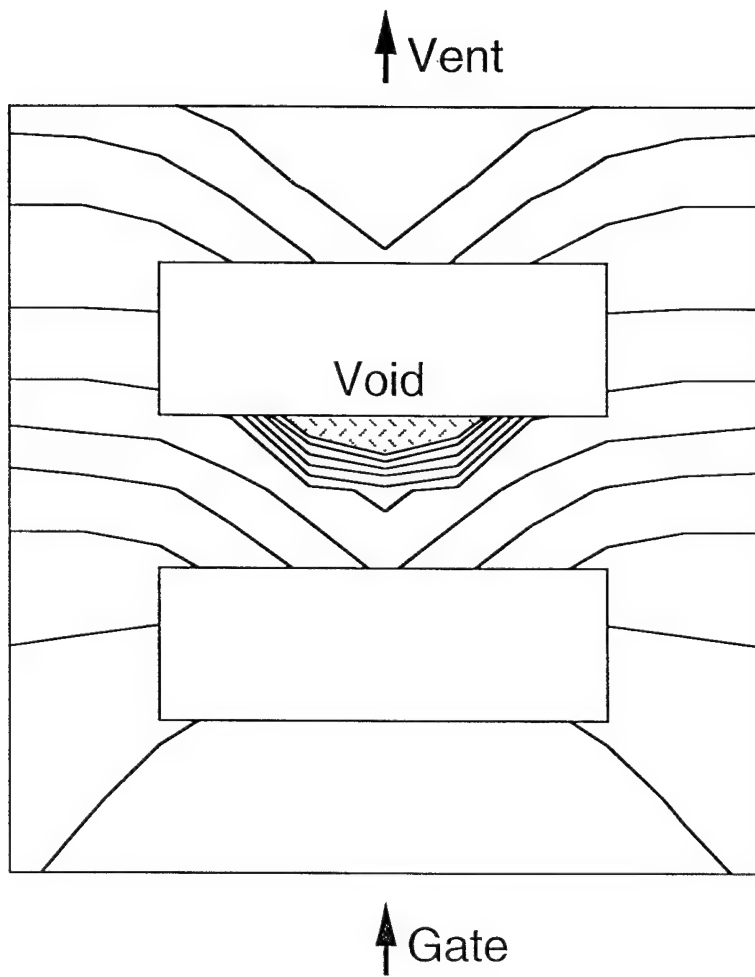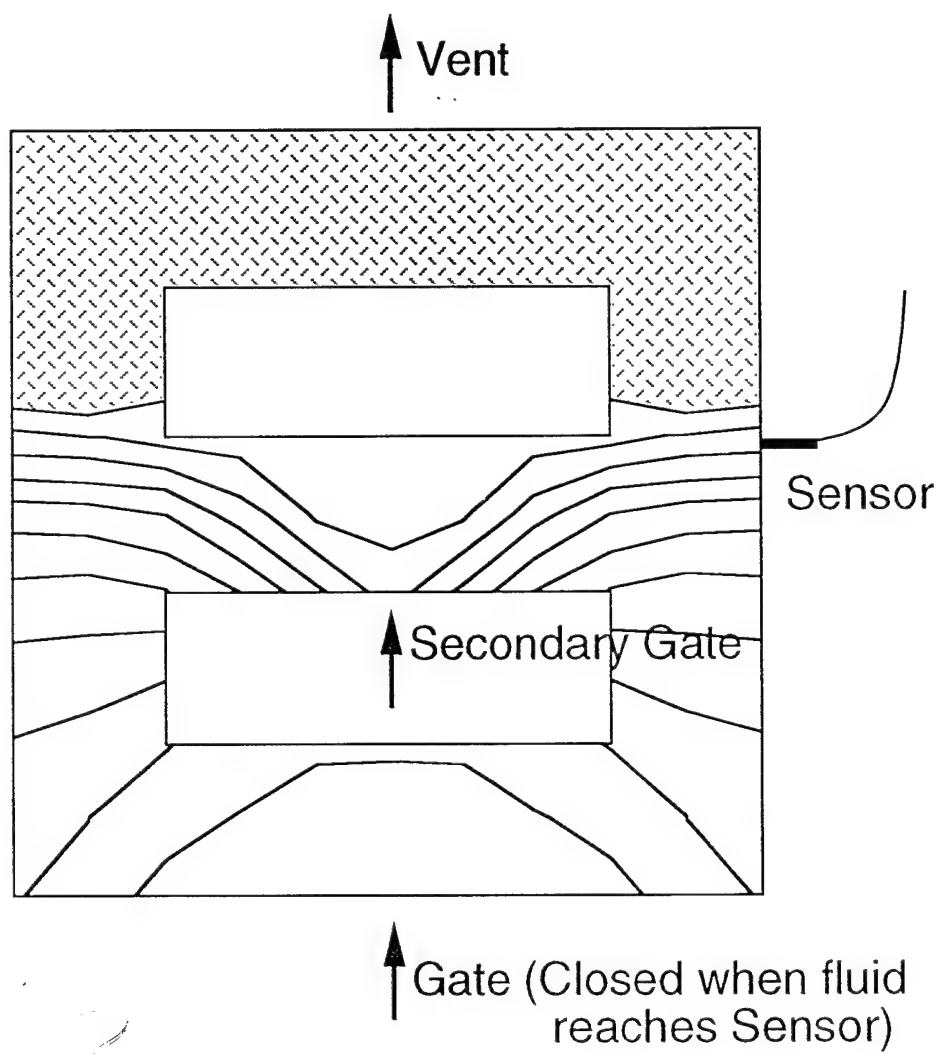
Figure 12

Operator Splitting Scheme for 3-D Temperature Solution Based on 2-D Flow Approximation

Baichen Liu* and Suresh G. Advani**

*Center for Composite Materials, Department of Mechanical Engineering,
University of Delaware, Newark, DE 19716*

In this work, an operator splitting numerical technique is used to solve for the temperature distribution in three dimensions during non-isothermal filling of anisotropic porous media in processes such as resin transfer molding (RTM). In these processes, the parts are manufactured by injecting resin into thin cavities so the flow is primarily in the plane of the part and is modeled as two dimensional flow. However, due to importance of conduction in the out of plane direction, the energy equation needs to be solved in 3-D. Scaling of the terms in the energy balance equation allows us to determine their significance. Important terms considered for this study in such processes are advection, conduction, and heat of curing reaction. The operator splitting scheme used to obtain the 3-D temperature solution takes advantage of the fact that advection is only important in the plane and conduction is only important in the thickness direction. When combined with a predictor-corrector method, this scheme converges rapidly to a stable temperature solution for the moving boundary problem. Because of its superior stability, this method uses large time steps to accelerate the calculation while maintaining good accuracy.

1. Introduction

Resin transfer molding (RTM) is a manufacturing process developed in recent years for high performance composite materials, such as structural parts for aircraft and automobiles. A typical RTM process cycle consists of four phases. The first phase is preform manufacturing which produces the fiber reinforcement in the shape of the finished part. The second phase is mold filling where resin is injected into the cavity of a mold with preplaced preform. The third phase is resin curing which may start during or after the second phase. The fourth phase is demolding which happens when the curing reaction

---

* Present address: The Dow Chemical Company, 1400 Building, Midland, MI 48667
** To whom correspondence should be addressed.

1

comes to a completion and the part solidifies to its designed rigidity [Advani, Bruschke, and Parnas (1994)]. Figure 1 is a schematic of the second phase of the process, mold filling, which is the focus of this study. It addresses the basic fluid mechanics and the associated heat transfer in a moving domain with a free surface. The method proposed in this work is also applicable for the third phase.

The second phase is the core of the process. The injected resin is driven by the inlet pressure to saturate the preform. The formulation to describe the flow is modeled as flow through porous media and shares same physics with other problems like those widely studied in the fields of oil recovery.

Because it allows the designer the best possible control over the fiber reinforcement in the final part, RTM has become a preferred method to manufacture structural composite parts. It has also attracted researchers to explore the possibility of simulating the process numerically. Many computer programs have been developed to solve for the pressure, velocity, flow front development and temperature distribution. While most investigators solved the isothermal flow in RTM processes [Bruschke and Advani, (1990), Coulter and Guceri, (1988), Fracchia, Castro, and Tucker III (1989), Molnar, Trevino and Lee, (1989),], some have modeled non-isothermal flow [Bruschke and Advani, (1994) Lin, Lee and Liou (1991)]. Although the isothermal assumption can give a preliminary prediction of the variables of interest, non-isothermal calculation is necessary for several practical reasons. The most commonly used resins for manufacturing polymer composites are thermosetting resins. Although it is possible to initiate the curing at a lower temperature by using an appropriate catalyst [Babbington, Barron, Enos, Ramsey and Preuss (1988)], heating is widely used because it is more controllable. In addition, the curing reaction of thermosetting resins is usually very exothermic [Lin, Lee and Liou (1991)]. Therefore, including the temperature into the governing equations for RTM simulations is logical if the heating is done at the time the mold is being filled.

Due to the lack of agreement on the energy balance equation for porous media [Tucker and Dessenberger (1994)], different approaches have been used. One of the differences in these approaches is the number of the phases appearing in the equation. While some believe that the properties of the fluid and the solid phases are so different that they should be treated separately, others consider it legitimate to use equilibrium model because the flow and reaction are slow enough for two phases to reach an equilibrium temperature. For the former model, there will be two sets of governing equations whereas for latter case, the equilibrium model allows us to reduce it to a single energy equation. The purpose of this paper is to report a successful solver for the temperature distribution. In this work, we used the equilibrium model, i.e., there is only one temperature for both

2

phases at given time and location as it has been experimentally demonstrated that the two phases do reach equilibrim temperature in a characteristic time that is much smaller than the process time [Lin, Lee and Liou (1991)].

The shape of most composite parts is shell-like as shown in Fig. 2. The thickness, h, is much smaller than other dimensions of the part, e.g., the length, L. The flow simulation can be done in two dimensions for three-dimensional surfaces (referred as 2.5 D by some authors) [Lin, Lee and Liou (1991), Bruschke and Advani, (1990)]. However, the temperature solution requires the third dimension to handle heat transfer through the thickness of the part [Lin, Lee and Liou (1991), Bruschke and Advani, (1994)]. The mathematical model in this work follows this approach. The pressure, flow rate, and flow front development are solved in the plane, while the temperature distribution is solved in three dimensions (see Fig. 2).

The main difference between this work and previously reported ones [Lin, Lee and Liou (1991), Bruschke and Advani, (1994)] is the time integration technique used for solving the temperature distribution. Lin, Lee and Liou (1991) used explicit finite difference time marching method. Since Chebyshev collocation spectral discretization was used in the through thickness direction and it is a conditionally stable discretization, there is a limit on the time step-size. Therefore, sub-time steps are used for each mold filling step to ensure stability.

Subbiah, Trafford and Guceri(1989) also used explicit finite difference time marching method. To improve the stability, upwind spatial discretization was used. Comparatively speaking, upwind finite difference has been found to be more stable than Chebyshev collocation spectral method [Liu and Beris(1988)]. However, using it explicitly does not guarantee stability. Therefore, there is still a limit on the time step-size [Subbiah, Trafford and Guceri(1989)].

The technique used in [Bruschke and Advani, (1994)] was a modified Crank-Nicholson method. In order to solve the implicit equation system obtained, a Gauss-Seidel iteration was used to achieve convergence. The disadvantage of this method arises due to two aspects: the implicit Crank-Nicholson method is not very stable and small time-steps must be used for each mold filling step, and the Gauss-Seidel iteration converges too slowly.

The numerical scheme adopted in this work performs much better with respect to these two aspects. For most simulation cases, there is no need to use multi-steps for the temperature solution. The scheme treats non-linear terms explicitly and the linear terms implicitly. This combination is a compromise between the high efficiency of the explicit

3

methods and the stability of the implicit methods. The simulations results shows this scheme works very well for the simulation of mold filling processes such as RTM.

In section 2 the general theory of energy balance for RTM process is presented, along with the scaling to estimate the importance of different terms in the equation. The numerical implementation of the simulation is given in section 3 and the details of the operator splitting technique used for the temperature solution are presented in section 4. Verification, simulation results and relevant discussion follow in section 5 and finally the conclusions about this contribution are stated.

2. Theory of energy conservation in RTM processes

The theory of the energy conservation in RTM processes has been studied in certain depth and there is general governing equation available [Tucker and Dessenberger (1994),Kaviany, (1991)]. Starting from the general consideration of the energy conservation. Tucker and Dessenberger (1994) obtained the following governing equation for heat transfer in RTM processes:

$$
\left[\phi \left(\rho C_p \right)_r + \left(1 - \phi \right) \left(\rho C_p \right)_f \right] \frac{\partial T}{\partial t} + \left(\rho C_p \right)_r \mathbf{v} \cdot \nabla T
$$
$$
= \nabla \cdot \left(\mathbf{k}_e \cdot \nabla T \right) + \phi H_R r_R + \eta \mathbf{v} \cdot \mathbf{S}^{-1} \cdot \mathbf{v} + \phi \left(\rho C_p \right)_r \nabla \cdot \left(\mathbf{D} \cdot \nabla T \right), \tag{1}
$$

where ϕ is the preform porosity (which is also $(1-v_f)$, here v_f is fiber volume fraction), ρ is density, with subscript "r" denoting resin or "f" denoting fiber preform, C_p is heat capacity, T is temperature, $\mathbf{v}$ is the velocity vector, $\mathbf{k}_e$ is the total effective conductivity tensor (see [Tucker and Dessenberger (1994)] for details), H_R is the heat of cure reaction, r_R is the rate of cure reaction, η is resin viscosity, S is the permeability tensor, and $\mathbf{D}$ is the thermal dispersion tensor (see [Tucker and Dessenberger (1994)] for details). Energy balance equation, eq. (1), essentially states that the temperature change is due to the heat from advection, conduction, cure reaction, viscous dissipation, and heat dispersion.

Using gap height of the mold, $h/2$, as the characteristic scale of length in z direction, L as the characteristic length in the in-plane direction, the maximum temperature difference, $\Delta T = T_w - T_0$, as the characteristic scale of temperature, the average flow velocity, $\bar{v}$, as the scale for velocity, and

$$
\hat{t} = \overline{\rho C_p} \frac{h^2}{4\bar{k}} \tag{2}
$$

as the characteristic time scale for heat transfer, where $\overline{\rho C_p}$ is the quantity in the brackets of eq. (1) and $\bar{k}$ is the average heat conductivity using the same averaging rule, one can re-cast eq. (1) in dimensionless form:

4

$$\frac{\overline{\rho C_p}}{(\rho C)_r}\frac{\partial \Theta}{\partial \tau} + Gz(\mathbf{u}\cdot\nabla\Theta) = \frac{h^2}{L^2}\left(\frac{\partial}{\partial\hat{x}}(k_{xx}\frac{\partial\Theta}{\partial\hat{x}}) + \frac{\partial}{\partial\hat{y}}(k_{yy}\frac{\partial\Theta}{\partial\hat{y}})\right) + \frac{\partial}{\partial\hat{z}}(k_{zz}\frac{\partial\Theta}{\partial\hat{z}}) +$$

$$Da\,\mathbf{r} + Br\left(\mathbf{u}\cdot\mathbf{K}^{-1}\cdot\mathbf{u}\right) + Pe\nabla\cdot\mathbf{B}\cdot\nabla\Theta \tag{3}$$

here **I** is a unit tensor and the dimensionless variables are defined as:

$$\Theta = \frac{T-T_0}{\Delta T}, \tag{4}$$

$$\tau = \frac{t}{\bar{t}}, \tag{5}$$

$$\mathbf{u} = \frac{1}{\bar{v}}\mathbf{v}, \tag{6}$$

$$\mathbf{r} = \frac{\mathbf{r}_R}{r_0}, \tag{7}$$

$$\mathbf{K} = \frac{1}{\bar{s}}\mathbf{S}, \tag{8}$$

$$\mathbf{B} = \frac{1}{\bar{v}d_p}\mathbf{D}, \tag{9}$$

where r_0 is the cure reaction rate of fresh resin at wall temperature, $\bar{s}$ is the characteristic scale for permeability, and d_p is the equivalent particle size for the preform. The dimensionless groups in eq. (3) are defined as:

$$Gz = \frac{h}{L}\frac{\bar{v}(\rho C_p)_r}{\bar{k}}, \tag{10}$$

$$Da = \phi\rho_r\left(\frac{h}{2}\right)^2\frac{H_R r_0}{\bar{k}\Delta T}, \tag{11}$$

$$Br = \frac{\eta\bar{v}^2}{\bar{k}\Delta T}\frac{h^2}{4\bar{s}}, \tag{12}$$

$$Pe = \frac{\phi(\rho C_p)_r\,\bar{v}d_p}{\bar{k}} \tag{13}$$

In the above, the dimensionless groups describe the importance of different terms with respect to conduction: the Graetz number, Gz, describes the importance of advection, the Damkohler number, Da, describes the importance of heat of reaction, the Brinkman number, Br, describes the importance of viscous dissipation, and the Peclet number, Pe, describes the importance of thermal dispersion.

The importance of each term in an equation is judged by its magnitude. The scaling used in the above analysis is to normalize those variables. As a result, most of the derivatives of those variables also become normalized with only one exception, the gradient of temperature along the flow direction. Therefore, the magnitude of each term, except the advection term, is represented by the magnitude of corresponding dimensionless group.

The scales used for temperature difference and length in the above scaling determine that the conduction term is of the order of unity. Notice that the scale of time in eq. (2) involves a group of parameters from the internal energy and conduction terms. Therefore, the rate of temperature change and the heat of conduction are of the same order of magnitude. This fact can be used as an intuitive guidance in evaluating the importance of other terms.

In order to analyze the remaining four terms, it is illuminating to first compute all these scales for a typical RTM process. It is reasonable to use centimeters as the scale of length because the thickness of most manufactured parts is usually a few millimeters. The flow velocity is in the neighborhood of 1 cm/s. The temperature difference is in the range of 10-100 K. Rarely there are resins that undergo temperature changes of more than several hundred K while isothermal assumption can be used if temperature change is less than 10K. The time scale of heat transfer is computed from eq. (2). Using typical values for these parameters leads to a value of about one minute. Table 1 gives the magnitude of these scales and some physical properties of resin and fiber used in the scaling.

Table 1. Magnitude of RTM properties and parameters.

Property / Parameter	Symbol	Magnitude
Mold half gap height	$h/2$	10^{-2} m
Mold Length	L	1 m
Heating temperature difference	ΔT	10-100 K
Average flow velocity	$\bar{v}$	10^{-2} m/s
Density (resin and/or fiber)	ρ	10^3 kg/m^3
Heat capacity	C_p	10^3 J/kg K
Resin viscosity	η	10^{-1} Pa s
Heat conductivity	k	1 W/m K

Using the physical properties of resins commonly used in RTM processes, the Graetz number computed is of the order of 100. Normally, the aspect ratio of planar dimension to gap height for thin-shell parts is about 100. This leads to a value of temperature gradient of the order of 0.01. Thus, the magnitude of the advection term in eq. (3) is also of the order of unity and is as important as conduction.

On the other hand, the heat of reaction, may vary on a much wider scale due to its sensitivity to temperature. The Damkohler number computed using the data given in Table 2 is about 0.1 at a temperature of 100 °C and a porosity at 0.5. It certainly should be considered in the simulation. For faster and more exothermic cure reactions, the heat of

6

reaction will be quite important. However, this Damkohler number drops to 0.003 at a temperature of 80 °C and it becomes reasonable to totally neglect this term.

Table 2. Parameters of resin curing reaction [Scott, (1988)] using kinetics model in [Kamal and Sourour, (1973)]:

$r_R = \left(k_1 + k_2\beta^m\right)(1-\beta)^n$, wherer $k_i = A_i \exp\left(-E_i / RT\right)$ and β is the resin cure extent.

Cure kinetics	Typical value
A_1	1.36×10^{28} s^{-1}
E_1	224.4 kJ/mol
A_2	1.25×10^{28} s^{-1}
E_2	223.0 kJ/mol
m	0.226
n	1.856
H_R	347.0 kJ/kg

If the permeability is of the order of 10^{-9} m^2, the Brinkman number is in the range of 0.01-0.1. Therefore, the viscous dissipation term is of marginal importance. In our presentation of operator splitting technique, this term is not included in the analysis. However, this term does not pose any special problem and may be addressed if it is important when permeability is very low.

The Peclet number computed, using the values in Table 1 and 2×10^{-4} m for d_p [Adams and Rebenfeld, (1987)], is 1. Since the dimensionless dispersion tensor is of the order of unity [Kaviany, (1991)], the dispersion term is of same importance as conduction. The dispersion term becomes more significant if the flow velocity is higher, but an efficient way to compute this term is yet to be developed. Therefore, this term is not included in the analysis and is not discussed when simulation results are presented. Both theoretical and numerical approaches for computing dispersion term are being investigated by the authors. This term can then be added to the conduction part, and we do not expect it to affect our proposed numerical scheme.

3. Numerical implementation for RTM simulation

An RTM simulation code LIMS (acronym for Liquid Injection Molding Simulation) has been developed at University of Delaware in the past [Liu, Bruschke and Advani (1994)].

7

The program solves a governing equation obtained by substituting Darcy's law into the continuity equation for two dimensions,

$$\nabla \cdot \left(\frac{1}{\eta} \mathbf{S} \cdot \nabla P \right) = 0. \tag{14}$$

Finite element method is used to solve for the pressure distribution with appropriate boundary condition of a prescribed pressure at the flow front, no flow through the walls and known pressure or flow rate at the inlet [Bruschke and Advani, (1990), Liu and Advani (1994), Bruschke and Advani, (1994)]. RTM is a moving boundary problem. In LIMS this moving boundary problem is treated as a series of pseudo-steady states as for low Reynolds number flows, inertia terms are insignificant.

Once the pressure distribution becomes available, a control volume approach is used to compute the moving boundary at the next time step. Pressure solution and flow front advancing are repeated until the mold is filled. More details about the method have been reported in [Liu, Bruschke and Advani (1994), Bruschke and Advani, (1994), Bruschke and Advani, (1990)].

The temperature distribution is obtained from solving eq. (1). The velocity information needed is calculated from the pressure distribution at the previous step by solving Darcy's law:

$$\mathbf{v} = -\frac{1}{\eta} \mathbf{S} \cdot \nabla P. \tag{15}$$

As mentioned before, the temperature solution must be solved for 3-D due to the importance of conduction in the thickness direction. For each pressure node, a number of temperature nodes are assigned. Program LIMS [Liu, Bruschke and Advani (1994)] uses a power distribution, $\zeta_i = (i/n)^\alpha$, for the temperature nodes, as shown in Fig. 3. If α is less than unity, the temperature nodes are more concentrated near the wall.

When solving eq. (1) numerically, it is assumed that heat conduction is negligible in the flow direction and advection is negligible in the through thickness direction.

The boundary condition may be stated in general terms [Bruschke and Advani, (1994)],

$$\left(\frac{\partial T}{\partial z} \right)_w = C(T_\infty - T_w), \tag{16}$$

which models the typical mold heating configuration shown in Fig. 4. The mold has a heating pipe at a distance a from the inner wall of the mold platen. The pipe is heated with a fluid at temperature T_∞. The constant for boundary condition, eq. (16), can be computed from

8

$$C = \frac{1}{k} \frac{1}{\frac{1}{h_h} + \frac{1}{h_m} + \frac{a}{k_m}}, \tag{17}$$

where h_h is the heat transfer coefficient between heating fluid and the pipe, h_m is the heat transfer coefficient between resin and the mold wall, and k_m is the heat conductivity of the mold material. The above boundary condition is versatile and different values of C lead to different boundary conditions ranging from adiabatic condition ($C=0$) to constant heat flux (finite C) to constant boundary temperature ($C \to \infty$).

4. Operator splitting technique

A general advection diffusion equation can be solved by using operator splitting techniques. The basic concept behind this technique is to split the updating of the unknowns into several steps. This technique is not limited for advection diffusion equations, any partial differential equation can be solved by this technique if it can be written in the form of

$$\frac{\partial u}{\partial t} = \sum_{i=1}^{n} f_i(u), \tag{18}$$

where u is any unknown dependent variable, and f_i's are functions of u. While this technique can be implemented in many ways (see [Marchuk, (1982)] for more detail), in this work the following procedure is used. The solution starts from

$$u = u^k, \quad \text{at} \quad t = t^k. \tag{19}$$

The terms on the right hand side are incorporated sequentially:

$$u^{k+i/n} = u^{k+(i-1)/n} + \Delta t \cdot f_i\left(u^{k+(i-1)/n}\right). \tag{20}$$

Each of above step incorporates one term (or a combination of terms, if so chosen). Here the notation i/n merely denotes the i-th step in the updating. It does not mean the current step to be a fraction of the time step Δt. More discussion is given later in this section when the operator splitting technique is applied to the energy balance equation for RTM processes. Equations (19) and (20) constitute the predictor of the technique. If better accuracy and stability are desired, following corrector can be used:

$$u^{k+1} = u^k + \Delta t \cdot \sum_{i=1}^{n} f_i\left(u^k\right). \tag{21}$$

Equation (3) can be rewritten into the form of Eq. (18) by moving the advection term to the right hand side and ignoring the inplane conduction, we get:

$$\frac{\partial \Theta}{\partial \tau} = -Gz(\mathbf{u} \cdot \nabla \Theta) + \nabla \cdot (\mathbf{I} + \mathbf{k}) \cdot \nabla \Theta + Da\, r + Br\left(\mathbf{u} \cdot \mathbf{K}^{-1} \cdot \mathbf{u}\right) + Pe\nabla \cdot \mathbf{T} \cdot \nabla \Theta. \qquad (22)$$

Advection, conduction, etc., are the f_i's which can be incorporated one term at a time. Theoretically, these terms can be incorporated in any order [Marchuk, (1982)]. However, from our past experience, it has been found that explicit marching scheme does not provide satisfactory temperature solution. It was necessary to use a small time step to obtain stable temperature solution [Bruschke and Advani, (1994)]. Thus, it is desirable to construct a more stable scheme when this operator splitting technique is implemented. This is achieved by following two rules:

1. the f_i's on the right hand side are incorporated in an order that the linear terms are handled implicitly at the end ;

2. the corrector, eq. (21), is used to make the whole scheme pseudo-implicit.

For equation (22), the conduction term is the last one to be incorporated, implicitly. The remaining terms are non-linear and are incorporated explicitly to save computation time.

To demonstrate this scheme, we further simplify eq. (22) into

$$\frac{\partial \Theta}{\partial \tau} = -Gz(\mathbf{u} \cdot \nabla \Theta) + \nabla^2 \Theta + Da\, r. \qquad (23)$$

Here we neglected the viscous dissipation and thermal dispersion terms. When the dispersion term becomes significant, it can be treated explicitly like the conduction term. The non-linearilty in the viscosity due to its temperature dependence should not cause any special problem and can be implemented in the non-linear terms explicitly. The interfacial heat flux term, $\nabla \cdot \mathbf{k} \cdot \nabla \Theta$, is not considered since it involves simulation on a micro scale. An efficient way of approximating this term is being investigated by the authors.

On the right hand side of eq. (23), the heat of reaction term is nonlinear because of the functional dependence of reaction rate on temperature, as given in Table 2. The other two terms are linear functions of Θ. However, we opt to incorporate the advection term explicitly. This is because the computation of $\nabla \Theta$ involves Θ's at neighboring nodes in plane. To compute this term implicitly is computationally expensive. For conduction term, if we assume that heat conduction in plane is negligible, it involves Θ's at only one node and can be handled implicitly.

The solution procedure of our scheme is as follows:

$$\Theta = \Theta^k, \quad \text{at } \tau = \tau^k. \qquad (24)$$

The three terms on the right hand side of eq. (23) are incorporated in the following order:

$$\tilde{\Theta}^{k+1/3} = \Theta^k - \Delta\tau \cdot Gz\left(\mathbf{u} \cdot \nabla \Theta^k\right), \qquad (25)$$

$$\tilde{\Theta}^{k+2/3} = \tilde{\Theta}^{k+1/3} + \Delta\tau \cdot Da\, r\left(\tilde{\Theta}^{k+1/3}\right), \qquad (26)$$

$$\tilde{\Theta}^{k+1} = \tilde{\Theta}^{k+2/3} + \Delta\tau \cdot \nabla^2 \tilde{\Theta}^{k+2/3}. \qquad (27)$$

10

The last step is subject to the boundary condition, eq. (16). In eqs. (25-27), the notation *i/n* denotes the *i*-th step in the updating and has nothing to do with the time step $\Delta\tau$. Based on the fact that the temperature rise is due to the contribution form three terms: advection, heat of reaction and conduction, the idea of this technique is to account the contribution of one term at one updating step. Therefore, after each step, a better estimation of the future temperature is obtained and is used for the next updating step. This process is carried until all the terms are accounted for. Equations (25-27) form the predictor of the method. The corrector is given by:

$$\Theta^{k+1} = \Theta^k + \Delta\tau \cdot \left[-Gz\left(\mathbf{u} \cdot \nabla\tilde{\Theta}^{k+1}\right) + \nabla^2\tilde{\Theta}^{k+1} + Da\ r\left(\tilde{\Theta}^{k+1}\right) \right]. \tag{28}$$

This is done by repeating steps (25-27) but with different values of Θ. Corrector eq. (28) can be used repeatedly for a certain number of iterations or until a convergence has been reached.

This temperature solver has been implemented in LIMS. The temperature solver is fully modularized in the program. Each of the terms contributing to the energy balance is incorporated separately, with a separate subroutine. The different terms can be incorporated in an order suitable for the problem being solved except that the conduction term must be incorporated last. Therefore, the accommodation of additional terms, the dispersion term as an example, poses no special problem.

5. Simulation results and discussion

Comparison of the numerical temperature solution with an analytical solution.

In order to verify the numerical method, we opt to compare its solution with available analytical solution. The analytical temperature distribution is obtained for following liquid flow and heat transfer system:

Liquid flows in between two parallel plates of infinite width and semi-infinite length. The flow is a plug flow entering from the edge located at the origin of the axis in the length direction. The plates are kept at a constant temperature while the influx of liquid is at a lower constant temperature.

For such an idealized problem, the differential eq. (3) for temperature distribution can be simplified to:

$$\frac{\partial\Theta}{\partial\xi} = \frac{\partial^2\Theta}{\partial\zeta^2}, \tag{29}$$

with boundary conditions:

$\Theta = 1$, at $\zeta = 1$; $\Theta = 0$, at $\xi = 0$; and $\dfrac{\partial \Theta}{\partial \zeta} = 0$, at $\zeta = 0$. $\hspace{2cm}$ (30)

The dimensionless variables in the above are defined as

$$\xi = \frac{4x}{h^2 \overline{v}} \cdot \frac{k}{\rho C_p}, \hspace{5cm} (31)$$

$$\zeta = \frac{2z}{h}. \hspace{7cm} (32)$$

The analytical solution for this problem is [Bird, Stewart and Lightfoot, (1960)]:

$$\Theta = 1 - \frac{2}{\pi} \sum_{i=0}^{\infty} \left[\frac{(-1)^i}{i+1/2} \exp\left(-(i+1/2)^2 \pi^2 \xi\right) \cos\left((i+1/2)\pi\zeta\right) \right]. \hspace{1cm} (33)$$

Figure 5 is the comparison between the analytical solution and the numerical simulation. The simulation is done with a mesh of 21 equidistant points for ξ from 0 to 1 and 11 equidistant temperature nodes through the thickness, for ζ from 0 to 1, at each mesh point. For each step the flow field is advanced, two sub time steps are used to produce the solution shown in Fig. 5. The curves in the figure are obtained for four ξ values, 0.1, 0.25, 0.5, and 1. The maximum error in the solution is 0.04 which means the maximum error in the temperature solution is 4% of the temperature difference, $\Delta T = T_w - T_0$. The simulation is also done with different number of temperature nodes. With 6 temperature nodes, the error is larger, 6%, while no improvement is seen when 21 nodes are used. This means that the solution obtained with 11 nodes is the converged solution for the method with the given mesh for flow field computation.

Computational efficiency of the temperature solver.

This technique is numerically more efficient than the one used previously [Bruschke and Advani, (1994)]. This is because this technique is computationally explicit while providing stability of an implicit methods. First, this technique uses same time step as that of mold filling. It is no longer necessary to cut the time-step of mold filling into multi-steps for temperature solution as it was in [Bruschke and Advani, (1994)]. This is because that this technique is close to a stable backward Euler's method. This has resulted in a reduction of the computational effort approximately by a factor of five. Second, the previous technique needs to use Gauss-Seidel iterations at each temperature solution step [Bruschke and Advani, (1994)]. For the technique proposed in this work, iteration is not necessary because the nonlinear terms are incorporated explicitly. Even if the corrector is used iteratively, it usually converges to a tolerance of 0.01 K within 2 to 4 iterations (more discussion will be given later). Dependent on the specific problem being solved, the overall

12

reduction of computational effort spent on temperature solution is about a factor of ten with guaranteed convergence.

The case used for the comparison between numerical and analytical solutions is used again here to conduct a performance comparison. The simulation is done on an SGI Elan 4000 computer. The time spent on temperature solving is 3.09 seconds. The temperature solver presented in [Bruschke and Advani, (1994)] takes 22.16 seconds to complete the same task.

Convergence of the predictor corrector method.

Figure 6 is the convergence of the corrector. The horizontal axis is the iteration number with the predictor as the zeroth iteration. The vertical axis is the error which is normalized with the error of the predictor. The data shown in Fig. 6 are picked at different times of the simulation session for method verification presented earlier in this section. The absolute error in the temperature at each time step drops with each iteration, forms a straight line on the semi-log plot. From this fact it can be concluded that the predictor corrector method used with the operator splitting technique is of linear convergence, i.e.

$$\left\| T - T^{k+1} \right\|_\infty < m \left\| T - T^k \right\|_\infty , \tag{34}$$

where T is the converged solution for temperature and T^k is the temperature solution at k-th iteration of the corrector. Since for this iterative correction procedure, the convergence is only linear, the speed of convergence is solely dependent on the constant m. In the simulations, the constant m is normally around 0.1 as those lines in the lower part of Fig. 6 indicate. This means within two corrector iterations, the maximum error reduces to 1% of that of predictor. Less frequently we have seen that this constant m can get a value at around 0.3 as seen from the two lines in the upper part of Fig. 6. To reduce the maximum error to 1% of that of predictor, four corrector iterations are needed for this value of m.

A case study.

A simulation of an RTM process is done for a part shown in Fig. 7. The part is a flat panel of one meter long and one meter wide. The panel has three sections of different thicknesses. The center potion is of 1 cm thick while the edges are 0.2 m wide and 2 cm thick. The preform is isotropic with a porosity of 0.6 and a permeability of 10^{-7} m^2. The resin is injected from one edge, its viscosity is 100 cP. The thermal properties are: resin thermal diffusivity, 10^{-7} m^2/s, resin conductivity, 0.2 W/mK, preform thermal diffusivity, 10^{-6} m^2/s, and preform conductivity, 1 W/mK. The resin is injected at 300 K and the

13

preform is heated to 350 K. The mold platens are kept at 350 K. To set this constant wall temperature, the boundary condition constant in eq. (16) is set to 5×10^5 /m

In order to obtain better temperature solution around the region where the thickness changes, the mesh used has three rows of mesh points around that region. The mesh consists of 11 rows of 11 equidistant mesh points, which gives a total of 121 mesh points. The rows are located at 0, 0.2, 0.29, 0.3, 0.31, 0.5 m from the center line in the flow direction. Associated with each mesh point are 21 equidistant temperature nodes through the thickness.

The first simulation was done with constant pressure at the injection gate. The injection pressure was 5×10^5 Pa. The simulation results for flow front development is shown in Fig. 8. Each contour line represents 6 s. It takes 60 s to fill the whole mold. The temperature solution obtained at the mid plane of the part is shown in Fig. 9. Each contour line represents 5 K. The results show that the temperature rises faster in the center portion of the panel where the part is thinner. If in-plane conduction was included, this jump would be smoother and one could expect faster convergence. Around the region where the thickness changes, the temperature exhibits sharp changes. This is due to the fact that heat conduction is neglected in plane. It is certainly necessary to account for the heat conduction in plane to simulate heat transfer problems with steep temperature gradient in plane. For parts without abrupt thickness changes, this technique is able to provide faithful solutions.

In the simulation, three temperature steps are used for each mold filling step. The temperature solution converges to a tolerance of 0.01 K in less than 5 corrector iterations. The simulation is done on the same SGI computer. The time spent on temperature solution is 3.60 seconds.

The simulation is repeated with constant injection rate boundary condition. All the conditions are the same as used in previous simulation, with one exception that the gate condition is a constant flow rate at 0.01 m^3/(s·m^2 gate area), i.e., at 1 cm/s linear velocity. This flow rate gives same total mold filling time as that of constant pressure simulation. The simulation result for flow front development is shown in Fig. 10. With regards to figures 8 and 10, it is worthwhile to note that unlike injection molding, the gapwise average velocity in RTM is independent of the gap thickness, hence the advancing fronts are straight even though the gap thickness is not uniform.

Each contour line represents 6 s. Note that the difference is that the contour lines are equidistant in this simulation, which is the expected result for constant flow rate. Because the flow development is different, it resulted in different temperature distribution. Figure 11 is the temperature solution obtained at the mid plane of the part. Each contour line

14

represents 5 K. It can be seen the temperature gradient in the left half of the part is less steep compared with the results of constant pressure simulation.

The temperature profiles are shown in Figs. 12 and 13. Figure 12 is the comparison of temperature profiles obtained at the mid plane of the thinner portion of the part. The profile is steeper for constant pressure case. Figure 13 is the comparison of temperature profiles obtained at the mid plane of the thicker portion of the part. The difference is less than that in the thinner portion. Flow with the constant pressure boundary condition is faster initially and as the mold approaches filled state, the flow velocity decreases. This advection effect can be contrasted with the constant flow rate case where the advection contribution is constant with time.

This type of detailed temperature distribution information is useful for the process design. It can be used to study the residual stress in the final part due to the temperature history, which in turn is the result of process conditions. In this example we assume that viscosity does not change much with temperature. Although one can account for this effect without any problem. Here the goal was to demonstrate the fast method to couple 2-D flow with 3-D heat transfer.

6. Conclusions

The newly implemented operator splitting technique is accurate and efficient. The accuracy of the technique comes from the predictor-corrector method. The corrector can be used until the required accuracy is reached. As we have shown, the corrector iteration converges fast. It is recommended that a corrector is used for most applications to achieve better accuracy. The efficiency of the technique comes form the splitting of linear and nonlinear terms and incorporate them in a correct order. The nonlinear terms are incorporated explicitly. This practice accelerate the computation significantly. The linear terms are incorporated implicitly. Although this requires solution of linear equation system, the computations are still very efficient. This is because, when it is assumed that the heat conduction is negligible in the plane, the linear equation systems for conduction term is small and involves only the temperature nodes at each mesh point. The numerical scheme was verified with an analytical solution and its convergence and efficiency were demonstrated. A case study was presented to emphasize its usage in situations where temperature distributions are important to the understanding of physics.

Acknowledgment

Nomenclature

Br   Brinkman number, eq. (12)

C_p heat capacity

D   dispersion tensor, see [Tucker and Dessenberger (1994)] for detail

Da   Damkohler number, eq. (11)

d_p particle diameter

Gz   Graetz number, eq. (10)

H_R heat of cure reaction

I   identity tensor

K   dimensionless permeability tensor, eq. (8)

k   dimensionless tensor for heat conductivity due to interfacial heat flux, see [10] for detail

$\overline{k}$ average heat conductivity, $\overline{k} = \phi k_l + (1 - \phi)k_s$

k_e heat conductivity tensor

Pe   Peclet number, eq. (13)

R   ideal gas constant

r   dimensionless cure reaction rate, eq. (7)

r_0 cure reaction rate of fresh resin at wall temperature

r_R cure reaction rate

S   permeability tensor

$\overline{s}$ characteristic permeability

T   dimensionless dispersion tensor, eq. (9)

u   dimensionless velocity, eq. (6)

ζ dimensionless distance from mid plane, eq. (32)

η viscosity

Θ dimensionless temperature, eq. (4)

ξ dimensionless axial location, eq. (31)

ρ density

τ dimensionless time, eq. (5)

ϕ preform porosity

16

References

Adams, K.L. and Rebenfeld, L. (1987): In-plane flow of fluids in fabrics: structure/flow characterization. Text. Res. J. **57**, pp.647-654 .

Advani, S.G., Bruschke, M. V. and Parnas, R. (1994): Chapter 12: Resin Transfer Molding. In Advani, S. G. (ed): Flow and Rheology in Polymeric Composites Manufacturing. pp 465-516. Amsterdam: Elsevier.

Babbington, D. Barron, J., Enos, J.H., Ramsey R. and Preuss, W. (1988): Evolution of RTM with vinyl-ester resins, Proceedings of the Fourth Annual ASM/ESD Conference on Advanced Composites, p.269 .

Bird, R.B., Stewart W.E. and Lightfoot, E.N.(1960): Transport Phenomena. New York:Wiley.

Bruschke, M. V. and Advani, S. G. (1994): A numerical approach to model non-isothermal, viscous flow with free surfaces through fibrous media. International Journal of Numerical Methods in Fluids. **19**, pp.575-603 .

Bruschke, M.V. and Advani,S.G. (1990): A finite element/control volume approach to mold filling in anisotropic porous media. Polymer Composites. **11**, p. 398.

Coulter,J.P. and Guceri, S.I. (1988): Resin impregnation during the manufacturing of composite material subject to prescribed injection rate. Journal of Reinforced Plastic Composites. 7, p. 200.

Fracchia, C.A., Castro, J. and Tucker III, C.L. (1989): A finite element/control volume simulation of resin transfer mold filling. Proceedings of the American Society for Composites Fourth Annual Technical Conference. pp. 157-164 .

Kamal, M.R. and Sourour, S. (1973): Kinetics and thermal characterization of thermoset cure. Polymer Engineering and Science. **13**, pp.59-64 .

Lin, R., Lee L.J. and Liou, M.J. (1991): Non-isothermal mold filling and curing simulation in thin cavities with preplaced fiber mats. International Polymer Processing. **6**, p. 356.

Liu, B. and Advani, S.G.(1994): Modeling and simulation of resin transfer molding (RTM)-gate control, venting and void formation. submitted to J. of Composites Manufacturing.

Liu, B., Bruschke, M. V. and Advani, S.G.(1994): Liquid Injection Molding Simulation- LIMS User's Manual- Version 3.0. Center for Composite Materials Report no . 94-18. University of Delaware, Newark, Delaware.

M. Kaviany, (1991): Principles of Heat Transfer in Porous Media New York:Springer-Verlag.

Marchuk, G.I. (1982): Methods of Numerical Mathematics. (New York: Springer-Verlag.

Molnar, J. A., Trevino L. and Lee, L.J. (1989) :Liquid flow in molds with prelocated fiber mats. Polymer Composites. **10**, p. 414 .

Scott, F.N. (1988): Processing Characteristics of Polyester Resin for the Resin Transfer Moulding Process. Ph.D. Thesis, University of Nottingham. England.

Subbiah, S., Trafford D.L. and Guceri, S.I. (1989): Non-isothermal flow of polymers into two-dimensional, thin cavity molds: a numerical grid generation approach. International Journal of Heat and Mass Transfer. **32**, p. 415 .

Tucker III, C.L. and Dessenberger, R.B. (1994): Chapter 8: Governing equations for flow and heat transfer in stationary fiber beds," In Advani, S. G. (ed): Flow and Rheology in Polymeric Composites Manufacturing. pp. 257-324. Amsterdam: Elsevier.

Figure Captions

Figure 1 Schematic of resin transfer molding process.

Figure 2 Schematic of a thin-shell RTM part.

Figure 3 Temperature nodes associated with each mesh point for flow calculation.

Figure 4 Schematic of an RTM mold heating configuration.

Figure 5 Comparison of the temperature solution of the numerical simulation with the analytical solution. Solid lines are results of analytical solution and open diamonds are results of numerical simulation. Results are shown for different values of dimensionless axial location, ξ.

Figure 6 Convergence of the corrector used for operator splitting scheme.

Figure 7 Schematic of a part with different thicknesses.

Figure 8 Numerical solution of the flow front development. Resin is injected from the inlet (left edge) at constant pressure of 5×10^5 Pa and each contour line represents 6 s. The mold is filled in 60 s.

Figure 9 Numerical solution of the temperature distribution at the mid plane of the part at the time the mold is filled. The injection pressure is constant at 5×10^5 Pa. Temperature is 300 K at the inlet (left edge) and each contour line represents 5 K temperature rise.

Figure 10 Numerical solution of the flow front development. Resin is injected from the inlet (left edge) at constant flow rate at 1 cm/s and each contour line represents 6 s. The mold is filled in 60 s.

Figure 11 Numerical solution of the temperature distribution at the mid plane of the part at the time the mold is filled. The injection flow rate is constant at 1 cm/s. Temperature is 300 K at the inlet (left edge) and each contour line represents 5 K temperature rise.

Figure 12 Numerical solution of the temperature at the mid plane of the thinner portion of the part at the time the mold is filled. The solid curve is the temperature profile obtained for constant pressure injection condition and the dashed curve is the temperature profile obtained for constant injection rate.

Figure 13 Numerical solution of the temperature at the mid plane of the thicker portion of the part at the time the mold is filled. The solid curve is the temperature profile obtained for constant pressure injection condition and the dashed curve is the temperature profile obtained for constant injection rate.

Vent

Resin

Fig 1

Fig 2

Mesh for pressure solution

Nodes for temperature solution

Fig. 4

Fig 5

Dimensionless distance from mid plane, ζ

Dimensionless temperature, Θ

1.0

0.5

0.25

ξ=0.1

Fig 6

Corrector iteration number, k

Error, $|\tau - \tau^k|_\infty / \|\tau - \tau^0\|_\infty$

Fig 7

0   **24**   **48**

Fig 8

300   **320**   **340**

Fig 9

0   24   48

Fig 10

300   320   340

Fig 11

Fig. 2

Fig. 13
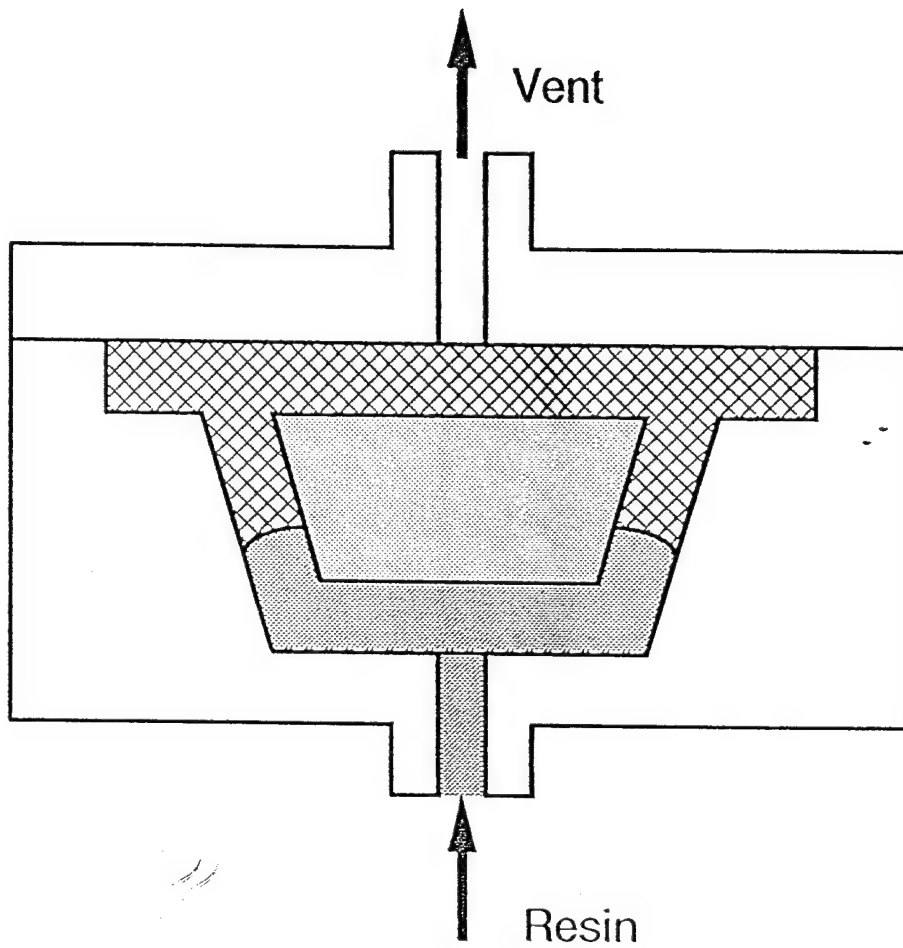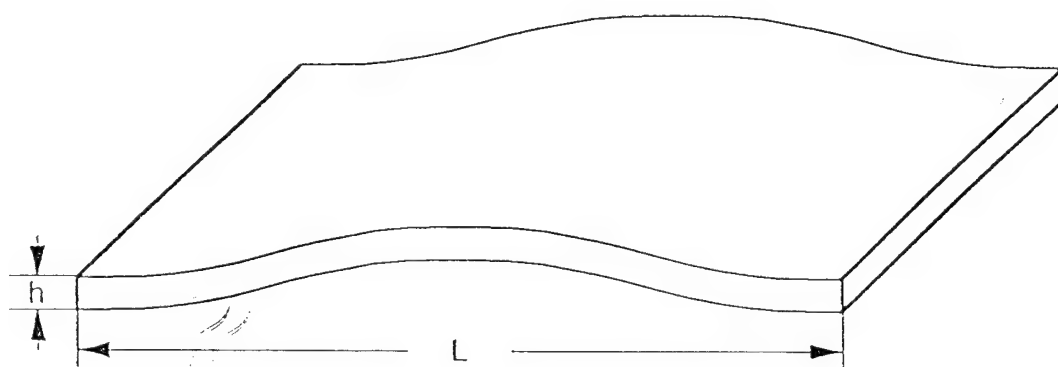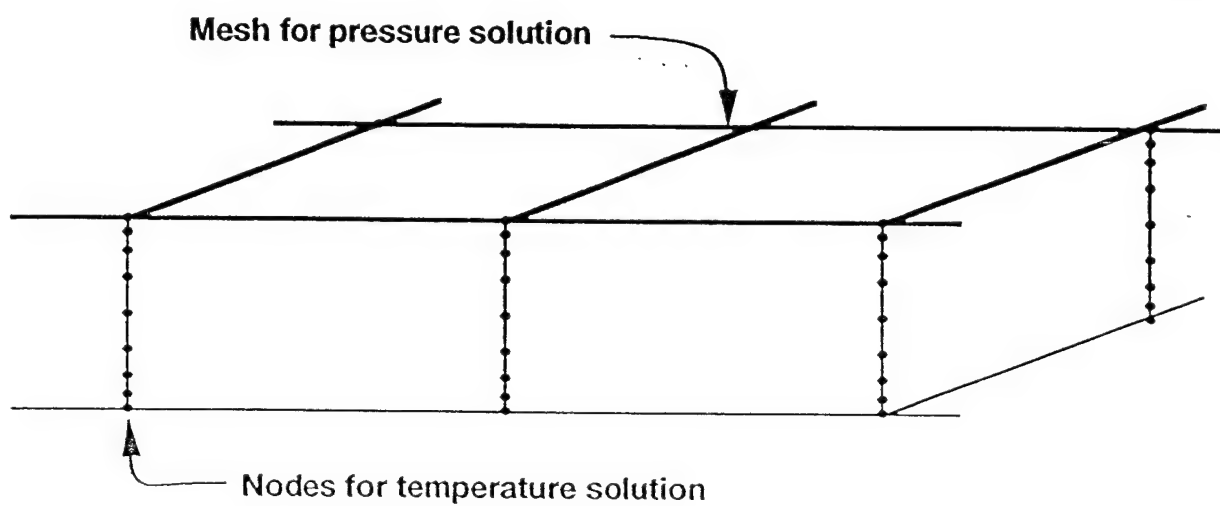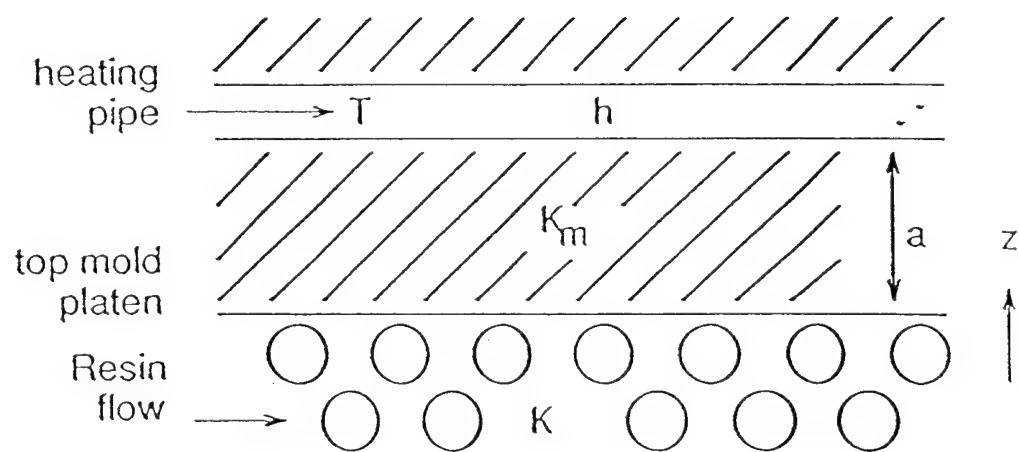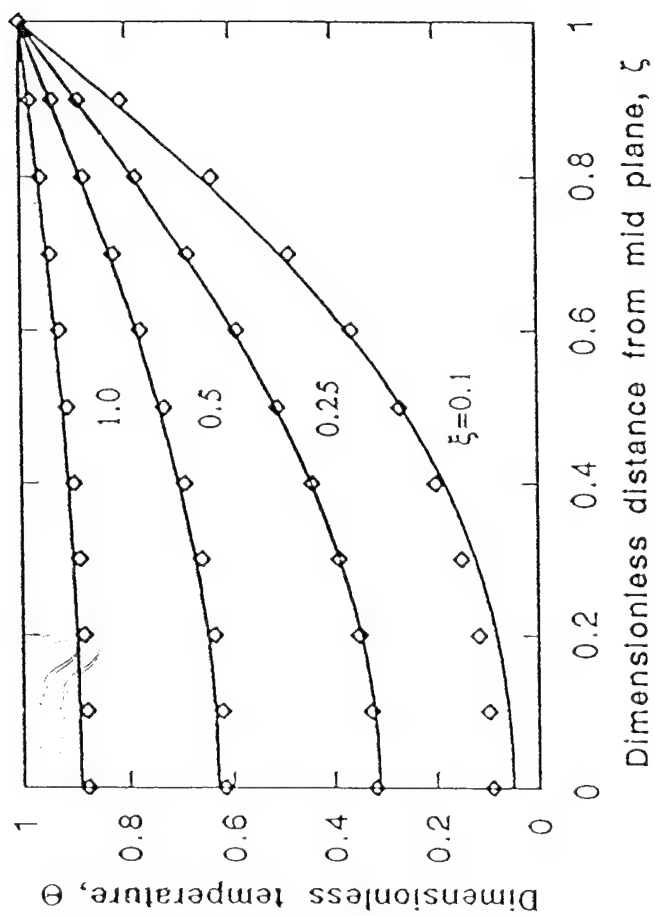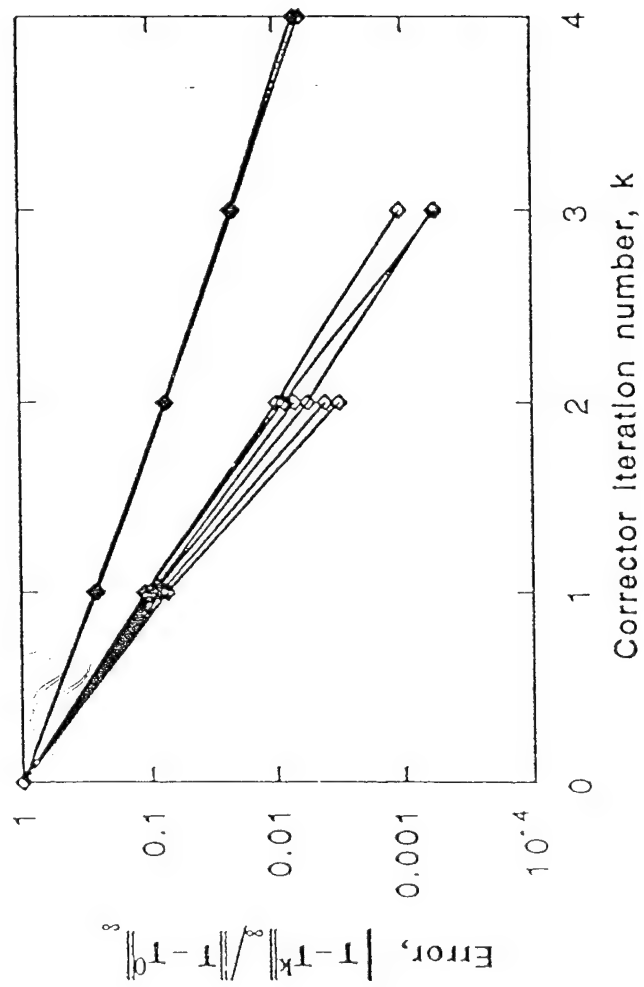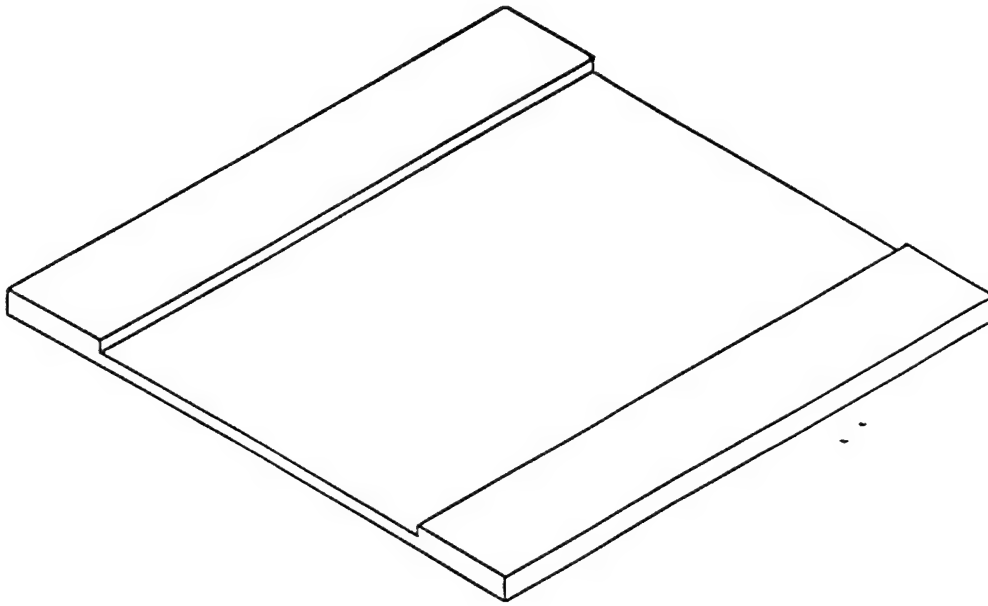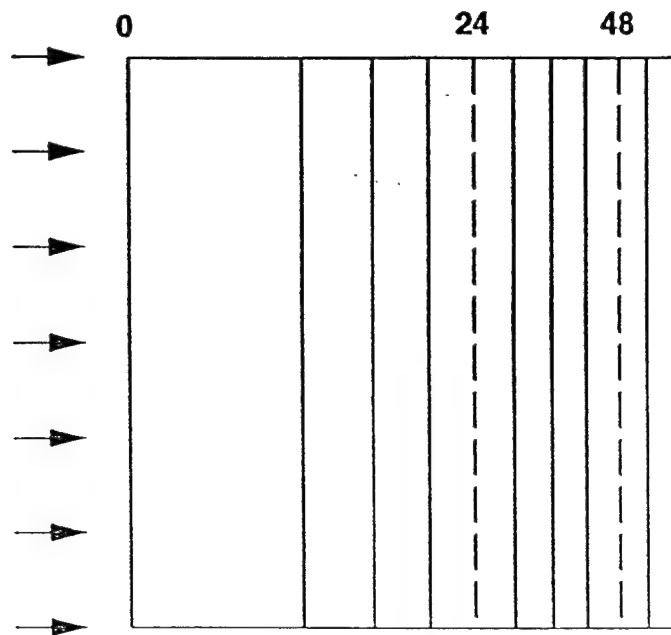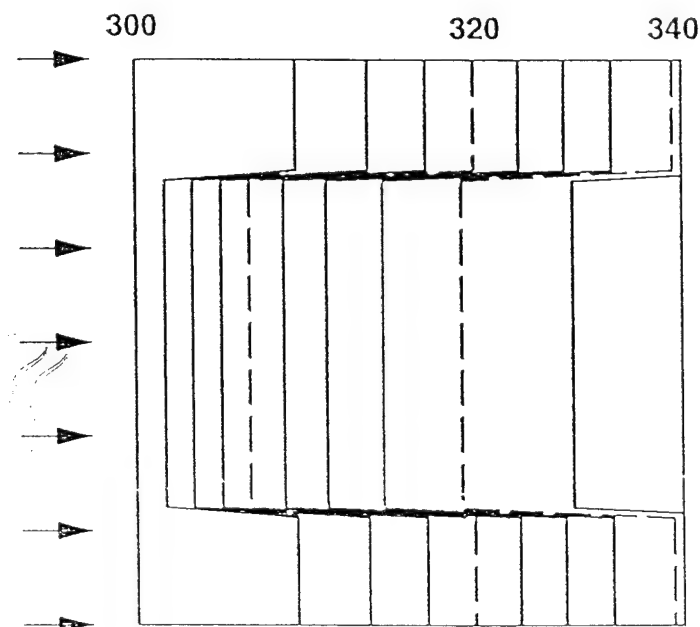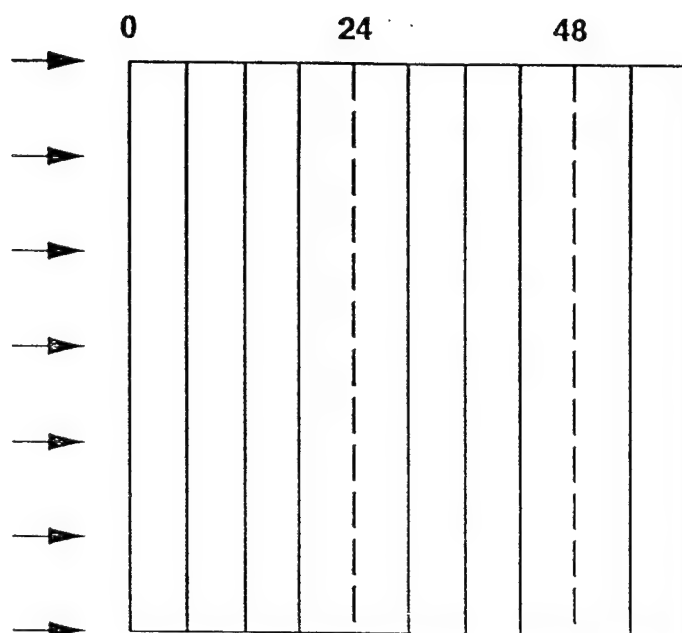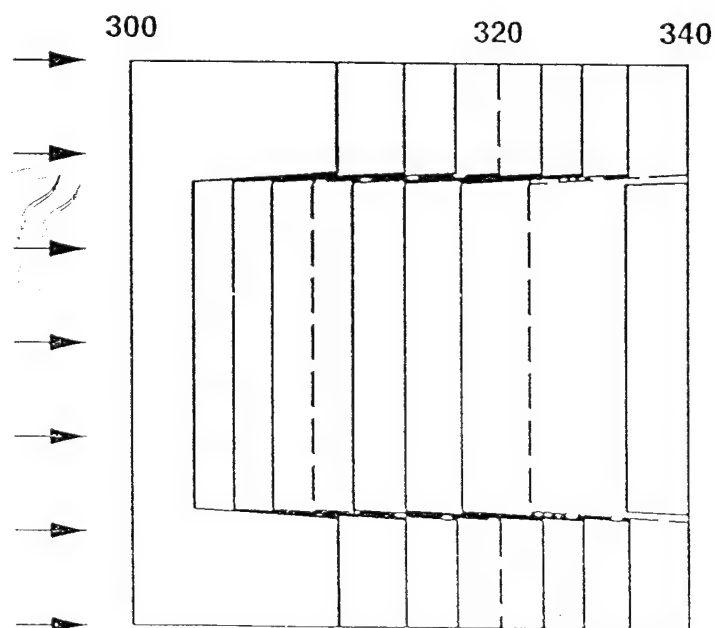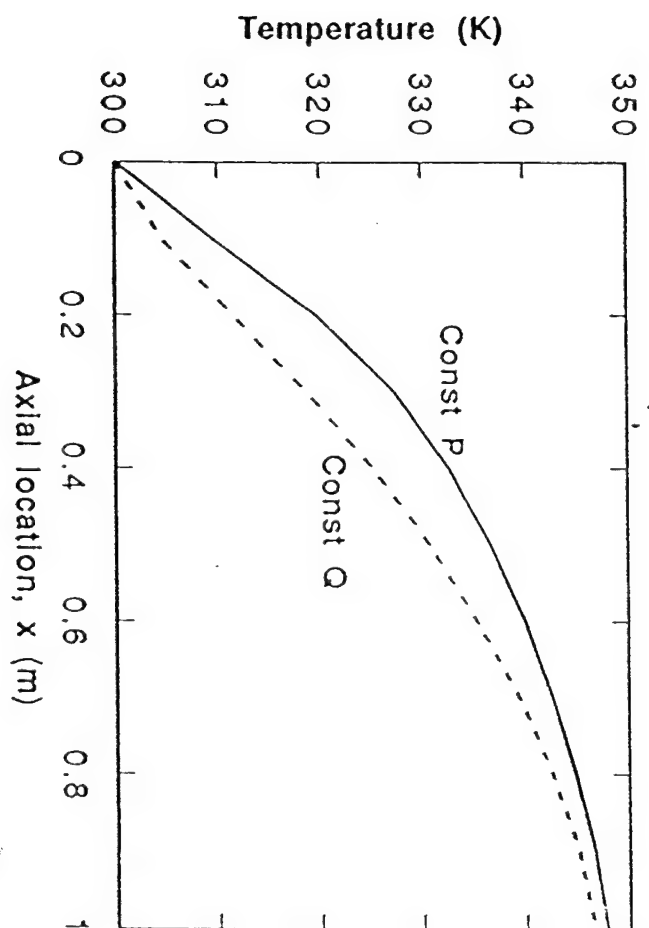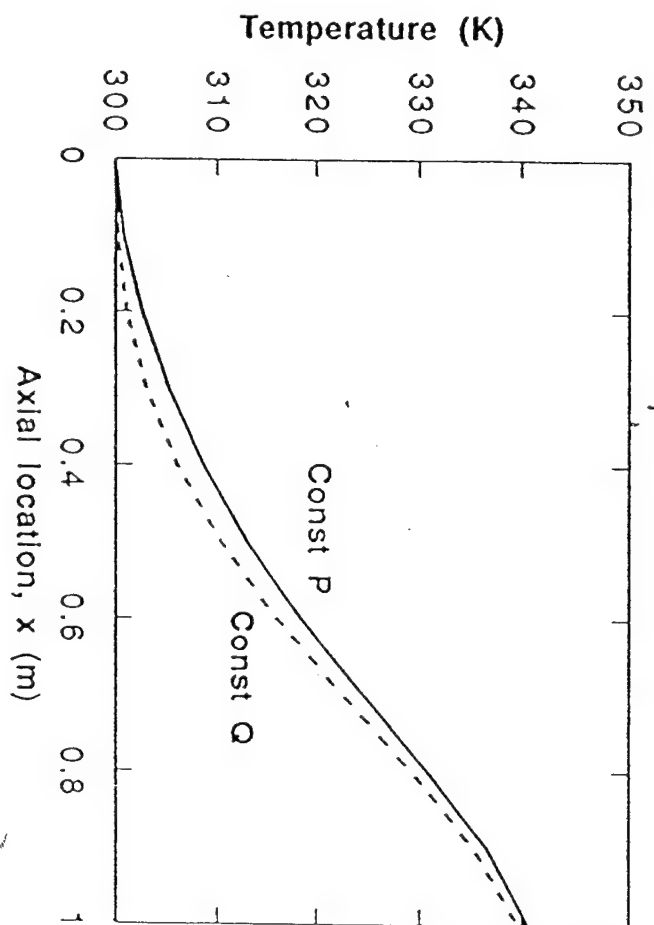
RTM: MODELING AND SIMULATION OF MOLD FILLING WITH INFLATABLE MOLDS

L. Lee Fong*and S. G. Advani[†]
University of Delaware
Newark, DE 19716

Kurt Fickie
Army Research Laboratory
Aberdeen Proving Ground, MD 21005

Abstract

Resin Transfer Molding (RTM) is a preferred method to manufacture structural composites. Conventional RTM tools usually consist of rigid mold walls which makes it difficult to control the processes such as preforming and resin impregnation. As a result, the preform is either too dense in fiber volume fraction or too sparse that race tracking is induced [1, 2]. The flexible tooling is aimed at overcoming these issues. Resin Transfer Molding with flexible walls is made up of one rigid tool half and one flexible matched half. The flexible mold half is capable of deflating or inflating depending on the process requirement. In mold filling, the flexible mold wall is pressed against the rigid wall by a predetermined pressure. For example, during the mold filling stage, the mold can deform such that it enhances the flow. Upon completion or near completion of mold filling, the flexible tool can be further inflated to consolidate the composite component. Other advantages include its capability to mold complex parts with one rigid mold half, less machining, easy demolding, and short cycle times. A deformation model for the flexible tool will be introduced in this research. The preform is described as a nonlinear spring. This model is implemented into a computer code, known as SLIMS (Second-generation Liquid Injection Molding Simulation). The simulation can be used as an analysis tool in composite design to optimize the mold filling as well as gate/vent design. In addition to provide an alternative to manufacture difficult-to-mold parts, the results from this modeling and simulation of deformable mold walls will demonstrate that the RTM with flexible tooling provides better process controllability. The physical properties of the preform, i.e., porosity and permeability, change as a result of changing thickness during the process to enhance the resin flow. The model presented in this paper helps predict the flow front progression and mold pressure inside the deformable porous preform during the mold filling process. Results indicate that flexible mold can speed up mold filling and reduce injection pressure at the same time.

---

*Center for Composite Materials
[†]Department of Mechanical Engineering

Contents

List of Figures

List of Tables

1 Introduction

Resin transfer molding has developed into a preferred method to manufacture high performance parts. One benefit of this process is that it consolidates several complex three dimensional parts into one molded piece. The key to accomplish this is the tool design. The conventional mold materials are metals or polymers which have the necessary rigidity and machinability. However, for certain parts, solid metal is not an ideal choice for RTM tooling. From the processing point of view, reduction of pressure drop is beneficial. This provides a stable mold filling with less fiber washout. Figure 1 shows a comparison between the conventional and the flexible mold configurations.

On the other hand, from design point of view, to mold certain parts with difficult or impossible to demold geometry, a flexible mold wall is very desirable. While a hard tooling makes clamping and demolding difficult, flexible mold provides a convenient alternative for mold design of these types of parts. Figure 2 shows an example of possible features which are commonly found in airframes. In this design, one can easily see the small draft angle and the stiffeners which can make demolding difficult. Moreoever, the beads and inserts in the bulkhead of this frame are features that are impossible to mold using rigid molds.

In addition, the flexible mold design can save the cost of manufacturing half of the rigid tool. Flexible tool takes up large volume without adding much weight to the overall tool. It can also be used to form hollow cavities. Demolding is easy when the flexible bladder is deflated. The mold closure is accomplished by proper inflating. The design also reduces secondary operations such as bonding, fastening or machining. However, injection pressure should be limited by the

Matched mold with rigid halves
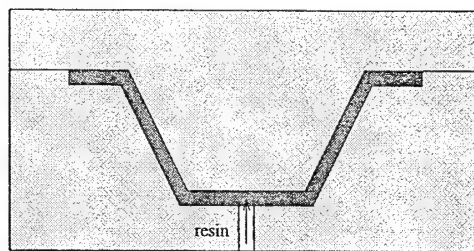
Matched mold with a flexible mold half
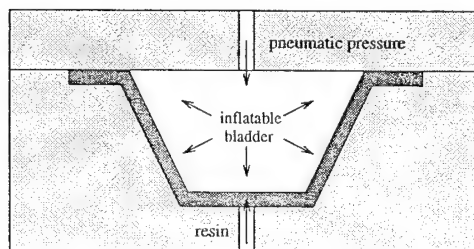
Figure 1: Conventional RTM tool versus flexible mold
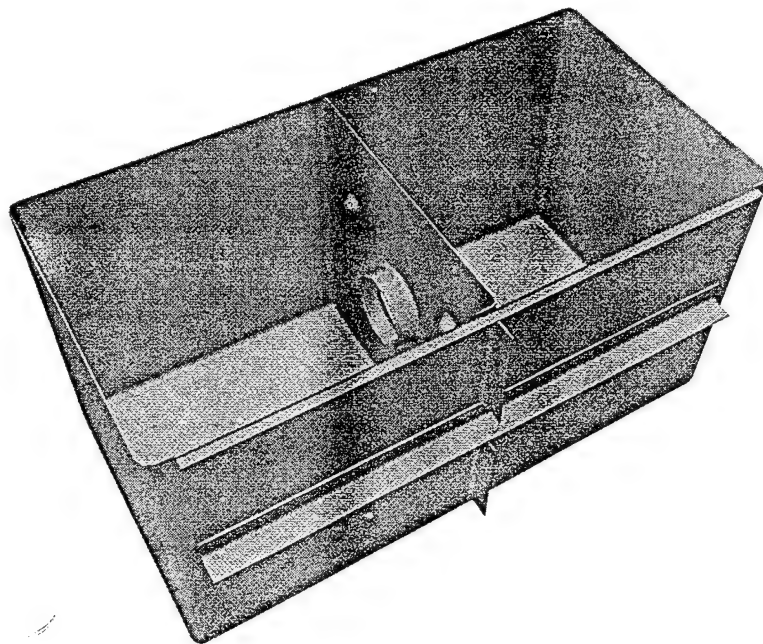
Figure 2: A structural part with various features commonly found in airframes

bladder pressure to avoid unconstrained gap thickness that can cause race tracking or channeling.

In studying RTM processes, many researchers have used numerical simulation. Many computer codes have been developed. To date, the available codes deal only the case of solid mold walls. The objective of this work is to propose a mathematical model for RTM with flexible wall boundary condition. The effect of flexible mold wall on processing will be investigated through numerical simulations.

2 Mathematical Modeling of Flexible Mold Wall

When a bladder is used as a means to form a cavity in the composite part, it is first under-inflated as the preform is loaded into the solid outer mold. Once the outer mold is closed, the bladder is inflated to the desired pressure before the resin is injected into the mold. The bladder inflation pressure is normally higher than resin injection pressure to avoid the bladder being pushed away from the preform to open up a flow channel. This situation may have its application in accelerating the mold filling. In this work, we only consider the case where bladder pressure is higher than that of the incoming resin. Different preform materials respond to this compression differently. A simple nonlinear spring model is proposed to depict the preform.

Since the bladder pressure is higher than the injection pressure, the preform is compressed by this pressure difference. The equation of motion for the bladder wall [3] can be written as:

$$-(p_b - p) = \rho b_t \frac{\partial^2 h}{\partial t^2} + D\frac{\partial h}{\partial t} + B\frac{\partial^4 h}{\partial x^4} + K(h - h_0) \tag{1}$$

where ρ, b_t, D and B are the density, thickness of the bladder wall, damping coefficient, and rigidity of the bladder material, respectively. K is the stiffness of the preform in the lateral direction. p is the resin pressure inside the preform, p_b is the bladder pressure. The thickness of the cavity, h, may vary during the filling process. When preplaced into the mold, the preform has a thickness ho when the bladder is inflated. The bladder is usually elastomeric and thin. Therefore, the first term on the right hand side of Equation 1 is negligible. Considering that the RTM process is a relatively

9

slow process, the time derivative in the second term on the right hand side is not significant. As the bladder is highly compliant and has a small rigidity, the third term on the right hand side may be neglected. Therefore, the simple form of this governing equation for RTM process using a bladder reduces to

$$- (p_b - p) = K(h - h_0) \qquad (2)$$

If the fiber preform deforms like an ordinary elastic spring, then corresponding load-deflection curve would be linear as depicted by the straight line in the figure. However, it should be pointed out that the stiffness of the preform, K, is not a constant in practice. This information can be obtained from the lateral compression tests of the fiber reinforcement material. The compressibility of preform has been studied elsewhere [4]. To account for the applied load-deflection effect of the preform, a nonlinear spring model will be used. The elastic constant of the preform, therefore, depends on the state of the preform. It is also worthwhile pointing out that the load-deflection response of fiber preforms may be sensitive to temperature. Therefore, temperature effect should be considered when the mold filling is non-isothermal. This is illustrated in Figure 3.

After transforming this relationship into a load-porosity curve as shown in Figure 4, one can readily determine the force exerted on the bladder by the preform based on the current gap thickness.

The porosity of the preform changes with the thickness. The relationship is:
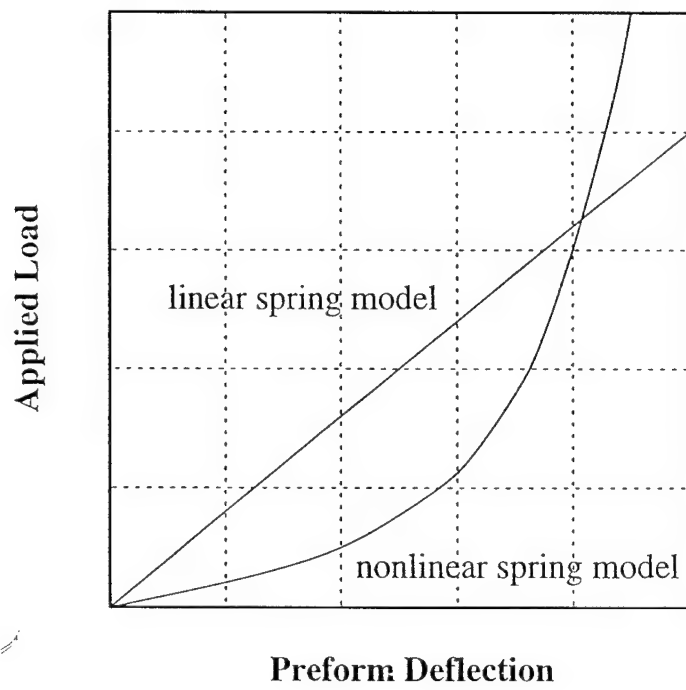
Figure 3: Applied load-deflection curve of a fiber preform
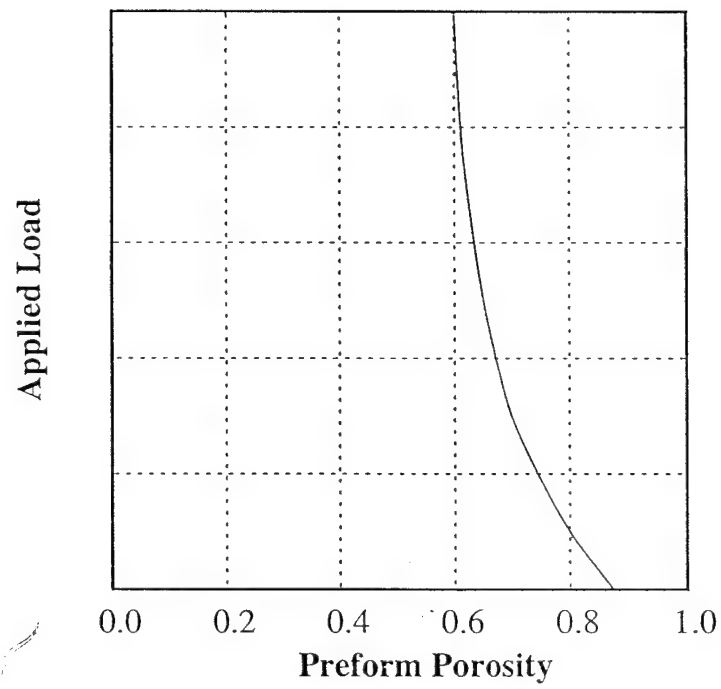
Figure 4: Applied load-porosity curve of a fiber preform

$$\phi = 1 - \frac{h_0}{h}(1 - \phi_0) \tag{3}$$

The preform permeability is generally a function of fiber architecture. The relationship used here is a simplified relationship for demonstration purpose [2].

$$k = c\frac{\dot{\phi}^3}{(1 - \phi)^2} \tag{4}$$

3   Mold Filling Simulation

Darcy's law for flow through porous media is used to relate the pressure and the resin flow in the preform. The generalized form of Darcy's law is

$$\vec{V} = -\frac{\bar{\bar{K}}}{\eta} \cdot \nabla P \tag{5}$$

where $\vec{V}$ is the superficial velocity of flow front, ∇P is the pressure gradient, and η is the fluid viscosity.

The fluid viscosity may be constant for Newtonian fluids or, for shear-thinning fluids, as a function of the pressure gradient. For steady, incompressible fluid flow, the continuity equation states that

$$\nabla \cdot \vec{V} = 0 \tag{6}$$

Substitution of (5) into (6) yields the elliptic equation

$$\nabla \cdot \left(\frac{\bar{\bar{K}}}{\eta} \cdot \nabla P \right) = 0 \tag{7}$$

which can be solved, along with appropriate boundary conditions, for the pressure. Boundary conditions along all boundaries (see Figure 5) are required. They are:

14

1. Along the mold wall or inserts the no-penetration conditions requires that the normal velocities are zero, or

$$\vec{V} \cdot \hat{n} = 0 \tag{8}$$

where $\hat{n}$ is the normal to the wall.

2. At the injection gates or inlets, two types of boundary conditions are provided - the pressure or the flow rate.

3. Along the flow front, the pressure is specified as the vent pressure in consistence with that of the vent.

A finite-element/control volume method [5, 6] is used for the filling simulation. The flow is assumed to be quasi-steady state. That is, the filling is assumed to take place at each time step. The solution is marched forward in time after the pressure field in the mold is calculated by a finite element method where the fill factor, f, is greater than zero. Then, the computed pressure field is used to calculate flow rates across the many control volumes in the flow domain and hence advance the flow front. The time step for each quasi-steady state is calculated from the time taken to fill the next partially filled control volume. This ensures the stability of the solution obtained under the quasi-steady state assumption. This solution procedure is repeated until all the control volumes are filled.
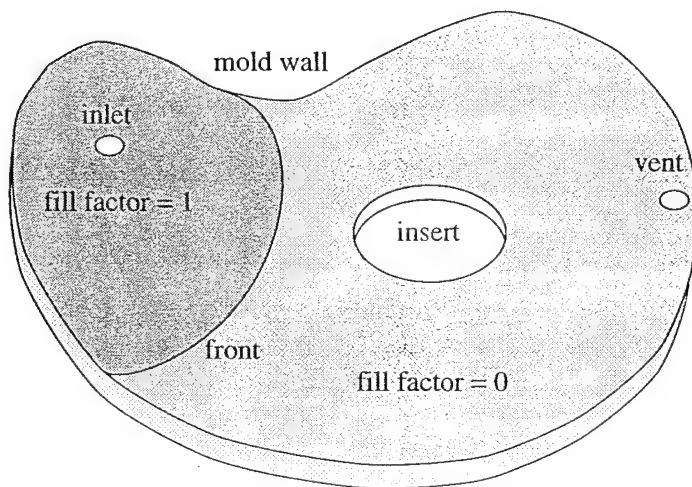
Figure 5: Boundary conditions in an injection mold with a flexible mold wall

Table 1: List of parameters in the one-dimensional mold filling simulation

injection BC	const pressure @ 0.55 MPa
cavity dimension	0.40 m x 0.10 m
gate type	line source
preform thickness	0.0016 m
porosity	0.55
resin viscosity	0.05 Pa*sec (50 cp)

4 Numerical solution and discussion

A finite element model will be used to demonstrate the mold filling simulation of the algorithm developed. The list of parameters used in numerical simulation is listed in Table 4. The model consists of 8 x 40 elements with the inlet located on one side of the 1-D mold. At the inlet, a constant pressure boundary condition is imposed.

Figure 6 is obtained from the numerical simulation of two cases: one with rigid walls and the other one with a flexible mold wall. From the case with rigid mold walls, the pressure drops linearly with respect to the flow distance. This is caused by the constant permeability of the preform inside the mold. The pressure curve for the case with flexible mold wall reflects the fact that the fluid flow in the filled region exhibits a smaller pressure drop. This reduction is beneficial to the molded parts as it causes less fiber washout and preform deformation due to the resin.

Figure 7 shows the result of computed gap thickness of the 1-D mold with flexible mold wall. The straight line show the thickness in a rigid tool. From this distribution, one can see that the gap height is a function of time during the filling process as well as a function of pressure. Near
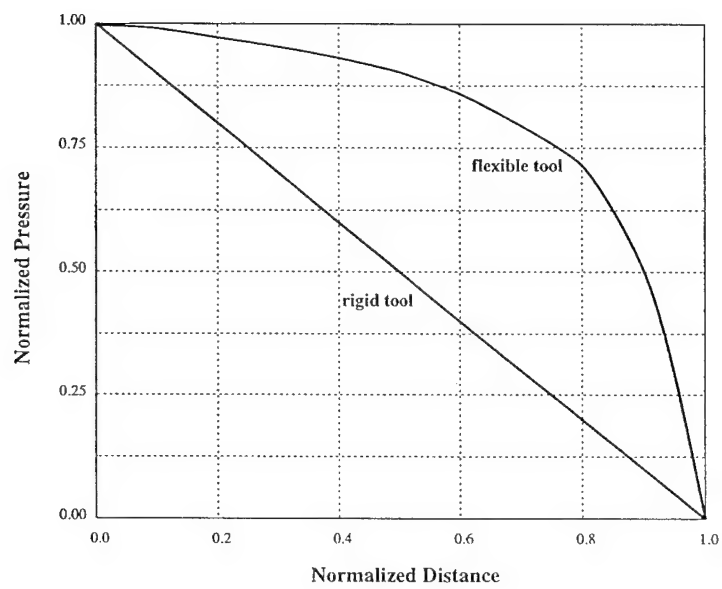
Figure 6: Comparison of pressure distribution

the injection gate, the resin pressure balances the applied pressure from the bladder and increases the gap thickness to its maximum in the 1-D mold. As a result, the resistance to the incoming flow has reduced significantly as shown in the previous figure.

Figure 8 shows the permeability calculated from a simple model. The same preform placed in a rigid mold has a permeability value of $7x10^{-11}$ or about 10 Darcy. After resin injection, the compliant preform expands and this value can increase by an order of magnitude. As a matter of fact, the filling time can decrease by the same order. However, the total volume in the mold increases due to the expansion of the cavity, an excess amount of fluid is necessary to complete the mold filling. This is reflected in the change of filling time from 64 sec. for the rigid tool to 9 sec. for the flexible one.
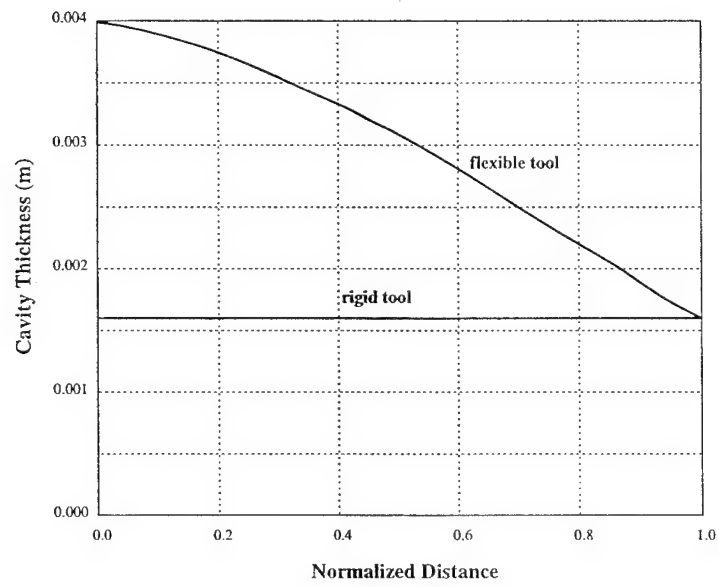
Figure 7: Comparison of gap thickness
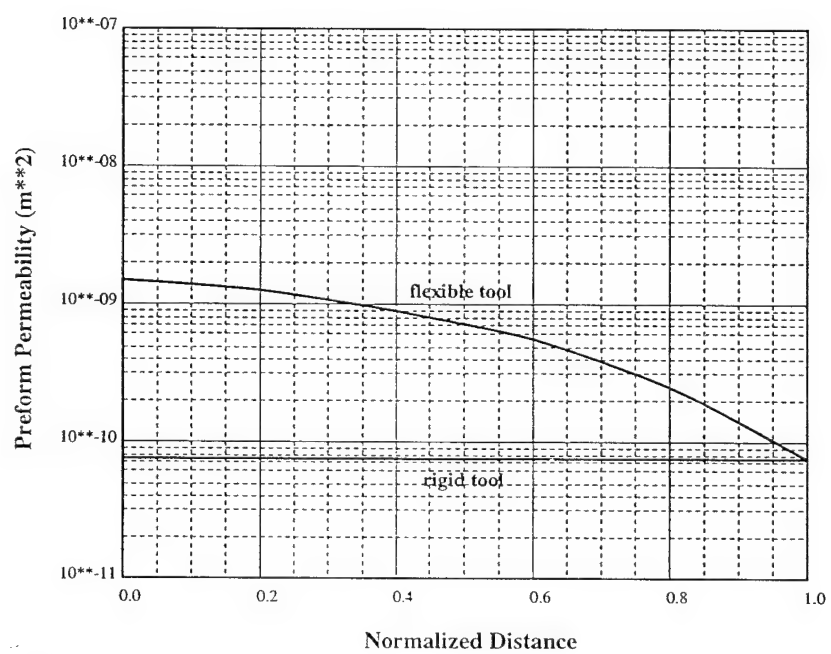
Figure 8: Comparison of permeability distribution

Table 2: Summary of the flexible mold filling of the one-dimensional mold

processing variables	parametric effect
filling time	9 sec (compared to 64 sec for rigid tool)
gap thickness	variable (0.0015 to 0.004 m)
fiber porosity	variable (0.55 to 0.83)
preform permeability	variable (10 Darcy to 100 Darcy)
pressure gradient at the gate	2.16 Pa/m (compared to 13.75 Pa/m)

5   Conclusions

Through the numerical study, the potential of the flexible tool design has been demonstrated. It has the advantage of reducing the pressure drop and overall filling time (see Table 5). This concept has been proven useful in molding an airframe structure where beads and inserts in the bulkheads render conventional tool design inapplicable.

Various effects may be now added into the simulation of the RTM at the current stage. For example, void entrapment due to inserts has been reported using the boundary condition at the vent [7]. The effect of different length scale in the fiber preform can be accounted for by solving the non-homogeneous working equation [8].

References

[1] M. V. Bruschke and S. G. Advani, *SAMPE Q.*, 1991, **23**, p. 2.

[2] L. Fong and L. J. Lee, *Journal of Reinforced Plastics and COmposites*, 1994, **13**, p. 637.

[3] A. D. Lucey and P. W. Carpenter, *J. Fluid Mech.*, 1992, **234**, p. 121.

[4] L. Fong, J. Xu, and L. J. Lee, *Polymer Composites*, 1994, **15**, p. 2.

[5] R. R. Varma and S. G. Advani, *Proc. of ASME Winter Annual Conference, Chicago, IL.*, 1994, , .

[6] B. Liu, M. V. Bruschke, and S. G. Advani, *CCM Technical Report, University of Delaware*, 1994, .

[7] B. Liu and S. G. Advani, *Proc. of the First ICCE Conference*, 1994, , p. 301.

[8] L. Fong and S. G. Advani, *Proc. of the First ICCE Conference*, 1994, , p. 17.

THE ROLE OF DRAPABILITY OF FIBER PREFORMS IN RESIN TRANSFER MOLDING

L. Lee Fong[*]and S. G. Advani[†]
University of Delaware
Newark, DE 19716

Kurt Fickie
Army Research Laboratory
Aberdeen Proving Ground

Abstract

Application of woven fiber mats in fabricating preforms for resin transfer molding (RTM) is a highly viable means of manufacturing affordable composites. Such light weight composites, having good mechanical properties, are being used in primary airframe structures in the aerospace industry. The success of RTM molded parts is largely determined by the filling process. Preform permeability plays an important role in the physics of mold filling process. In general, the preform permeability is a function of the fiber tow and mat construction. Drape, in this report, refers to the act of bringing a flat workpiece into contact with an arbitrary tool surface. As a result, the draping of the woven mats tends to cause the mat to deform to the tool geometry. This effect has received little attention in the literature. This paper takes into account the role of drapability of fiber mats in the manufacturing process. It has been shown that drape of mats causes the fiber orientation to change and the fiber volume fraction to be inhomogeneous. Results demonstrate the use of a geometry-based computation scheme in predicting the fiber volume fraction as well as the deformation. Permeability of the draped preform can be estimated through previously developed models and the influence on the flow of resin and processing parameters is also shown through a case study. It is found that the prediction of pressure inside the mold is no longer intuitive when the influence of draping is not negligible.

[*]Center for Composite Materials
[†]Department of Mechanical Engineering

1

Contents

List of Figures

List of Tables

1 Introduction

Resin Transfer Molding (RTM) is an economic process for producing polymer matrix composites. RTM offers several significant advantages over conventional composites manufacturing processes [1]. Among these advantages, RTM allows fabrication of large structural components in short cycle times. This is accomplished by the use of fiber preforms. Preforms allow fast and precise fiber placement. Recently the spectrum of RTM applications has been extended to airframes. The current work is focused on issues in resin transfer molding of primary airframe structures.

The fiber reinforcements usually come in the form of mats. Draping refers to the act of casting a flat piece of mat into a desired shape. Preforming through draping of the mats offers a number of advantages over traditional fiber placement techniques. These include short fabrication time and the process allows automation in mass production.

For bi-directional mats, woven or stitched, draping an arbitrary tool surface depends on two deformation modes. They are shear deformation and inter-yarn slip [2]. A mat of this nature is treated as a net that consists of many cells [3]. Therefore, draping over a surface of double curvature requires the net to map on the surface by changing the internal angles in each cell. This kinematic model is justified by the fact that the contact of fiber mats with the tool surfaces is often assisted by matched mold halves or diaphragms. With the normal support, the cross-over point of warp and weft tows becomes a pivoting joint. The four sides of a cell are made up of fiber tows. These tows, under the preforming condition, are inextensible. At high deformation regions in a preform, slippage may be necessary to drape the tool surface. The length of cell segment can

be changed as a result of slippage to accommodate for this effect. Normally the length of the cell segment will increase as a result of inter-yarn slippage.

The purpose of the current work is to relate the draping of mats to the molding process. This has a twofold significance. First, draping analysis serves to assess the formability of a preform over a given geometry. High shear deformation in a preform can cause out-of-plane deformation. This deformation, or buckling, can result in wrinkles or folds. This can be predicted given the lock angle of the cell, which indicates the onset of the out-of-plane buckling. Additionally, the fiber orientation as well as fiber volume fraction is obtained from the draping analysis. Second, in order to predict the moldability of a part, a computational tool has been developed. However, the vital parameter required to simulate the resin flow inside a fiber preform is permeability. This quantity is often obtained from flow visualization and measurement of raw stock mats. The values obtained from the experiments are used in the computational tool to simulate flow in a complex mold. This may result in inaccurate prediction of flow front patterns. As a consequence, expensive preforms and defective parts are scraped in numerous trial runs and some tools even need to be redesigned.

This report briefly reviews the shear model adopted for bi-directional fabric. From this, we obtain effective permeability through superposition. In a case study, we first perform a draping analysis. This analysis is intended to find out the geometry-dependence of the preform permeability. Then a liquid molding simulation that requires permeability as an input variable is used to study the influence of deformation on flow. Results from the draping analysis show that fiber volume fraction becomes inhomogeneous and fiber orientation change resulting in permeabilities that also change in magnitude and direction. Through the mold filling simulation, we further demonstrate that if the

preform property change is taken into account, it does result in flow front patterns different from those when preforming-induced deformation is ignored. A qualitative study will show the mold cavity pressure as well as the inlet pressure will deviate significantly from the predicted values when the changes in preform properties are ignored.

2 Integrated Simulation

Let the tow segment lengths of a bi-directional fabric be r_{warp} and $\boldsymbol{r_{weft}}$. These two quantities will depend on structure of the fabric and the degree of shearing each cell of the fabric. In order to map the two-dimensional fabric over a three-dimensional tool geometry in a piecewise linear manner, the following assumption must hold. This assumption requires that the r_{warp} and r_{weft} are chosen such that

$$r_{warp} \ll \rho_{min} \tag{1}$$

$$r_{weft} \ll \rho_{min} \tag{2}$$

where ρ_{min} represents the smallest radius of curvature of the tool geometry. This assumption ensures that details of the tool surface are not smoothed out. In this scheme, a smaller tow segment length can help improve the accuracy.

Consider a cell unit as shown in Figure 1, the unknown position of joint (m+1, n+1) can be uniquely determined given that the rest of the three joints are known. This is achieved by solving for the loci of all possible joint location, which is the equation of a sphere of radius r_{warp} centered at the joint (m+1, n).

$$\|p(m + 1, n + 1) - p(m + 1, n)\| = r_{warp} \tag{3}$$

9
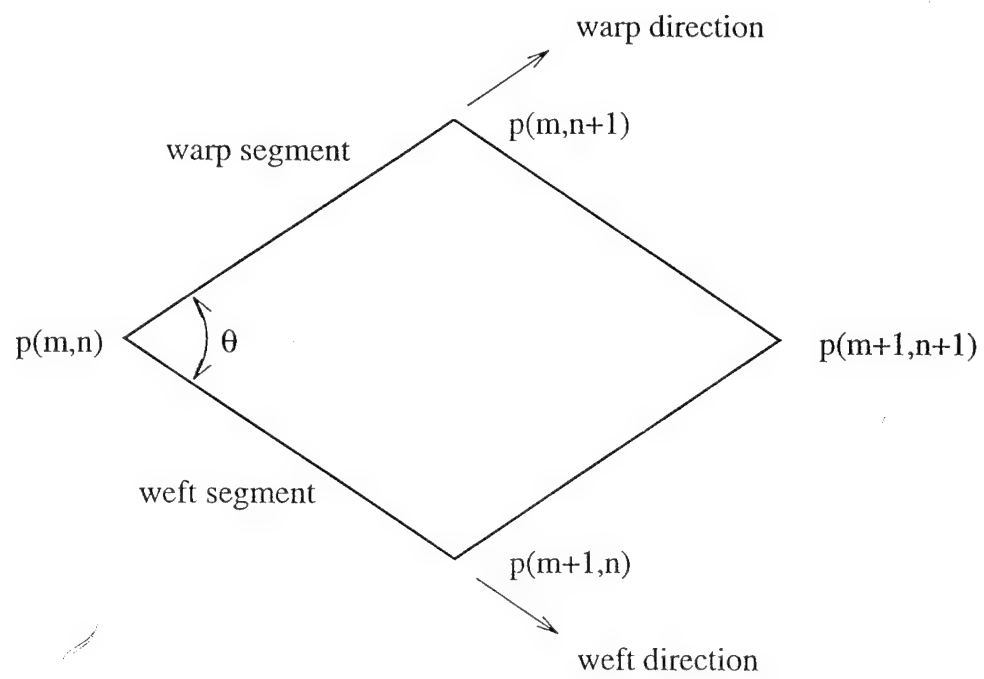
Figure 1: A deformed unit cell in a bi-directional reinforcement fabric

where r_{warp} is a function of the internal angle of the cell at joint $p(m, n)$. Likewise, one can formulate the loci of the sphere stemming from joint position $p(m, n+1)$ as in Equation (4). Note that each of the $p(i, j)$ in the above equations is a three-dimensional position vector. With three unknowns, an additional equation is needed to solve for the new joint position $p(m+1, n+1)$. This equation can be found from the tool surface.

$$\|p(m+1, n+1) - p(m, n+1)\| = r_{weft} \tag{4}$$

To represent the tool surface in a single mathematical equation is, in most cases, rather formidable. Therefore, surface tessellation is often needed. Conventional finite element mesh or curved surface patch may be used to discretize the geometry Γ into smaller and more manageable units S_i. Each S_i is a facet or a curved surface patch used to piece together the tool surface. Therefore,

$$\Gamma = S_1 \cup S_2 \cup \ldots \cup S_n \tag{5}$$

As mentioned, S_i can take a form ranging from triangular finite elements to curved surface patches. If the S_i is a bicubic spline surface patch [4, ?] defined in terms of two parametric variables u and v, then each cell can be represented in the following form

$$S_i = U \ M \ B_i \ M^T \ V^T \tag{6}$$

11

$$U = [u^3 \; u^2 \; u \; 1] \qquad\qquad (7)$$

$$V = [v^3 \; v^2 \; v \; 1] \qquad\qquad (8)$$

where M is transformation matrix, M^T is the transpose of M, and B_i is a matrix containing geometric coefficients of the i-th element such as x, y, z coordinates of control points. Note that S_i may take other forms depending on the availability of surface modellers.

Equations (3), (4), (5) are the working equations for the draping analysis. These equations are nonlinear and solution procedure is iterative. A closer look at these equations shows that initially p(m+1, n) and p(m, n+1) must be given in addition to the starting point where draping calculations initiate. Without these conditions, the draping of fabric preforms can have more than one unique configuration. To achieve a unique solution requires certain constraints. They can be specified in terms of known yarn paths which may depend on the deformation history of the tool-preform interaction. However, with the aid of clamping device, a common practice in sheet forming, the constraint paths can be controlled. Therefore, choice of constraints is left as a design freedom. Fig. 2 shows a number of cells before and after deformation. The relative fiber content of the preform compared to the undeformed mats can be readily computed by [12].

$$V_f = \frac{\rho_m}{\rho_f} \cdot \frac{n}{h} \qquad\qquad (9)$$

where V_f is the fiber volume fraction, dm is the density of the mat, df is the density of the fiber in a preform made up of n layers placed in a cavity of thickness h. Also,

before draping
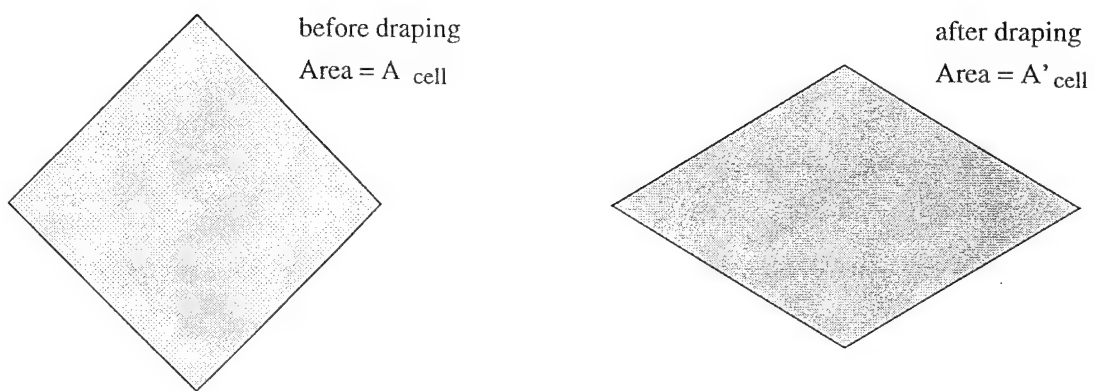Area = A $_{cell}$

after draping
Area = A' $_{cell}$

Figure 2: The change of area of a unit cell before and after deformation

$$\rho_m = \rho_{m0} \cdot \frac{A_{cell}}{A_{cell'}} \qquad (10)$$

where dm0 is the density of the mat before deformation.

The permeability of mats in the cell is generally complicated by many factors. The can be addition of binder in the mat, the undulation of fiber tows, or the use of fiber stitches. In order to provide a qualitative analysis of such effect, the following assumptions are used in obtaining the permeability.

- inter-tow space is eliminated (only one length scale is considered)

- the material is orthotropic and the permeability tensor is symmetric three-dimensionality of the flow front is negligible

- the effective permeability of preform is a result of pore space oriented in the warp direction superimposed with that of the weft direction

With the assumptions, the effective permeability can be expressed as

$$k = \sum_{i=1}^{n} \frac{h_i}{h} \cdot k_i \qquad (11)$$

where is permeability tensor of i-th constituent mat (of thickness hi) in a preform made up of n layers. Since the principal directions of are known from the draping analysis, their magnitudes can be found by considering fluid flows along and across the filaments [6, ?]. The work by Gebart [6]

14

provides a simple modified Kozeny-Carman equation to account for effect. Equation (12) and (13) are non-dimensionalized permeability.

$$\frac{k_{para}}{r_f^2} = \frac{8}{c}\frac{(1-V_f)^3}{V_f^2} \tag{12}$$

$$\frac{k_{perp}}{r_f^2} = c_1\left(\sqrt{\frac{(V_f)_{max}}{V_f}} - 1\right)^{\frac{5}{2}} \tag{13}$$

where r_f is the radius of the filament, and k_{para} and k_{perp} are permeabilities along and transverse to fiber tow, respectively. The constants c, c_1, and $(V_f)_{max}$ are geometric constants depending on the packing configuration. Other models provide similar results. However, a rigorous model to account for deformation is being developed.

The addition of Equation (11) is performed at the element level with respect to the local coordinate system. The orientation of the tow qwarp is used to transform the permeability into the local coordinate system with respect to an element. Therefore, the components of the permeability tensor from the warp tow can be expressed as

$$\left(\begin{array}{cc} k_{xx} & k_{xy} \\ k_{yx} & k_{yy} \end{array}\right) = \left(\begin{array}{cc} cos\theta_{warp} & sin\theta_{warp} \\ -sin\theta_{warp} & cos\theta_{warp} \end{array}\right) \left(\begin{array}{cc} k_{para} & 0 \\ 0 & k_{perp} \end{array}\right)_{warp} \left(\begin{array}{cc} cos\theta_{warp} & -sin\theta_{warp} \\ sin\theta_{warp} & cos\theta_{warp} \end{array}\right) \tag{14}$$

where k_{para} and k_{perp} are obtained from Eq. (12) and Eq. (13). Similarly, the components of the permeability tensor from the weft tow is

$$\begin{pmatrix} k_{xx} & k_{xy} \\ k_{yx} & k_{yy} \end{pmatrix} = \begin{pmatrix} cos\theta_{weft} & sin\theta_{weft} \\ -sin\theta_{weft} & cos\theta_{weft} \end{pmatrix} \begin{pmatrix} k_{para} & 0 \\ 0 & k_{perp} \end{pmatrix}_{weft} \begin{pmatrix} cos\theta_{weft} & -sin\theta_{weft} \\ sin\theta_{weft} & cos\theta_{weft} \end{pmatrix} \quad (15)$$

It is obvious that the resultant permeability tensor, k, in Eq. (11) is also a second order tensor. The obtained is valid for thin shell-like parts only. The concept of effective permeability does not hold as the gap height of the mold cavity increases and the flow front is no longer uniform in the thickness direction. By solving for the eigenvalues and eigenvectors of , we can obtain the principal values as well as the orientation of the effective permeability as shown in Fig. 3. Note that the local coordinate system always has its x-axis emanating from node 1 to node 2 as shown in Fig. 4.

Therefore, k_{11} and k_{22} represent the principal permeability values after the superposition of permeability ellipses. Fig. 4 shows the orientation of the effective permeability expressed by an angle a with respect to the edge formed by $node1$ and $node2$ in an element used for flow simulation. Darcy's law for flow through porous media is used to describe the pressure-velocity relationship. The generalized form of Darcy's law is

$$\vec{V} = -\frac{\bar{\bar{K}}}{\eta} \cdot \nabla P \quad (16)$$

where $\vec{V}$ is the superficial velocity of the flow front, is the pressure gradient, and is fluid viscosity. The fluid viscosity may be constant for Newtonian fluids or, for shear-thinning fluids, as a function of the pressure gradient. For steady, incompressible fluid flow, the continuity equation states that
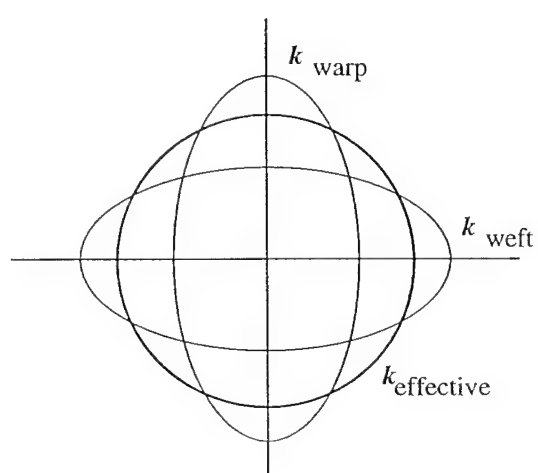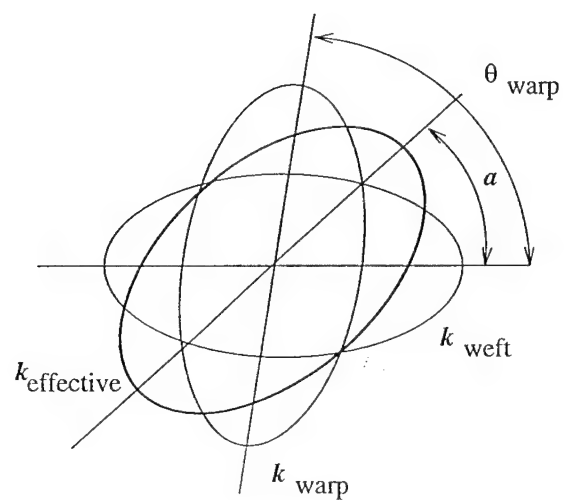
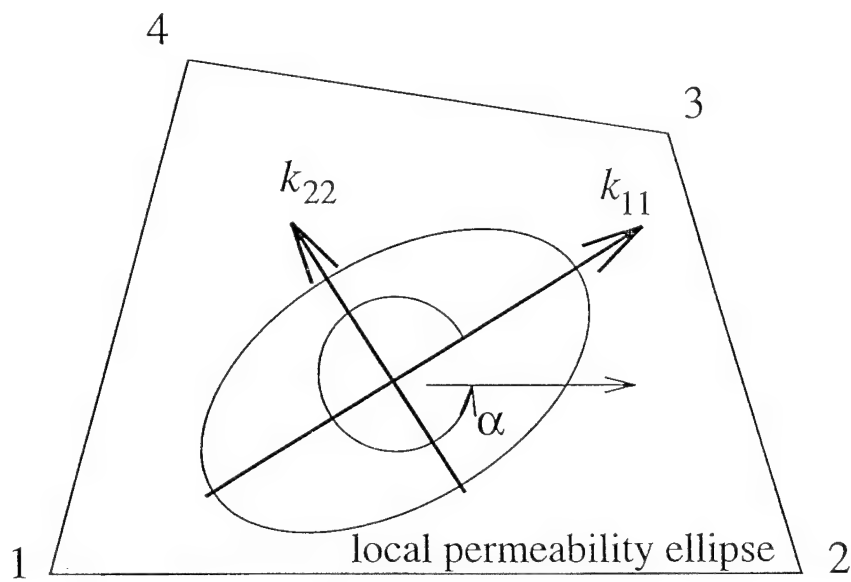Figure 3: Superposition of permeability ellipses

Figure 4: The effective permeability in an element

$$\nabla \cdot \vec{V} = 0 \qquad (17)$$

Substitution of (16) into (17) yields the elliptic equation

$$\nabla \cdot \left(\frac{\bar{\bar{K}}}{\eta} \cdot \nabla P \right) = 0 \qquad (18)$$

which can be solved, along with appropriate boundary conditions, for the pressure. Boundary conditions along all boundaries (see Fig. 5) are required. They are:

1. Along the mold wall, ∂R_1, or inserts, ∂R_4, the no-penetration conditions requires that the normal velocities are zero, or

$$\vec{V} \cdot \hat{n} = 0 \qquad (19)$$

where $\hat{n}$ is the normal to the wall.

2. At the injection gates or inlets, ∂R_2, two types of boundary conditions are provided - the pressure or the flow rate.

3. Along the flow front, ∂R_3, the pressure is specified as the vent pressure in consistence with that of ∂R_5.

A finite-element/control volume method [8] is used for the filling simulation. The flow is assumed to be quasi-steady state. That is, the filling is assumed to take place at each time step.

19
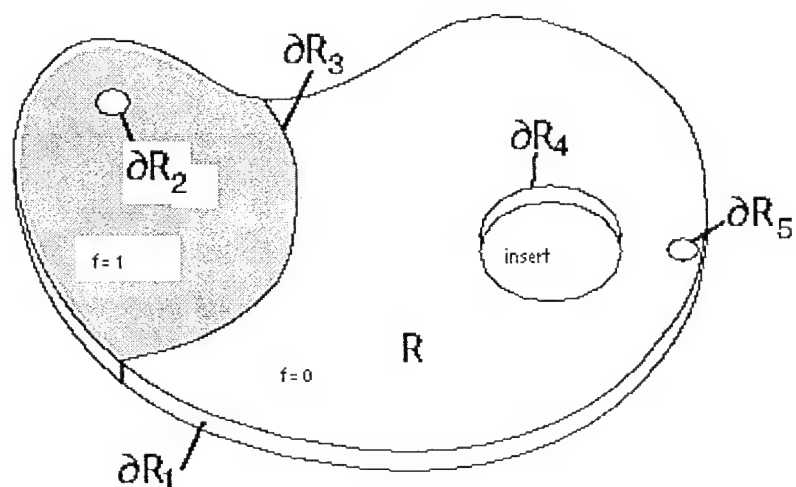
Figure 5: Boundary conditions in an injection mold

The solution is marched forward in time after the pressure field in the mold is calculated by a finite element method where the fill factor (f) is greater than zero. Then, the computed pressure field is used to calculate flow rates across the many control volumes in the flow domain and hence advance the flow front. The time step for each quasi-steady state is calculated from the time taken to fill the next partially filled control volume. This ensures the stability of the solution obtained under the quasi-steady state assumption. This solution procedure is repeated until all the control volumes are filled.

3 Case Study - Mold Filling Simulation of a Hemispherical Shell

A dome shaped part will serve as an example of this integrated draping and resin transfer molding simulation. The hemisphere in the part has a radius of 1.0 m and a flange of 0.3 m in width. First, a square bi-directional mat is draped. The workpiece is initially configured that warp and weft tows are perpendicular to each other. Then draping starts at an arbitrary point on the tool. The algorithms described in the previous section are implemented as shown in Fig. (6). The draping analysis program, or known as $DRAPER$, starts the calculation with the provided initial conditions and tool geometry. As it progresses through each cell in the mat, starting with those cells where $p(m,n)$, $p(m+1,n)$, and $p(m,n+1)$ are known, the draped configuration can be obtained.

The permeability module in the above figure makes use of Eq. (9) - (13). User may interface with this module to assign boundary conditions (inlet location and pressure/flow rate) as well as the viscosity model used for resin flow. The output from this module contains: principal permeabilities, orientation in local coordinates of an element, and the fiber volume fraction in an element. Then the interface module in the above figure generates necessary input parameters for a Liquid Injection Molding Simulation program [9], or known as LIMS. The processing conditions are given in Table 3.

The output from LIMS consists of pressure and flow front information at each nodal point. The flow fronts at different time are represented in contours. The predicted pressure at specified nodal points during the mold filling is also plotted. In order to show the effect of draping, normalized pressure is used in the parametric study. The normalized pressure is obtained by
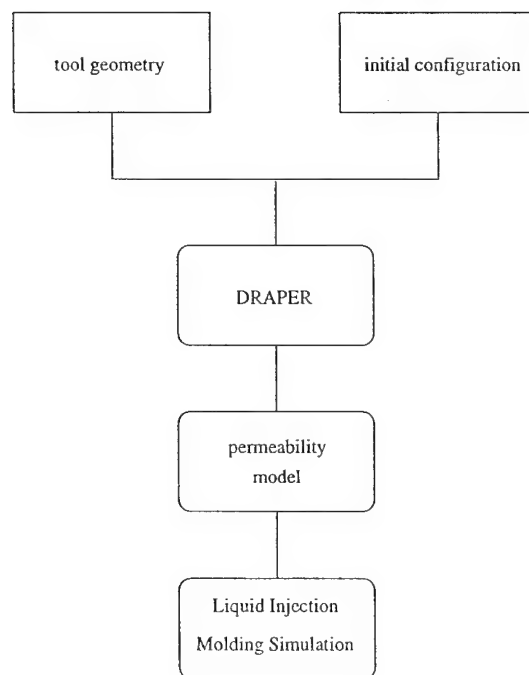
Figure 6: Schematic of the integrated simulation for resin transfer molding

Table 1: Processing Conditions Used in Simulation

injection BC	const flow rate
gate location	edge gate
preform thickness	0.0032 m (1/8 inch)
porosity	0.7
resin viscosity	0.05 Pa*sec (50 cp)

dividing the pressure value with a reference value.

4 Results

The above programs, *DRAPER* and LIMS, were implemented on a workstation. The preform consists of 2500 (50x50) cells while the mold geometry is discretized into 720 elements. In this section, we present results of the integrated simulation. Deformation caused by draping itself is an important issue as to how a shape can be draped successfully. *DRAPER* can be used to allow a designer to assess formability of preforms. We also look into the effect of permeability change due to draping on resin transfer molding through the mold filling simulation of LIMS.

4.1 Simulation of Draping of Hemispherical Preform

The initial constraints used in this case study are prescribed along the central tows in both the warp and weft directions. The length of the cell segment is assumed to be constant. In the draped configuration shown in Fig. 7, the degree of deformation varies from cell to cell. The minor angles in the preform range from 90 degrees (undeformed) to a minimum of 35 (largest shear deformation) approximately. The shear also results in fiber volume fraction increase. This information can assist a designer in material selection, setup of processing conditions and part design. Or, a process engineer can use this information to find out where to make necessary cuts in order to accommodate for such induced deformation. As a rule of thumb, formability of preform mat relies on absorption of such deformation by the reinforcement material. A good material can withstand high deformation without wrinkle formation [10]. The fiber preform is trimmed such that it has a flange of constant width. The finite element mesh used in mold filling simulation is made up of both rectangular and

triangular elements. The permeability of each element is assigned to the value of the cell that is closest to the centroid of that element.

The information of shear deformation in each cell also provides insight into the composites processing than wrinkle prediction. The compression induced by draping increases the fiber content in a preform. In the current example, draping induced deformation gives a fiber volume fraction distribution ranging from 0.3 to 0.7 approximately. By using the permeability model described in section 2, this translates into a change in k_{11} (the first principal permeability) from $3.3x10^{-11}\ m^2$ to $1.5x10^{-13}\ m^2$ under the assumption that only one length scale is being considered.

4.2 Simulation of Mold Filling before and after Modification

Even though the preform is axisymmetric, the orientation of the preform deserves some attention. In this section, the preforms are oriented such that its x-axis coincides with that of the injection mold. Using the given conditions, the flow front patterns are obtained by LIMS and displayed through a commercial postprocessor [11]. The hemispherical part is a three-dimensional structure. For visual comparison, only the top view is shown. Fig. 8 shows the simulations of flow fronts in the mold for two cases. In the first case, only the fiber volume fractions aregiven while the permeability is that of the undeformed mat. The flow front patterns from such calculation are represented by thin lines.

The first case is a common situation faced by many design engineers where the preforming is neglected. Such practice, though seems harmless, may lead to molding defects when flow fronts entrap unexpected voids or when the mold leaks because of pressure buildup due to increase in the
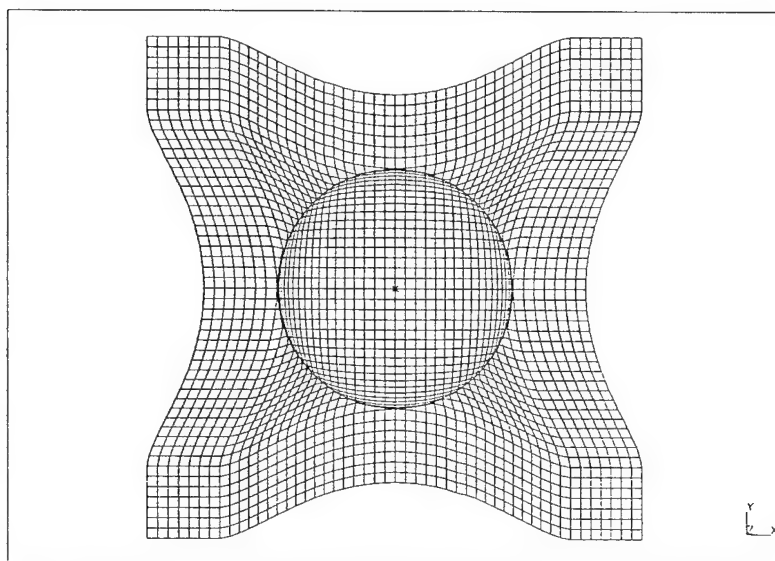
Figure 7: Draped configuration of a fabric over the hemispherical dome
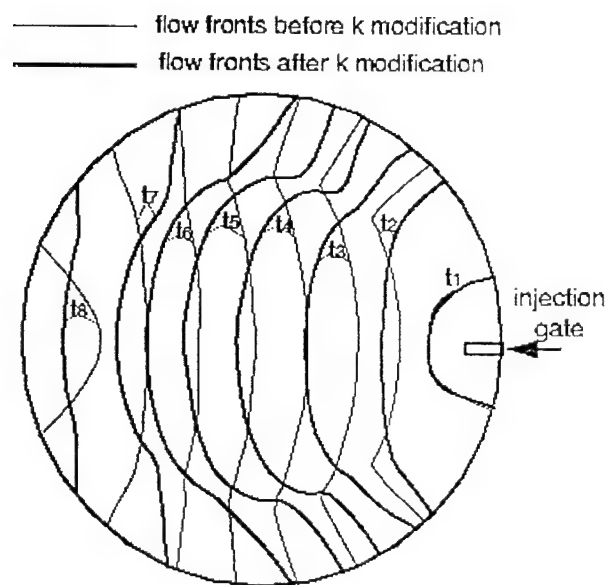
Figure 8: Flow front progression before and after permeability modification

flow resistance.

The thick lines in Fig. 8 represent the flow front advancement after accounting for the fiber deformation by modifying the permeability. The filling times of the two simulations are normalized for a head-on comparison. The differences between the two are obvious. The shapes of the flow fronts become convex as compared to the concave flow fronts in the dome region. As one can see, the flow front is slowed down (at t4 and t5) in the flange of the part. As we recall, the highest deformation tends to be localized in some of the areas in the flange, which contribute to the high flow resistance and slow down the flow front progression. Even though the flow front patterns are changed, the effect on over all mold filling is not clear at the first glimpse. Therefore, we will look at one important processing variable, pressure, to investigate the preforming induced variations. The importance of the role of draping or the effect of preforming will be demonstrated by the following example.

One advantage of resin transfer molding is its ability to mold large parts using less expensive press or by the weight of the mold itself. However, insufficient mold clamping can result in resin leakage and incomplete filling. It is important to account for the pressure increase when the overall flow resistance is increased. Fig. 9 shows the simulated inlet pressure before and after applying the permeability modification. In this figure, the gate pressure at the end of mold filling without applying permeability modification is used as the reference. Both simulations use constant flow rate as the inlet boundary condition. Initially, a small pressure exists at the inlet. These pressures are of the same magnitude when the preform is oriented at 0 degree with respect to the axis for the mold geometry. However, the difference between the two pressure curves begins to

increase as resin advances in the mold. An increase of 50% to 60% of the pressure compared to that with unmodified permeability is observed during the filling simulation. This is caused by an increase in flow resistance as the flow front progresses through the preform.

Fig. 10 shows the comparison of the cavity pressures in the same setting. The cavity pressure values are taken from an identical location in the mold cavity at a distance of 0.37 m (see Fig. 11) away from the inlet. In this figure, the cavity pressure at the end of mold filling without applying permeability modification is used as the reference. This is shown by the time delay of about 9 seconds. Based on one's intuition, a high inlet pressure will normally imply a high cavity pressure. However, we will see that this intuition is sometimes incorrect when the preform is not uniform and homogeneous.

4.3   Simulation of Mold Filling at A Different Gate Location

As mentioned earlier, the selection of the gate location can also affect the molding process when the fiber content is not uniform. In this section, we simulate the flow front progression of the same hemispherical shell by injection at a different gate location. Change of inlet location is achieved by rotating the x-axis of the preform by 45 degrees with respect to the x-axis of the mold cavity in the direction shown in Fig. 11). This type of variation in preform placement can be easily introduced in axisymmetric parts such as the hemispherical shell. We will compare the flow front pattern with the simulation obtained previously in which the x-axis of the preform coincides with the x-axis of the mold cavity.

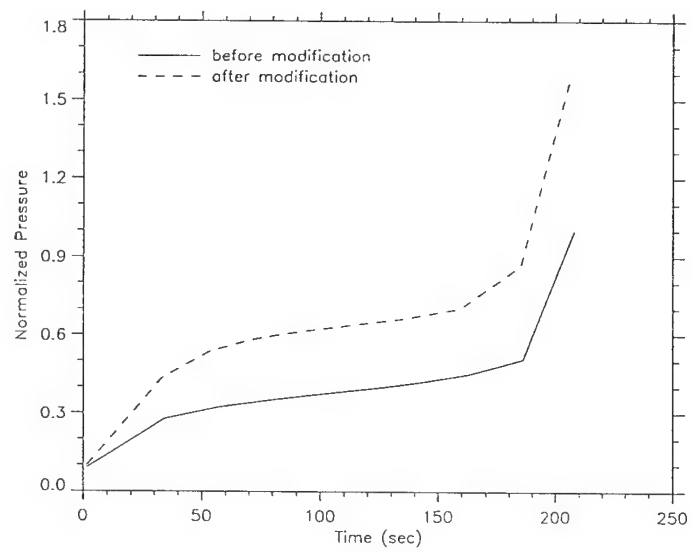The mold filling simulation is shown in Fig. 12. Flow fronts of two filling simulations at

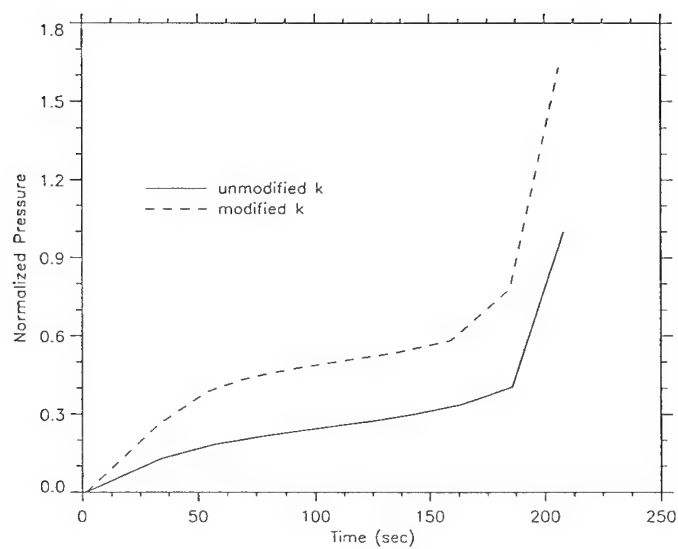Figure 9: Inlet pressure history before and after modification

Figure 10: Cavity pressure history before and after modification
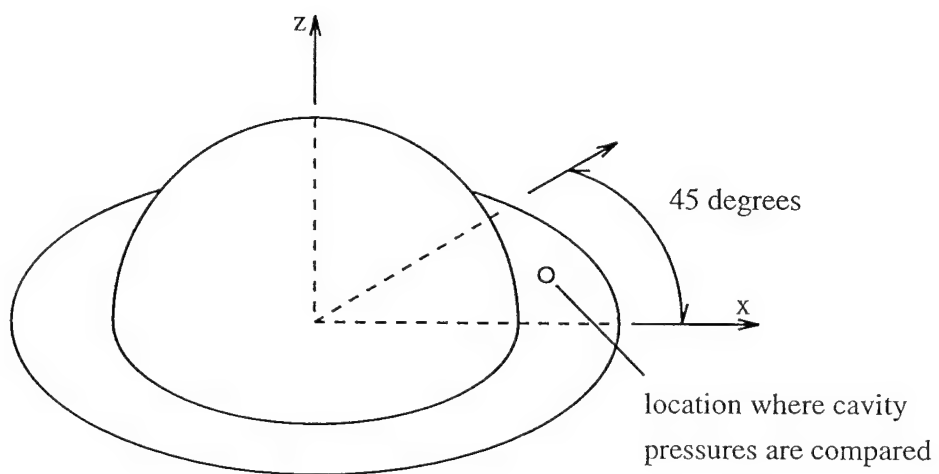
Figure 11: Rotation of the hemispherical preform

eight time steps are compared. Both cases have taken the draping effect into account. The thick lines represent the flow fronts for the preform oriented at 45 degrees with respect to the x-axis of the mold. The thin lines represent the flow fronts for the preform oriented at 0 degrees with respect to the x-axis of the mold. One can tell that the two settings for identical preforms result in totally different filling patterns. Although the part is axisymmetric, the mold filling is sensitive to the orientation of the preform. Flow front in the flange slows down at t5 and t6. This is understood as the high deformation areas are rotated which are causing the flow front advancement to lag that in the center. Fig. 13 shows the pressure history of two filling simulations consist of identical preforms. In this figure, the gate pressure at the end of mold filling before preform rotation is used as the reference. For the same mold configuration, the two pressures in this figure tend to represent two limits. The upper bound of the inlet pressure is achieved when the injection takes place at low permeability region. The lower bound of the inlet pressure can be observed when the injection gate is chosen close to high permeability region. From the simulations, the upper bound pressure is almost twice that of the lower bound pressure. This indicates that there is a potential run-to-run variation if the fiber preforms are handled indiscriminately.

In the previous section, we observed that the order of mold pressures tend to follow that of inlet pressures. That is, if inlet pressure is larger, then so should the mold pressure. From the simulation, Fig. 14 shows that a high injection pressure does not result in a high cavity pressure. In this figure, the cavity pressure at the end of mold filling before preform rotation is used as the reference. This is difficult to visualize by intuition alone. However, an explanation seems apparent in the light of the permeability variation inside the preform. Qualitatively, the permeability is

low in areas where fiber content is high. Because of the high deformation induced by draping at the corners (located 45 degrees from the x-axis), the preform with the 45 degrees rotation happen to represent the difficult-to-penetrate flow regions. Therefore, the pressure difference between the inlet and the point of interest is diminished by the high flow resistance. Note that if k was not modified by draping analysis to account for deformation, the LIMS simulation will show that the results are not sensitive to change in gate location.
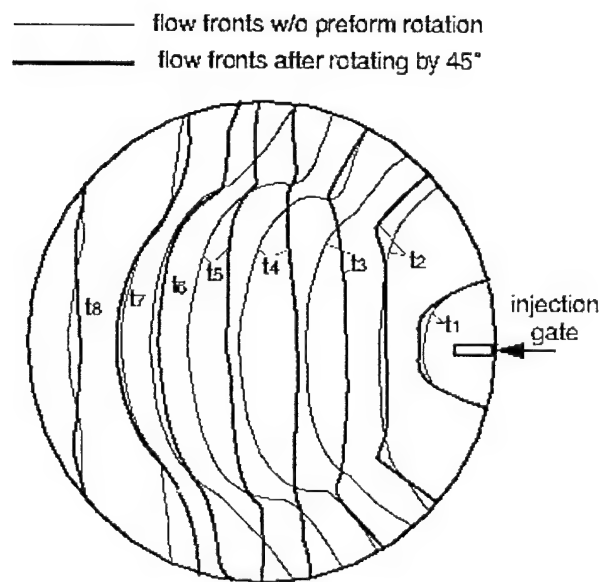
Figure 12: Comparison of flow fronts location before and after preform rotation
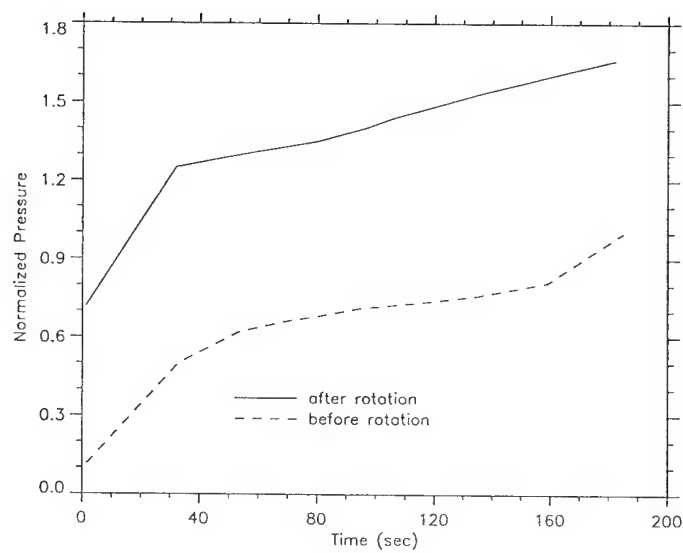
Figure 13: Inlet pressure history before and after preform rotation after accounting for permeability modification
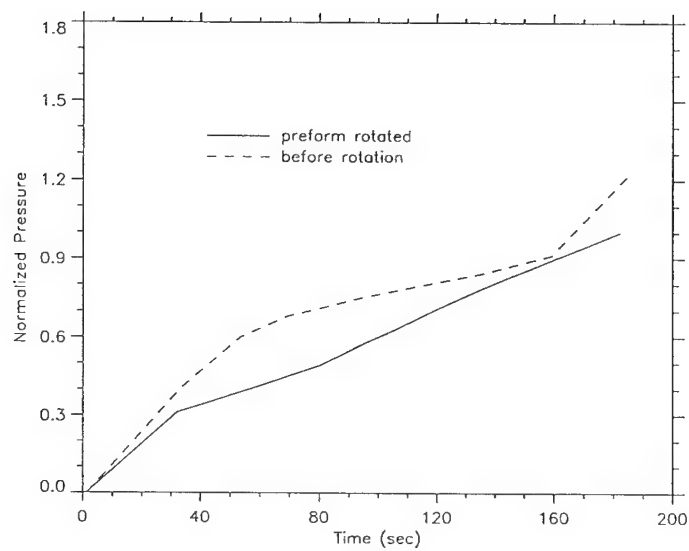
Figure 14: Cavity pressure history before and after preform rotation after accounting for permeability modification

Table 2: Parametric Effect of Draping in simulation

processing variables.	parametric effect
filling time	10 % increase
volume fraction	70 % increase
injection pressure	50 % increase
mold pressure	50 % increase

5   Conclusions

In our effort to capture the processing physics in resin transfer molding, we have demonstrated an integrated simulation that allows a design engineer to model the resin flow inside fiber preforms. Our approach is different from conventional simulation as preform properties are now taken into account. Table 5 summarizes the effects on processing due to fiber deformation for the case study. In this work, the versatility of the integrated approach has not only dealt with the formability of preforms through the draping algorithm, but also the moldability of resin transfer molded parts.

As the RTM is marching into the phase of higher sophistication [13], the experience-based craft should turn into a simulation-based technology where processing physics is incorporated into computer simulations.

References

[1] Advani, S. G. , M. V. Bruschke and R. Parnas, *Flow and Rheology in Polymeric Composites Manufacturing*, Chapter 12: Resin Transfer Molding, 1994, **Chapter 12: Resin Transfer Molding**, p. 465.

[2] Potter, K. D., *Composites*, 1979, **132**

[3] Mack, C. and H. M. Taylor, *J. Textile Inst.*, 1956, **47**, T447.

[4] Forrest, A. R., *Computer Graphics and Image Processing*, 1972, **1**, 341.

[5] Van West, B. P., R. B. Pipes, M. Keefe and S. G. Advani, *Composites Manufacturing*, 1991, **2**, 1.

[6] Gebart, R. B., *SICOMP Technical Report*, 1990, **90-006**.

[7] Bruschke, M. V. and S. G. Advani, *Journal of Rheology*, 1993, **37**, 479

[8] Bruschke, M. V. and S. G. Advani, *Polymer Composites*, 1990, **11**, 398.

[9] Liu, B., M. V. Bruschke and S. G. Advani, *CCM Technical Report 94-18* 1994.

[10] PDA Engineering, PATRAN Plus User's Manual, 1991.

[11] Fong, L., J. Y. Xu, and L. J. Lee, *Polymer Composites*, 1994, **15**, 2, p134

[12] Fong, L., and L. J. Lee, *Journal of Reinforced Plastics and Composites* 1994, **13**, 7, p. 637

[13] Polymer Composites. *Polymer Composites*, 1994, **to appear**

THE SIMULATION OF DRAPING PROCESS

Pavel Šimáček

Suresh G. Advani

Center for Composite Materials and Department
of Mechanical Engineering, University of Delaware

Introduction

Resin Transfer Molding process provides an attractive low cost alternative for manufacturing composite parts. The simulation of this process is important because of several reasons. First, we need to properly design the process parameters, such as mold geometry and pressure and time needed to fill this mold. Second, we need to properly design the part itself to assure it meets demands.

Both the processing and the final mechanical properties depend significantly on the reinforcement geometry. In processing it dictates the permeability — resistance to flow — of the preform in mold. If final properties of a part are considered, the reinforcement geometry gives stiffness, and has large influence on strength, fracture toughness or transport properties.

The geometry of preform within mold is generally different from that of the flat workpiece used to create the preform. This is because of two factors. First, during covering of the mold surface large — mostly shearing — deformation occurs within the plane of the workpiece as it is deformed out off plane to three-dimensional shape. The other factor is the pressure applied during the mold closing. It compacts the structure mainly in the transverse direction.

This report is concerned with the first of the above-mentioned mechanisms, the

draping of the mold. During draping of a woven fabrics on the mold surface, several mechanisms change its structure. First, the angle between warp and weft changes — shearing deformation. Some additional deformation is possible due to tow-tow slip or extension of undulated fiber tows. However, in most practical cases the first mechanism is dominant.

Possible Approaches to Draping Simulation

The numerical simulation of the draping process presents several problems. From the numerical point of view, non-uniqueness of the solution is a very important one. This means that, in order to obtain solution we have either to select a branch at every possible bifurcation or introduce some additional criteria (Boundary conditions) to avoid this problem.

Behavior of the media is second problem. The woven material is showing two directions of inextensibility and wide range of resistance-free shearing deformation. This is not — unfortunately — unlimited and at a certain angle fabrics will not deform any more (it locks) and attempt to increase the shearing deformation leads to wrinkling.

Both of these elements present difficulty, both from experimental — establishing of the proper locking angle — and computational point of view. From the simulation point of view, the possibility of wrinkled surface leads to necessity to be able to change some geometrical aspects (boundary conditions) of draping according to the shearing deformation attained and, possibly, to cut the draping fabric and remove a part of the sheet to allow proper draping.

It is possible to obtain the elastic solution for the fabric treated as a membrane with two directions of inextensibility, progressively stiffening shearing response and large deformations. Nonetheless, a number of problems persist, rendering this solution impractical:

- The solution is non-unique. Since all points are being placed at once, this

would require to specify boundary conditions and/or optimization criteria to obtain a properly posed system.

- The inextensibility is problematic, since it requires mixed formulation and usually yields spurious modes in the stress (tension) part. This is a difficulty with one direction of inextensibility. To authors knowledge nobody ever tried two directions of inextensibility.

- The reaction between the mold and fabric are necessary for this approach. They need to be specified, but it is extremely difficult to obtain even an estimate of realistic values. The repeatability of these values in real process should be also subjected to scrutiny.

- The wrinkling would not be easily predicted, since the sheared elements would become absolutely rigid instead of yielding to load by instability — buckling. However, if large deformations are allowed, buckling on length scales larger than the element size could be modeled.

These difficulties cause that using the geometric model is the only way to obtain the solution in real time and using only the data currently available to us. This approach is built on the geometric considerations and assumption of no slip between weft and warp yarns.

Geometric Model: Node placement

The lower level of the draping simulator is the algorithm which, starting with known position of some nodes can find a position of the additional ones based on a length of warp and weft between the nodes already placed and the node being placed. Note that the utilized relation is valid only if there is no force effect on the yarns between the two nodes — barring the potential normal reaction from the mold surface.

Assuming no interaction but the normal force, the tow (warp or weft) connecting two points is following the geodesics curve — i.e., the shortest possible

line. On a flat surface this reduces to a straight line. On developable surface, this curve maps to straight line after developing the surface. Most works including [3][4][5] are using this approach. The approach outlined in the following does this as well. The method really depends on approximation of the surface, giving two distinct possibilities:

- Model the surface as an assembly of flat elements (i.e., linear triangles). Then the geodesics reduce to straight lines and can be easily solved for. Actually, since the surface is developable, closed form solution is available regardless on how many triangles the line crosses. However, unless carefully optimized, the closed form solution would require developing of about 2^N panels to plane, where N is the number of triangles the yarn segment crosses. This renders the solution unsuitable for large N, i.e., small panels and long distances between nodes on fabric. As a result, existing implementations require the final point to be at the same panel or restrict the number of triangular boundaries crossed [3].

- Modeling the surface as a smooth (C^1) assembly of curved elements. The geodesics then have to be followed numerically. For a geodesics given by an initial point and tangent this is a rather straightforward approach. Unfortunately, if we want two geodesics of given starting points to intersect at given distances, some iterative scheme is necessary to solve for initial tangents. This is nonlinear system of equations for two unknowns. Obviously, the problem can be cast into nonlinear minimization problem in two variables. Utilization of this approach is suggested herein.

There is the third possibility, i.e., curved panels on C^0 surface, but it does not offer much of advantage. The only one would be easier mapping of the surface.

Comparison of the previously mentioned approaches

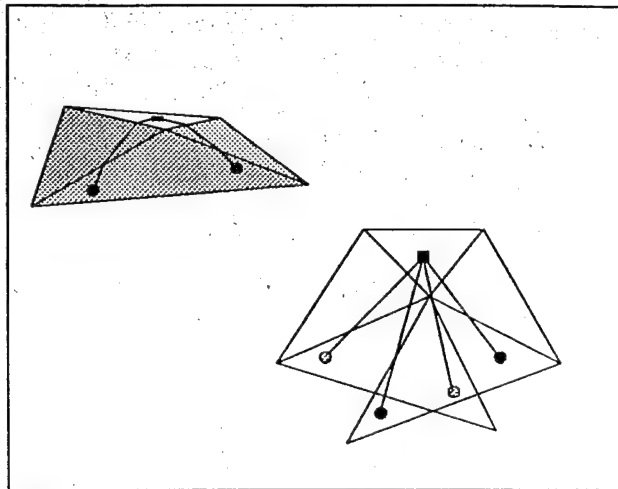Each of the approaches mentioned above has both advantages and potential

Figure 1

problems. The flat triangular panels require tremendous number of elements on the surface in locations where the curvature is small. This in turn forces the size of fabric cell to be small. As far as the solution goes, a scheme which solves the problem in closed form is available. It utilizes the developability of the surface. The approach, together with the possible complications, is outlined in Figure 1. The known points are circles, the computed one is rectangular. Developing the surface works easily, however, once more than one boundary comes into play, it is *non-unique*, yielding more paths possible. Clearly, the shortest paths is right, i.e., the point which does not come closer than the required distance to *any* possible projection of the original points is the solution. This is not iterative solution but rather a selection of one of finite number of closed form solutions. Nevertheless, considerable amount of bookkeeping would be required to utilize this algorithm over larger patches of triangles. Perhaps this is the reason it has not been implemented — as far as authors know — in the general form. Note that each additional triangle between the known point and the sought one doubles the number of possible mappings, yielding the already mentioned 2^N number of options to select from.

On the other hand, the flat triangles allow for fast solution, fast projection of spatial points or vectors on the surface of element and painless handling of singular lines on the surface.

The curved panels can reflect the geometrical structure of mold by very few panels, as demonstrated in the Figure 2. This can be considered to be a quarter of box structure. Using cylindrical, plane and spherical panels, only seven entities ar required. This model might actually correspond to the geometry of the box generated by CAD program. Comparing this with
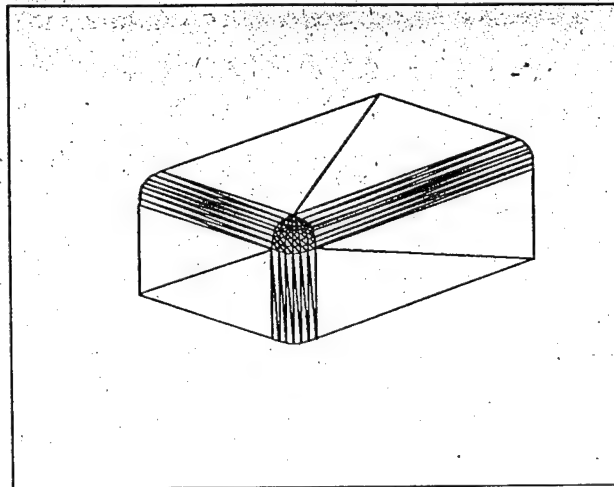
Figure 2

triangular mesh on the surface, it is great simplification. Also, it allows following geodesics for an arbitrary length — assuming the surface is smooth — with only linear increase in computational time. The third advantage is associated with the following section. The ability to find and/or follow geodesics allows for more realistic estimates of the location of some nodes specified as a boundary condition.

Nonetheless, there are also some serious drawbacks. Numerical solution can be quite lengthy. Introducing the singular line (break) where the surface normal is not continuous can be handled but requires additional bookkeeping. Finally, we are interested in Cartesian coordinates of nodes. The transfer from local coordinates to global Cartesian ones is rather simple. However, the opposite direction is not so easy and finding a nodal projection on curved surface may be a difficult task for some entities.

The authors opinion is that, if a reasonable draping simulation is to be attempted, *BOTH* approaches should be implemented. At this points, rather restricted implementation of the former is available. It does not solve the problem in closed form but rather uses iterative solver [3]. The later approach, as far as the authors knowledge goes, is untried. Its implementation is a subject of current work. To use the former approach it would be desirable to improve the algorithm.

One final note. The literature is flooded with 'elastic' solutions which assume elastic extensional stiffness of fibers in fabric and zero shearing stiffness. This solution is actually very close to the ones described above. The only difference is that the approach above uses pointwise collocation, while the 'elastic' solution uses Galerkin method. These solutions have little to do with elasticity and seems to be computationally more intensive. Comparison of this 'elastic' solution and the two approaches considered above is presented in [6]. However, this reference should not be considered a final word, since only a hemispherical surface is considered therein. It makes use of algorithms dependent on smoothness of the surface much easier.

Geometric Model: Boundary Conditions for Node Placement

The previous section showed how we can, knowing the position of a node on warp yarn and a node on weft yarn, compute the position of the node where these two tows intersect. Note that this tacitly assumes that there is no slip between tows and no forces but normal reaction from surface act on the tows between the points of interest.

Obviously, to start placing nodes on the surface we *apriori* need to know positions of some nodes on the surface. We will speak about these 'fixed' nodes as about the boundary conditions.

The boundary conditions are complicated subject. Consequently some assumptions are generally made to simplify the problem. Some works [4] assume nodes fixed along the lines of symmetry. Since general approach can not rely on this feature, it seems unwise to follow. The work [3] uses a bit different approach — there is supposed to be a single warp yarn and a single weft yarn whose position is fixed - prescribed once and for ever. In the case the object is sufficiently symmetric, these are assumed to be lines of symmetry and correspond to the previous approach. No other cases were ever solved.

There are just two problems with the "symmetry" type solution:

- It cannot be applied to non-symmetric molds and even to some symmetric ones if a general orientation of yarns is required.

- Even if the mold is symmetric, the symmetric solution is not necessarily the most desirable. This is associated with the intensity of the shearing deformation. Since we may be forced to cut the preform, one cut — albeit a "bigger" one — may be preferable to multiple cuts. This is demonstrated in Figure 3.
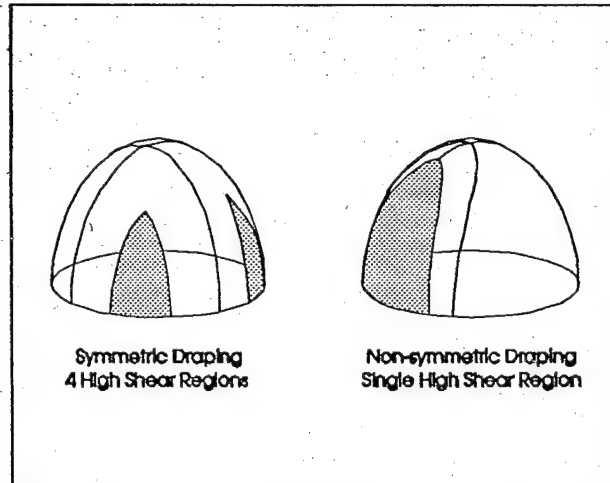

Symmetric Draping
4 High Shear Regions

Non-symmetric Draping
Single High Shear Region

Figure 3

Zero Shearing Stiffness Assumption

Previous approaches assume the material to allow unlimited shearing deformation. This allows for a simple boundary conditions without any element of adaptability as described beforehand, but it contradicts to common experience, by which most of the fabrics shows a "locking" phenomenon — the shearing stiffness grows progressively with shearing deformation. There is a very sharp jump to "infinite" value for certain angle.

This behavior is directly associated with wrinkling of the fabric. This can be easily demonstrated. The fabric can be easily assumed to behave as a true membrane, i.e., it is basically incapable of carrying compressive stress in any direction. Now take the square piece of fabrics as shown in the Figure 4. This can be loaded at the intersections by tension. as shown. Varying the tension in x and y directions, the fabric will shear to arrange for the carrying all the load as a tension in the warp and weft yarns on the boundary — since it cannot carry compression and only negligible amount of shearing load. Once the shearing limit is reached, the fabric within the quadrangle can
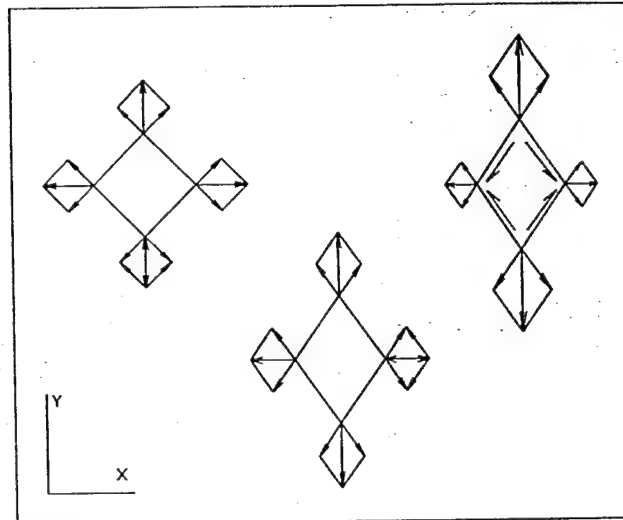
Figure 4

no longer adjust and it has to be loaded with (no longer negligible) shearing stress. This corresponds to the compression in x direction and the membrane buckles.

The previous example demonstrates only that excessive shearing deformation will lead to wrinkling. The opposite is trivially not true, i.e., wrinkling can be caused by other type of loads as well.

The previous approaches, as noted, are ignoring the limits on shearing. This allows them to give solution for arbitrary boundary conditions, regardless of its physical possibility. The limits can, however, be treated by adjusting the draping process. There are two ways to make this adjustment:

- When excessive shearing is detected, boundary conditions could be rearranged in order to restrict shearing within the critical zone. Usually there is no crucial reason to locate a given yarn along a fixed line, so this approach is rather acceptable.

- The critical part of the preform can be cut out. The cut edges can be designed to touch or overlap a given amount once the mold is draped. The feasibility of this solution is dependent on manufacturing considerations.

Little was done in this area beforehand, but it is worth exploring. The problem is again the *non-uniqueness* of the above mentioned solutions. Thus, heuristic improvements may be the best way to cope with the problem. There are also some additional problems to handle, for example, additional boundary conditions are necessary once a cut is made.

Note that, strictly speaking, the first method might be applied using Draper, the code used in [3]. This would mean editing the input file after results are known. While time consuming, this approach is certainly possible. Nonetheless, Draper has no way to accommodate the second approach.

The authors intention is to develop an algorithm capable of handling these two methods, i.e., draping with the potential to remove part of preform and to change — possibly interactively — boundary conditions. This approach can be described by the following pseudo-code:

```
DO WHILE there are some unaccounted nodes
   obtain the location of the next boundary condition

   CHANGES<-TRUE
   NODES_REMOVED<-0
   DO WHILE CHANGES=TRUE
     CHANGES<-FALSE
     FOR all unaccounted nodes
         IF can place this node THEN
             place the node
             CHANGES<-TRUE
             IF the node is sheared to much THEN
                 remove the node from preform
                 NODES_REMOVED<-NODES_REMOVED+1
             ENDIF
```

```
        ENDIF
    NEXT node
LOOP


IF NODES_REMOVED>0 THEN
    DO WHILE change the last BC makes sense
        restore nodes killed or placed since the last BC was handled
        change last BC
        return last BC to input queue
    LOOP
ENDIF
LOOP
```

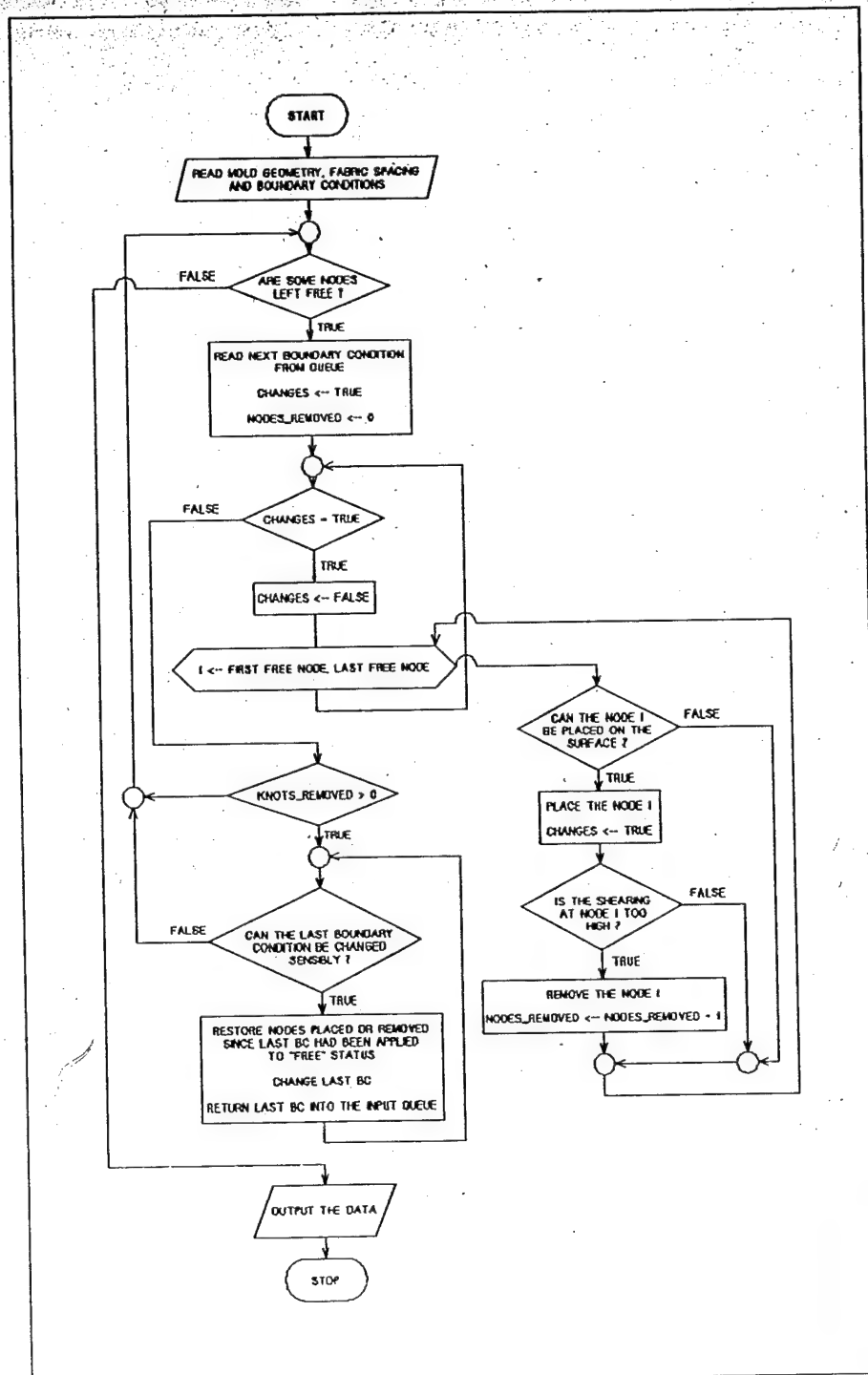The flowchart of this algorithm is presented in Figure 5.

Figure 5

Implementation

The previous pseudo-code does not explain details of working, but many of the procedures are not finished yet. We will, however, provide some information concerning the already implemented details.

Obviously, the nodes (intersections of warp and weft yarns) can be no longer arranged in array. First, if cutting is to be allowed, several things can happen with a node during draping. It can be removed from the preform. It can also be split into two nodes, each belonging to one side of wedge cut. Than there has to be a possibility of reversing the process of placing the node on surface. Consequently, the nodes have to be organized as a doubly linked list and separate list is kept for placed, removed and 'uncertain' nodes. Despite the fact that this complicates the program, it does not influence its efficiency too much because of its incremental algorithm. To generate appropriate input data, use of program is recommended.

Boundary conditions implemented are of two types. First, the node can be placed on the surface to given position. This allows a superset of boundary conditions used in previous program. Use of this kind of boundary condition is, however, not recommended, as it allows user to violate inextensibility of tows. Second kind of boundary condition describes the direction in which warp or weft yarns lay. This should allow relatively easy changes in optimization routine, as this condition preserves distances between nodes.

Removal of excessively sheared nodes has been implemented. However, optimization and undo features are still being worked on.

Surface description so far includes only rotationally symmetric panels (cone, cylinder, sphere, plate) but the solution does not need to be symmetric. Additional elements are under development.

Code has been verified on examples already done with both the previous code

and experimental techniques, such as hemisphere with base plate and cone mold. Export of permeability data into LIMS through filter has been implemented and tried. It allows to use permeability values tabulated as a function of shearing deformation and mold thickness to generate a proper material entities in otherwise complete LIMS mesh.

Conclusion

This is meant to summarize intended changes and improvements implemented in the currently developed code over the existing code (DRAPER):

- The search for a node location on surface should allow for curved surface, using the differential equations describing the geodesics curve. The flat panelled surface might be kept, but certain changes are needed to alleviate limits on distance between nodes compared to the panel size.
- The overall algorithm is to allow for wider range of boundary conditions. For example, yarn between two fixed points should be sufficient instead of specifying all nodes.
- Removing the overly sheared fabrics should be implemented, giving at least admissible shape of the preform before draping.
- Backtracking of the boundary conditions should allow at least some flexibility in reducing the removed/overly sheared areas. However, unless the user might be prompted for a recommended change, heuristic algorithms for such an improvement are necessary. The backtracking itself should allow to "undo" as little as possible of the work done, hopefully without any change in the input files.

References

[1]   Simacek, P., *"Numerical Modeling of the Sheet-Forming Process,"* Report 94-27, Center for Composite Materials, University of Delaware, 1994

[2]   Simacek, P., Kaliakin, V.N., Pipes, R.B., "Pathologies Associated with the Numerical Analysis of Hyper-Anisotropic Materials," *International Journal for Numerical Methods in Engineering*, Volume 36, 1993, pages 3487-3508

[3]   Fong, L., Advani, S.G., Fickie, K.D., "The Deformation of Bi-Directional Fabric in Composite Processing Using resin Transfer Molding," submitted to ...

[4]   Long, A.C., *"Drape Analysis for Beaded Stiffened Panel,"*, Report, University of Nottingham, 1995

[5]   Van West, B.P., Pipes, R.B., Keefe, M.,"Simulation of Draping of Directional Fabrics over Arbitrary Surfaces," Report 90-14, Center for Composite Materials, University of Delaware, 1990

[6]   Van Der Weeën, "Algorithms for Draping Fabrics on Doubly Curved Surfaces," in *International Journal for Numerical Methods in Engineering*, Volume 31, 1991, pages 1415-1426

EFFECT OF DRAPING OF FIBER PREFORMS ON PROCESS PARAMETERS DURING MANUFACTURING WITH RESIN TRANSFER MOLDING

Simon Bickerton and Suresh G. Advani
Department of Mechanical Engineering
University of Delaware

and

Kurt Fickie
Army Research Laboratory
Aberdeen Proving Ground

and

Lihwa Fong
Center for Composite Materials
University of Delaware

ABSTRACT

Resin Transfer Molding (RTM) is a composite material manufacturing process during which resin is injected into a mold cavity filled with a fibrous reinforcing preform. Application of woven and stitched fiber mats in fabricating preforms for RTM is a highly viable means of manufacturing affordable composites. Preform permeability plays an important role in the physics of the mold filling process. In general, the preform permeability is a function of the fiber tow and mat construction. Draping, in this paper, refers to the act of bringing a flat workpiece into contact with an arbitrary tool surface. As a result, the draping of the woven mats tends to cause the mat to deform to the tool geometry. This paper demonstrates the effect of preform draping on the mold filling process. A mold was built to provide a conical mold cavity. Fluid flow-front progression has been recorded, and injection pressure measured during mold filling experiments. Draping the preform has effected flow-front progression and significantly increased required injection pressure. Experimental results obtained are compared with the numerical predictions given by the draping code and mold filling simulation developed at the University of Delaware. Reasonable agreement has been found for flow front progression, while simulated pressures were much lower than those measured experimentally.

1

INTRODUCTION

The first step in the RTM process consists of placing of the preform within the mold cavity. The fiber preform will provide the finished piece with the majority of its structural properties. After the mold is sealed, resin is injected, heat being applied to the mold to cure the resin at the completion of filling. The finished composite product is then removed from the mold [1].

Successful filling of the mold is required for successful manufacturing. Liquid Injection Molding Simulation (LIMS) is a numerical simulation of the RTM process developed at the University of Delaware [2] [3], which provides the tools to design the correct injection scheme, before the expensive task of manufacturing the mold is undertaken.

A large portion of RTM preforms are manufactured using fabric style reinforcement materials. Preforms are constructed using a variety of methods, 'Draping' referring to the act of bringing a flat workpiece into contact with an arbitrary tool surface, causing the deformation of the preform material. The work presented in this paper is applicable to bi-directional reinforcement materials, woven or stitched.

The ability to predict the final configuration of the reinforcement material after draping is of interest to both preform manufacturers, and manufacturers who use draped preforms to fabricate composite structures [4]. The final orientation of reinforcement fibers within the preform will be a major factor in determining the structural properties of the finished piece. Within an RTM molding scenario, fiber orientation and local variations of fiber volume fraction due to draping can have significant effect on the mold filling process.

This paper presents brief details on the draping analysis code developed at the University of Delaware, DRAPER. This simulation was designed to predict the final configuration of reinforcement material draped over an arbitrary surface. The results produced by our draping simulation have been used to predict the changes in the local permeability tensor at each location of a draped preform. This is vital information required by LIMS to model the mold filling process for cases in which deformation of the preform is significant.

A mold has been constructed that provides a complex tool surface, requiring the preform to undergo significant deformation. The mold cavity is a thin shelled cone, with hemispherical nose. Results of experimental flow visualization will be presented, along with measured injection pressure history. Experimental results will be compared with results obtained from LIMS simulations. The simulations carried out were based on the permeability predictions calculated from DRAPER results.

THEORY

Brief theory is presented here on mold filling simulation, draping analysis, and local permeability tensor predictions based on draping analysis results. For more detailed information, the papers cited in this section should be reviewed.

NUMERICAL FLOW MODELLING

Practice has converged on modelling the mold filling stage of RTM as flow through porous media [5][6]. These simulations are based on Darcy's law, which relates;

$$v_d = -\frac{K}{\mu} \nabla P \tag{1}$$

where μ is the viscosity of the fluid, P its pressure, and K is the permeability tensor, representing the resistance of the porous media in different directions. The permeability tensor is related to the architecture of the preform. v_d is the volume averaged Darcy velocity [7].

The version of LIMS employed in this study considers flow through porous media in planar sections, averaging velocities through the thickness of a part. The simulation is based on a two dimensional version

of Darcy's law,

$$
\begin{pmatrix} v_x \\ v_y \end{pmatrix} = -\frac{1}{\mu} \begin{pmatrix} K_{xx} & K_{xy} \\ K_{yx} & K_{yy} \end{pmatrix} \begin{pmatrix} \partial P/\partial x \\ \partial P/\partial y \end{pmatrix}
\tag{2}
$$

where v_x and v_y are the Darcy velocities in the x and y directions [3].

DRAPING ANALYSIS

For bi-directional fabrics, woven or stitched, draping an arbitrary tool surface depends on two deformation modes. These modes are; shear deformation and inter-yarn slip [8]. A mat of this nature can be treated as a net that consists of many cells [9]. Therefore, draping over a surface of double curvature requires the net to map on to the tool surface by changing the internal angles in each cell. This kinematic model is justified by the fact that the contact of fiber mats with the tool surfaces is often assisted by matched mold halves or diaphragms. With the normal support provided, the cross-over points of warp and weft tows become pivoting joints.

The four sides of a cell are made up of fiber tows. These tows, under the preforming condition, are inextensible. In high deformation regions of a preform, slippage may be necessary to drape the tool surface. The length of a cell segment can be changed as a result of slippage to accommodate for this effect. DRAPER assumes that tow slippage is negligible [10][4].

Shear deformation of the preform material alters local permeability through two mechanisms. Reorientation of the tows within the material alters the direction of the principal values of permeability. Shearing of the tow unit cells decreases the inter-tow spacing, thus increasing the local volume fraction of the preform, decreasing the local average permeability.

PERMEABILITY PREDICTIONS

Results easily obtainable from the draping code include; α, the minimum shear angle between warp and weft tows, and V_f, the local fiber volume fraction of the preform. At this point in time, we have assumed that the local permeability tensor of the preform is dependent only on α and V_f. Therefore:

$$
K = f(\alpha, V_f)
\tag{3}
$$

where α quantifies the change in the direction of the principal axes of the permeability tensor, and V_f allows one to change the magnitude of the local permeability components.

Modelling the effects of draping on the local permeability tensor is still in the early stages. Our model is based upon the decomposition of each layer of bidirectional material into two layers of unidirectional material. A local permeability tensor is predicted for each unidirectional material, based on computed values of α and V_f, and the two layers are superimposed together [10]. It is possible to account for the influence of V_f on the local permeability tensors by applying modified Kozeny-Carman equations [10]. The effect due to orientation of tows is introduced through the use of standard tensor transformations.

EXPERIMENTAL STUDY

A mold was designed to provide a tool surface of double curvature, requiring the preform to undergo extreme deformation in several areas of the mold cavity. The cavity shape decided upon was a cone of angle 21 degrees, capped with a hemispherical dome of radius 1.0". The cavity is 1/8" thick at all places. A solid model of the male half of the the mold is shown in Figure 1. The required deformation of the preform was such that only one type of bi-directional material was found that could drape the tool surface without wrinkling. The reinforcement material used was NCS 81053A, manufactured by JB Martin.

A two piece mold was built, with the female side being machined from optical grade clear acrylic. With this design, the fluid flow front could be recorded to video tape as the mold filled. The fluid used to represent a resin system was dilute corn syrup, dyed for ease of visibility. A video camera was placed directly above the mold, capturing a plan view of the flow front progression.
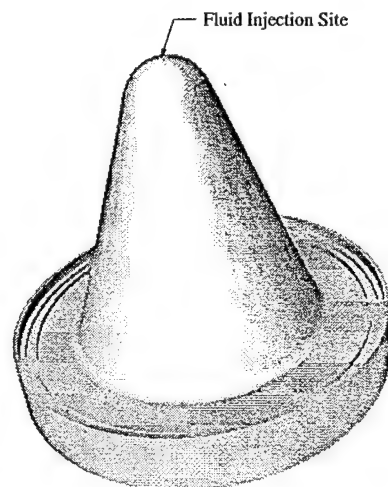

Figure 1: Solid model of tool surface.

For the particular experiment presented here, corn syrup of viscosity 106.5 centipoise, was injected at a constant volume flowrate of 2.10 cm^3/s. The preform was constructed of four layers of bi-directional material, providing an undeformed fiber volume fraction of 30.3%, before draping. The fluid was injected at the tip of the hemispherical section, air being vented at two points on the flange of the cone section.
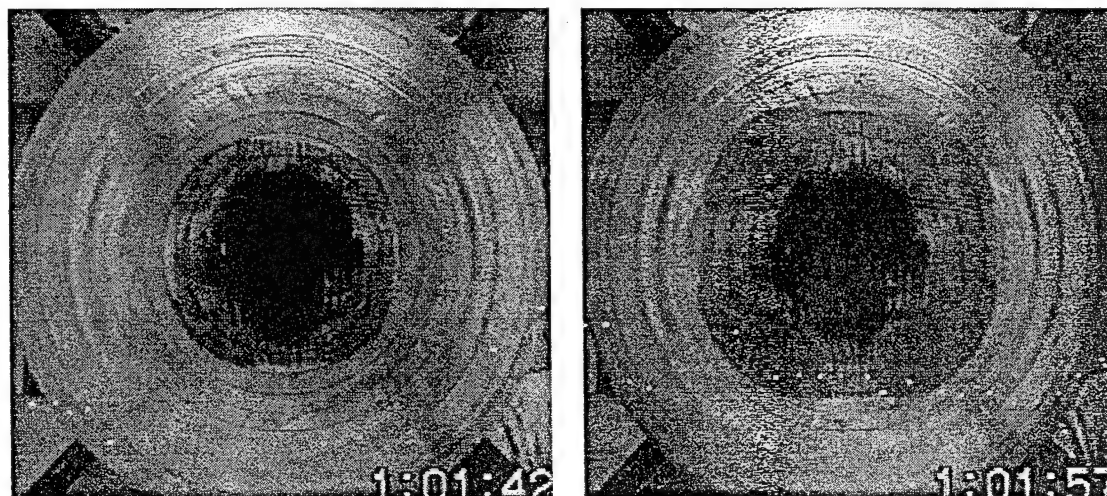
Figure 2: Frames digitized from flow visualization experiment. a) 14 sec. b) 29 sec.

Two video frames captured at 14 and 29 seconds into the experiment are presented in Figure 2. All experiments completed in this mold show definite evidence of flow front deformation due to preform draping. The injected corn syrup flowed faster through the regions of the preform sheared to the highest angle, producing a '4-pointed star' pattern. This pattern is evident in Figure 2, however, the viewing angle used tends to play down this effect.

The faster flow of the fluid through these regions demonstrates the contrasting roles played by the two mechanisms influencing local permeabilities. Though volume fraction is maximum in the highest sheared

portions of the mold, and it is reasonable to expect that the flow front would be slower in these areas, this was not the case. Reorientation of the tows in these regions has altered the direction of the principal permeabilities, causing preferential flow to occur in these areas.

A pressure transducer was situated in the fluid injection line just prior to entering the mold. In this manner, injection pressure histories were recorded for all experiments completed. The experimental pressure history measured for this particular experiment is plotted in Figures 4 and 6. This curve will be compared to pressure histories predicted by LIMS.

The increase in required injection pressure due to draping was found to be very large. Corn syrup was injected into the center of a flat, square mold cavity of 1/8" thickness. The fluid viscosity was 361 centipoise, and the injection flowrate was 5.7 cm^3/s. Though fluid viscosity and flowrate were much larger than those used in the cone experiment, the maximum pressure reached was only 12.83 Psi. This result demonstrates the importance of studying draping of preforms, correct prediction of mold pressures being vital simulation results.

NUMERICAL SIMULATION

The experiment described in the previous section will be numerically modelled using the simulation abilities that are available to us at this time. Both numerical flow front and injection pressure history predictions will be compared with the experimental results presented.

A numerical representation of the tool surface was generated. A draping analysis was preformed, a plan view of the resulting cell deformation pattern is shown in Figure 3. Notable are the four areas of highest deformation situated at ninety degree intervals. This pattern was observed experimentally, shearing angles comparing well at first inspection. Currently, work is underway to measure both local shearing angle and fiber volume fraction experimentally.
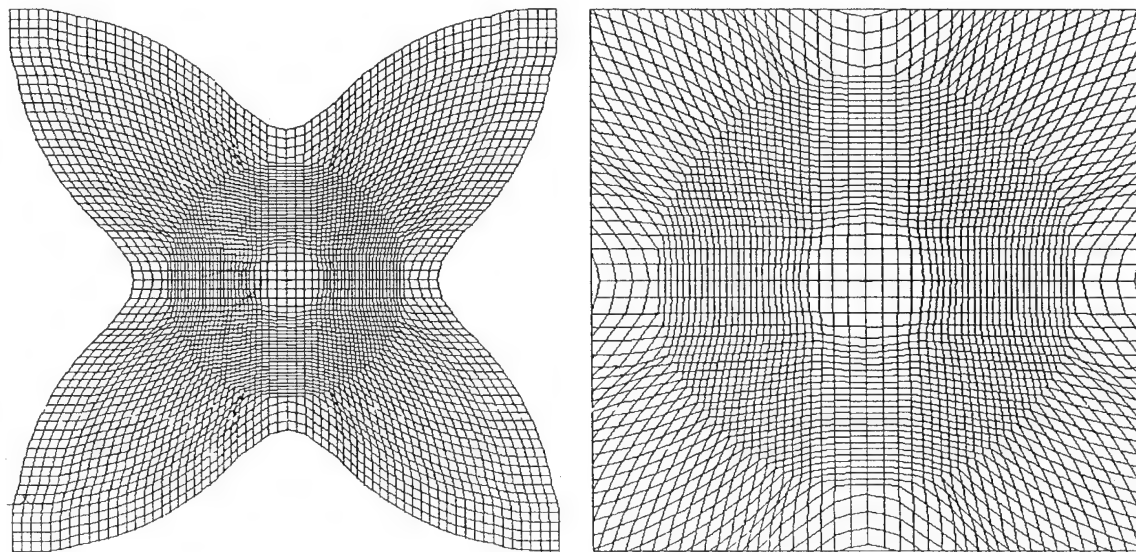

Figure 3: Cell deformation pattern predicted by DRAPER. A close up is shown to the right.

The obtained draping results were used to calculate local permeability tensors for each element of a LIMS finite element model. The initial method used, encorporated both local fiber volume fraction, and minimum shear angle. However, subsequent flow simulations revealed that this approach over emphasized the influence of fiber volume fraction, the predicted flow fronts showing the experimentally observed '4-pointed star' pattern out of phase by 45 degrees.

The injection pressure history calculated using LIMS is presented in Figure 4. This is compared with

the experimental results. The numerically predicted pressures are roughly one order of magnitude larger than the experimental values. This large error may be due to the unrealistically low values of permeability predicted by the modified Kozeny-Carman equations, or possibly high volume fractions calculated by the draper.
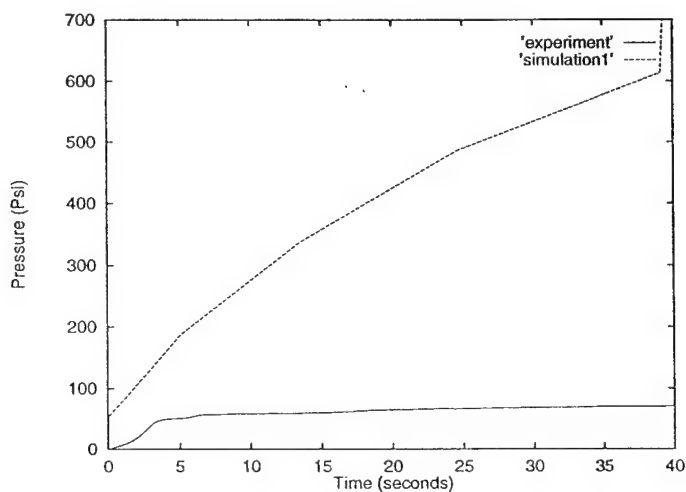

Figure 4: Experimental and numerically calculated pressure histories.

A second approach was adopted, for which local permeability tensors were calculated from the minimum shear angle alone. Component permeability tensors were obtained by decomposing permeability measurements of the the undeformed preform material. Numerical flow front progression results are shown in Figure 5. The black contours represent flow front position at four second time intervals. The flow fronts predicted by LIMS compare reasonably well with those recorded experimentally, reproducing the observed '4-pointed star' pattern. However, the numerically predicted star shape appears to be more pronounced. LIMS predicted the filling time of the mold cavity to be 48.1 seconds, while the mold filled in approximately 60 seconds during the experiment. Differences between numerical and experimental filling times are likely to be caused by inaccurate fiber volume fraction predictions.
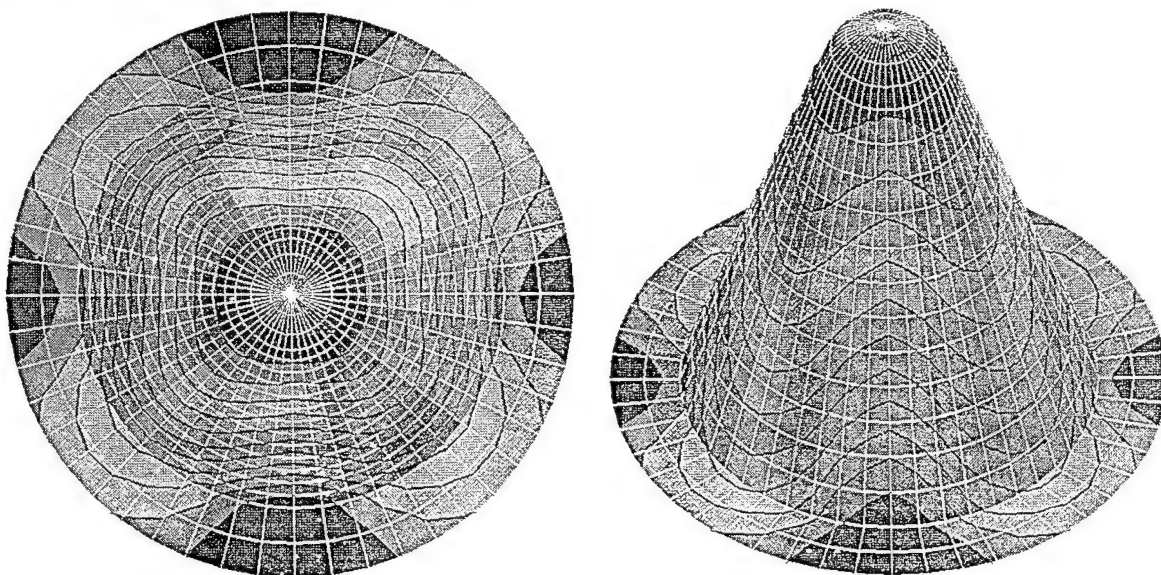
Figure 5: LIMS flow front predictions.

The injection pressure history for the second simulation, calculated using LIMS, is presented in Figure

6. The experimentally measured history is also shown. Notable is the large difference between the two pressure histories, simulation predicting pressures 5-10% of those experienced experimentally. This large error is probably due to the method of predicting draped permeability tensors, which does not take into account local increases in fiber volume fraction due to draping.

Discrepancies between numerical and experimental flow front and pressure histories signify the need for a new local permeability tensor prediction method that accounts for both local volume fraction, and tow orientation.
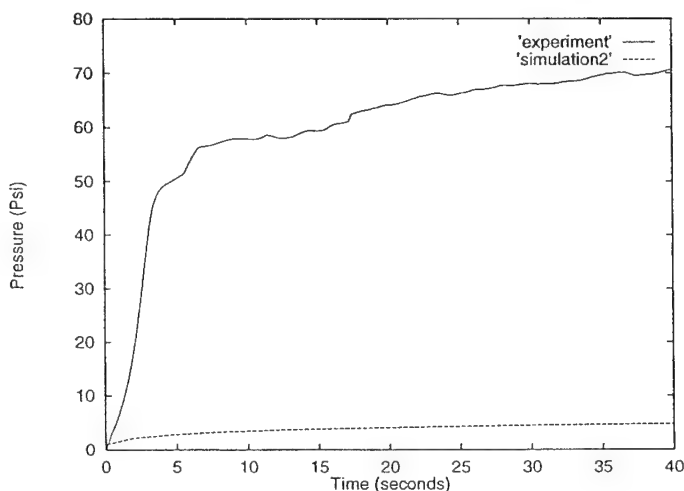
Figure 6: Experimental and numerically calculated pressure histories.

CONCLUSIONS

An experimental case study has been undertaken, demonstrating the effects of draping RTM preforms on the mold filling process. The deformation caused by draping the preform has been shown to effect flow front progression, and drastically increase required injection pressures. A numerical study has been completed, utilizing previously developed mold filling, and draping simulations. From our draping results, we have employed simple methods to predict local permeability tensors, information required for flow simulations. Simulations of the presented experiment show good agreement with recorded flow front data, while simulated injection pressure was 5-10% of the experimental values. The results presented signify the need for experimental verification of our draping code. This work is underway, and involves the manufacture of cone pieces using an aluminum mold. These pieces will be analyzed, yielding local fiber volume fraction and tow orientation. Models presented for calculating local permeability tensors are ad hoc. Further development will allow us to capture the correct physics of the manufacturing process.

REFERENCES

[1] S. G. Advani, M. V. Bruschke, and R. Parnas. *Flow and Rheolofy in Polymeric Composites Manufacturing. Chapter 12: Resin Transfer Molding.* Edited by Suresh G. Advani, Elsevier Publishers, Amsterdam, 1994.

[2] S. G. Advani, B. Liu, and M. V. Bruschke. *Liquid injection molding simulation - LIMS User's Manual - version 3.0.* University of Delaware, Newark, 1994.

[3] M. V. Bruschke and S. G. Advani. Filling simulation of complex three dimensional shell-like structures. *Sampe quarterly,* pages 2–11, 1991.

[4] B. P. Van West, R. P. Pipes, M. Keefe, and S. G. Advani. The draping and consolidation of commingled fabrics. *Composites Manufacturing*, 2(1):10–22, March 1991.

[5] W. B. Young, K. Han, L. H. Fong, and L. J. Lee. Flow simulation in molds with preplaced fiber mats. *Polymer Composites*, 12(6):391–403, December 1991.

[6] M. V. Bruschke and S. G. Advani. A finite element/control volume approach to mold filling in anisotropic porous media. *Polymer composites*, 11(6):401–402, 1990.

[7] H. Darcy. Les fontaines publiques de la ville de Dijon, Dalmont, Paris. 1856.

[8] K. D. Potter. The influence of accurate stretch data for reinforcements on the production of complex structural moldings. *Composites*, 10(3):161–167, July 1979.

[9] C. Mack and H. M. Taylor. The fitting of woven fabric to surfaces in three dimensions. *J. Textile Inst.*, 47:447–488, 1956.

[10] L. Fong and S. G. Advani. The role of drapability of fiber preforms in resin transfer molding. In *Proceedings of the 9th American Society for Composites*, page 1246, 1994.

ACKNOWLEDGEMENTS

Experimental Investigation of RTM, within a Box Mold

Simon Bickerton and Suresh G. Advani[*]
Department of Mechanical Engineering
University of Delaware
Newark, DE 19711

Abstract

Resin Transfer Molding is emerging as an important manufacturing process, for producing complex composite pieces. This report deals with the mold filling stage of the process, in particular, an experimental study of the filling of a five sided box. Flow front progression, as well as pressures, have been measured experimentally for a variety of mold filling situations. Parameters varied from experiment to experiment include; fiber volume fraction, preform type, fluid viscosity, fluid injection speed, and injection location. A large number of experiments have been completed, providing a valuable source of experimental data for modeling and numerical simulation of the RTM process.

---

[*]Author to whom correspondence should be addressed.

1

Contents

1 Introduction

Resin Transfer Molding, or RTM, provides an excellent method for the production of complex composite pieces. The process has a number of benefits including;

- The process is a relatively quick, low cost operation.

- It produces a net shape, with minimal machining required.

- It produces pieces with tight tolerances, and good surface quality.

The mold filling stage of RTM is very important in determining the finished quality of the product. If the mold is not filled completely, and air is entrapped within the mold, porosity, dry spots, or other defects may be produced in the finished piece, seriously degrading its quality. It is therefore necessary to form an understanding of the mold filling stage, ensuring that your mold filling strategy will be successful.

This work focuses on the mold filling stage of RTM, the objective being to study the mold filling of a moderately complex three dimensional mold cavity. A mold was built, allowing the visualization of the fluid flow front as it filled the mold. The mold cavity is a five sided rectangular box, with a base and four sides. Accommodation was made for the measurement of pressure at several points within the mold. A more detailed discussion of the goals of this study is presented in Section 2, Objectives.

Racetracking is a common phenomena encountered during the filling of RTM mold cavities. Racetracking occurs whenever the fluid filling the mold encounters an air cavity, or region of the mold not completely filled with the preform material. Due to the lower resistance to flow in such air cavities, the fluid will tend to fill these regions first, significantly altering the form of the flow front.

The deformation of the flow front due to racetracking can be difficult to predict, as the formation of air cavities within the mold is itself difficult to predict. It is therefore common

for racetracking to cause the formation of dry spots in the finished piece, as the placement of vents does not allow air within the mold to escape.

In the past, several numerical packages have been developed to simulate the mold filling stage of RTM. As racetracking can have a serious effect on dry spot formation, and hence finished product quality, the prediction of racetracking should be incorporated in such simulations. At this time racetracking has not been modelled, and the development of a model to account for racetracking is a long term goal of this work. The study discussed in this report serves as an initial investigation into racetracking, as this effect was documented in all the experiments undertaken. This study will also supply a database of experimental data, which will be useful for comparison to any RTM simulations developed in the future.

2   Objectives

The study detailed in this report had a number of objectives, which will be described in this section.

The main objective of this study was to build a database of experimental data from mold filling experiments performed in a moderately complex RTM mold. A mold was to be built, so that the fluid flow front progression could be recorded as the mold was filled. The experiment was designed so that the effects of a number of parameters could be investigated. These parameters included:

- Fiber volume fraction of the preform.

- Type of material used for preform.

- Fluid viscosity.

- Fluid injection speed.

- Injection location.

Pressure data was also to be recorded during the experiments. The mold was to be built so that injection point pressures, and pressures at other points in the mold could be recorded. This was to be feasible for a number of possible injection locations.

Both experimental flow front and pressure data would be used for comparison with numerical simulation results. The data gathered will also be useful for comparison with future versions of such numerical solutions.

This study will also serve as an initial investigation into the effects of racetracking. The importance of racetracking could be studied in various different situations, by considering its effect when varying the experimental parameters listed above.

3 Mold Design and Construction

A mold was required that would produce a moderately complex three dimensional mold cavity. A cavity shape was required that contained folded edges and corners. The cavity shape decided on was a rectangular five sided box, with a base and four sides. The shape and dimensions of the mold cavity are presented in Figure 1. This shape requires the fluid to flow around, and along corners. It was felt that this orientation would encourage the formation of air cavities in the assembled mold (e.g. containing the preform), and hence lead to the occurrence of racetracking during the experiments.

4"

8"

5 1/2"

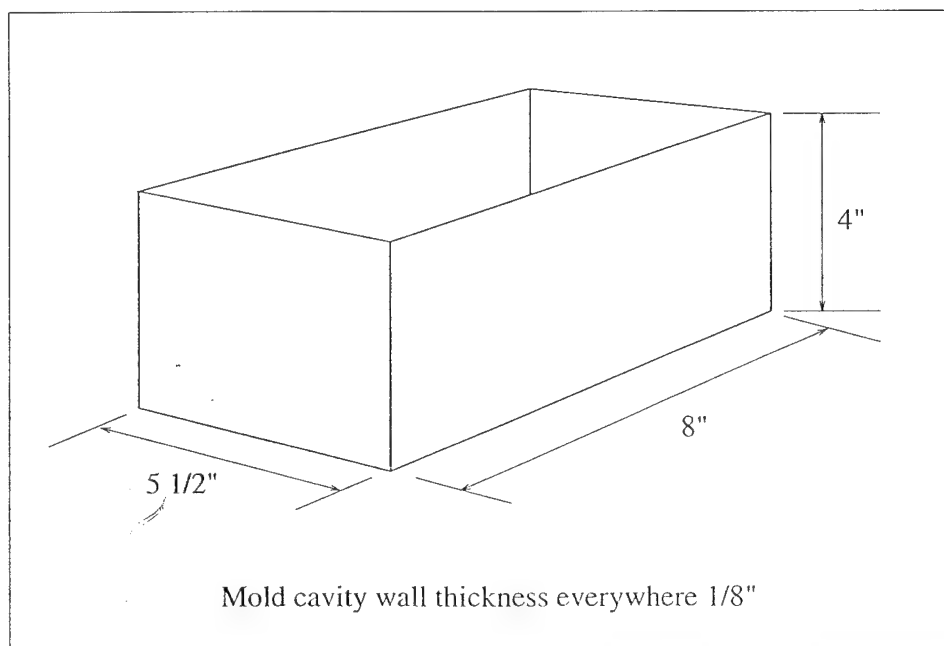Mold cavity wall thickness everywhere 1/8"

Figure 1: Mold cavity dimensions

The main aim of this experimental study was to record the progress of the fluid flow front as the mold cavity was filled. To allow the flow front to be visually tracked, it was decided that the female part of the mold be constructed from a clear plastic material. As it had been found that flexing of materials such as Plexiglas had been a problem in past studies, the stiffer material Lexan, was used to construct the female part of the mold. The basic design
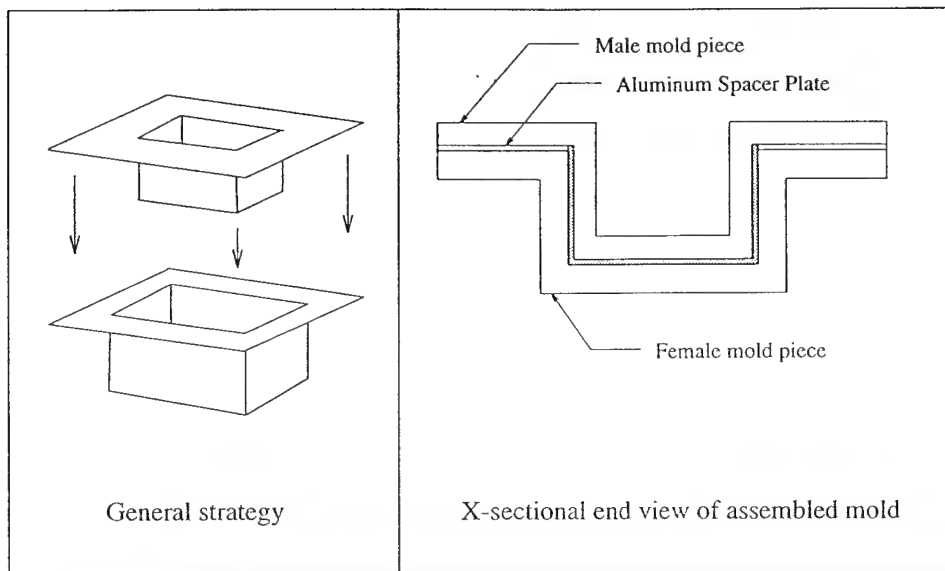
Figure 2: Basic mold design

of the mold is represented in Figure 2.

The mold was designed so that a wide variety of experiments could be performed. Both injection ports, and pressure transducer ports were located at the centers of the five faces of the box. Ports that were not required for a particular experiment could be plugged. Multiple vent locations were also provided at eight different points. These could be plugged with small screws when not in use. Details of vent and inlet positions are presented in Appendix A.

To aid with comparison to numerical solutions, and provide a visual reference, a 1/2" grid was drawn on the inner side of the female Lexan part. This feature can be seen in Figure 5. Figure 3 shows the finished mold.

4 Experimental Set-up

The experimental set-up used in this study provided a facility for undertaking mold filling experiments with constant flow rate injection. Figure 4 schematically represents the set-up.

The fluid used to simulate a viscous resin is placed within the piston and cylinder arrangement pictured in Figure 4. This fluid, diluted corn syrup in this study, will be injected into the assembled mold at a constant flow rate. To achieve a constant flow rate, the piston must be depressed at a constant speed. The cylinder is depressed by a hydraulic cylinder. By varying the flow of oil into the hydraulic cylinder, a range of constant flow rates can be obtained. The actual flow rate obtained for each experiment is calculated by measuring the speed at which the hydraulic cylinder extends.

The fluid leaves the piston and cylinder at a constant flow rate, and is transported to the mold through clear plastic tubes. The fluid is injected from the inside of the male side of the mold. Tubes and fittings have been obtained to allow for experiments with multiple injection points. Injection can occur simultaneously at one, two, or three injection points. With the correct fittings fluid could be injected into all five injection ports simultaneously (However this would serve little purpose).

During an experiment, the mold is situated on the wooden frame pictured in Figure 3. This frame serves two purposes. Firstly, the frame raises the mold up of a bench, allowing fluid injection tubes to be attached to the inside of the male mold piece. Secondly, the frame serves as a steady mount for the placement of the four mirrors. The purpose of the mirrors will be discussed shortly.

To record the progression of the flow front in the mold, the experiment is filmed using a Sony Video 8 Handycam. The handy cam is placed directly above the mold, and an overhead view of the mold is recorded to video tape. This angle views the base of the mold directly, and mirrors are required to capture the remaining four sides of the mold in the same video frame. Four mirrors are used, placed at approximately 45 degrees to the four mold sides.

An example of the view obtained is presented in Figure 5.

In addition to flow front data, pressure data has been collected from the majority of experiments completed. The mold was constructed so that pressure transducers could be placed across from any of the five injection sites. These pressure measurement sites can also be used for measuring non injection point pressures. The pressure transducers employed were CMC Technologies, 0-150 psi, model APT-FL. The electrical signal produced by the transducers was fed through a CMC Analog Pressure Transducer Interface (model PD4-4T2), and into a Macintosh Metro 20 Computer. The voltage data was logged using Quicklog v3.0.4. A small amount of post processing yields the required pressure versus time data.
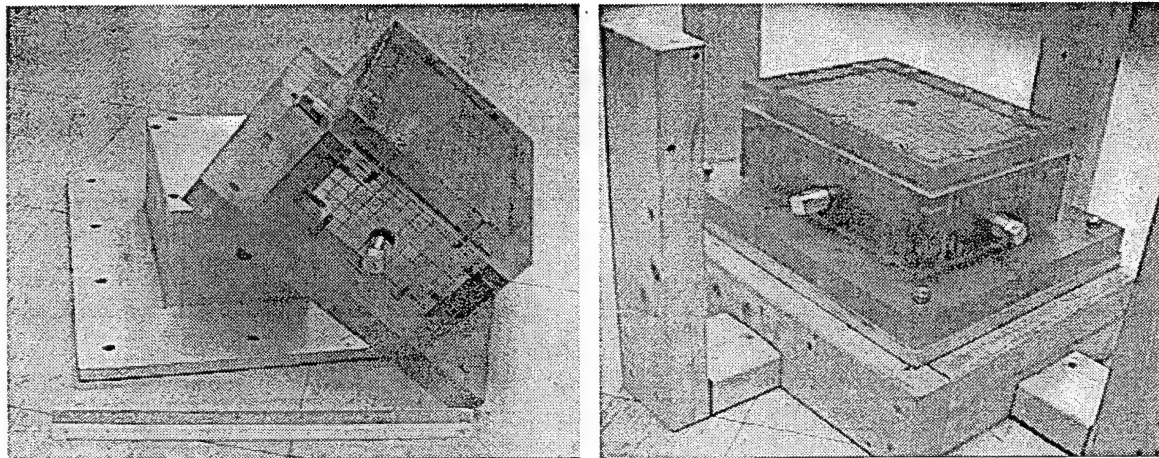
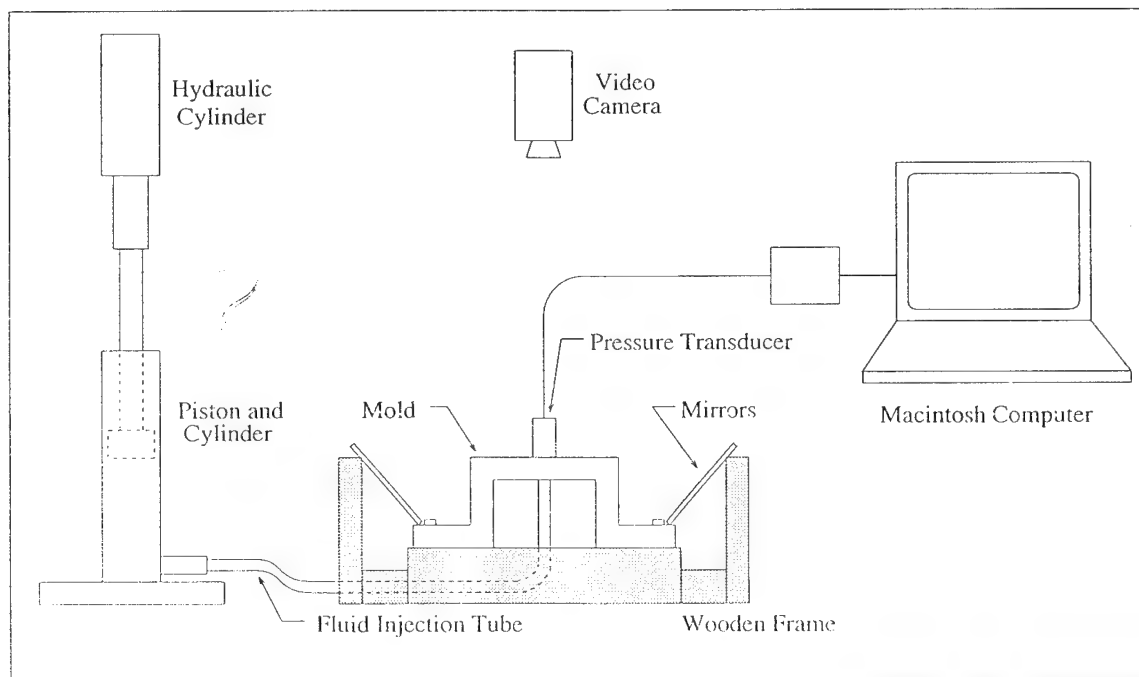Figure 3: Left: Mold in pieces, Right: Mold assembled on wooden frame

Figure 4: Schematic of experimental set-up

5 Experimental Procedure

This section details some of the procedures thought to be important to the completion of the mold filling experiments.

5.1 Preparation of the Fluid

The fluid chosen to simulate the resin used in an actual RTM run was corn syrup. Corn syrup is found to be convenient for a number of reasons:

- It is a Newtonian fluid, hence viscosity is easily characterized.

- It is soluble in water, making it easy to mix a range of viscosities.

- As it is soluble, it is practical for cleaning purposes.

- It will not degrade Lexan surfaces, as most resins will.

The corn syrup is diluted to approximately the desired viscosity, being in the range of 100 to 300 centapoise in this study. Black clothing dye is then added to the mixture. The dye is an important ingredient, as the corn syrup water mixture is very nearly clear. The addition of the dye increases the visibility of the fluid within the mold significantly. Water or extra corn syrup is added to bring the fluid to the desired viscosity. All viscosity measurement was carried out using a Brookfield digital viscometer.

5.2 Preparation of the Fibrous Preform

For all of the experiments carried out, the fibrous preform was constructed from layers of fiberglass reinforcement fabric. The different styles of mat included:

- Random mat

- Unidirectional mat

- Bidirectional mat

Details about the reinforcement fabrics used, will be presented in Appendix A.

The preform shape used in the vast majority of experiments is pictured in Figure 32, contained within Appendix A. This shape allowed for the easiest construction of the assembled mold, with the four side tabs draping neatly over the four box sides.

The fiber volume fraction of the preform used in each experiment needed to be calculated. This is required if the permeability of the preform is to be used for numerical simulation purposes.

The fiber volume fraction was calculated by taking a known area of a single layer of the material in question, placing this in a measuring cylinder partly filled with water, and measuring the volume of water it displaced. Dividing the volume of the section of material by its area will give its volume/unit area. The fiber volume fraction used in each experiment can be calculated from the following equation:

$$V_f = \frac{(No.\ of\ layers) * (Area\ of\ mold\ cavity) * (V)}{Total\ volume\ of\ the\ mold\ cavity} \tag{1}$$

where V_f is fiber volume fraction, and V is the volume per unit area of the preform material.

5.3   Pressure Data Conversion

The raw data collected from the pressure transducers was in the form of a voltage versus time file. A small fortran program was written to convert this to pressure versus time files in the desired units.

6 Experimental Strategy

The experimental data gathered during this study, will form a database of information useful for comparison with current and future numerical models of the mold filling stage of RTM. While data from a few experiments would be very valuable, a large number of experiments have been carried out, with the aim being to study several areas of interest. These areas of interest, and the corresponding experiments, are discussed in this section.

At this point, 46 mold filling experiments have been carried out during this study. In this section, the experiments are represented by a number. For full details of each experiment (preform information, fluid viscosity, etc) see Appendix A.

This section will be divided into discussions on the flow front progression study, and the pressure measurement study.

6.1 Fluid Flow Front Progression Study

The experiments detailed in this report can be grouped in several ways, to study the effects of different parameters. Each parameter will be discussed, and relevant results presented in Section 7.1.

6.1.1 Effects of Fiber Volume Fraction on Racetracking

It should be expected that as the fiber volume fraction (or in effect the density) of the preform increases, the level of distortion of the flow front caused by racetracking would increase. This could be explained as follows. Racetracking will tend to occur where an air cavity, or other form of low porosity region, is formed within the assembled mold. As the fiber volume fraction of the preform around the air channel increases, the fluid will find such a channel easier and easier to flow through, in comparison with the surrounding preform.

To verify this fact, observations can be made from several of the experiments completed.

15

Three experiments (17, 11, and 5) were completed with different fiber volume fractions of random mat. All other variables are constant for these experiments.

Three other experiments will be discussed. These experiments used a different injection position, one that was found to be more suitable for the study of racetracking. Experiment 24 is a random mat experiment, while experiments 34 and 35 used a bidirectional preform.

6.1.2   Effects of Fluid Viscosity on Racetracking

It should be expected that there will be no effect due to fluid viscosity on the magnitude of the racetracking effect. A simple explanation of this fact might consider that a change in the viscosity of the fluid flowing through an air channel, and in the neighboring preform, will have no effect on the relative resistances to flow through each area. As long as the resistance to flow through the two regions forms a constant ratio, there should be no effect on the extent of racetracking. This argument is valid for an isothermal filling process, however local changes in viscosity due to temperature variations may prove to be significant.

Two sets of experiments can be examined in the consideration of viscosity effects, six experiments with two levels of permeability. Experiments 9, 10, and 11, are random mat experiments with a fiber volume fraction of 14%. Experiments 2, 4, and 8, are random mat experiments with 7% fiber volume fraction.

6.1.3   Effects of Fluid Flowrate on Racetracking

As for viscosity, it is expected that there should be no effect on the magnitude of racetracking due to injection flowrate. This can be argued as for viscosity effects, the fluid speed within the preform and air channels, having no effect on the ratio of resistances to flow.

Two sets of random mat experiments can be examined to acknowledge this claim. Experiments 5, 6, and 7, were carried out with 7% fiber volume fraction, while experiments 9, 12, and 14, had 14% fiber volume fraction. The injection speeds are given in Appendix A.

Another set of 14% fiber volume fraction random mat experiments will be considered. Experiments 25, 26, and 27, were carried out with fluid injected at one of the short ends of the box.

6.1.4 Effects of Preform Material Type on Flow Front Progression

The majority of experiments were carried out using random mat preforms, as random mat proved to be the easiest material to work with. Fourteen experiments were carried out using unidirectional and bidirectional mats (5 unidirectional, 9 bidirectional). The major importance of producing experimental data from a variety of preform materials, is to provide data for comparison with numerical simulations of RTM.

The principal values of permeability of the random mat used were very similar. Hence, if fluid were to be injected at a point in a planar mold, circular flow fronts should be expected. The principal values of permeability measured for the unidirectional and bidirectional mats used, were significantly different. Flow fronts due to a point injection would be expected to be elliptical in shape. It was therefore expected that the general flow front shape would depend on preform material, and preform orientation within the mold.

6.1.5 Effects of Injection Location on Flow Front Progression

The majority of experiments were completed with the fluid being injected at one point, the center of the base of the box. Several experiments were completed with random and bidirectional preform, with different injection locations. Full details of these experiments are given in Appendix A.

The random mat experiments of interest are, 24 to 30, and 38 to 42. The bidirectional experiments of interest are, 34 to 37, 43 and 44.

6.2 Pressure Measurement Study

As for the flow front study, several topics of interest will be discussed, and the relevant experiments listed. Results will be presented in Section 7.2.

6.2.1 Effects of Fiber Volume Fraction on Injection Pressure

As the fiber volume fraction within a mold is increased, the resistance to fluid flow should increase. Therefore it should be reasonable to expect that pressures within the mold will increase with higher volume fractions.

The pressure files of the following experiments can be compared to investigate the effects of fiber volume fraction; 5, 11, 17, 21, and 32. Experiments 5, 11, and 17 used random mats, while 21 used unidirectional, and 32 bidirectional.

6.2.2 Effects of Fluid Viscosity on Injection Pressure

As viscosity of the resin injected within a mold increases, larger pressures should be required to drive the resin through the preform. Pressure data files from several experiments can be compared to investigate this fact.

The same experiments used to consider the effect of viscosity on racetracking will be used to investigate the effect on injection pressure (Experiments 2,4,8, 9, and 11). Experiment 10 cannot be considered, as experimental error caused pressures not to be measured.

6.2.3 Effects of Fluid Flowrate on Injection Pressure

If resin is injected into a mold at higher and higher flowrates, the pressure required to drive the flow should increase. This is analogous to pumping fluid through a pipe at greater and greater flowrates, the shear stress that must be overcome being strongly related to the fluid velocity.

The same experiments considered in the investigation into the effect of flowrate on race-tracking, will be studied. Experiments 5, 6 and 7, are 1 layer random mat, with three different injection speeds. Experiments 25, 26, and 27, are 2 layer random experiments using a different injection site.

6.2.4 Effects of Injection Location on Injection Pressure

In the design of an RTM mold, one is interested in obtaining an injection scheme that will minimize the pressures experienced within the mold. If this is achieved, significant materials cost savings can be made.

Several experimental pressure files can be studied, to examine the effect of injection location. Experiments 11, 25, and 29 will be studied, these using three different types of single point injection. Experiment 40, a two point injection, will also be considered.

7 Results and Discussion

This section will present all of the results relevant to the topics discussed in Section 6. All of the flow front progression and pressure data for all of the experiments completed in this study will not be included.

7.1 Fluid Flow Front Progression Study

Flow fronts will be compared in this section by tracing flow fronts at distinct times, onto a folded out grid representing the 5-sided box. Due to the symmetry contained in most of the experiments, the flow front figures present only half of the mold. In general, flow fronts presented in a chart are chosen so that they match at certain points within the mold.

7.1.1 Effects of Fiber Volume Fraction on Racetracking

Flow fronts recorded during experiments 5, 11, and 17, are presented in Figure 6. The flow fronts have been recorded at a similar point in time. This should give some information about the extent of the effect of racetracking at this particular point in the experiments. The approach is very similar for the remainder of flow front charts presented in this section.

Examining Figure 6, it is noticeable that the effect of racetracking in all three experiments is relatively small. Experiments 5, 11, and 17 had volume fractions of 7%, 14%, and 21% respectively. We should therefore expect that racetracking should be most evident during experiment 17. This appears to be true, however, it is difficult to draw solid conclusions when racetracking has such little effect. This was true of all of the experiments that were completed using this injection scheme. As the fluid flows around the corners that surround the base of the box, the main component of the flow is perpendicular to the air channels that have been set up in these corners.

Racetracking was found to be more prominent in experiments where the injection scheme

caused fluid to flow with a main component parallel to the air channels set up within the mold. Unfortunately, the majority of experiments designed to assess the effect of various parameters on racetracking, were carried out with the injection site at the center of the base of the box.

Flow fronts recorded during experiments 24 and 34 are presented in Figure 7. These experiments were completed with fluid injected at the center of one of the short ends of the box. Experiment 24 used a random mat preform with fiber volume fraction 14%, while 34 used a bidirectional mat of volume fraction 35%. Though these experiments are quite different in a number of respects, the effect on racetracking due to the large difference in volume fraction is significant. The effect of high volume fraction on racetracking was noted for all of the unidirectional and bidirectional mat experiments.

Also included in Figure 7 is a flow front recorded during experiment 35. This experiment was identical to experiment 34, with the orientation of the preform within the mold being rotated 90 degrees. This graphically shows the effect due to the orientation of the preform.

7.1.2   Effects of Viscosity on Racetracking

Flow fronts recorded during experiments 9, 10, and 11, are presented in Figure 8. These three experiments were identical except for the viscosity of the fluid. As expected, the effect of the varying viscosities on racetracking seems to be negligible. This was also found to be true when examining the set of experiments 2, 4, and 8.

Unfortunately this sort of study was not completed using other injection locations that would magnify the effect of racetracking. Experiments carried out with injection at the center of one of the side walls would be preferable.
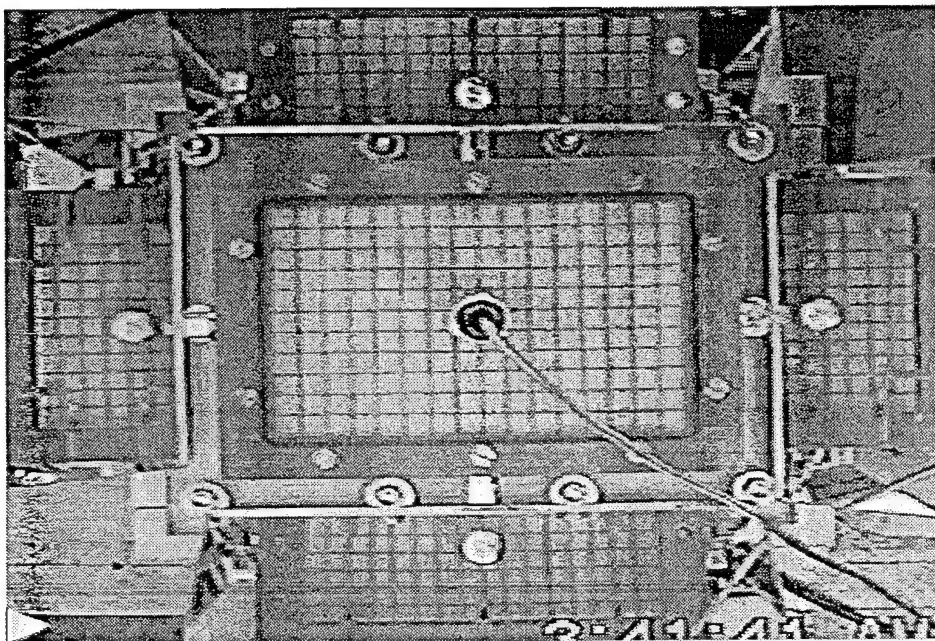
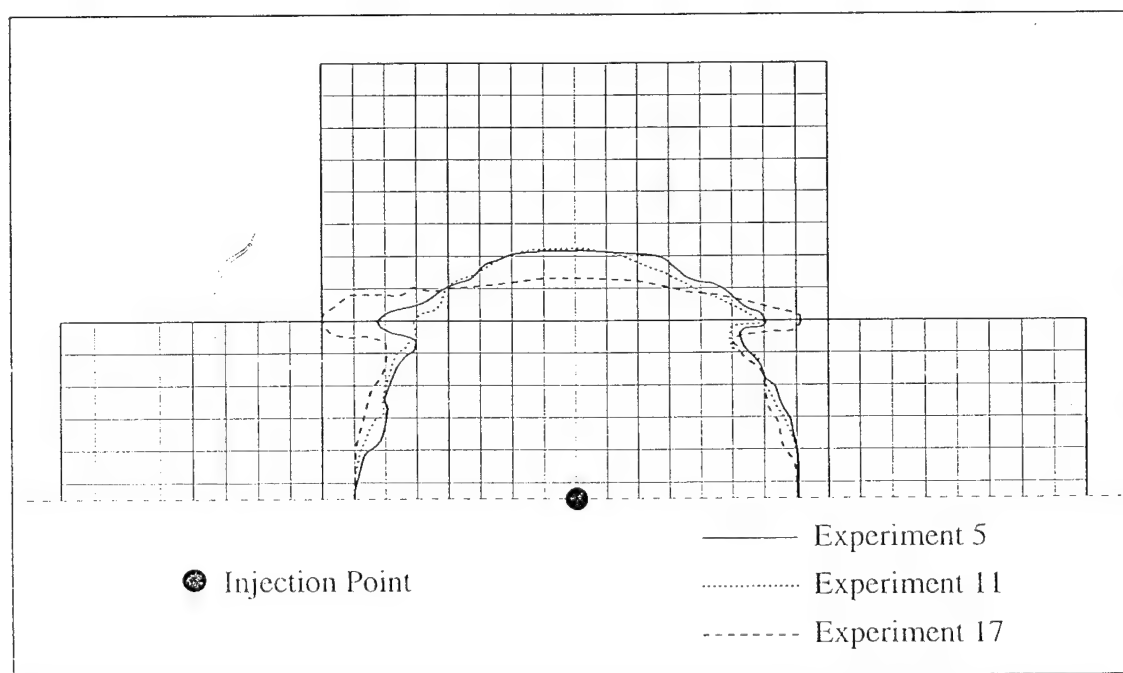Figure 5: View of mold from above. Sides of mold seen in mirrors

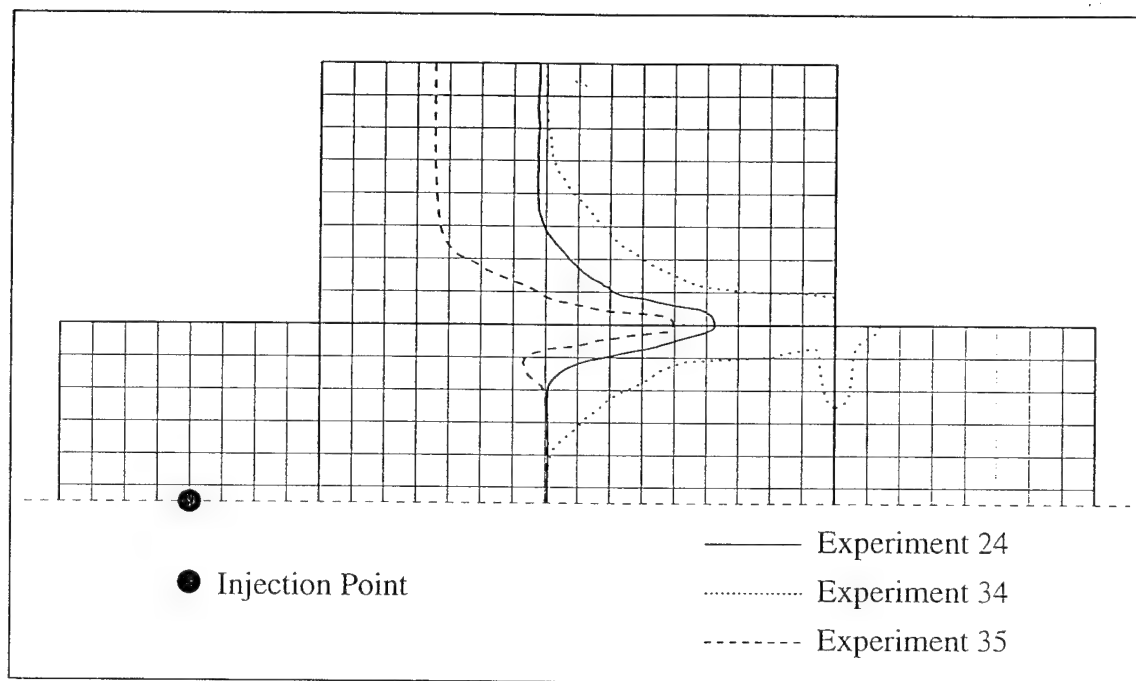Figure 6: Flow Map for Experiments 5, 11, and 17

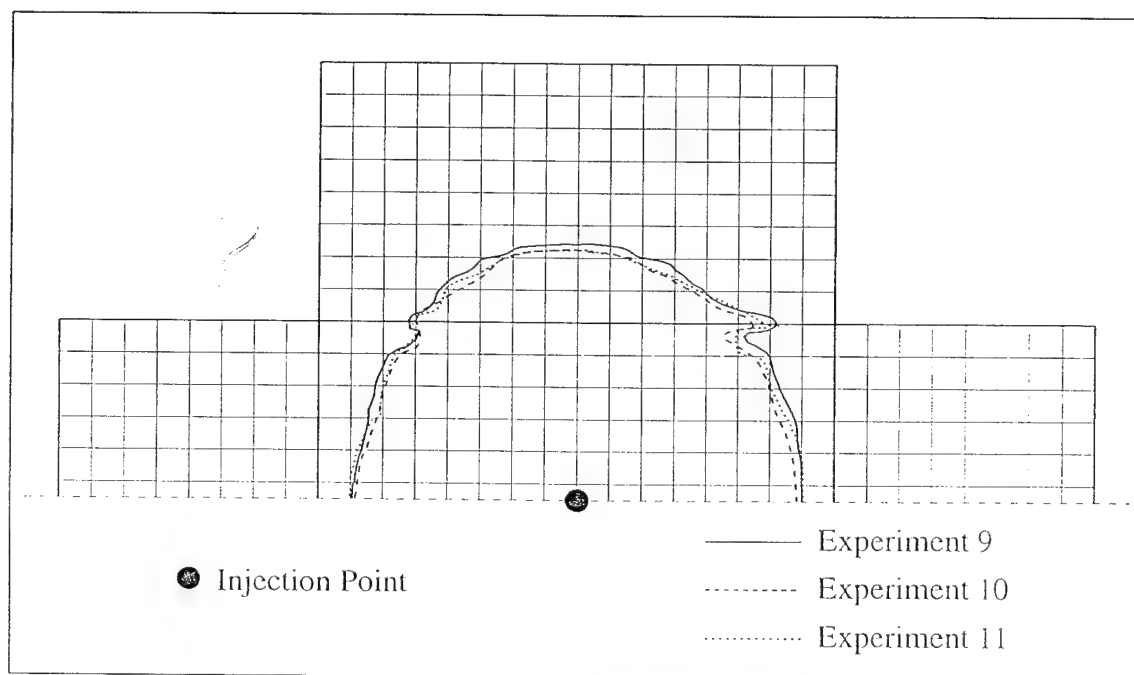Figure 7: Flow Map for Experiments 24, 34, and 35

Figure 8: Flow Map for Experiments 9, 10, and 11

7.1.3 Effects of Fluid Flow rate on Racetracking

Experiments 9, 12, and 14, were 14% volume fraction random mat experiments completed with three different injection speeds. Flow fronts from these experiments are presented in Figure 9. As described in the previous sections, the magnitude of racetracking in experiments completed using an injection point at the center of the box base, is such that it is hard to draw solid conclusions. This was also found to be true for experiments 5, 6, and 7.

Experiments 25, 26, and 27, form a group of experiments similar to 9, 12, and 14, with injection being at the center of one of the short sides of the box. This orientation was found to be the preferred orientation for studying the effect of various factors on racetracking. Flow fronts produced during these experiments are presented in Figure 10.

On examination of Figure 10, it seems that at a point during each experiment at which the flow fronts coincide at the center of the base of the box, the magnitude of the racetracking effect varies significantly. The injection speeds of the experiments 26, 25, and 27, form the ratio 4:2:1 respectively. It should be noted that the flow fronts of the experiments represented in Figure 10 were not present at similar points in time. Figure 10 suggests that as injection speed is increased, the magnitude of the racetracking effect is reduced. This is an unexpected result.

Flow fronts from the same experiments are presented in a slightly different way in Figure 11. These flow fronts have been recorded when tips of the deformed flow front reached the corner of three faces. This shows how the remainder of the fluid flow fronts lag behind, dependent on the injection speed used.

This unexpected result, may raise questions about the repeatability of the size of air channels that are set up within the mold. The experiments were carried out in a careful manner, so as to keep conditions within the mold as consistent as possible. However, the size of the air channels within the mold were not measured. It was noted that the size tended to vary with preform material, or fiber volume fraction, but appeared fairly constant for
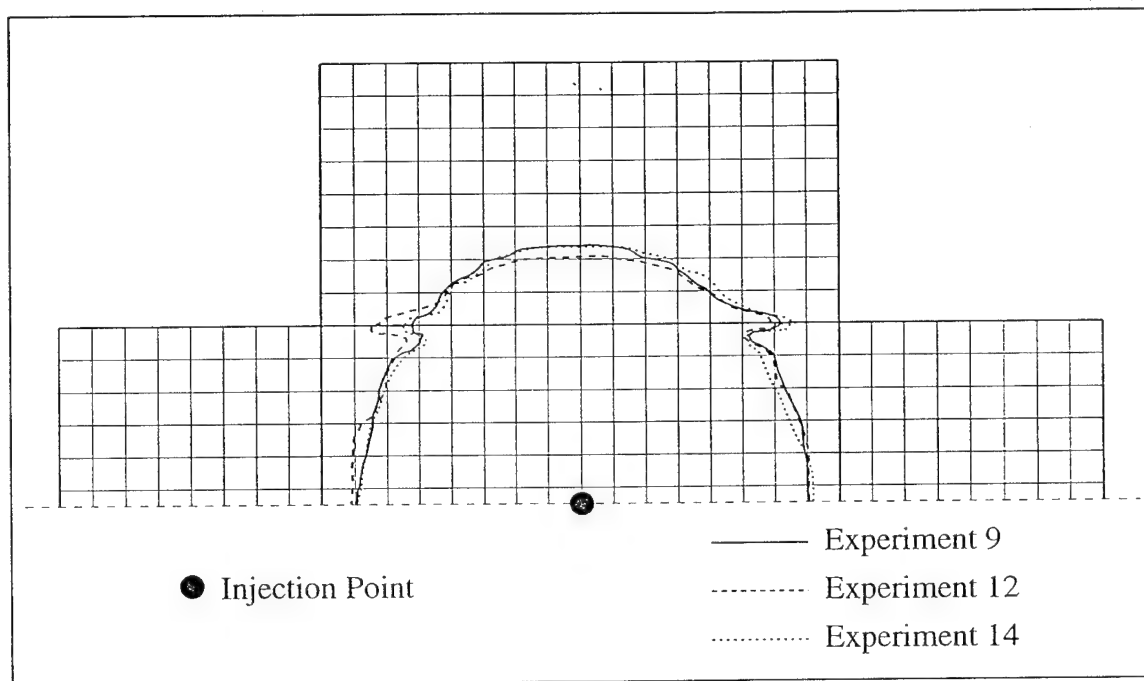
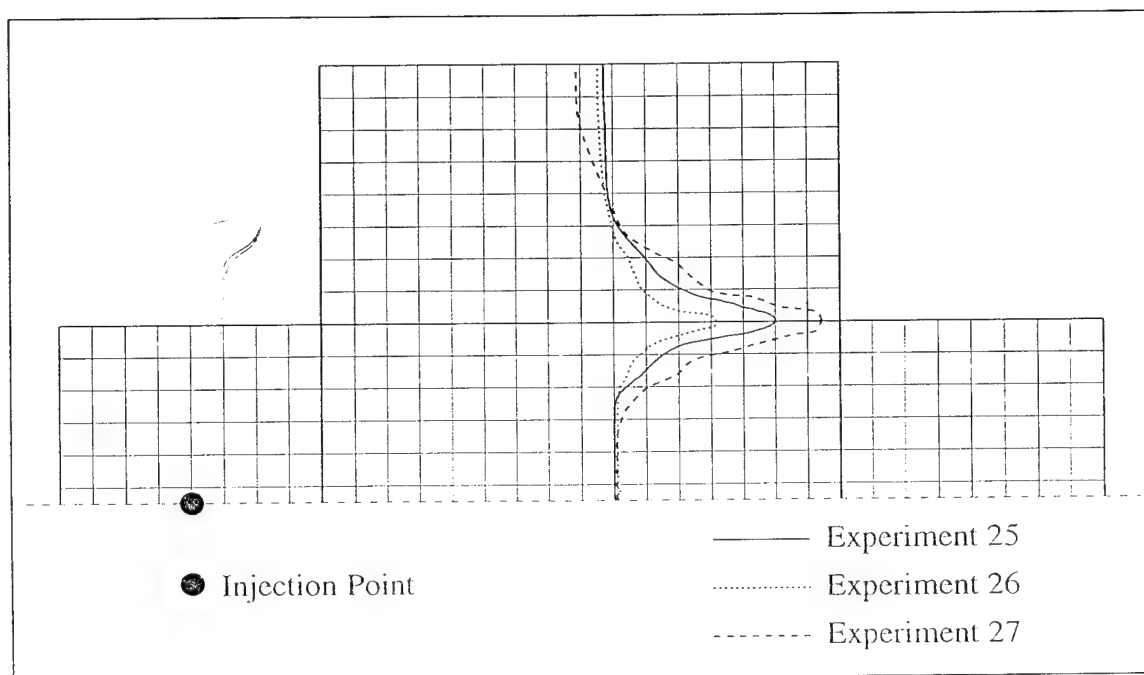Figure 9: Flow Map for Experiments 9, 12, and 14

Figure 10: Flow Map for Experiments 25, 26, and 27

experiments with similar preform characteristics. To be able to state that fluid injection speed is an important factor in the consideration of racetracking, experiments should be completed, for which the size of air gap within the mold is known to be constant.

7.1.4 Effects of Preform Material on Flow Front Progression

As predicted, the style of preform material used influenced the shape of the flow front within the mold. Digitized frames taken during four experiments will be presented to demonstrate this point.

Figure 12 presents frames recorded during experiment 28, a random mat experiment, and experiment 36, a bidirectional experiment using the same injection orientation.

Figure 13 presents two experiments using two point injection, experiment 39 using random mat preform, and experiment 43 bidirectional.

7.1.5 Effects of Injection Location on Flow Front Progression

To demonstrate the effect of injection location on flow front progression, digitized frames taken from four experiments will be presented. Experiments 12, 24, 28, and 39, used random mat preforms, and represent the four injection schemes used in this study. These frames are presented in Figure 14.

7.2 Pressure Measurement Study

Several plots of pressure versus time will be included in this section. Time is plotted in seconds (s), and pressure in pounds per square inch (Psi). Pressure curves will be labelled 'out(experiment no.)', the curve for experiment 17 being labelled 'out17'.
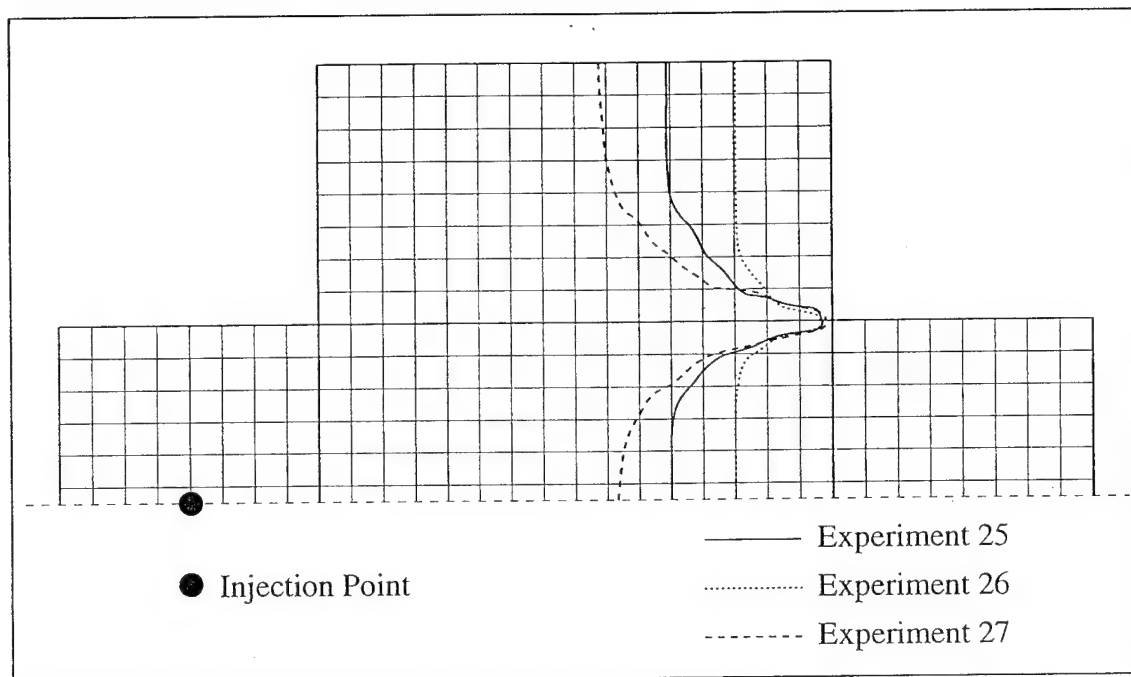
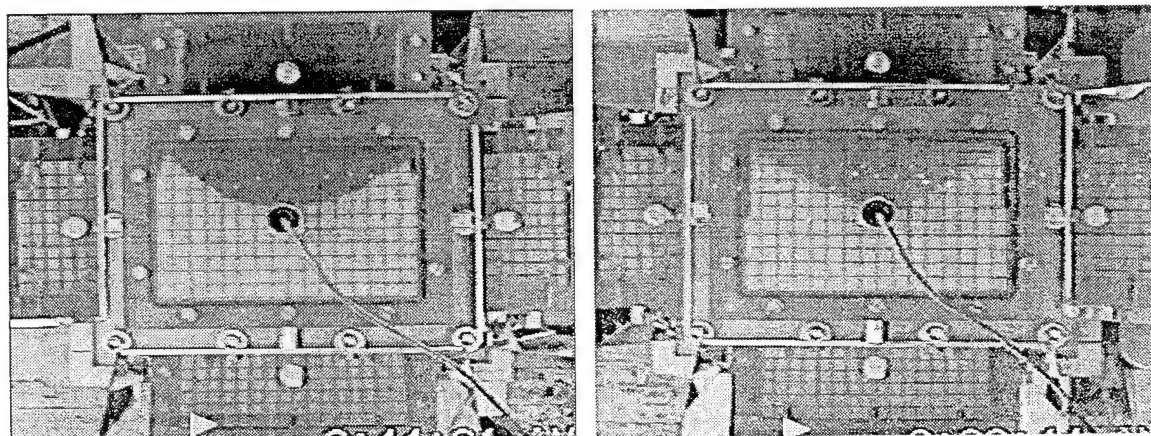Figure 11: Flow Map for Experiments 25, 26, and 27

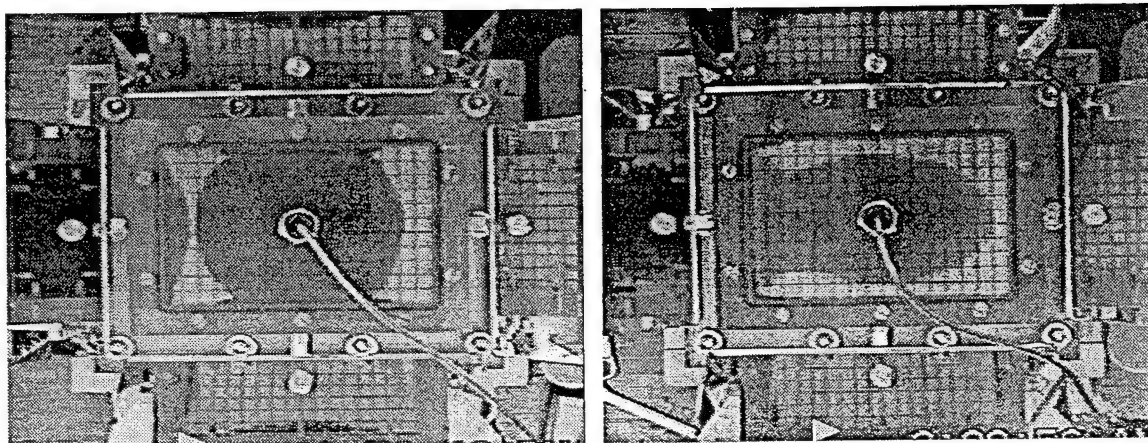Figure 12: Left: Experiment 28, Right: Experiment 36

27

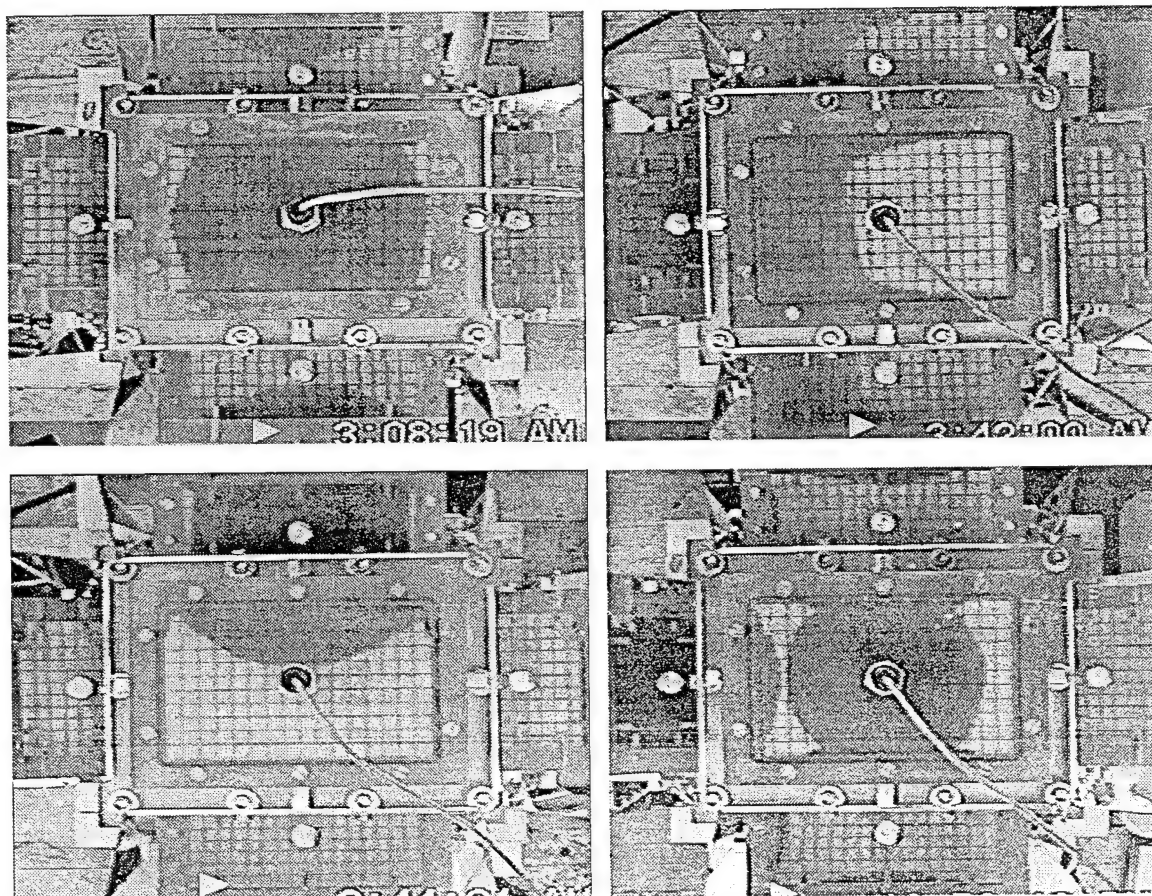Figure 13: Left: Experiment 39, Right: Experiment 43

Figure 14: Top Left: Experiment 12, Top Right: Experiment 24, Bottom Left: Experiment 28, Bottom Right: Experiment 39

7.2.1 Observations of General Pressure Curve Shape

The majority of experiments were completed using single fluid injection points. For these experiments which injection site pressure was measured, a common shape of pressure curve was found. This can be observed by examining the various pressure plots presented in this section. Figure 15 presents the curves for experiments 17, 29 and 33. Experiment 17 was carried out using a random mat preform, with injection at the center of the box base, while experiment 33 used bidirectional mat with a similar injection scheme. Experiment 29 employed random mat preform, with injection at the center of one of the long sides of the box. Though these experiments are varied in their nature, the three pressure curves show very similar trends.

The pressure curves can generally be broken down into three regions. Initially, pressure rises quickly with the gradient of the slope decreasing with time. A second stage develops, during which the gradient of the slope remains approximately constant. When the mold is close to filling, the rate of increase of pressure begins to rise again. This third stage is not evident on some pressure curves, as injection and pressure measurement were often stopped prematurely. The three stages are shown for experiment 17 in Figure 16.

On comparison of pressure histories and their corresponding flow front progressions, it seems that the slope of a typical pressure curve is closely related to the circumferential length of the flow front. Examining several experiments, it seems that the following holds for many injection orientations. During the first stage noted in Figure 16, the circumferential length of the flow front is increasing with time, as the slope of the injection pressure curve decreases. During the second stage, the length of the flow front reaches a fairly constant value due to the shape of the mold cavity, and corresponds to a portion of the pressure curve with constant slope. During the third stage, the flow front length begins to decrease with time, and this seems to correspond to a steady increase in the slope of the pressure curve towards the end of the experiment. The stages of mold filling corresponding to the pressure curve for experiment 17 are presented in Figure 17.
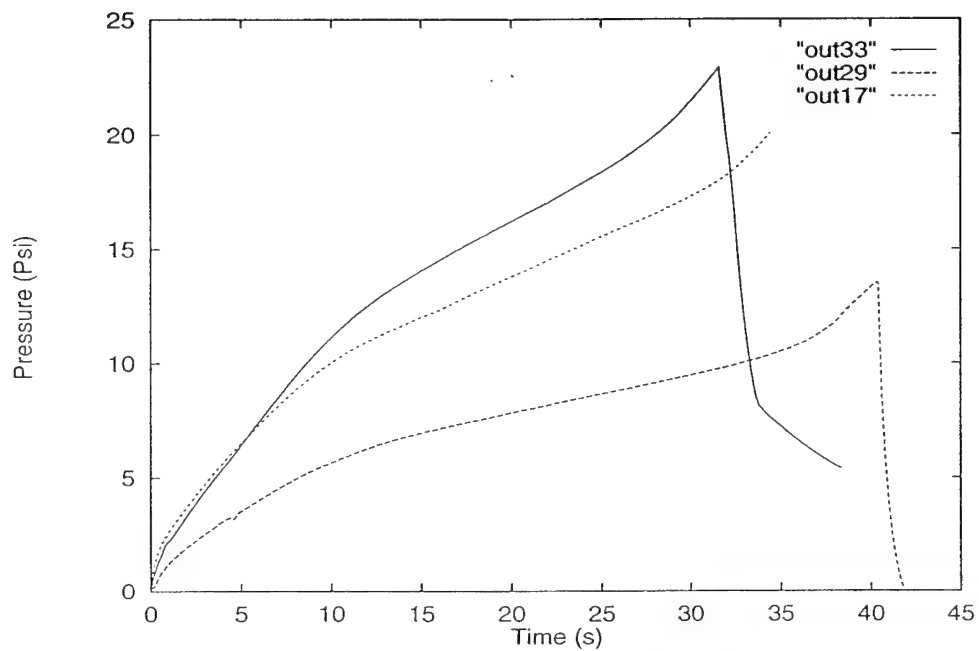
29

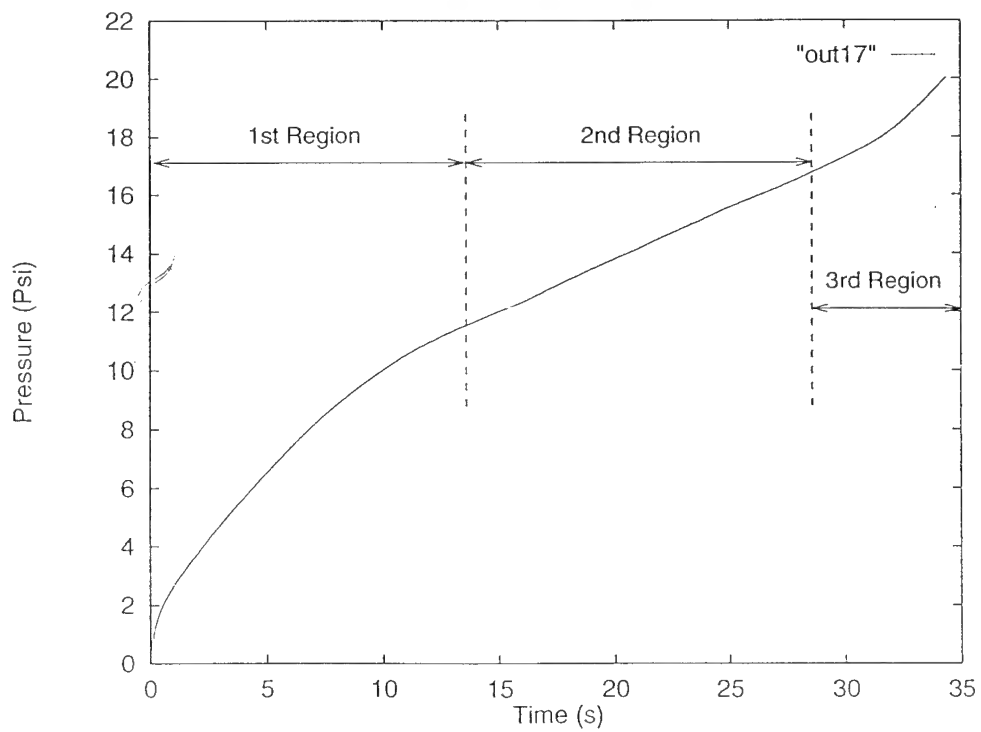Figure 15: Injection pressure plot, experiments 17, 29, and 30

Figure 16: Experiment 17 pressure plot showing three regions of interest

This discussion can be furthered by considering the pressure data measured during experiment 40. Experiment 40 employed a random mat, with fluid injection at two points (center of base, center of short side). Pressure was measured at both injection sites, the curves being presented in Figure 18. Curve Out40.1 represents the pressure measured at the center of the base.

For the first 9 or 10 seconds of injection, the flow fronts generated by each of the injection sites do not interfere with each other. During this time the pressure curves presented in Figure 18 rise in a logarithmic manner. Inflection points occur in the curves at the point at which the two flow fronts begin to merge , and the rate of increase of pressure steadily increases. Studying the flow front progression, it seems that the total length of flow front decreases as the mold fills past the time of this inflection. This observation is in agreement with single injection point experiments.

Double injection point experiments were also completed using bidirectional preform material. One injection pressure was measured for both of experiments 43 and 44 (center of base), with the bidirectional mat being oriented differently within the mold for each experiment. The injection pressure curves for these experiments are presented in Figure 19.

As for experiment 40, the inflection points on the curves presented in Figure 19 correspond to the merging of the two flow fronts within the mold.

7.2.2 Effects of Fiber Volume Fraction on Injection Pressure

The pressure versus time curves for experiments 5, 11, and 17, are plotted in Figure 20. These curves show clearly the increasing pressure experienced within the mold, with increasing volume fraction from 7 to 14 to 21%.

To compare even higher volume fraction results, pressure curves for experiments 17, 21, and 32, have been presented in Figure 21. The pressure data gathered from experiment 21 shows irregular shape, but clearly shows the greater pressures encountered when injecting
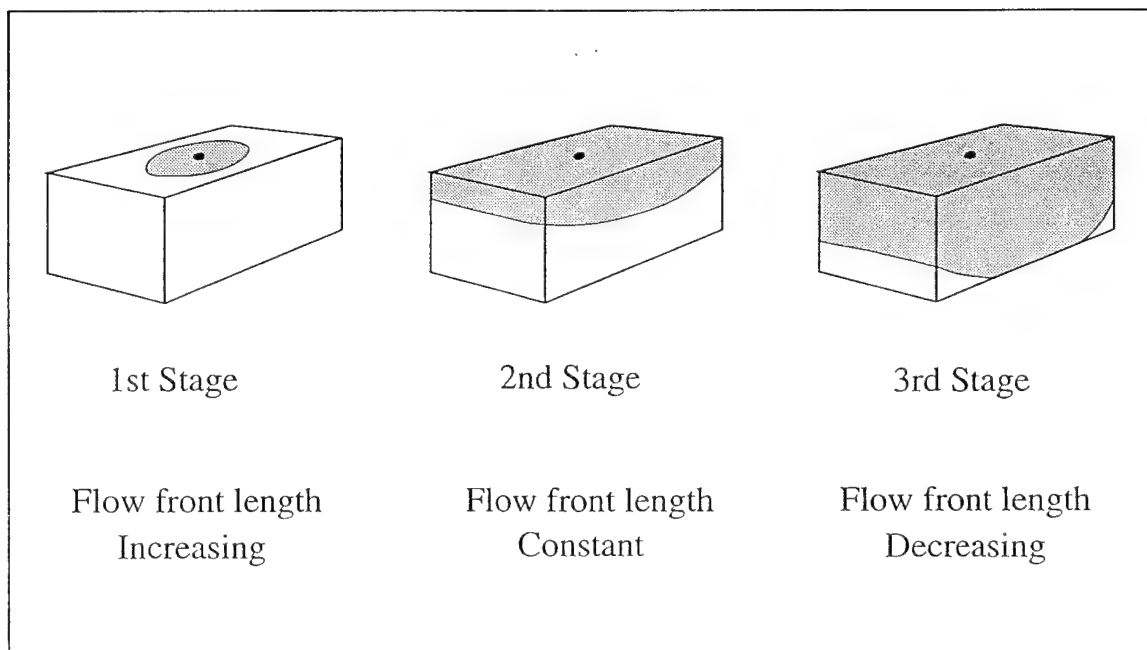
Figure 17: Three stages of flow front advancement during experiment 17
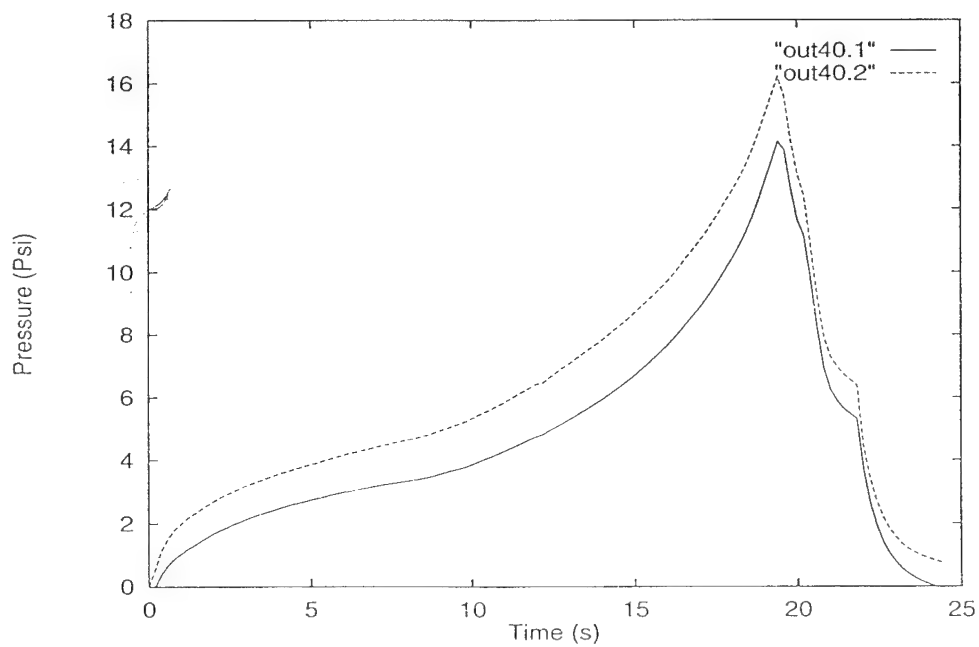

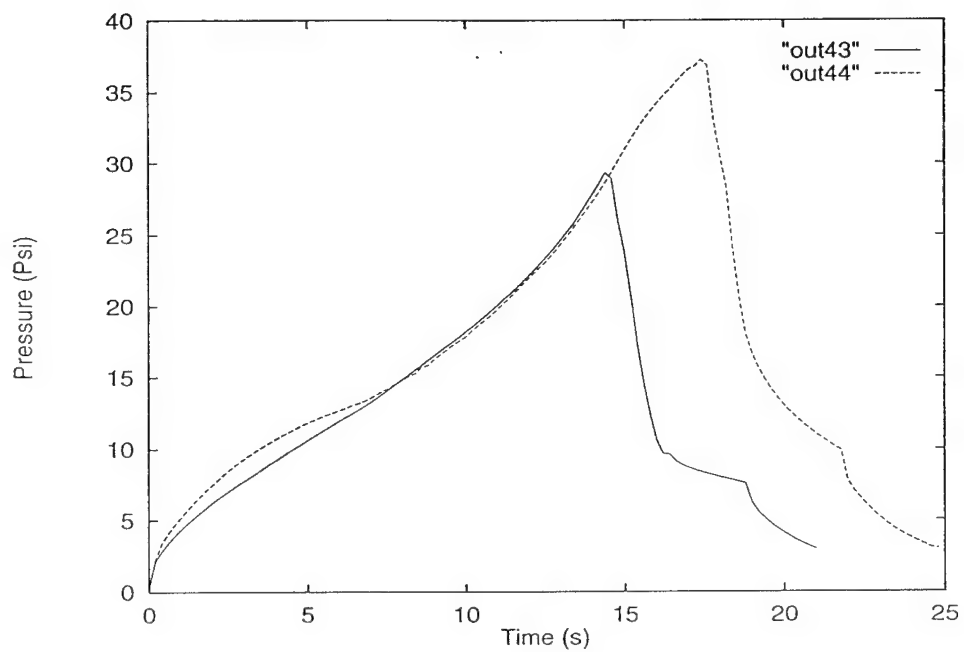Figure 18: Injection pressure plot, two points, experiment 40

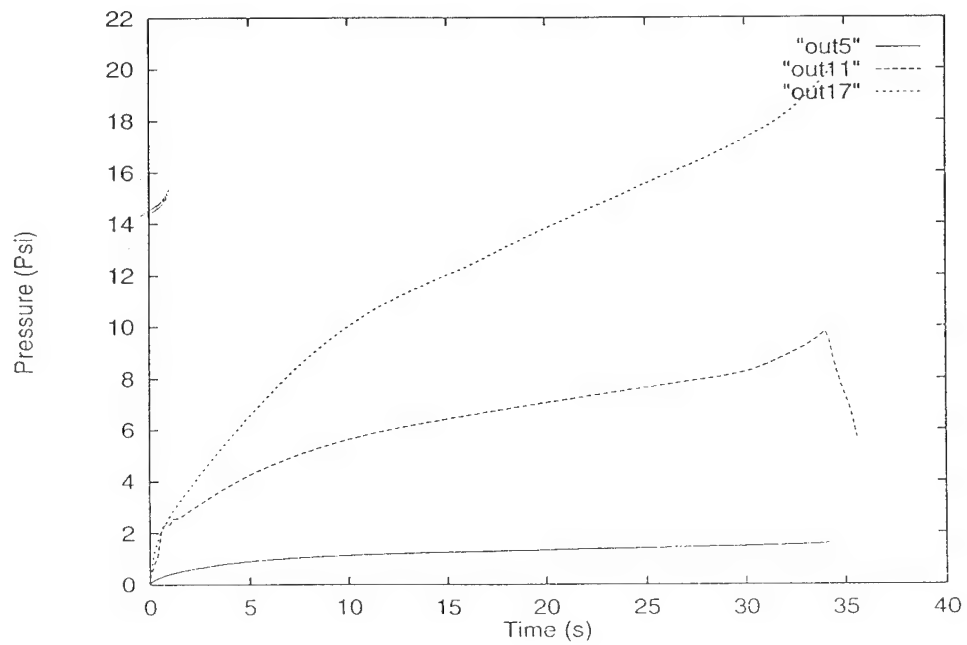Figure 19: Injection pressure plots, experiments 43 and 44

Figure 20: Injection pressure plots, experiments 5, 11, and 17

through a 33% volume fraction preform. The data gathered from experiment 32 seems to lie very close to the curve for experiment 21, though the fiber volume fraction was measured to be 35%. This seems to be due to the lower viscosity of fluid injected into the mold.

7.2.3 Effects of Fluid Viscosity on Mold Pressure

Three experiments using 1 layer of random mat will be examined first. The pressure curves for experiments 2, 4, and 8, are presented in Figure 22. This figure clearly shows the effect of increasing fluid viscosity on mold pressure. A similar result was found when comparing the injection pressures measured during experiments 9 and 11, both two layer random mat experiments. These pressure curves are presented in Figure 23.

The majority of RTM mold filling simulations are based on Darcy's law:

$$v_d = -\frac{K}{\mu} \nabla P \tag{2}$$

where μ is the viscosity of the fluid, P its pressure, and K is the permeability tensor. v_d is the volume averaged Darcy velocity.

Due to the form of Darcy's law, it is reasonable to expect that the pressure curves in Figure 22 should be related very simply by fluid viscosity. It should be possible to collapse the curves on top of each other, by scaling each by the appropriate viscosity ratio. The pressure curves of experiments 2 and 8, have been scaled by multiplying the pressure at each time by the ratio of viscosity for experiment 4, to the viscosity for the experiment in consideration. The resultant curves are compared to the pressure curve for experiment 4, in Figure 24.

By examining Figure 24, it is noticeable that the three curves do not collapse on to each other exactly. The curves out4 and chout8 compare nicely, while chout2 has not scaled so well.
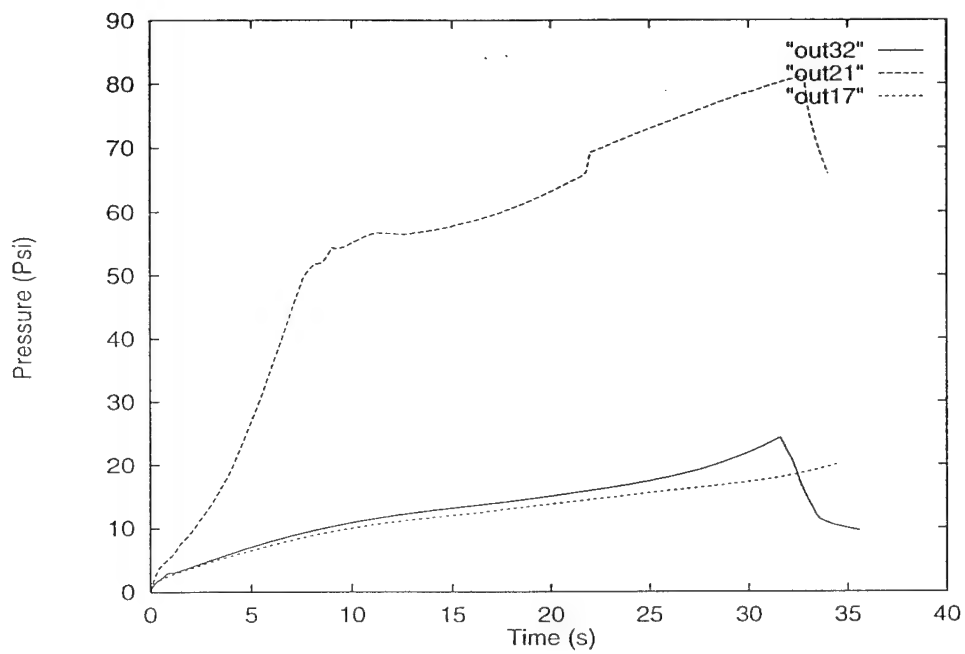
Figure 21: Injection pressure plots, experiments 17, 21, and 32
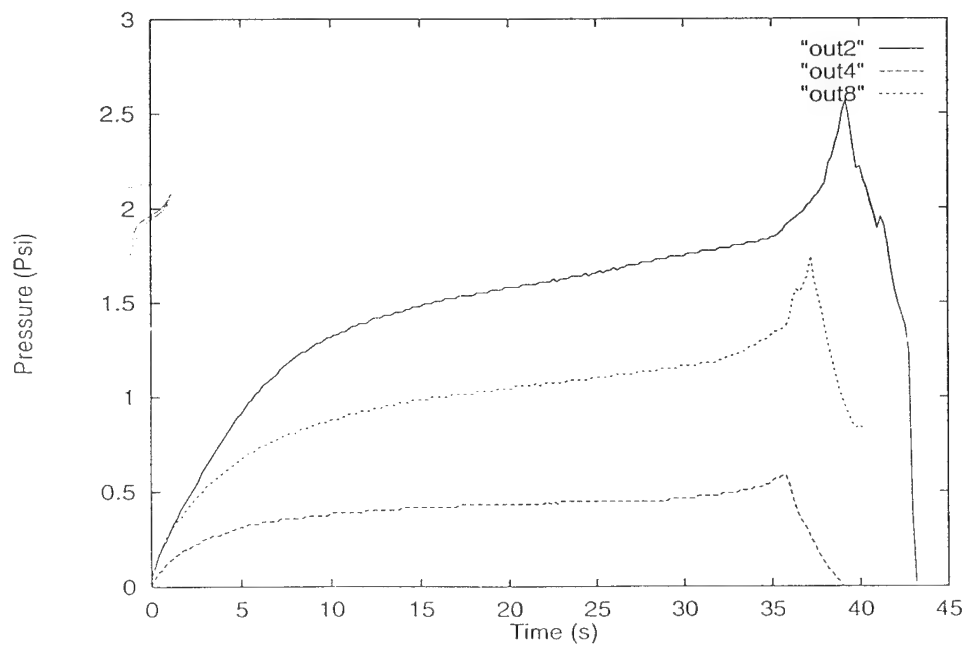

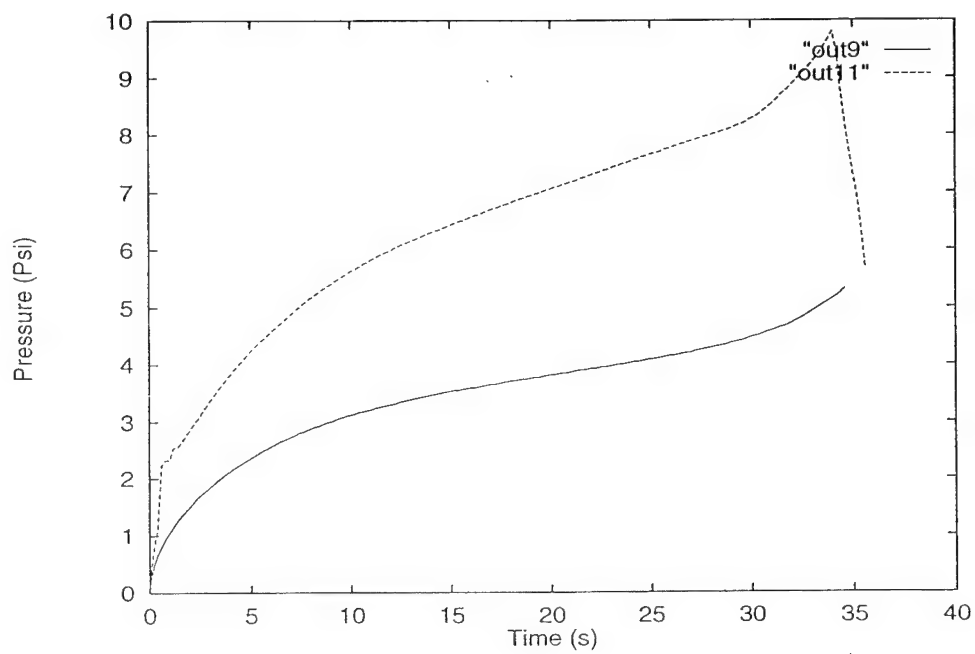Figure 22: Injection pressure plots, experiments 2, 4, and 8

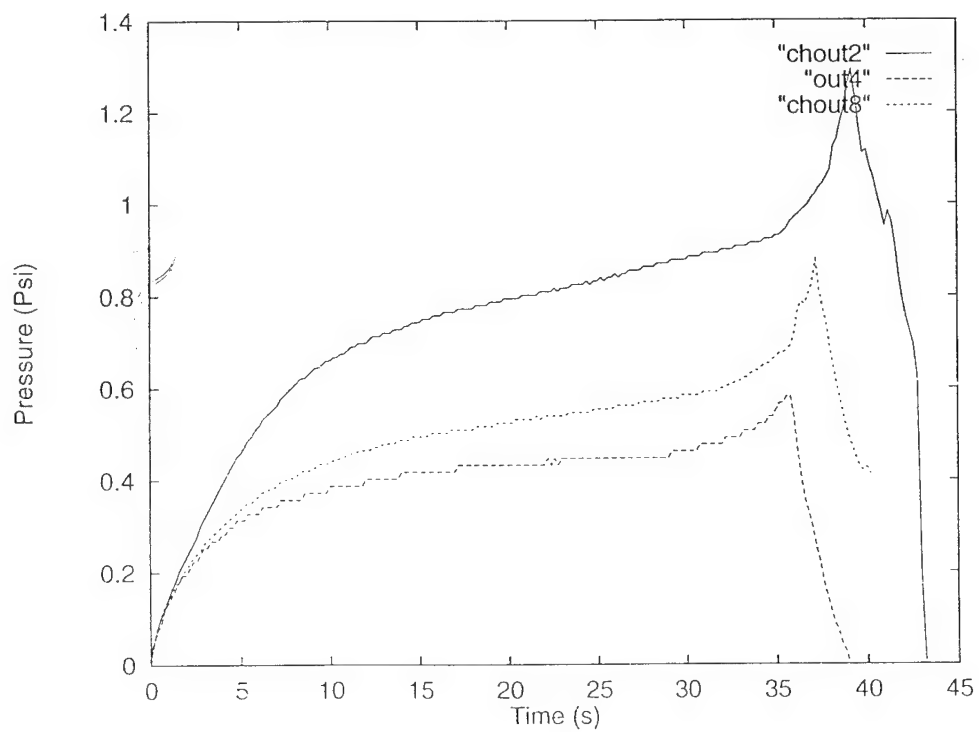Figure 23: Injection pressure plots, experiments 9 and 11

Figure 24: Injection pressure plots, experiments 17, 21, and 32

7.2.4 Effects of Fluid Flow rate on Injection Pressure

Two sets of experimental pressure curves will be compared in the discussion of this topic. These experiments used random mat preforms, with two different injection locations.

Figure 25 compares the pressure curves for the single layer random mat experiments 5, 6, and 7. The injection speeds form the ratio 2:4:1 respectively.

Figure 26 compares the pressure curves obtained from experiments 25, 26, and 27. Two layer random mat preforms were used in these experiments, with the fluid being injected at site 1 (described in Appendix A). The injection speeds for experiments 25, 26, and 27, form the ratio 2:4:1 respectively.

Both graphs display the expected trends, increasing injection speed causing higher mold pressures.

7.2.5 Effects of Injection Location on Injection Pressure

Figure 27 presents the pressure curves of experiments 11, 25 and 29. These experiments used 2 layer random mat preforms, with injection points at site 1 for experiment 25, site 2 for experiment 11, and site 3 for experiment 29. All other variables are approximately equal for these experiments.

Although readings were not taken long enough during experiments 11 and 29 to observe a final peak pressure, there seems to be significant difference between the injection scheme pressures. The pressures recorded during experiments 11 and 29 seem to be significantly lower than that measured during experiment 25. These curves would suggest to a mold designer that the injection scheme used in experiment 25 should be avoided to keep pressures within the mold to a minimum. Though pressures were measured at one point, and do not reflect how pressure behaved in other portions of the mold, pressure will be largest at the injection point.

The larger pressures encountered in experiment 25 could be explained by considering
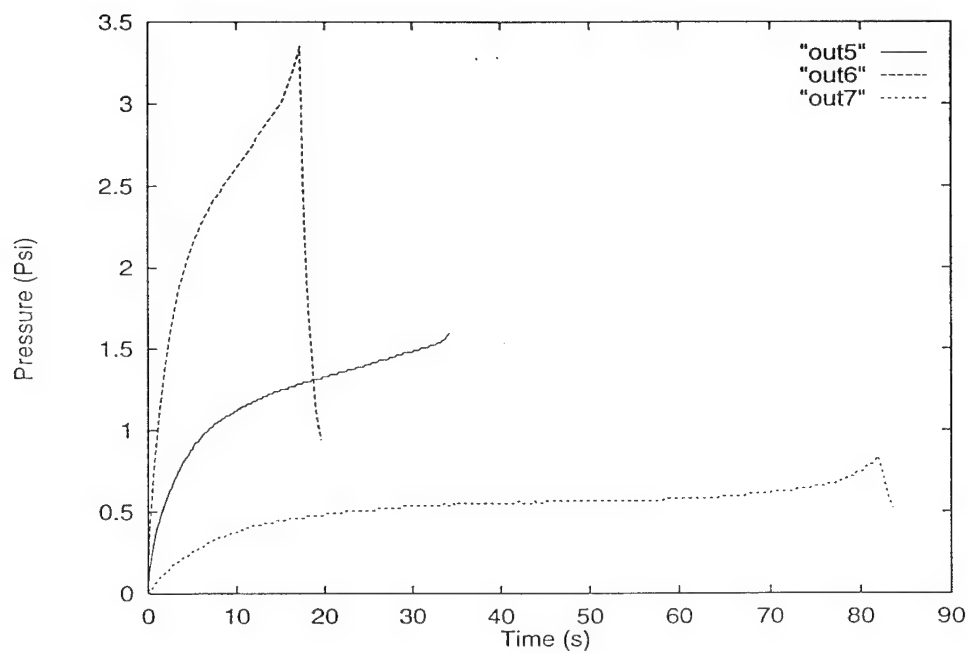
Figure 25: Injection pressure plots, experiments 5, 6, and 7
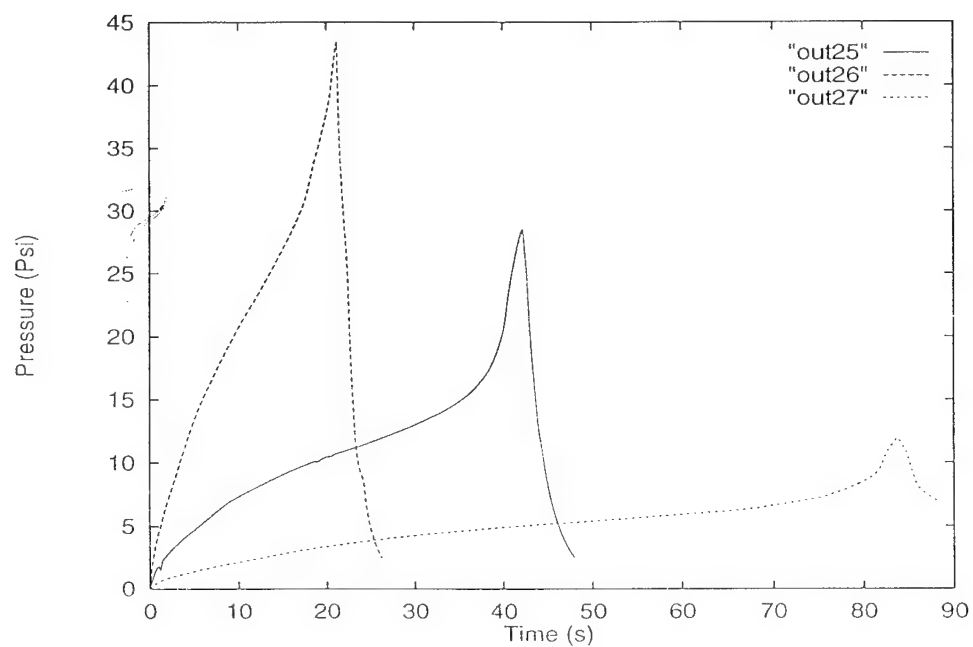
Figure 26: Injection pressure plots, experiments 25, 26, and 27

the behavior of the circumferential length of the flow front during mold filling. Due to the injection point location in experiment 25, the length of the flow front reaches a steady state length that is smaller than those found in experiments 11 and 29. As explained in Section 7.2.1, a smaller flow front length seems to cause a steeper pressure gradient, hence the pressure curve of experiment 25 steadily rose above those of the other two experiments. The relative levels of pressure measured in experiments 11 and 29 also back up this statement, the steady state length of the flow front in experiment 11 being the longest.

Experiment 40 is a random mat experiment using a two point injection scheme. The pressures measured during experiment 40 are compared to those of the previously discussed experiments in Figure 28. The viscosity of fluid used in this experiment was approximately 2/3 of that used in experiments 11, 25 and 29. Assuming that pressure can be scaled using ratios of viscosity, both pressure curves obtained from experiment 40 were scaled to give an approximate comparison to the other experiments.

It can be noted from Figure 28, that the pressure curves of experiment 40 peak much sooner, as the flow rate into each injection site was approximately equal to the flow rates used in experiments 11, 25 and 29. However the pressure values reached in experiment 40 are of comparable value to the other pressure curves presented. Hence, by injecting at two points at once, a mold may be filled in half the time, with similar pressure levels to single point injection.

Figure 27: Injection pressure plots, experiments 11, 25, and 29

Figure 28: Injection pressure plots, experiments 11, 25, 29, and 40

40

8 Conclusions

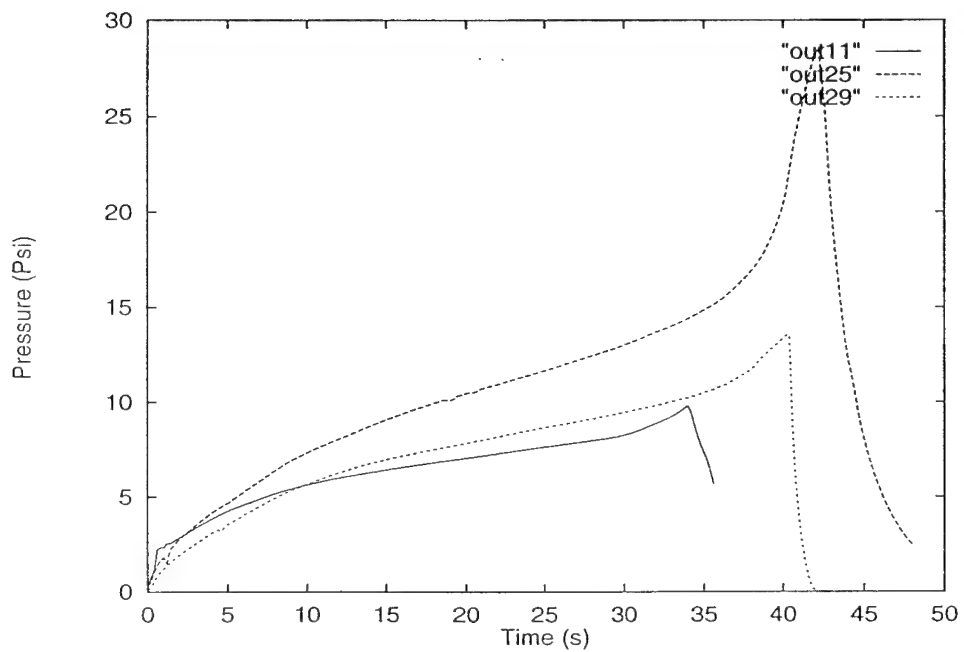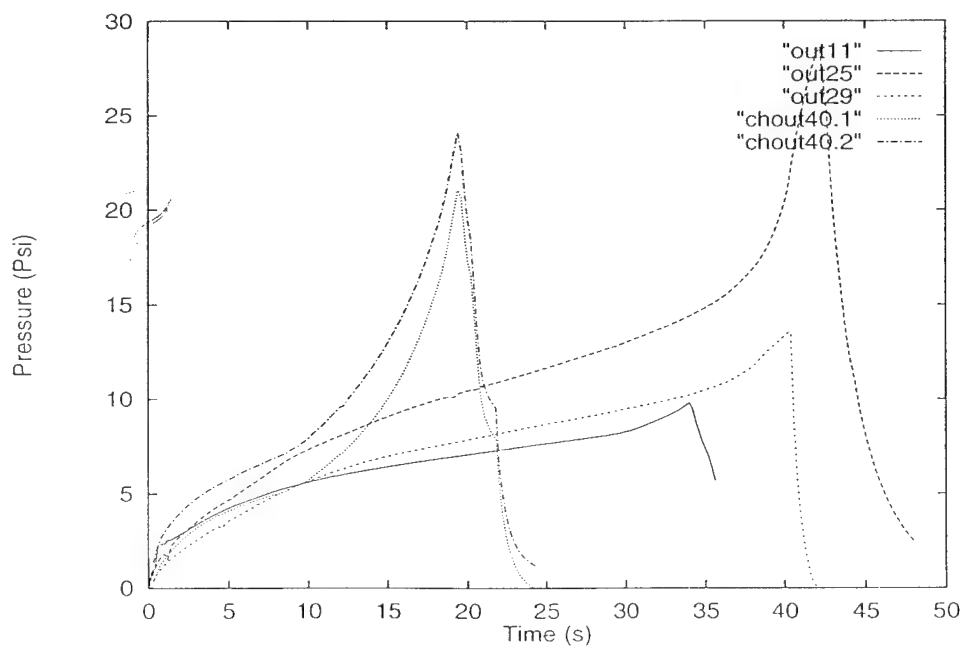The main goal of this study has been achieved, with a large amount of experimental flow front and pressure data being recorded, which will serve as a valuable resource for RTM numerical simulation work. Through comparison between several sets of experiments, different observations were made about flow front progression, and mold pressure.

The effects of fiber volume fraction, and fluid viscosity, on racetracking , were found to be negligible, as expected. However, the injection scheme used in the experiments to investigate the effects of fluid viscosity, did not encourage substantial racetracking effects. Hence, this issue should be investigated further.

Contrary to expectations, the experiments examined seemed to suggest that the magnitude of the racetracking effect does depend on the velocity of the fluid in the main body of the preform. It was noted that lower fluid injection speeds produced larger deformations of the fluid flow front due to racetracking.

Some observations were made about the general shape of the pressure curves produced during experimentation. On comparison between fluid flow front progression, and injection pressure curves for a substantial number of experiments, it has been noted that there is a relationship between the slope of the pressure curve, and the circumferential length of the flow front at any particular time. It has been found that the slope of the pressure curve decreases as the flow front length grows, remains constant when the flow front length is constant, and increases as the flow front length decreases.

The effects of fiber volume fraction, fluid viscosity, and fluid flowrate, on injection pressure, were found to be as expected, with pressure required to fill the mold increasing as all three of these variables increased.

Pressure curves for different injection locations were compared. Injection at the center of the base of the box was found to produce the lowest mold pressures for a single point injection. Pressures measured during a double point injection were found to be of similar

magnitude to single point, with the mold being filled in half the time.

9   References

[1] Richard S. Parnas, J. Grant Howard, Thomas L. Luce and Suresh G. Advani. ,"Permeability Characterization: Part 1. A Proposed Standard Reference Material for Permeability," submitted to POLYMER COMPOSITES.

A   Experimental Details

It is intended that all of the information about each experiment completed will be given in this appendix. This should prove to be a useful resource for information needed to carry out numerical simulations of each experiment. The data presented includes:

- The viscosity of the injected corn syrup.

- The total flowrate of corn syrup injected.

- The name of the movie file containing the recorded flow front progression.

- The name of the files containing pressure versus time histories.

- The pressure measurement sites employed in each experiment.

- The sites through which corn syrup was injected in each experiment.

- The location of vents during each experiment.

- The style of reinforcement mat used to construct the preform.

- The number of layers of reinforcement mat making up the preform.

- The orientation of the preform within the mold.

- The shape of the preform used.

- The measured fiber volume fractions of the preform used.

The majority of these items are straight forward quantities, while others will require further discussion to clarify various points.

A.1 Pressure Measurement and Fluid Injection Sites

Pressure measurement and fluid injection is available at five different points on the box mold. Each pressure measurement port is located immediately opposite a corresponding injection inlet. During this study, a variety of injection schemes were employed. The injection and pressure measurement points are given reference numbers in Figure 29.

It should be noted that the values given for injection flow rates are total flow rates. If the experiment uses multiple injection points, the flow rate at each injection point, is given by dividing the total flow rate by the number of injection points.

A.2 Venting Locations

Venting points are available at eight points within the mold. These vents may be plugged with small screws when not in use. As for the various injection sites, these vents are given reference numbers in Figure 30. Four pairs of points are labelled with the same number, as these points on the preform are brought together at a single point when the mold is assembled.

Whenever a particular injection scheme was used, the same venting points were employed. Table A.1 gives the relationship between injection sites and venting points.

Injection site(s) used	Vent points used
1	V5, V7
2	V1, V3, V5, V7
3	V3, V5
1, 2	V5, V7

Table A.1: Venting points used with particular injection sites.

A.3 Preform Type and Orientation

Three styles of reinforcement mat have been used during this study to construct the preforms. Depending on the material used, the orientation of the preform within the mold can have a

Box sides folded down.
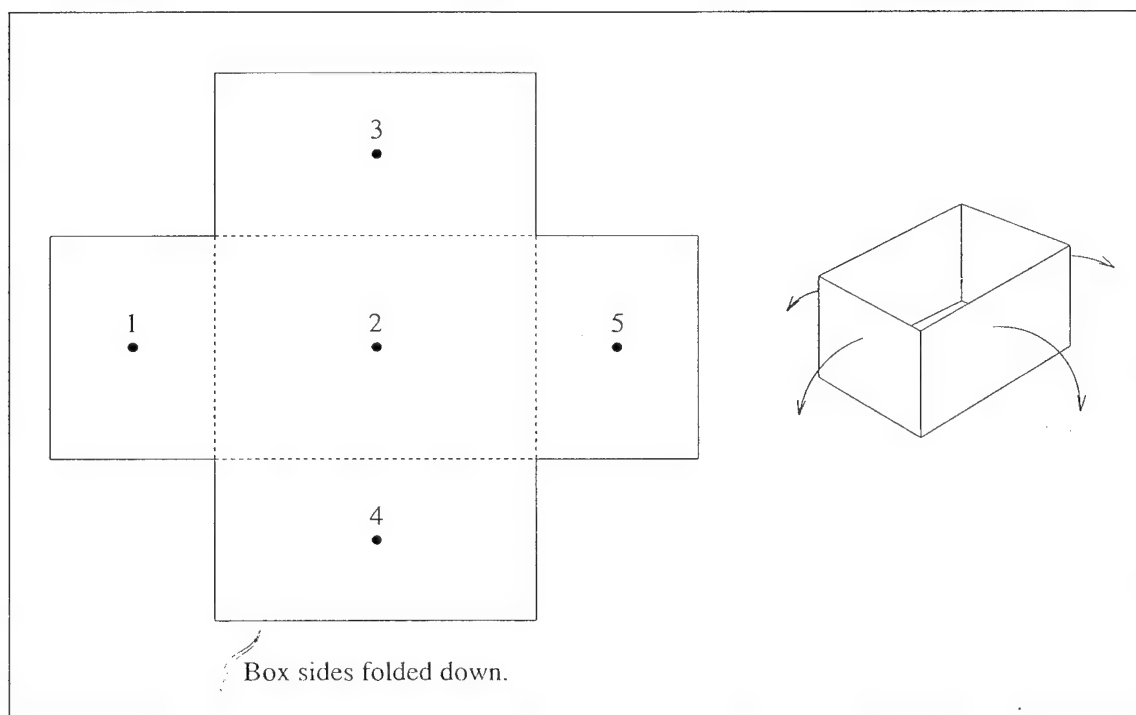
Figure 29: Reference number scheme for injection, and pressure measurement sites.
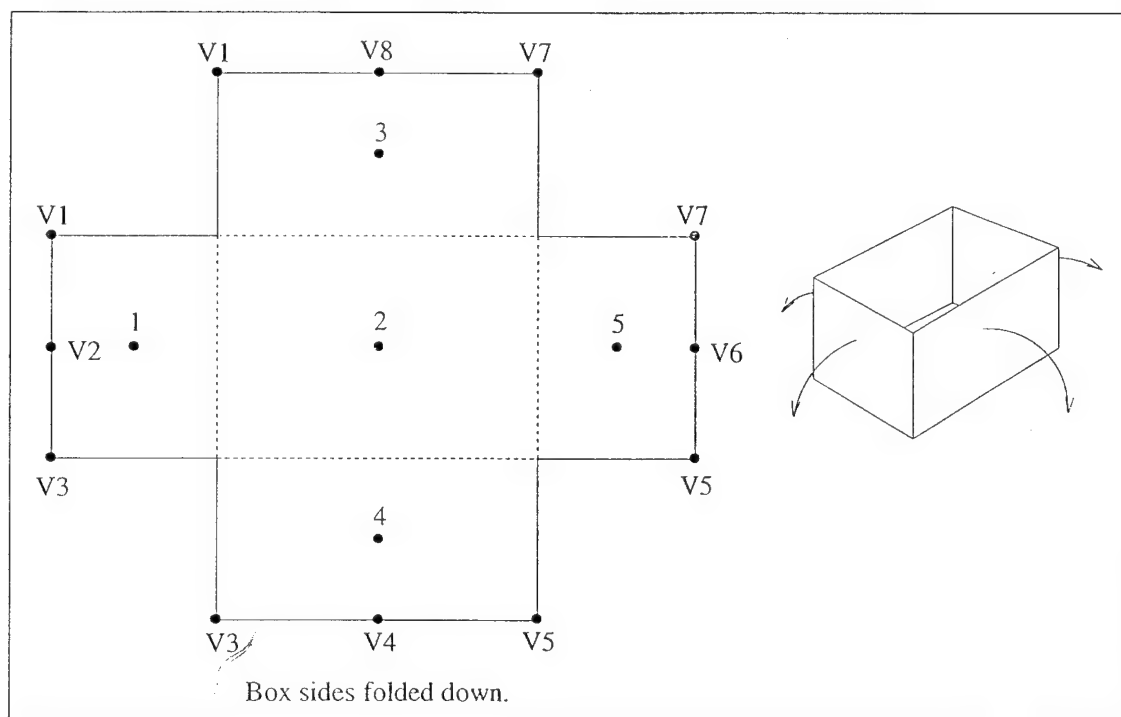
Figure 30: Reference number scheme for vents

large effect on the flow front progression.

The reinforcement fabrics used were as follows:

- Random Mat: Owens/Corning Reinforcements, random fiber mat.

- Unidirectional Mat: Certainteed, 313-UD woven roving (Product number: 313500).

- Bidirectional Mat: Knytex Reinforcement Fabrics, CD180A (Product number: N309401).

The majority of the preforms used, were constructed using fiberglass random mat. For this material, the permeabilities in the principal directions are nearly equal, and so we can consider the material to be basically isotropic in this respect. If fluid were to be injected at the center of a planar mold containing this material, the flow front shape would be very close to circular. Hence, the orientation of the random mat preforms was not important, but was maintained constant during the random mat experiments.

The remainder of the preforms used, were manufactured using unidirectional, and bidirectional fiberglass mats. These materials proved to be anisotropic, the permeabilities in the principle directions being significantly different. If fluid were to be injected at the center of a planar mold containing these materials, the flow front shapes would be elliptic in shape. Hence, the orientation of the preform in these experiments was very important. The orientations used are presented in Figure 31, and are given reference numbers. The grey ellipses demonstrate the orientation of the expected flow front patterns.

A.4 Preform Shape

The vast majority of experiments were carried out using preform shape '1', pictured in Figure 32. Two experiments were completed using preform shape '2'.
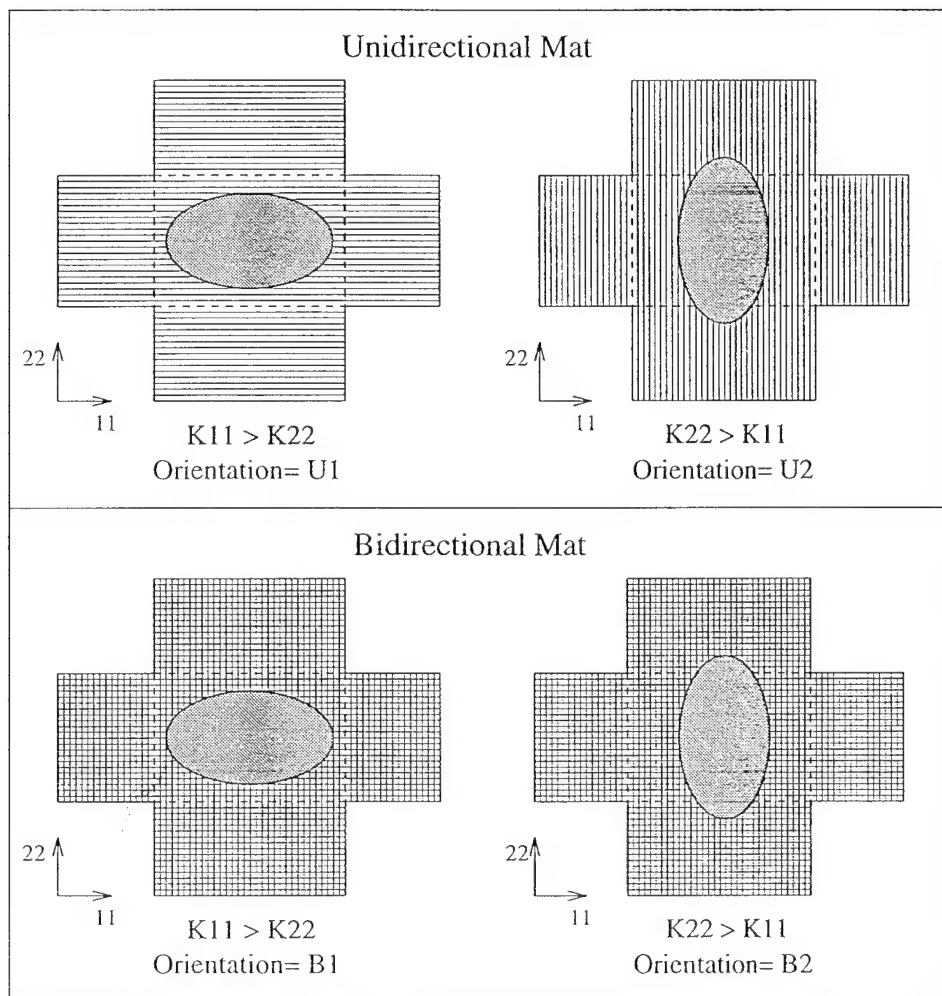
Figure 31: Preform orientation codes for Unidirectional and Bidirectional mats
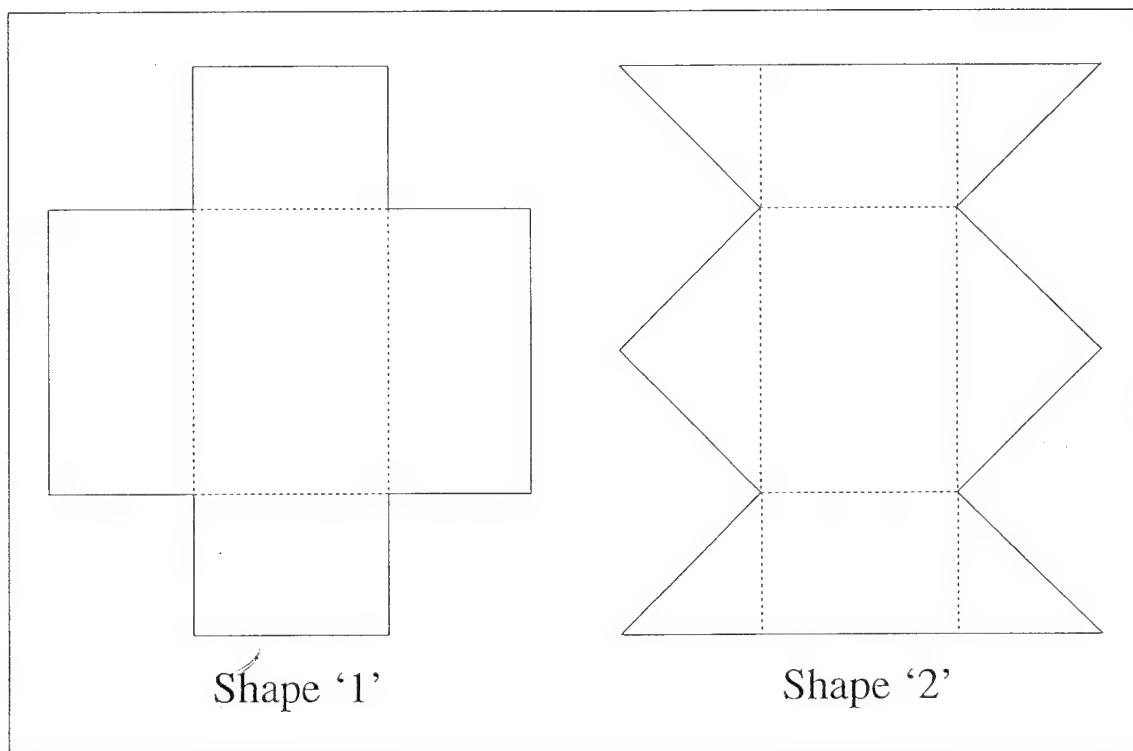
Figure 32: Preform shapes

50

A.5 Preform Permeabilities

At this time only the permeabilities of the random mat preforms have been quantified. The permeabilities for the various fiber volume fractions of random mat are given in Table A.2 [1].

Volume Fraction (%)	Permeability (m^2)	
	K11	K22
7.0	1.3e-8	1.3e-8
14.0	5.8e-9	5.8e-9
21.0	2.7e-9	2.7e-9

Table A.2: Permeability of Fiberglass Random Mat

For the experiments using a bidirectional preform, a fiber volume fraction of 35% was used. Estimations of the permeability values for this material are provided. These were obtained from pressure data measured during a radial flow permeability measurement experiment. Attempts will be made to provide more precise values, and make these available in the future.

It is again emphasized that the following values are approximations. The given values will not successfully describe the ellipticity experienced during the experiment, but do provide a good measure of the order of magnitude of permeability.

K11: 1.43e-9 m^2

K22: 1.83e-9 m^2

Unfortunately, permeabilities for the unidirectional material used could not be obtained. As for the bidirectional material, attempts will be made in the future to provide reliable numbers.

A.6 Experimental Data

The information discussed in this appendix will be presented in a series of three tables. Table A.3 presents the fluid viscosity, injection flow rate, movie file, and pressure file associated with each experiment.

Table A.4 presents the preform type, number of layers in preform, and volume fraction of preform for each experiment.

Table A.5 presents the injection, and pressure measurement sites used, as well as the preform shape.

Experiment	Viscosity (Pa.s)	Flowrate (cm^3/s)	Movie File	Pressure Files
1	0.2890	7.44	EXP1R1.mv	out1
2	0.2735	7.44	EXP1R2.mv	out2
3	0.2735	7.44	EXP1R3.mv	out3
4	0.0985	7.44	EXP1R4.mv	out4
5	0.2400	7.44	EXP1R5.mv	out5
6	0.2400	14.67	EXP1R6.mv	out6
7	0.2400	3.38	EXP1R7.mv	out7
8	0.1960	7.54	EXP1R8.mv	out8
9	0.1960	7.54	EXP2R9.mv	out9
10	0.1000	7.54	EXP2R10.mv	none
11	0.2980	7.54	EXP2R11.mv	out11
12	0.2030	15.53	EXP2R12.mv	none
13	0.2030	4.00	EXP2R13.mv	out13
14	0.2030	4.00	EXP2R14.mv	none
15	0.2910	7.44	EXP1R15.mv	none
16	0.2920	7.44	EXP1R16.mv	out16
17	0.2920	7.44	EXP3R17.mv	out17
18	0.2940	7.44	EXP6U18.mv	out18
19	0.2960	7.44	EXP6U19.mv	out19
20	0.3050	7.33	EXP6U20.mv	out20
21	0.2875	7.33	EXP6U21.mv	out21
22	0.2850	7.33	EXP6U22.mv	out22
23	0.2850	7.33	EXP2R23Z.mv	out23
24	0.2850	7.33	EXP2R24Z.mv	out24
25	0.2915	7.33	EXP2R25Z.mv	out25
26	0.2915	15.08	EXP2R26Z.mv	out26
27	0.2990	3.69	EXP2R27Z.mv	out27
28	0.2990	7.33	EXP2R28Z.mv	out28
29	0.2990	7.33	EXP2R29Z.mv	out29
30	0.3030	15.08	EXP2R30Z.mv	out30
31	0.1970	7.23	EXP4B31.mv	none
32	0.1975	7.23	EXP4B32.mv	out32
33	0.1995	7.23	EXP4B33.mv	out33
34	0.2020	7.44	EXP4B34Z.mv	out34
35	0.2010	7.33	EXP4B35Z.mv	out35
36	0.1980	7.33	EXP4B36Z.mv	out36
37	0.1970	7.33	EXP4B37Z.mv	out37
38	0.1980	15.08	EXP2R38Z.mv	out38

Experiment	Viscosity (Pa.s)	Flowrate (cm^3/s)	Movie File	Pressure Files
39	0.1980	15.08	EXP2R39Z.mv	out39
40	0.1980	15.08	EXP2R40Z.mv	out40.1, out40.2
41	0.2030	7.33	EXP2R41Z.mv	out41.1, out41.2
42	0.2030	7.33	EXP2R42Z.mv	out42.1, out42.2
43	0.1980	15.53	EXP4B43.mv	out43
44	0.1950	15.53	EXP4B44.mv	out44
45	0.1950	7.23	EXP2R45.mv	out45
46	0.1950	7.23	EXP2R46Q.mv	out46

Table A.3: Fluid viscosity, injection flow rate, movie file, and pressure file

Experiment	Preform Type	No. of Layers	Volume Fraction (%)	Preform Orientation
1	Rand	1	7	-
2	Rand	1	7	-
3	Rand	1	7	-
4	Rand	1	7	-
5	Rand	1	7	-
6	Rand	1	7	-
7	Rand	1	7	-
8	Rand	1	7	-
9	Rand	2	14	-
10	Rand	2	14	-
11	Rand	2	14	-
12	Rand	2	14	-
13	Rand	2	14	-
14	Rand	2	14	-
15	Rand	1	7	-
16	Rand	1	7	-
17	Rand	3	21	-
18	Unidir	6	33	U1
19	Unidir	6	33	U1
20	Unidir	6	33	U1
21	Unidir	6	33	U1
22	Unidir	6	33	U2
23	Rand	2	14	-
24	Rand	2	14	-
25	Rand	2	14	-
26	Rand	2	14	-
27	Rand	2	14	-
28	Rand	2	14	-
29	Rand	2	14	-
30	Rand	2	14	-
31	Bidir	4	35	B2
32	Bidir	4	35	B2
33	Bidir	4	35	B1
34	Bidir	4	35	B2
35	Bidir	4	35	B1
36	Bidir	4	35	B2
37	Bidir	4	35	B1
38	Rand	2	14	-

Experiment	Preform Type	No. of Layers	Volume Fraction (%)	Preform Orientation
39	Rand	2	14	-
40	Rand	2	14	-
41	Rand	2	14	-
42	Rand	2	14	-
43	Bidir	4	35	B1
44	Bidir	4	35	B2
45	Rand	2	14	-
46	Rand	2	14	-

Table A.4: Preform type, number of layers in preform, and volume fraction

Experiment	Injection Sites	Pressure Sites	Preform Shape
1	2	2	1
2	2	2	1
3	2	2	1
4	2	2	1
5	2	2	1
6	2	2	1
7	2	2	1
8	2	2	1
9	2	2	1
10	2	2	1
11	2	2	1
12	2	2	1
13	2	2	1
14	2	2	1
15	2	2	1
16	2	2	1
17	2	2	1
18	2	2	1
19	2	2	1
20	2	2	1
21	2	2	1
22	2	2	1
23	2	2	1
24	1	2	1
25	1	1	1
26	1	1	1
27	1	1	1
28	3	2	1
29	3	3	1
30	3	3	1
31	2	2	1
32	2	2	1
33	2	2	1
34	1	2	1
35	1	2	1
36	3	2	1
37	3	2	1
38	1, 2	2	1

Experiment	Injection Sites	Pressure Sites	Preform Shape
39	1, 2	2	1
40	1, 2	1, 2	1
41	1	1, 2	1
42	1	1, 2	1
43	1, 2	2	1
44	1, 2	2	1
45	2	2	2
46	2	2	2

Table A.5: Fluid injection sites, pressure measurement sites, and preform shape

CHARACTERIZATION OF CORNER AND EDGE PERMEABILITIES DURING MOLD FILLING IN RESIN TRANSFER MOLDING

Simon Bickerton
Department of Mechanical Engineering
University of Delaware
Newark, DE 19716

Suresh G. Advani
Department of Mechanical Engineering
University of Delaware
Newark, DE 19716

ABSTRACT

During the fiber preform lay-up in an RTM mold, air cavities or other regions of high porosity are set up near the edges and corners of the mold and the inserts within the mold. Such high porosity regions offer the injected resin least flow resistance, causing the resin flow front to flow much faster in these regions, this effect is generally known as racetracking. Numerical simulations to model RTM can account for the effects of racetracking once one can specify the permeability or the resistance to flow in these regions. A systematic experimental study was conducted in a 1-dimensional mold to investigate the role of air gap, preform type, volume fraction and process and material parameters on flow. Experimental flow fronts were matched with numerical flow fronts at all times during filling, by adjusting the permeability values for the edge elements in the numerical simulation. This allowed us to construct a phenomenological model for permeability in an air gap, as a function of air gap size, preform fiber volume fraction, and preform material.

NOMENCLATURE

A, C, D	Coefficients
K	Permeability (m^2)
P	Pressure (Pa)
Q	Fluid injection flowrate (m^3/s)
V_f	Preform volume fraction
b	Air gap width (m)
v_d	Volume averaged Darcy velocity (m/s)
μ	Fluid Viscosity ($Pa.s$)

Subscripts:

bulk   of the preform material
gap   in the air gap

INTRODUCTION

The first step in the RTM process consists of the placing of the preform within the mold cavity. The preform will provide the finished piece with the majority of its structural properties. After the mold is sealed, resin is injected, heat being applied to the mold to cure the resin at the completion of filling. The finished composite product is then removed from the mold (Advani et al., 1994b).

This study focuses on the mold filling stage of RTM. Successful filling of the mold is required if a satisfactory part is to be produced. An incorrect injection scheme can produce dryspots in the finished piece, rendering it useless. Liquid Injection Molding Simulation (LIMS) is a numerical simulation of the RTM process developed at the University of Delaware (Advani et al., 1994a)(Bruschke et al., 1991), which provides the tools to design the correct injection scheme, before the costly task of manufacturing the mold is undertaken.

Racetracking is a common phenomena encountered during the filling of RTM mold cavities (Bruschke et al., 1990). Racetracking occurs when the injected resin encounters an air cavity, or region of the mold not completely filled with the preform material. Due to the lower resistance to flow in such air cavities, the resin will tend to fill these regions first, significantly altering the shape of the flow front. The position of the flow front due to racetracking can be difficult to predict, as the formation of air cavities within the mold is itself difficult to predict, and there are very few models to assign permeabilities to these high porosity regions.

Such unpredictable behavior of the resin flow front can lead to the entrapment of air in the mold, causing dryspots in the finished piece. For numerical simulations to successfully predict the mold filling stage of RTM, a model that will account for permeability changes near the corners and edges needs to be incorporated.

A simple method to numerically simulate racetracking is investigated. This paper details an experimental study to measure the permeability ratio between air gap and bulk preform (K_{gap}/K_{bulk}), for a random fiberglass reinforcing material.

A series of experiments have been completed in a planar rectangular mold, constructed from acrylic. LIMS has been employed where elements representing the air gap have been assigned a single value of permeability higher than that of the preform, for a variety of air gap widths, b, so as to match numerical and experimental flow fronts. For each experiment, a value of K_{gap}/K_{bulk} was settled upon that provided the best flow front match for all time steps. Groups of experiments were completed for three different volume fractions, V_f.

The experimental data gathered has been analyzed, and an empirical model developed. This model provides the K_{gap} value required for use with the two-level permeability method of numerically simulating racetracking. The model has been developed for one style of preform material, and is dependent on b, V_f, and K_{bulk}.

THEORY

The mold filling stage of RTM is generally modelled as flow through porous media. The majority of RTM simulations available are based on Darcy's law:

$$v_d = -\frac{K}{\mu} \nabla P \tag{1}$$

where μ is the viscosity of the fluid, P its pressure, and K is the permeability tensor,

1

representing the resistance of the porous media. v_d is the volume averaged Darcy velocity (Darcy, 1856).

Successful prediction of the filling of an RTM mold relies on the determination of the permeability tensor throughout the mold (Davé et al., 1990). Permeability is vital material information provided to LIMS. The proposed two-level permeability method lends itself readily to the finite element format of LIMS and other similar packages, where it can be assigned locally.

The proposed method simulates racetracking by assigning higher permeability values to elements representing air channels, or regions of high porosity in the mold cavity. Examples of such regions in a mold may occur at edges, corners, inserts and stiffeners. Models are required to predict the values of permeability applied to these high porosity regions.

It was proposed that K_{gap}, the permeability within an air cavity, could have the following functional dependence.

$$K_{gap} = f(V_f, \; b, \; K_{bulk}, \; \mu, \; Q, \; Preform \; material \; type) \tag{2}$$

where Q is the flowrate at which fluid was injected.

Experiments have been completed to establish whether μ and Q influence K_{gap}. For the molding situation studied, under conditions comparable with RTM operations, it was found that fluid viscosity μ, and injection flowrate did not influence K_{gap}. Therefore, models developed will be based on the following functional relationship.

$$\frac{K_{gap}}{K_{bulk}} = f(V_f, \; \frac{b}{\sqrt{K_{bulk}}}, \; Preform \; material \; type) \tag{3}$$

EXPERIMENTS

Experiments were completed in a simple two piece mold, the male and female pieces constructed from 1/2" clear acrylic plate. The mold cavity was of a planar rectangular shape, measuring 19" by 4", having a thickness of 1/8". A 1cm grid was marked on one face of the mold for easy reference between experiment and numerical simulation.

The preforms used during this study were composed of 1 to 3 layers of random mat fiberglass reinforcement. The mat used was M721, manufactured by Advanced Textiles. The preforms were cut at a variety of widths, small enough to create an air gap of width b along one edge of the mold cavity. The air gap width b, was measured for each experiment using simple image processing techniques. Figure 1 presents the mold cavity, and position of preform relative to injection and venting sites.

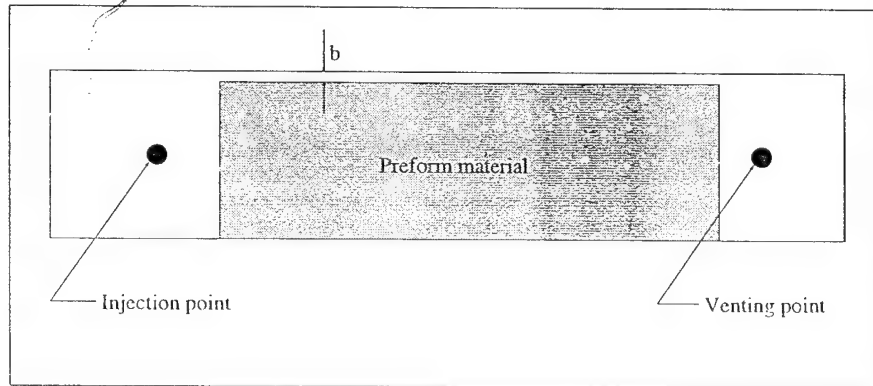Experiments were completed with a constant flowrate fluid injection system. The

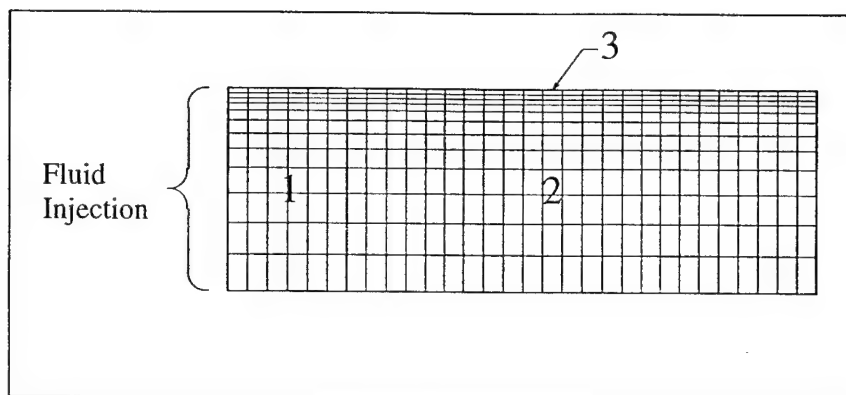Figure 1: Schematic of preform and mold cavity.

2

Figure 2: Schematic of typical finite element mesh.

experimental setup allowed the setting of a wide range of flowrates. The injection position is shown in Figure 1.

The fluid used to represent resin was a mixture of corn syrup, water, and clothing dye. This fluid is Newtonian, and hence viscosity is easily characterized. Black clothing dye was used to enhance the visibility of the fluid within the mold.

Each experiment was filmed from directly above using a Sony Handy-cam video camera. Several experiments were completed for three different volume fractions, 7%, 14%, and 21%. Footage of each experiment was placed in Silicon Graphics movie format, one frame being digitized every second of experiment real time. Digitizing the experiments in this format provided an excellent media for comparison with numerical results.

For each experiment completed, a finite element mesh was created for input to LIMS. Each mesh contained three material regions, region 1 was a low permeability region of material, included to allow the flow front to settle to a one dimensional flow before entering the preform. Region 2 represents the preform material, region 3 representing the air gap. The regions of the mesh are presented in Figure 2, a schematic of a typical mesh. The width of region 3 was adjusted for each experiment, according to the actual air gap present in the mold.

K_{bulk}, the permeability of the fiberglass preform, was taken from Parnas (et al., 1994). A value for K_{gap} was set in the LIMS input file in region 3 before numerically simulating the flow fronts. Parameters measured for each experiment, and included in the LIMS input, included fluid viscosity, injection flowrate, K_{bulk}, and b. The resulting flow fronts calculated by LIMS were compared to the digitized movie of the experiment in consideration. The simulation was repeated, each time varying K_{gap}, until numerical and experimental flow front patterns matched at all times. In this way, the ratio K_{gap}/K_{bulk} was obtained from each experiment. Figure 3 provides an example of the match obtained between numerical simulation and experiment.

A mesh refinement study was completed to assess how the level of detail of the mesh effected the resultant flow front pattern calculated by LIMS. Meshes were created containing 2, 4, and 8 rows of elements in region 3 (see Figure 2). All other variables were identical for these three simulations. The extra elements used to represent the air cavity did not significantly alter the resulting flow fronts. A similar study was completed to assess the effect of the level of the grading of the mesh in region 2. Again, the effect on the flow fronts was negligible.

RESULTS AND DISCUSSION

K_{gap}/K_{bulk} values obtained from each experiment are plotted versus the nondimensional gap width $b/\sqrt{K_{bulk}}$, in Figure 4. With the higher volume fraction experiments, it proved to become increasingly difficult to set up the preform within the mold. This is reflected

in the increased scatter of the data with increasing volume fraction.

For each group of data points corresponding to a certain volume fraction, a polynomial fit was attempted. Higher order polynomials gave contradicting forms, suggesting linear fits to be more suitable.

As the width of an air gap becomes small, K_{gap} will approach K_{bulk}. Therefore, K_{gap}/K_{bulk} was assigned a value of 1.0 for a nondimensional gap width of 0.0, in each group of data points. A linear fit was found for each data set, that was forced to pass through the point (0.0,1.0). In this way, each set of data was fitted to Equation 4.
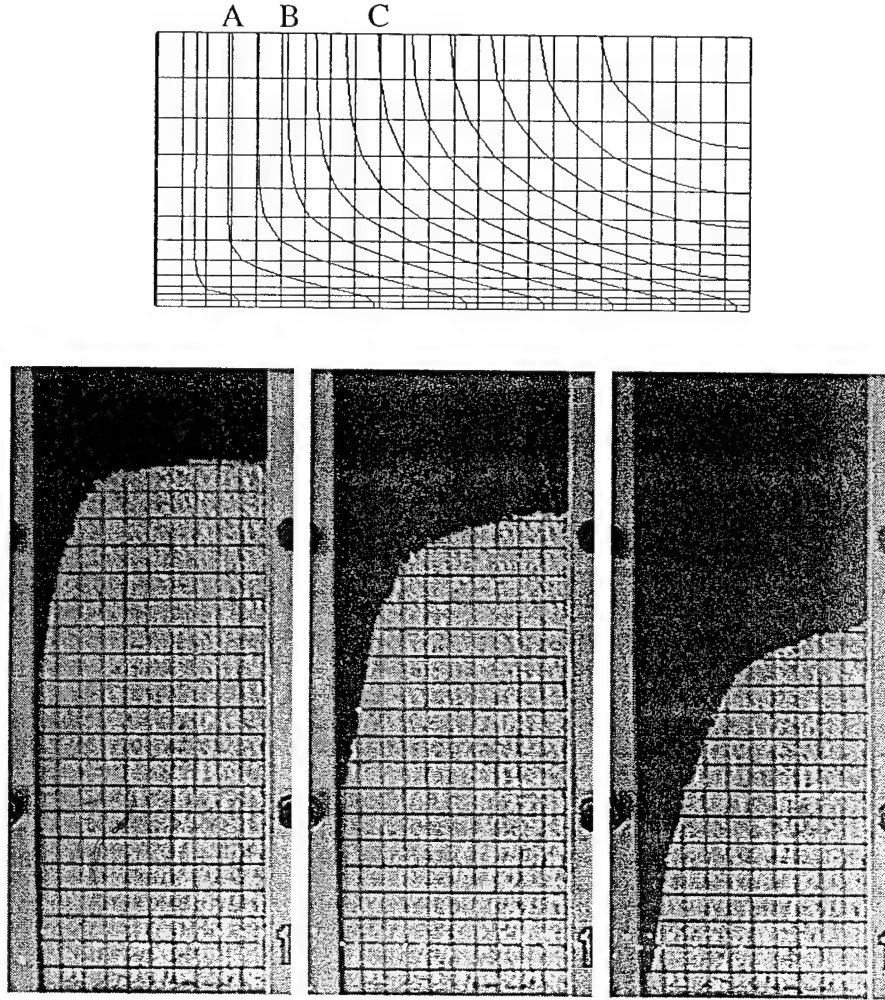

Figure 3: Example of match between experimental and numerical results. The digitized frames A to C (left to right) correspond to the labelled contours of the numerical result above.

$$\frac{K_{gap}}{K_{bulk}} = 1.0 + C\left(\frac{b}{\sqrt{K_{bulk}}}\right) \tag{4}$$

The values of the coefficient C, obtained for each volume fraction V_f, are presented in Table 1. The three values of C obtained are plotted versus V_f in Figure 5. An exponential
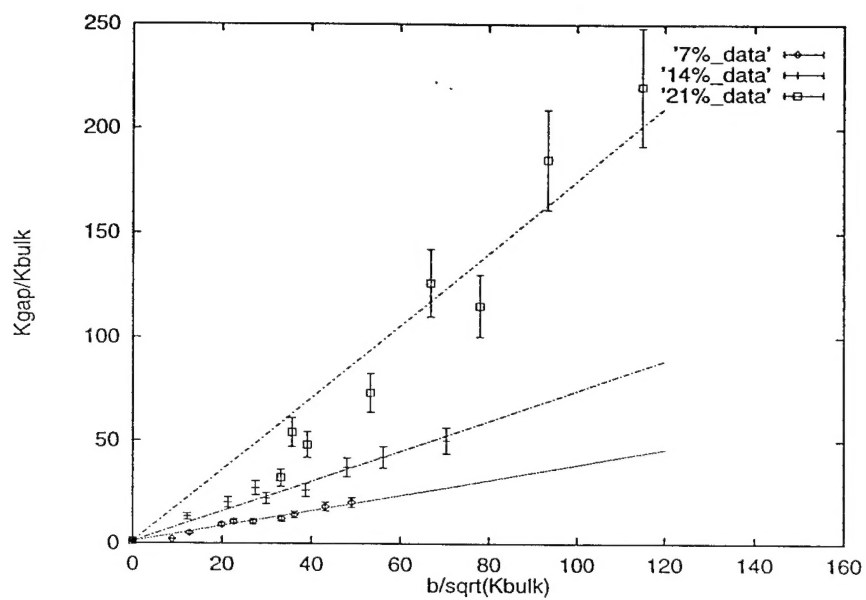
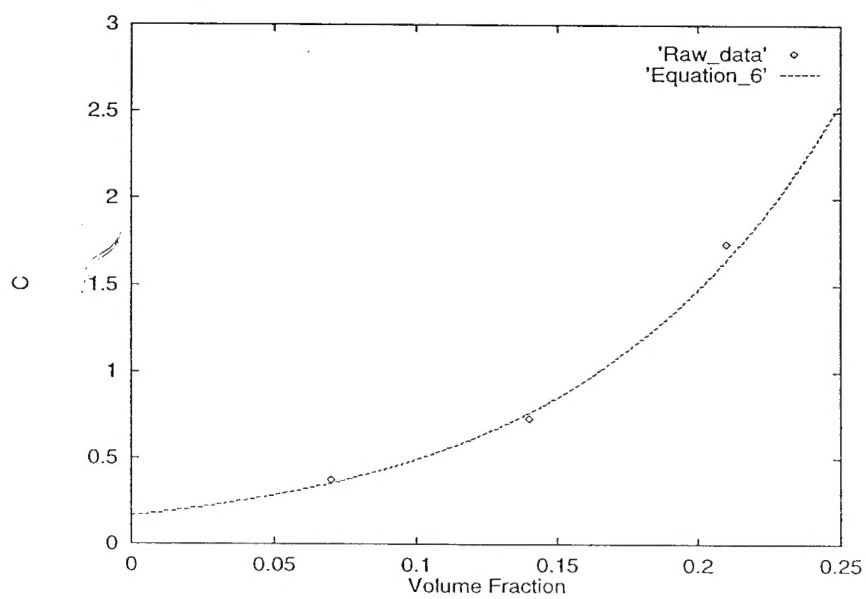Figure 4: Kgap/Kbulk versus Non-dimensionalised cavity width.

Figure 5: C versus Preform volume fraction.

Volume Fraction (V_f)	C
0.07±0.005	0.373
0.14±0.010	0.730
0.21±0.015	1.739

Table 1: C coefficients.

curve was found to fit the data well. The form of equation applied is given in Equation 5.

$$C = Ae^{DV_f} \tag{5}$$

where A and D are coefficients to be determined. The curve fitted to the data is presented in Figure 5. The resultant form of the equation is as follows:

$$C = 0.1642e^{10.991V_f} \tag{6}$$

K_{gap}/K_{bulk} has been found to vary as predicted by Equation 7. Equation 7 is of the form given by Equation 3. This relation is recommended for use up to a preform volume fraction of 0.21.

$$\frac{K_{gap}}{K_{bulk}} = 1.0 + 0.1642e^{10.991V_f}\left(\frac{b}{\sqrt{K_{bulk}}}\right) \qquad 0.00 < V_f < 0.21 \tag{7}$$

A predictive model for K_{gap} has been developed from experiments, for one type of random mat fiberglass reinforcement. The model provides an RTM simulation with the permeability expected in a planar air cavity. This process will be repeated with different styles of material, to determine whether these materials follow similar trends. In this manner, it may be possible to determine a simple model for K_{gap}/K_{bulk} for the majority of materials used to construct RTM preforms, and will allow us to predict racetracking in RTM simulations.

SUMMARY

A simple method to model racetracking in RTM molding was investigated. It was found that a dual permeability model, applying a value K_{gap} in the air cavity concerned, higher than that of the bulk preform, K_{bulk}, produced flow fronts that closely matched those found in experiments. LIMS was used in conjunction with experimental flow front visualization results, to measure the ratio K_{gap}/K_{bulk}, for a variety of preform volume fractions, and air cavity widths. The study was completed using preforms constructed of random mat fiberglass reinforcement. The data gathered was analyzed, and a predictive empirical model developed.

ACKNOWLEDGEMENTS

REFERENCES

Advani, S.G., Liu B., and Bruschke, M.V., 1994a,"*Liquid injection molding simulation - LIMS User's Manual - version 3.0.*" University of Delaware, Newark.

Advani, S.G., Bruschke, M.V., and Parnas, R., 1994b,"Chapter 12: Resin Transfer Molding, in"*Flow and Rheology in Polymeric Composites Manufacturing*, Edited by Suresh G. Advani, Elsevier Publishers, Amsterdam, pp. 465-516.

Bruschke, M.V., and Advani, S.G, 1990,"A Finite Element/Control Volume Approach to Mold Filling in Anisotropic Porous Media," *POLYMER COMPOSITES*, Vol. 11, No. 6, pp. 401-402.

Bruschke, M.V., and Advani, S.G, 1991,"Filling simulation of complex three dimensional shell-like structures," *SAMPE QUARTERLY*, pp. 2-11.

Darcy, H., 1856,"Les fontaines Publiques de la Ville de Dijon", Dalmont, Paris.

Davé, R., and Houle, S., 1990," *The Role of Permeability During Resin Transfer Molding,*" Proceedings of the American Society for Composites Fifth Technical Conference, pp. 539-547.

Greenkorn, R.A. 1983," *Flow Phenomena in Porous Media,*" Marcel Dekker, New York.

Parnas, R.S., Howard, J.G., Luce, T.L., and Advani, S.G., "Permeability Characterization: Part 1. A Proposed Standard Reference Material for Permeability," *submitted to POLYMER COMPOSITES.*

Scheidegger, A.E., 1974," *Physics of Flow through Porous Media,*" Univ. Toronto Press, Toronto.

High Performance Computing and Modeling of
Composite Manufacturing Processes such as Resin Transfer Molding

by

Suresh G. Advani
Associate Professor of Mechanical Engineering
Affiliated Faculty with Center for Composite Materials
University of Delaware
Newark, DE 19716
phone: 302 -831-8975
fax   302-831-3619
e.mail advani@me.udel.edu

Abstract

This report summarizes the research conducted under Research Agreement No.
DAAH04-93-G-0087. The focus was to understand and model the composite
manufacturing process called Resin Transfer Molding (RTM) and develop numerical
simulations to move towards virtual manufacturing in an attempt to reduce the prototype
costs. Experiments were carried out to understand and isolate the important features of
this process and mathematical models were developed to create a process model. These
models were incorporated in numerical simulations to make them useful for
manufacturing of complex structures. Numerical procedures were also developed in the
process to make the simulations stable and faster. The results of numerical simulations
were compared with two elaborate experimental programs, a five sided box and a cone,
to verify the authenticity of the numerical simulation and the mathematical models.
Different versions of the numerical simulation developed are being used at ARL,
Aberdeen and by TACOM. This report gives a brief summary of the work and the details
of the work are reported as appendices.